The Role of ABCC5 in Metabolism and Signalling in Prostate Cancer

Jessica Abele

Exeter College

University of Oxford

A thesis presented for the degree of

Doctor of Philosophy

Hilary 2024

Abstract

Advanced prostate cancer (PCa) treatment remains challenging, requiring new drug targets and therapies to improve outcomes for patients. Studies have linked ABCC5 overexpression to unfavourable tumour grading, shortened recurrence-free survival, and reduced overall survival in PCa. However, the precise mechanisms and pathways governed by ABCC5 in the context of PCa remain elusive. This thesis aims to advance our comprehension of ABCC5's role in PCa as limitations persist due to the scarcity of in-depth functional studies and the absence of the ABCC5 crystal structure. This study proposes a novel dual perspective, suggesting that shorter ABCC5 isoforms might be responsible for epigenomic regulation, particularly within the nucleus, while protein from full-length transcripts could play a distinct role in mitochondria, associated with heme metabolism and apoptosis. The categorisation of ABCC5's roles into these two compartments offers a fresh insight into its potential functionality, contributing to our understanding of its diverse impact on PCa biology. In the nucleus, ABCC5 impacts pathways related to SUMOylation and cell cycle regulation. Whereas, in the mitochondria, promoter analysis emphasises ABCC5's connection to the heme metabolism, while caspases in the protein network highlight ABCC5's participation in mitochondrial apoptotic pathways. Further, structural similarities with PCAT1 raise questions about an enzymatic function and potential protein modification mediated by ABCC5. Future research should explore these novel targets and investigate this proposed dual functionality to deepen our comprehension of ABCC5's function in PCa.

Declaration

This thesis and the work presented in it were completed at the University of Oxford (Department of Physiology, Anatomy and Genetics) between October 2019 and March 2024, under the supervision of Prof. Heidi de Wet, Prof. Jaideep Pandit and Prof. Helen Christian. This work is wholly my own, and any contribution to the thesis made by others has been acknowledged. The work submitted here does not form part of another thesis in this or any other university.

Acknowledgements

I want to begin by expressing my gratitude to my supervisor, Prof. Heidi de Wet, for allowing me to continue my DPhil in her lab. Her guidance, support, advice, and encouragement have been instrumental in my success. Furthermore, I am incredibly grateful to my co-supervisor Prof. Dr. Jaideep Pandit. His unwavering support and encouragement throughout the ups and downs of my journey have been invaluable, and I am truly thankful for his guidance. I must also extend my heartfelt appreciation to my co-supervisor, Prof. Dr. Helen Christian, for helping me navigate the unexpected challenges I faced and for generously sharing her personal experiences. I would also like to thank Chelsea for her invaluable contributions. Her knowledge, experience, and availability for scientific discussions and brainstorming sessions have been immensely helpful. Moreover, her friendship both in and out of the lab has been a source of great support. Additionally, I want to acknowledge the other members of the de Wet group, including Tascia and Gosia, for their continuous assistance, and support, and for fostering a friendly and welcoming environment. I am also grateful to all my friends from Exeter College, OURFC, and beyond. Your presence has enriched my experience in the UK, and I am thankful for the wonderful memories we have shared. Finally, I would like to express my heartfelt gratitude to my family, especially my parents, Carola and Thomas, and my brother, Matteo. Their unwavering support and love have been the foundation of my journey, and I am profoundly grateful for everything they have done for me.

Realise deeply that the present moment is all you have. Make the now the primary focus of your life.

— Eckhart Tolle

Table of Contents

1 Introduction **1**

1.1 Prostate Cancer 1

1.1.1 Incidence and Mortality 1

1.1.2 Clinical Diagnosis 2

1.1.2.1 Prostate Anatomy 2

1.1.2.2 Screening and Diagnosis 4

1.1.2.3 Tumour Grading and Staging 4

1.2 Management 8

1.2.1 Active Surveillance 8

1.2.2 Watchful Waiting 9

1.2.3 Surgery 10

1.2.4 Radiotherapy 10

1.2.5 Systemic Therapy 11

1.2.5.1 Hormonal Therapy 11

1.2.5.2 Chemotherapy 13

1.2.5.3 Immunotherapy 13

1.3 Prognosis 14

1.4 Advanced Prostate Cancer 15

1.5 ABC Transporters 17

1.5.1 ABCC Family 21

1.6 ABCC5 23

1.6.1 Substrates 26

1.6.2 Structure 29

1.6.3 Paralogues ABCC11 and ABCC12 32

1.7 ABCC5 in Cancer 34

1.8 ABCC5 in Prostate Cancer 37

1.9 Summary and Hypothesis 41

2 Material and Methods **43**

2.1 Computational Analysis 43

2.1.1 Meta-analysis of ABCC5 Correlated Genes 43

2.1.2 Metascape Pathway and Process Enrichment 46

2.1.3 REVIGO GO Term Enrichment Analysis 46

2.1.4 Homology Modelling with DALI 47

2.1.5 Gene Promoter Motif Analysis 47

2.1.6 Protein-Protein Interaction Network Construction 48

2.2 Mice Work 50

2.2.1 Mice 50

2.2.2 Tissue Isolation 50

2.2.3 Histology and Cryosectioning 50

2.2.4 Immunofluorescence of Cryosections or Floating Sections 51

2.3 RNA/DNA and Protein 52

2.3.1 Plasmid DNA Purification 52

2.3.2 Reverse Transcription and qPCR 52

2.3.3 Protein Sample Preparation and Measurement 56

2.3.4 SDS-PAGE and Western Blot 57

2.4 Prostate Cancer Cell Work 61

2.4.1 Cell Culture 61

2.4.2 ABCC5 Knockdown 62

2.4.3 ABCC5 Overexpression 63

2.4.4 Immunofluorescence in Cell Culture 64

2.4.5 Colony Formation Assay 64

2.4.6 Cell Migration Assay 65

2.4.7 Caspase Assay 66

2.5 Data Analysis 67

2.6 Reagents 67

3 Decoding Cancer Gene Networks and ABCC5's Potential Functions 69

3.1 Introduction 69

3.1.1 Meta-analysis TCGA Dataset 69

3.1.2 Functional Prediction via Homologous Proteins 70

3.1.3 Aims 71

3.2 Results 72

3.2.1 Meta-analysis of Genes Correlating with ABCC5 from TCGA Datasets 72

3.2.2 ABCC5 Gene Expression Dependent Analysis 77

3.2.3 Functional Prediction via Homologous Proteins 83

3.2.3.1 DALI Server Modelling against PDB Database . 83

3.2.3.2 Alignment of ABCC5 and PCAT1 86

3.2.3.3 DALI Server Modelling against AlphaFold Database 87

3.3 Discussion 91

3.3.1 ABCC5's Connection to the SUMO-specific Endopeptidase Pathway 91

3.3.2 Does ABCC5 have a Potential Enzymatic Function? . . . 93

3.3.3 ABCC5 Involvement in Heme Transport 95

3.4 Summary and Limitations 97

4 Exploring Co-Expressed Genes of ABCC5 in Human Prostate Cancer: Discovering Diverse Functional Pathways and Potential Transcription Factors 99

4.1 Introduction 99

4.1.1 Preclinical Challenges Investigating Prostate Cancer . . . 99

4.1.2 Transcriptional Regulation 103

4.1.3 Aims 104

4.2 Results 105

4.2.1 Prostate Cancer Analysis with ABCC5 105

4.2.2 Transcription Factor Analysis 114

4.2.3 ABCC5 Knockdown and Overexpression Validation . . . 118

4.2.4 Transcription Factor Assessment 121

4.2.4.1 Zinc Finger Transcription Factors 122

4.2.4.2 Other Transcription Factors 129

4.3 Discussion 136

4.3.1 Chromatin Regulation Cluster 137

4.3.2 Cell Division Cluster 139

4.3.3 Transcription Regulation Cluster 140

4.3.4 Protein Modification and SUMOylation Cluster 142

4.3.5 P53 Activity Regulation Cluster 143

4.4 Summary and Limitations 144

5 Proteome Studies Uncover ABCC5 Connections to Apoptosis and Mitochondrial Pathways 146

5.1 Introduction 146

5.1.1 Protein Co-Expression and Interaction Network Analysis . 146

5.1.2 Promoter Motif Analysis 147

5.1.3 Cancer Hallmarks 147

5.1.4 Aims 148

5.2 Results 149

5.2.1 Protein Interaction Network 149

5.2.2 Transporter Proteins 154

5.2.2.1 Motif Analysis 154

5.2.2.2 Role of ABCC5 Paralogues 162

5.2.3 Cancer Pathway-Associated Proteins 164

5.2.3.1 Sustaining Proliferative Signalling and Replicative Immortality 165

5.2.3.2 Resistance to Cell Death 172

5.2.3.3 Mitochondrial Involvement via SHMT2 176

5.3 Discussion 180

5.3.1 Exploring ABCC5 Interactors and Linking Gene Promoter Motifs to Prostate Cancer 180

5.3.2 Potential Interrelationship between ABCC11 and ABCC5 in Prostate Cancer 184

5.3.3 Contradicting Results Regarding the Role of ABCC5 in Prostate Cancer Cell Proliferation and Related Proliferation Pathways 186

5.3.4 Is ABCC5 Connected to the Induction of Apoptosis via Caspase Activity? 189

5.3.5 Is SHMT2 Potentially the Link Connecting ABCC5 to Mitochondrial Involvement? 191

5.4 Summary and Limitations 194

6 Antibody Validation for the Detection of ABCC5 197

6.1 Introduction 197

6.1.1 Antibody Testing and Validation 197

6.1.2 Aims 198

6.2 Results 199

6.2.1 Screening of Commercial Antibodies 199

6.2.1.1 Immunofluorescence 199

6.2.1.2 Western Blot 206

6.2.2 Antibody Design 210

6.2.3 Screening of Antibody Serum 215

6.2.4 Screening of Customised Antibodies 218

6.2.4.1 Immunofluorescence 218

6.2.4.2 Western Blot 225

6.2.5 Custom Antibodies from the Borst Group 228

6.2.5.1 Validation of ABCC5 Antibodies through Colocalisation Analysis with ABCC5-GFP 228

6.2.5.2 Validation of ABCC5 Antibodies through ABCC5 Knockdown 229

6.3 Discussion 231

6.3.1 Challenges in ABCC5 Detection: Overcoming Antibody Limitations 231

6.3.2 Is the ABCC5$^{-/-}$ Mouse a Complete Knockout? 235

6.4 Summary and Limitations 238

7 General Discussion and Conclusion 240

7.1 Epigenomic Regulation in Prostate Cancer: Potential ABCC5-Mediated Regulatory Pathways 242

7.2 Decoding ABCC5's Role in Mitochondria: Unravelling Links to Heme Biosynthesis and Apoptotic Pathways 245

A Appendices 336

A.1 Appendix 337

A.2 Appendix 342

List of Figures

1.1 Prostate anatomy 3

1.2 Gleason's score for histological grading of PCa 5

1.3 ABC transporter structure 18

1.4 ABCC5 structure 23

1.5 Post-translational modifications ABCC5 30

1.6 ABCC5 AlphaFold structure 31

1.7 Kaplan-Meier Plot illustrating the impact of ABCC5 gene expression on PCa patient survival 38

1.8 Expression of ABCC5 mRNA based on patient's Gleason score . . 39

2.1 Histogram of number of datasets individual genes appear in 45

2.2 Meta-analysis on genes that correlate with ABCC5 from TCGA datasets 45

2.3 Protein-protein interaction analysis workflow 49

3.1 Meta-analysis of genes correlating with ABCC5 from TCGA datasets 73

3.2 Scatterplot of GO terms for molecular function correlated with ABCC5 in multiple cancers 75

3.3 Scatterplot of GO terms for biological process correlated with ABCC5 in multiple cancers 76

3.4 Scatterplot of GO terms for cellular compartment correlated with ABCC5 in multiple cancers 77

3.5 Venn diagram illustrating the distribution of cancer types according to *ABCC5* expression status in tumour and healthy tissue . . . 78

3.6 *ABCC5* Expression-Dependent Gene Clustering in Tumour and Healthy Tissue Reveals Distinct Molecular Signatures 80

3.7 Functional Pathway Analysis 82

3.8 Comparative analysis of homologous proteins to ABCC5 for functional inference 84

3.9 Sequence alignment of PCAT1 (PDB: 7T54_1) and ABCC5 . . . 86

3.10 Sequence alignment between ABCC5 (human) and CydC (*E. coli*) (PDB: essr) 90

4.1 Overview of the prostate cancer cell line characteristics used in this study 101

4.2 Functional analysis of positively correlated genes with ABCC5 in prostate adenocarcinoma using g:Profiler 106

4.3 Meta-analysis results based on all-cancer and PCa datasets 107

4.4 Top non-redundant enriched terms for positively correlated genes with *ABCC5* in prostate cancer, colour-coded by p-values 108

4.5 Enhanced visualization of metascape enrichment network showing intra-cluster and inter-cluster connections among enriched terms 109

4.6 Clustergram analysis of the top two BP GO groups 110

4.7 Clustergram analysis of the top three REACTOME pathway groups 112

4.8 Clustergram analysis of the top three CC GO groups 113

4.9 Clustergram analysis of the top MF GO group 114

4.10 Visualisation of Gene Ontology Molecular Function (GO:MF) Enrichment and Correlation Analysis 118

4.11 Validation of ABCC5 knockdown and overexpression in LNCaP and PC-3 cells 121

4.12 *ZNF75A* expression levels upon *ABCC5* KD and OE 122

4.13 *ZNF169* expression levels upon *ABCC5* KD and OE 123

4.14 *ZNF182* expression levels upon *ABCC5* KD and OE 124

4.15 *ZNF224* expression levels upon *ABCC5* KD and OE 125

4.16 *ZNF250* expression levels upon *ABCC5* KD and OE 126

4.17 *ZNF471* expression levels upon *ABCC5* KD and OE 127

4.18 *ZBTB43* expression levels upon *ABCC5* KD and OE 128

4.19 *ZXDC* expression levels upon *ABCC5* KD and OE 129

4.20 *DMTF1* expression levels upon *ABCC5* KD and OE 130

4.21 *MDM4* expression levels upon *ABCC5* KD and OE 131

4.22 *PRDM15* expression levels upon *ABCC5* KD and OE 132

4.23 *SUPT7L* expression levels upon *ABCC5* KD and OE 133

4.24 *TAF11* expression levels upon *ABCC5* KD and OE 134

4.25 *TRIM52* expression levels upon *ABCC5* KD and OE 135

5.1 ABCC5-associated protein network 151

5.2 Clustering of proteins 152

5.3 Scatterplot of GO terms for molecular function correlated with the proteins of Cluster 1 and Cluster 2 153

5.4 Binary heatmap of motif occurrence in transporter protein gene promoters 155

5.5 Motif overlap analysis 158

5.6 Heatmap of motif occurrence across promoter sequences of the transporter proteins 160

5.7 Mining consensus GO terms from promoter motif analysis 161

5.8 *ABCC11* expression levels upon ABCC5 KD and OE 163

5.9 *ABCC12* expression levels upon ABCC5 KD and OE 164

5.10 *NRF1* expression levels upon ABCC5 KD and OE 165

5.11 *PARP1* expression levels upon ABCC5 KD and OE 166

5.12 *PTK2* expression levels upon ABCC5 KD and OE 167

5.13 *ESR1* expression levels upon ABCC5 KD and OE 168

5.14 Impact of ABCC5 on colony formation in LNCaP cells 169

5.15 Impact of ABCC5 on colony formation in PC-3 cells 170

5.16 Impact of ABCC5 on LNCaP cell migration 171

5.17 Impact of ABCC5 on PC-3 cell migration 172

5.18 *CASP6* expression levels upon ABCC5 KD and OE 173

5.19 *CASP7* expression levels upon ABCC5 KD and OE 174

5.20 *CASP8* expression levels upon ABCC5 KD and OE 175

5.21 Caspase activity levels upon *ABCC5* KD and OE 176

5.22 *SHMT2* expression levels upon ABCC5 KD and OE 177

5.23 Relationship between SHMT2 expression and prostate cancer stage 178

6.1 Relative expression of ABCC5 in wt mouse prostate compared to negative control 200

6.2 Staining of wild-type (WT) mouse prostate tissue with commercial anti-ABCC5 antibodies 202

6.3 Optimisation of secondary antibody background staining with Visublock reagent 202

6.4 Staining of WT mouse prostate tissue with commercial anti-ABCC5 antibodies 204

6.5 Staining of PC-3 cells with commercial anti-ABCC5 antibodies . 206

6.6 Anti-ABCC5 antibody testing - Western Blots 209

6.7 Antibody design 211

6.8 Structural alignment of ABCC5, ABCC11, and ABCC12 212

6.9 Relative expression of ABCC11 and ABCC12 213

6.10 Alignment of the antibody target sequences of human ABCC5 with ABCC11 and ABCC12 214

6.11 Screening of anti-ABCC5 serum 217

6.12 Colocalisation staining with ABCC5-GFP overexpressing PC-3 cells and anti-ABCC5 antibodies 219

6.13 Detection of ABCC5 KD mediated by siRNA with immunofluorescence 221

6.14 Detection of ABCC5 KD mediated by siRNA with immunofluorescence 222

6.15 Staining of LNCaP, PC-3, HEK, and GLUTag cells with ab89 . . . 223

6.16 Staining of LNCaP, PC-3, HEK, and GLUTag cells with ab90 . . . 224

6.17 ABCC5 staining of WT and ABCC5 KO mouse prostate tissue with ab89 and ab90 225

6.18 Western blot analysis for ABCC5 antibody specificity in LNCaP and PC-3 cells 227

6.19 Colocalisation staining with overexpressed ABCC5-GFP in PC-3 cells and anti-ABCC5 antibodies 229

6.20 Detection of ABCC5 KD mediated by siRNA with immunofluorescence 230

6.21 Schematic overview of ABCC5 and the respective antibody binding sites 232

6.22 Genomic overview of Abcc5$^{-/-}$ CRISPR/Cas9 KO design and mouse ABCC5 isoforms 236

A.1 Multiple Sequence Alignment of Proteins identified in DALI analysis with ABCC5 (015440). 338

A.2 Structural alignment of ABCC5 and CydC (PDB: essr) from the DALI server alignment. The letters describe different structural elements: H: helix, E: strand, L: coil 341

A.3 Staining of wild-type mouse prostate tissue with commercial anti-TH antibody compared to the primary control 342

A.4 Staining of PC-3 cells with commercial anti-ABCC5 antibodies . 344

A.5 Prediction of ABCC5 all-helical membrane protein by MEMSAT-SVM and MEMSAT3 servers 346

List of Tables

1.1 ISUP PCa grade groups 6

1.2 Tumour Node Metastasis classification of PCa 6

1.3 Staging of PCa based on tumour node metastasis classification . . 8

2.1 Databases used for PPI Network 48

2.2 Plasmids 52

2.3 Human Primers. 53

2.4 List of Primary Antibodies used for Western Blotting. 58

2.5 List of Secondary Antibodies used for Western Blotting. 60

2.6 Overview of the Characteristics of the PCa Cell Lines used in this Study 62

2.7 siRNA Sequences 63

2.8 Solutions and Buffers. 67

3.1 Homology modelling hits of ABCC5 against human and *E. coli* AlphaFold structural database 88

5.1 Enriched motifs in promoter sequences of submitted proteins. (P-value * <0.05, E-value * <0.05, Q-value * <0.05) 156

6.1 Commercial antibody characteristics (ms=mouse, hu=human). . . 199

A.1 Homology modelling of ABCC11 and ABCC12 against human and *E. coli* AlphaFold structural database. 339

Abbreviations

ABC ATP-binding cassette

ACC Adrenocortical carcinoma

ADT androgen deprivation therapy

AML acute myeloid leukemia

AR androgen receptor

AS Active surveillance

BCR biochemical recurrence

BLCA Bladder urothelial carcinoma

BP biological process

BPS Blocking and Permeabilisation solution

BRCA breast invasive carcinoma

CASP caspase

CC cellular compartment

CESC cervical squamous cell carcinoma

CHOL cholangiocarcinoma

COAD Colon adenocarcinoma

CRPCa Non-metastatic castration-resistant PCa

DALI Distance-matrix Alignment for Structural Homology

DLBC lymphoid neoplasm diffuse large B-cell lymphoma

DMTF1 cyclin D binding myb-like transcription factor 1

DRE digital rectal examination

EBRT external beam radiotherapy

ESCA oesophageal carcinoma

ESR1 estrogen receptor 1

FAK focal adhesion kinase

GBM glioblastoma multiforme

GnRH gonadotropin-releasing hormone

GO Gene Ontology

GSH glutathione

HDAC histone deacetylase

HNSC head and neck squamous cell carcinoma

IF immunofluorescence

IHC immunohistochemistry

KD knockdown

KICH kidney chromophobe

KIRC kidney renal clear cell carcinoma

KIRP kidney renal papillary cell carcinoma

KLF Krüppel-like factor

KO knockout

LGG brain lower grade glioma

LH luteinising hormone

LHRH luteinising hormone-releasing hormone

LIHC liver hepatocellular carcinoma

lncRNA long non-coding RNA

LUAD lung adenocarcinoma

LUSC lung squamous cell carcinoma

MAMs mitochondrial-associated membranes

mCRPCa castration-resistant metastatic PCa

mCSPCa metastatic hormone-sensitive PCa

MDM4 mouse double minute 4

MDR multidrug resistance

MEMSAT-SVM transmembrane protein topology predictor support vector machines

MESO mesothelioma

MF molecular function

MSD membrane-spanning domain

NBD1 nucleotide-binding domain 1

NBDs nucleotide-binding domains

NCI National Cancer Institute

NHGRI National Human Genome Research Institute

NRF1 nuclear respiratory factor 1

OE overexpression

OV ovarian serous cystadenocarcinoma

PAAD pancreatic adenocarcinoma

PARP1 poly(ADP-ribose) polymerase 1

PBS phosphate-buffered saline

PCA principal component analysis

PCa prostate cancer

PCAT1 peptidase containing ATP-binding cassette

PCPG pheochromocytoma and paraganglioma

PDB Protein Data Bank

PFA paraformaldehyde

PPI Protein-Protein Interaction

PPIs protein-protein interaction networks

PRAD prostate adenocarcinoma

PRDM PRDI-BF1 and RIZ homology domain-containing

PSA prostate-specific antigen

PSIPRED PSI blast-based secondary structure prediction

PTC premature stop codons

PTK2 protein tyrosine kinase 2

RARP robotic-assisted RP

RBP RNA-binding protein

READ rectum adenocarcinoma

RP radical prostatectomy

RT Radiotherapy

SARC sarcoma

SD standard deviation

SENP Sentrin/SUMO-specific proteases

SHMT2 serine hydroxymethyltransferase 2

SKCM skin cutaneous melanoma

SLC solute carrier

SP Specificity Protein

SUMO Small Ubiquitin-like Modifier

SURs sulfonylurea receptors

TCGA The Cancer Genome Atlas

TF Transcription factors

TGCT testis germ cell tumours

THCA thyroid carcinoma

THF tetrahydrofolate

THYM thymoma

TMDs transmembrane domains

UBC ubiquitin C

UCS uterine carcinosarcoma

UVM uveal melanoma

WT wild-type

ZXDC Zinc finger, X-linked, duplicated family member C

1 | Introduction

1.1 Prostate Cancer

1.1.1 Incidence and Mortality

Prostate cancer (PCa) is the second most diagnosed cancer in men globally and the fifth leading cause of cancer death in men (1). In the UK, PCa is the most frequently diagnosed cancer in men, with around 52,300 new cases reported each year. It also ranks as the second highest cause of cancer-related deaths among males, accounting for 14% of all male cancer fatalities (2). Incidence rates of PCa show significant geographical variation, with the highest occurrences reported in Northern Europe, Western Europe, the Caribbean, Australia/New Zealand, and North America. Conversely, the lowest rates are found in Central and Eastern Asia, as well as Northern Africa. Similarly, mortality rates vary across regions and populations, with Central and Southern Africa, as well as the Caribbean, recording the highest rates, while Asia generally reports lower mortality rates (3; 1).

Autopsy studies revealed that incidental detection of PCa occurred across all populations, with prevalence escalating in tandem with age - a well-established risk factor for the disease. This underscores the inherent risk of overdiagnosis associated with PCa screening protocols that detect PCa that would stay indolent across the patient's lifetime (4). Nevertheless, PCa mortality has declined significantly in many developed countries due to the widespread use of prostate-specific antigen (PSA) screening and improvements in treatment options. However, mortality rates remain high in some low- and middle-income countries with limited access to screening and treatment (5; 6).

Despite the age risk factor, several other risk factors have been identified, includ-

ing family history, race/ethnicity, and certain lifestyle factors (7). Men with a familial history of breast or PCa face heightened risks of developing PCa. The risk is notably elevated if PCa has been diagnosed in a first-degree relative (8; 9). Interestingly, among individuals diagnosed with localised PCa, having a familial history of the disease does not increase the risk of biochemical recurrence or cancer-specific mortality (10). Research consistently shows that race/ethnicity plays a significant role in PCa risk, with black men facing a 60% higher risk for developing PCa compared to white men (11). While genetic aetiology may contribute to this increased risk, the precise causes and biological differences across racial groups remain uncertain and migration-associated gene-environment interactions could also further contribute to increased risk (12; 11).

Numerous lifestyle factors have been extensively debated regarding their relationship to PCa. More recently, case-control studies have shown that tobacco smoking is associated with an increased risk of PCa and can also be associated with advanced stage and worse prognosis (13; 14; 15). Furthermore, research also emphasises the negative impact of obesity on PCa outcomes, as it is associated with higher mortality rates attributed to an increased risk of advanced PCa (16; 17). Interestingly, some studies have suggested a potential role of alcohol consumption in PCa, although this remains a topic of considerable debate (18; 19).

1.1.2 Clinical Diagnosis

1.1.2.1 Prostate Anatomy

The prostate gland, an integral male reproductive system organ, exhibits a complex anatomical structure comprising distinct lobes and zones, each responsible for specialised functions critical to its overall physiological role. Anatomically, the prostate consists of three main lobes: the anterior, posterior, and lateral lobes,

which encase the urethra and seminal vesicles (20). Functionally, the prostate is divided into zones based on histological and clinical characteristics, namely the peripheral zone, transition zone, and central zone as seen in **Figure 1.1** (21). The peripheral zone constitutes the largest portion, enveloping the distal urethra and accounting for approximately 70% of the glandular volume (22). Notably, it is the primary site where PCa commonly arises, underscoring its clinical significance (23).

The healthy gland is made up of ducts and acini embedded in supportive stromal tissue. The ducts and acini are encased by basal epithelial cells that produce the basement membrane and lined with a single layer of epithelial cells. The stroma also contains fibroblasts that primarily support the ducts in the adult prostate (24). The epithelial cells in prostate tissue express high levels of the androgen receptor (AR), which drives hormone dependency in prostate cancer. Additionally, these cells secrete prostate-specific antigen (PSA), a serine protease activated by the AR (25). Elevated PSA levels are often seen in men with prostate cancer and are used for disease detection and diagnosis (26; 27).

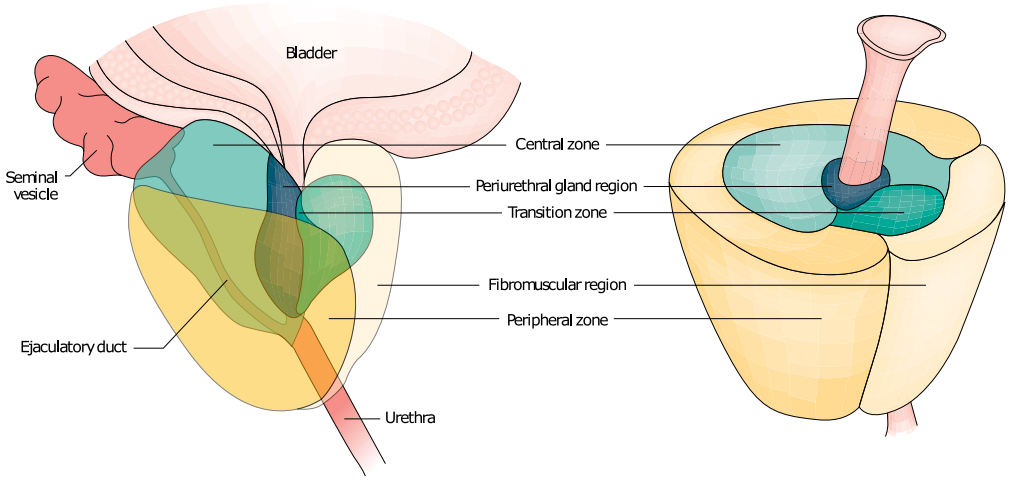

Figure 1.1: The prostate can be divided into five anatomical regions: the central zone, the periurethral region, the transition zone, the peripheral zone and the fibromuscular region. Adjusted from (28).

1.1.2.2 Screening and Diagnosis

Screening for PCa typically involves the utilisation of various techniques aimed at identifying potential abnormalities within the prostate gland. Among these techniques, the PSA blood test and digital rectal examination (DRE) stand out as the primary modalities for initial assessment (29; 30; 31). The PSA test evaluates the levels of PSA, a protein mainly produced by the prostate gland, in the bloodstream. Elevated PSA levels can serve as an indication of possible abnormalities within the prostate, such as cancer (26; 27). However, the reliability of PSA testing remains contentious due to its lack of specificity and sensitivity (32). PSA levels can be affected by various factors besides cancer, including genetic predisposition, prostatitis, and benign prostatic hyperplasia (33; 34). Moreover, meta-analyses have indicated that screening does not significantly impact overall mortality over 10 years (35). While DRE can provide valuable insights, particularly in cases where PSA results are inconclusive, its reliability for detecting early-stage PCa is still being debated (36; 37). Additionally, the discomfort associated with DRE discourages up to 22% of individuals from undergoing screening, highlighting concerns about the methods employed for screening (38; 39). Following initial screening, a definitive diagnosis of PCa relies on histological verification obtained through prostate tissue biopsy (40). While biopsy remains the gold standard for diagnosis, advancements in imaging modalities have enhanced the procedure, leading to approaches such as transrectal ultrasound-guided biopsies (41; 42). Recent clinical research suggests the use of magnetic resonance imaging due to its non-invasive nature for detecting concerning lesions (43).

1.1.2.3 Tumour Grading and Staging

Originating from the epithelial cells lining the prostatic acini and glandular ducts, adenocarcinomas represent approximately 95% of all prostate malignancies (44).

The histological grading of prostate tumours plays a crucial role in determining clinical behaviour and treatment response. The Gleason grading system, introduced in 1974, revolutionised the histological assessment of PCa by providing a standardised method for grading tumour aggressiveness (45; 46). The Gleason grading system evaluates two primary tumour patterns found in biopsy samples; each assigned a score from 1 to 5. These scores are combined to calculate the Gleason score, ranging from 2 to 10. Lower Gleason scores suggest tumours with better differentiation and less aggression, whereas higher scores indicate tumours with poorer differentiation and greater aggression as seen in **Figure 1.2** (47; 48; 49).

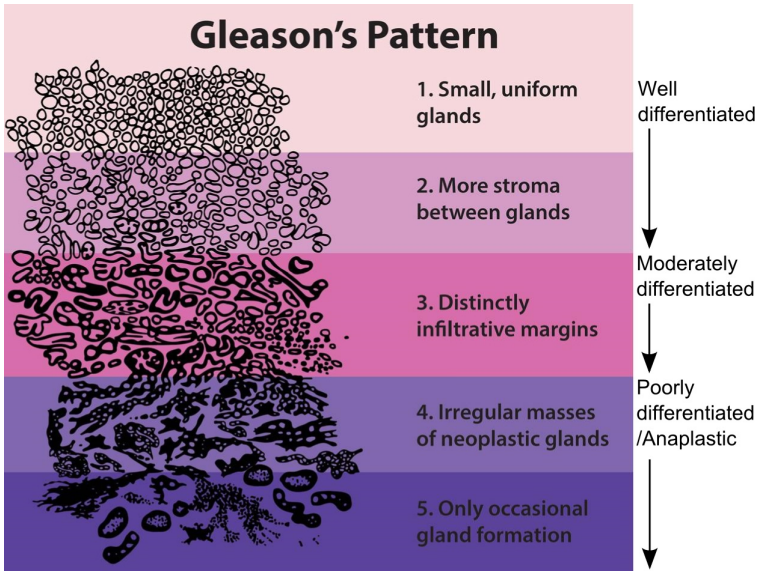

Figure 1.2: Gleason's score for histological grading of PCa (44).

The Gleason grading system can be extended to the 6th digit International Classification of Diseases for Oncology (ICD-O) grade or differentiation code with the assistance of the following **Table 1.1**.

Table 1.1: International Society of Urological Pathology (ISUP) PCa grade groups (50)

Grade group	Gleason score	Gleason pattern
1	$\leq$6	$\leq$3+3
2	7	3+4
3	7	4+3
4	8	4+4, 3+5, 5+3
5	9 or 10	4+5, 5+4, 5+5

Numerous studies have demonstrated the prognostic significance of the Gleason score in predicting disease progression and patient outcomes (51; 52). While the Gleason grading system provides insights into tumour aggressiveness, staging plays a crucial role in understanding disease progression and guiding treatment decisions. The Tumour, Node, Metastasis (TNM) system, developed by the Union for International Cancer Control, categorises tumours based on the size of the primary tumour (T), involvement of regional lymph nodes (N), and presence of distant metastasis (M). The TNM classification assigns stages I through IV to PCa, indicating disease progression from least advanced (stage I, confined to the prostate gland) to most advanced (stage IV, involving distant metastasis) as seen in **Table 1.2** (53; 54). PCa is typically classified into four stages as seen in **Table 1.3**.

Table 1.2: Tumour Node Metastasis classification of PCa (54)

Primary Tumour (T)	
Tx	Primary tumour cannot be assessed
T0	No evidence of primary tumour

T1	Clinically inapparent tumour not palpable or visible by imaging
T1a	Tumour incidental histologic finding in $\leq$5% of tissue resected
T1b	Tumour incidental histologic finding in $\geq$5% of tissue resected
T1c	Tumour identified by needle biopsy (e.g. of elevated PSA level)
T2	Tumour confined within prostate
T2a	Tumour involves one-half of 1 lobe or less
T2b	Tumour involves more than one-half of 1 lobe but not both lobes
T2c	Tumour involves both lobes
T3	Tumour extends through the prostatic capsule
T3a	Extracapsular extension (unilateral or bilateral)
T3b	Tumour invading seminal vesicle(s)
T4	Tumour fixed or invades adjacent structures other than seminal vesicles
Regional Lymph Nodes (N)	
NX	Regional lymph nodes were not assessed
N0	No regional lymph node metastasis
N1	Metastasis in regional lymph node(s)
Distant Metastasis (M)	
M0	No distant metastasis
M1	Distant metastasis
M1a	Nonregional lymph nodes(s)

M1b	Bone(s)
M1c	Other site(s)

Table 1.3: Staging of PCa based on tumour node metastasis classification (54)

Stage			
Stage I	T1, T2a	N0	M0
Stage II	T2b, T2c	N0	M0
Stage III	T3, T4	N0	M0
Stage IV	Any T	N1	M1
	Any T	Any N	M1

1.2 Management

Management of PCa depends on several factors, including the stage of the disease, the patient's age and overall health status, and the presence of other medical conditions. The management of PCa can be broadly classified into four categories: active surveillance, surgery, radiation therapy, and systemic therapy. The choice of treatment depends on the stage and grade of the cancer, as well as the patient's overall health status and preferences (55; 28; 56).

1.2.1 Active Surveillance

Active surveillance (AS) represents a strategic approach in managing PCa by closely monitoring patients diagnosed with low-grade, early-stage disease, who are deemed at low risk of disease progression. This strategy aims to defer surgical or therapeutic interventions until symptoms manifest or disease progression oc-

curs, thus minimising potential treatment-related morbidities (57). AS protocols entail regular monitoring through PSA tests, DREs, and prostate biopsies, facilitating the detection of any evidence of tumour growth or metastasis (58). The criteria for AS selection include parameters such as clinical stage T1c, PSA density <0.15 ng/ml, Gleason score $\leq$6 (ISUP grade $\leq$1), <3 positive prostate biopsy cores, and <50% cancer per core (59). These criteria aim to identify patients with clinically insignificant PCa who are suitable candidates for AS, thereby avoiding unnecessary overtreatment of indolent tumours. Studies have reported favourable outcomes for patients managed through AS, demonstrating a low rate of progression to metastatic disease or death from PCa (60; 61). The Hopkins cohort study further confirms the success of AS, demonstrating exceedingly low rates of metastasis and PCa mortality among eligible patients. Specifically, after 15 years of follow-up, the study reported only a 0.4% risk of metastasis and an even lower 0.1% risk of PCa mortality (62). Studies also confirmed that patients with AS reported similar levels of anxiety or depressive symptoms to patients who received treatment (63).

1.2.2 Watchful Waiting

Watchful waiting, in contrast to AS, offers a distinct approach to managing PCa, particularly suited for patients unsuitable for delayed treatment, with limited life expectancy, or a preference for deferring immediate intervention (64; 65). Unlike AS, which involves close monitoring with potential for curative treatment, watchful waiting primarily addresses symptomatic management rather than seeking a cure. This strategy is tailored for patients deemed unfit for radical treatments or when treatment-related harms outweigh benefits (66; 67).

1.2.3 Surgery

Surgery is a common approach for treating localised PCa, with radical prostatectomy (RP) being the most prevalent method. This surgical intervention entails removing the entire prostate gland, along with the seminal vesicles and nearby lymph nodes. It can be executed through traditional open surgery or less invasive approaches such as laparoscopic or robotic-assisted RP (RARP) (68). RARP has emerged as a preferred option due to its advantageous features, such as decreased blood loss, shorter hospitalisation periods, and enhanced functional results in contrast to conventional laparoscopic techniques (69). Although RARP shows promising outcomes, long-term assessments are still needed, and concerns persist regarding the higher costs associated with robotic surgery compared to laparoscopic techniques (70). Despite its effectiveness, radical prostatectomy is not without its drawbacks. Reported side effects include erectile dysfunction, infertility, and urinary incontinence, which can significantly impact the quality of life for patients post-surgery (71; 72; 73). Furthermore, a considerable proportion of about 20-40% of patients experience biochemical recurrence (BCR) following RP (74; 75). BCR is defined as an initial rise in PSA levels above 0.2 ng/mL, followed by a confirmatory increase on subsequent tests (76). This recurrence necessitates long-term follow-up evaluations, typically spanning at least 10 years, to enable early intervention in case of cancer recurrence (77).

1.2.4 Radiotherapy

Radiotherapy (RT), including external beam radiotherapy (EBRT) and brachytherapy, is a crucial treatment modality for localised PCas, utilising high-energy radiation to target and destroy cancerous cells while preserving surrounding healthy tissues (78; 79). Interestingly, recent research also suggests use in newly diag-

nosed low-burden metastatic PCa as it improves overall survival (80). EBRT involves delivering radiation externally to the pelvic region, typically over multiple sessions (81). This technique utilises conformal, intensity-modulated, or volumetric-modulated RT to precisely target the tumour while minimising exposure to adjacent tissues (82; 83; 84). On the other hand, brachytherapy entails internal radiation delivery via implanted radioactive seeds, such as Iodine-125, Palladium-103, or Caesium-131 (85; 86).

Brachytherapy provides targeted radiation delivery to the tumour, offering enhanced precision and the advantage of high radiation doses directly to the affected area. However, its use is restricted in cases of severe urinary obstruction, rectal abnormalities and a large prostate (87; 88). While RT can effectively target cancer cells, it may also lead to side effects including erectile dysfunction, rectal bleeding, diarrhoea, radiation proctitis, radiation cystitis, fatigue and lymphedema (89; 90; 91).

1.2.5 Systemic Therapy

Systemic therapy encompasses the administration of drugs or other agents distributed throughout the body to eradicate cancer cells. This approach may involve chemotherapy, hormone therapy, immunotherapy, or targeted therapy. Systemic therapy is typically used in patients with advanced or metastatic PCa (92).

1.2.5.1 Hormonal Therapy

Hormonal therapy, also known as androgen deprivation therapy (ADT), is based on the hormone-sensitive nature of PCa, which thrives on the presence of testosterone, a key androgenic steroid hormone (93; 94). By diminishing circulating testosterone levels, hormonal therapy aims to impede the fuelling of PCa cell proliferation. This reduction in testosterone can be achieved through surgical in-

tervention by removing the testes bilaterally, also called bilateral orchidectomy, which used to be the gold standard (95). This method is cost-effective and results in lower levels of testosterone (96). However, the psychological impact on patients is tremendous, and therefore, intervention using medication is preferred by patients (97). Medication on the other hand can either directly stop testosterone production or obstruct its interaction with cancerous cells.

The first category encompasses agents such as luteinising hormone-releasing hormone (LHRH) agonists and gonadotropin-releasing hormone (GnRH) antagonists. LHRH agonists initially provoke a surge in luteinising hormone (LH) release, but with sustained use, they suppress LH production, thereby leading to a decline in testosterone levels (98; 94). GnRH antagonists, on the other hand, directly inhibit the secretion of both GnRH and LH, resulting in a similar reduction in testosterone levels without the initial surge seen with LHRH agonists (99; 100).

The second category of hormonal therapy involves hindering testosterone from binding to cancer cells. This is achieved through androgen receptor blockers and ADT. ADT induces a significant reduction in systemic androgens while also preventing androgen receptor activation, positioning it as a pivotal treatment modality for metastatic PCa (101; 102). Despite its efficacy, hormonal therapy is associated with notable side effects. These encompass a spectrum of complications ranging from cardiovascular and metabolic aberrations to diminished bone density and cognitive disturbances that significantly increase the risk of dementia. Hence, while hormonal therapy remains integral to PCa management, its administration necessitates vigilant monitoring and mitigation of potential adverse effects (103; 104; 105). Patients usually transition from metastatic hormone-sensitive PCa to castration-resistant metastatic PCa (mCRPCa) characterised by the acquisition of resistance to hormonal therapy (106).

1.2.5.2 Chemotherapy

Chemotherapy targets rapidly dividing cells, aiming to inhibit the proliferation of dividing cancer cells (107). Cytotoxic drugs can be administered either as neoadjuvant or adjuvant therapy. Neoadjuvant chemotherapy precedes surgery or radiotherapy to mitigate micro-metastases, potentially shrink the primary tumour, and prevent treatment failure (108; 109). Adjuvant chemotherapy, on the other hand, is administered post-surgery or radiotherapy to eradicate micro-metastases (110; 111). Taxane-based chemotherapy, such as docetaxel and cabazitaxel, has been pivotal in extending overall survival in men with mCRPCa. The approval of docetaxel by the United States FDA in 2004, based on studies demonstrating its efficacy in mCRPCa, marked a significant advancement (112). Subsequently, cabazitaxel gained FDA approval in 2010 for PCa treatment (113).

1.2.5.3 Immunotherapy

Immunotherapy represents a therapeutic avenue in PCa treatment, harnessing the body's immune system to combat tumours (114). Notably, vaccine-based therapies and immune checkpoint inhibitors have emerged as novel therapeutics in immunotherapy. Sipuleucel-T, the first FDA-approved immunotherapy for cancer, exemplifies vaccine-centred therapy by utilising the patient's antigen-presenting cells to induce a cytotoxic T-cell response against prostatic-acid-phosphatase, a specific-antigen found in PCa cells (112; 115). Pembrolizumab, a monoclonal antibody targeting programmed cell death protein 1, stands as the sole immune checkpoint inhibitor with FDA approval for PCa treatment (116). Other classes of immunotherapy, including CAR-T cell therapy, bispecific antibodies, and small molecule kinase inhibitors, are being explored. However, many studies have failed to meet their primary endpoints, including new immune checkpoint inhibitors and vaccines (117; 118; 119; 120).

Despite the diversity of immunotherapy modalities, their efficacy in PCa remains limited due to the tumour's "cold" immune environment. Successful antitumor immune responses in PCa require the generation of tumour-reactive T-cells, physical interaction between target and effector cells, and a supportive microenvironment conducive to immune effector functions. However, PCa often lacks distinct characteristics necessary for a robust immune response, presenting challenges in establishing effective immunotherapy strategies for this cancer type (121; 122). In conclusion, the management of PCa is complex and depends on several factors, including the stage and grade of the cancer, the patient's age and overall health status, and the presence of other medical conditions.

1.3 Prognosis

The prognosis of PCa varies significantly across different stages of the disease, highlighting the importance of early detection and tailored treatment approaches. For localised disease, where the cancer is confined to the prostate gland, the prognosis is generally favourable. Approximately 80% of men are diagnosed at this stage, and their ten-year survival rate can reach as high as 99% (2; 123). This encouraging outlook is largely attributed to advancements in screening methods such as PSA testing, which allows for the detection of tumours at an earlier, more manageable stage. Consequently, many of these tumours progress slowly and can be effectively treated (124). In cases of local aggressive disease, where the cancer has spread beyond the prostate but remains within the nearby region, the prognosis becomes less favourable. Around 15% of men are diagnosed with this stage of the disease. Although treatment options exist, the likelihood of disease progression and recurrence increases, impacting overall survival rates (2; 123). The most concerning prognosis is associated with metastatic disease, where the cancer has

spread to distant parts of the body. Approximately 5% of men are diagnosed at this advanced stage, and their five-year survival rate drops significantly to only 34% (125; 126). Metastatic PCa presents considerable challenges in treatment and management, often requiring aggressive interventions to prolong survival and maintain quality of life.

1.4 Advanced Prostate Cancer

Advanced PCa encompasses various stages characterised by disease progression beyond localised forms. Non-metastatic castration-resistant PCa (CRPCa) has become resistant to hormone therapy despite the absence of detectable metastases on routine imaging (127). While metastatic hormone-sensitive PCa (mCSPCa) has spread beyond the prostate gland and is responsive to hormone therapy. Initially, ADT is the standard treatment, aiming to suppress testosterone levels and inhibit androgen receptor (AR) signalling, thus impeding cancer growth. However, despite treatment, metastatic lesions can develop in lymph nodes, bones, liver, and lungs (128; 93; 129). The progression to mCRPCa underscores the pivotal role of AR signalling in PCa progression.

Androgens, primarily testosterone and dihydrotestosterone, bind to the AR, which is a transcription factor, and activate its downstream signalling pathway, leading to the regulation of various genes that control cell growth, proliferation, differentiation, and survival. Androgen signalling is essential for normal prostate development and function, but it also contributes to the development and progression of PCa (130; 131; 132). Mechanisms contributing to castration resistance include alterations in the AR pathway, such as AR gene amplification (133; 134), mutations (135; 136), splice variants (137; 138), and changes in AR co-regulators (139; 140). Metastasis in PCa commonly occurs in lymph nodes adjacent to the

primary tumour, followed by metastases to distant sites such as the liver, lungs, and bones (141; 3). Interestingly, the development of bone metastases happens several years after the removal of the primary tumour (142). Bone metastases typically manifest as lesions with combined osteoblastic and osteolytic features. This results in complications encompassing pain, fractures, nerve compression and hypercalcemia. Current treatment approaches primarily focus on symptom management rather than curative measures (143; 144).

1.5 ABC Transporters

The ATP-binding cassette (ABC) transporter family is one of the largest and most diverse families of membrane proteins found in both prokaryotic and eukaryotic organisms (145). The first ABC transporters were initially identified in the 1970s during investigations into bacterial nutrient uptake (146). Utilising ATP binding and hydrolysis, these transporters enable the movement of a diverse range of substances across membranes (147). In prokaryotes, these transporters play a crucial role in fundamental survival processes, including the uptake of nutrients and the expulsion of toxic compounds (148). In eukaryotes, the transport function encompasses a wide array of substrates, ranging from ions and lipids to peptides and xenobiotics (149). In the human genome alone, 48 ABC transporter genes exist, categorised into seven subfamilies by their sequence homology and functional characteristics. These seven subfamilies are represented across the majority of eukaryotic genomes and are therefore of ancient origin (150). Spanning from ABC-A to ABC-G, the subfamilies of human ABC transporters exhibit structural and functional variations. Each subfamily is defined by unique substrate specificities and cellular functions (151; 152)).

ABC transporters exhibit a modular architecture that consists of transmembrane domains (TMDs) and nucleotide-binding domains (NBDs). The standard functional unit is characterised by two TMDs connected to two cytoplasmic NBDs (153). Embedded within the lipid bilayer, the TMDs form the pathway for substrate translocation. These TMDs have lower sequence conservation which facilitates functional specification within transporter subfamilies (154). In contrast, NBDs exhibit high conservation irrespective of species, substrate specificity, or transport direction (155). NBDs play a pivotal role in facilitating ATP binding and hydrolysis.

Structurally, NBDs are comprised of the RecA and helical subdomains (156). The RecA subdomain features essential conserved motifs, the Walker A and Walker B motifs. The Walker A motif is key for ATP binding and is characterised by the sequence (GXXGXGK(T/S)T, X = any amino acid residue). In contrast, the Walker B motif is crucial for coordinating Mg2+ ions during ATP hydrolysis, typically displaying the motif (hhhhDE, h = hydrophobic residue) (156; 157). Additionally, the RecA domain includes other conserved loops, namely the A-loop, Q-loop, D-loop, and H-loop (158; 159; 160). The helical subdomain, on the other hand, contains the ABC signature motif, also known as the C-loop, which plays a crucial role in coordinating ATP hydrolysis (161). To be functional, the NBDs in ABC transporters dimerise in a head-to-tail arrangement, a process facilitated by ATP binding within the dimer interface as seen in **Figure 1.3** (162).

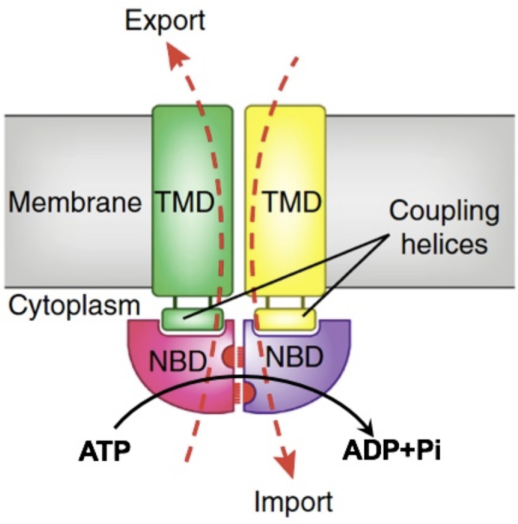

Figure 1.3: ABC transporter structure. Organisation of ABC transporter domains including TMDs, NBDs and coupling helices. Coupling helices convey conformational changes between the NBDs and TMDs. The NBD interface highlights the P loops (red circles) and ABC signature motifs (dashed lines) in the head-to-tail arrangement. Image from (163).

In addition to the specified TMDs and NBDs, ABC transporters often feature additional domains either at the N- or C-terminus or inserted between the TMD and NBD domains. A few examples include the cystic fibrosis transmembrane conductance regulator, an ion channel featuring a distinctive unstructured regulatory domain that facilitates channel opening (164). A significant porphyrin-binding domain is found in the large extracellular loop of ABCG2 (165). While the sulfonylurea receptors (SURs) ABCC8/SUR1 and ABCC9/SUR2 form a functional complex with either KIR6.1 or KIR6.2 to assemble the final transporter (166).

Human ABC transporters exhibit diverse domain compositions and the structural arrangement of these transporters distinguishes between full transporters and half transporters. A full transporter manifests as either NBD-TMD-NBD-TMD or TMD-NBD-TMD-NBD, while a half transporter is characterised by a single TMD and a single NBD (150; 145). The two symmetric halves of ABC transporters can be expressed either as separate subunits, which function as homodimers or heterodimers upon assembly or as monomers containing two nonidentical halves within a single polypeptide. Each half of the transporter consists of at least an NBD and a TMD (167). Notably, some transporters are encoded with only a single TMD or NBD, constituting a single domain structure. Non-transporter ABC proteins, only contain NBDs at both the N- and C-termini (150).

In the context of eukaryotic ABC transporters, only subfamilies A-D and G possess transmembrane domains and actively function as transporters (150; 152). Within subfamilies A and B, dimers can form through either two TMD-NBD half transporters or the presentation as full transporters within a single polypeptide chain (168; 169). In contrast, subfamily C exclusively encodes full transporters, housing all four domains on a single polypeptide chain (170). Subfamily D primarily comprises dimerised half transporters, with exceptions observed in specific land plants (171). Remarkably, subfamily G introduces a unique arrangement

by swapping the positions of TMDs and NBDs and predominantly exists as half transporters within the human system (165; 172). Deviating from the conventional transporter structure, ABCE and ABCF proteins solely consist of NBDs, leaving them as soluble proteins (173; 174).

The physiological significance of eukaryotic ABC transporters is underscored by their association with various human diseases. Mutations in some ABC transporters have been associated with several human genetic diseases and immune deficiencies. Examples include ABCA1 (Tangier disease and familial HDL deficiency) (175), ABCA3 (surfactant deficiency) (176), ABCA4 (Stargardt disease and age-related macular degeneration) (177), ABCB2 and ABCB3 (immune deficiency) (178), ABCC2 (Dubin-Johnson syndrome) (179), ABCC7 (cystic fibrosis) (180) and ABCG5 and ABCG8 (sitosterolemia) (181).

Beyond the association with Mendelian disorders, ABC transporters are also involved in the pathophysiology of various other diseases. They play a significant role in multidrug resistance (MDR) in cancer through the facilitation of chemotherapeutic agent export (182). P-glycoprotein (P-gp) and breast cancer resistance protein (BCRP/ABCG2) emerge as pivotal drug transporters associated with treatment resistance across a spectrum of cancers (183; 184). Persistent exposure to chemotherapeutic agents has been correlated with the upregulation of ABC transporters, intensifying the risk of MDR. Beyond P-gp and BCRP, the ABCC subfamily, notably ABCC1 (MRP1) (185) and ABCC2 (MRP2) (186), contribute substantially to MDR. Despite substantial progress, the intricate molecular regulatory mechanisms governing ABC-transporter-mediated MDR in cancer remain elusive, posing challenges in translating promising preclinical insights into successful clinical applications (187).

1.5.1 ABCC Family

The exploration and delineation of drug and conjugate efflux pumps belonging to the MRP/ABCC subfamily began with the research on MRP1 (ABCC1) (185). Following, its characterisation as an ATP-dependent unidirectional efflux pump for anionic conjugates (188; 189), the term "multidrug resistance protein" was coined. This nomenclature emerged from observations indicating that the overexpression of ABCC transporters led to heightened resistance against various categories of drugs (185). The ABCC subfamily comprises a total of 12 transporters, denoted as ABCC1 to ABCC13, which exhibit a significant degree of sequence and structural similarity. These transporters are systematically grouped into three categories: the multidrug resistance protein subgroup, encompassing nine members; the sulfonylurea receptor subgroup, consisting of two members; and CFTR/ ABCC7 (190; 166; 150). Within the multidrug resistance protein subgroup, further classification in long and short MRPs is possible.

The long MRPs are characterised as transporter proteins possessing an extra NH2-proximal membrane-spanning domain (MSD) in addition to their set of membrane-spanning domains (MSD1 and MSD2). Members of this category include ABCC1/ MRP1, ABCC2/ MRP2, ABCC3/ MRP3, ABCC6/ MRP6, and ABCC10/ MRP7 (191). On the contrary, the short MRPs are characterised by having two membrane-spanning domains (MSD1 and MSD2) which include ABCC4/ MRP4, ABCC5/ MRP5, ABCC11/ MRP8, and ABCC12/ MRP9 (190; 192). The short MRPs preserve the linker region located NH2-proximal to MSD2, similar to the long MRPs, but there is diversity in the length of this linker among the various transport proteins (193). As an illustration, in MRP4, the anticipated length of the linker is around 75 amino acids, and the NH2-terminus of this transporter aligns closely with CFTR (194). Conversely, the linker in MRP5 is longer, spanning approxi-

mately 170 amino acids (195). The functional implications of these differences are currently unknown.

1.6 ABCC5

ABCC5 is a transmembrane protein characterised by the conventional architecture of two transmembrane domains, each consisting of six membrane-spanning helices and two intracellular nucleotide-binding domains (NBD1 and NBD2) as seen in **Figure 1.4**. The gene is located on chromosome 3q27 and is comprised of 31 exons that encode a protein of 1747 amino acids with a molecular weight of approximately 190 kDa (196; 197; 198).

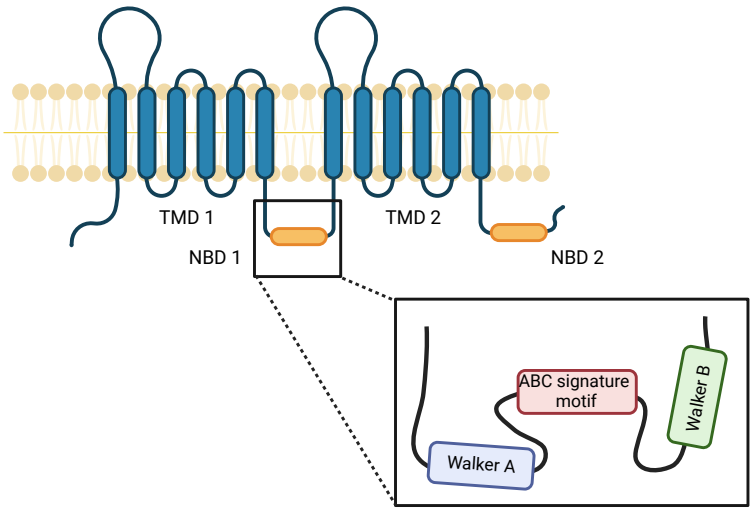

Figure 1.4: ABCC5 structure. Topological overview of ABCC5 protein showing two transmembrane domains (TMD1 and TMD2) with their corresponding nucleotide-binding domains (NBD1 and NBD2). Created with BioRender.com.

ABCC5 mRNA exhibits widespread expression in diverse human tissues, with prominent levels detected in the brain, gastrointestinal tract, muscle, and heart (196; 199). In cardiac tissue, ABCC5 is not only present in myocytes but also in endothelial cells. A study highlighted increased ABCC5 expression in individuals with ischemic cardiomyopathy, emphasising its potential relevance in cardiovascular health (200). Within the brain, ABCC5 has been demonstrated to be present

in brain capillary endothelial cells, indicating its potential involvement in substrate transport across the blood-brain barrier (201). Furthermore, ABCC5 presence has been confirmed in pyramidal neurons and astrocytes (202; 203). Another report indicates the absence of ABCC5 in brain cortex microvessels, ventricular epithelium, and choroid plexus (204), highlighting the variability depending on the specific brain tissue. Further, the expression of ABCC5 was also shown in human and mouse erythrocytes (205).

Several studies also evaluated the presence and role of ABCC5 across different gestational stages in the placenta and highlighted a decreasing trend in ABCC5 expression with advancing gestational age (206) while increased ABCC5 levels were associated with trophoblast differentiation (207). Furthermore, ABCC5 has been identified in mouse extraembryonic foetal membranes, providing additional insights into its distribution during mid to late gestation (208). In a distinctive developmental context, a study involving sea urchin embryos underscored the essential role of ABCC5 in hindgut invagination, emphasising its significance in morphogenesis during embryonic development (209). Additionally, zebrafish embryos had developmental retardation upon the blockage of endogenous ABCC5 activity, implicating ABCC5 in crucial developmental processes (210).

A specific genetic variant within the ABCC5 gene has been associated with anterior chamber depth and primary angle closure glaucoma in Asian populations (211), as well as among individuals from northern China (212). Furthermore, ABCC5 expression has been confirmed in the cornea and suggested in the efflux of antiviral and glaucoma drugs (213; 214). The creation of the initial model of homozygous Abcc5$^{-/-}$ mice on a Friend leukaemia virus B (FVB) background did not yield any discernible phenotype (205). The Abcc5$^{-/-}$ mice were viable and fertile, showing no apparent differences in their behaviour compared to wild-type counterparts (215). Interestingly, ABCC5 was also proposed as a susceptibility

gene for type 2 diabetes (216), while a later study in ABCC5 KO mice showed a reduction in fat mass and GLP-1 plasma levels (217). Ultimately, highlighting a potential metabolic role of ABCC5.

The cellular localisation of ABCC5 within mammalian cells has been widely reported to be in the outer plasma membrane (218; 219; 220; 221). Moreover, ABCC5 has been found in intracellular vesicles (217) and the nucleoplasm (222; 199). The recombinant expression of human ABCC5 in mouse embryonic fibroblasts resulted in co-localisation with Golgi and endosomal recycling organelles (223). In a more recent study, the examination of ABCC5 in mouse testes showed its co-localisation with mitochondria-associated membrane (MAM) markers; however, it was absent in purified mitochondrial fractions (224). Furthermore, paclitaxel-induced the intracellular redistribution of ABCC5, leading to its enrichment in lysosomes (225).

The variability in reported cellular localisation of ABCC5 may stem from unreliable commercially available antibodies targeting ABCC5. This unreliability is likely attributed to the sequence homology shared among ABC proteins. Presently, there is no consensus regarding the precise subcellular localisation of ABCC5 protein within the scientific community. In addition to the uncertainty surrounding ABCC5's subcellular localisation, there is also variability in its expression patterns. Three novel splice variants originating from two additional exons within intron 5 of the ABCC5 gene were identified in the human retina. Notably, one of the protein-coding variants produced a truncated ABCC5 protein isoform with unknown functional properties in the retina (226). SF3B1 mutations, encoding a component of the spliceosome, were associated with differential alternative splicing of ABCC5, in uveal melanoma, emphasising the impact of spliceosome-related mutations on ABCC5 expression dynamics (227). Hence, cellular location as well as variants remain a topic of debate and further research

is necessary.

1.6.1 Substrates

As previously illustrated, the function of ABCC5 in normal physiology remains incompletely understood, although it has been implicated in several processes. This physiological role is closely linked to its substrate transport function, particularly concerning the types of substrates it transports. The hindgut invagination in sea urchin embryos, as previously discussed, is mediated by cAMP, which is a proposed substrate of ABCC5 (209). Initial research on vesicles from ABCC5-transfected hamster fibroblasts showed ATP-dependent transport of cGMP (K_m 2.1 μm) and cAMP (K_m 379 μm) (228). However, another study on HEK293 cells suggested ABCC5 as a low-affinity cyclic nucleotide transporter (229), which was supported by another study in HEK cells that didn't observe increased uptake of cGMP in ABCC5-overexpressing cells (230). A study on erythrocytes showed ambiguous data as ABCC5 KO mice exhibited a lower transport rate, although this effect was not significant (205). In a more recent investigation, cGMP transport rates at concentrations of 1 mM were reported, suggesting a low-affinity, high-capacity type of mechanism (231). Various potential inhibitors of ABCC5 were also tested based on the premise of ABCC5-mediated cGMP transport. Several studies focused on drugs that inhibit phosphodiesterase 5, including sildenafil (232), vardenafil, tadalafil (233) and vardenafil-analogues (234). Another study focussed on sex hormones including testosterone and progesterone (235). Ultimately, the majority of these studies reported some level of inhibition; however, due to the uncertainty of ABCC5 transporting cGMP and the fact that many phosphodiesterase 5 inhibitors also bind to ABCC4 and ABCB1, specificity cannot be claimed (233; 234; 235).

Initial studies on cGMP transport prompted several groups to also investigate

the potential transport of nucleotide analogues by ABCC5. HEK293 cells were shown to be resistant to the cytotoxicity of thiopurine anticancer drugs, including 6-mercaptopurine (6MP) and 6-thioguanine (TG), upon ABCC5 overexpression (236). This finding was supported by a study investigating the transport of different metabolites of 6MP and TG by ABCC4 and ABCC5, which concluded that all major metabolites are transported by both transporters, although the substrate specificity varies (237). Another study concluded that ABCC5 was able to transport (2-phosphono- methoxy- ethyl) adenine (PMEA) as well as the pyrimidine-based antiviral 2',3'- dideoxynucleoside 2',3'- didehydro- 2',3'- dideoxythymidine 5'- monophosphate (d4TMP) (230). Data from HEK293 cells showed that ABCC5 overexpression led to resistance against 5-fluorouracil and its metabolites in cytotoxicity assays. Corresponding data from vesicles reported saturation at K_m 1.1 mM of 5-fluorouracil, and uptake was inhibited by MK571 (238).

Another substrate of ABCC5 that emerged is heme and the role of ABCC5 in heme homeostasis. Studies have demonstrated the essential role of ABCC5 in heme export, as evidenced by targeted depletion experiments *C. elegans* leading to embryonic lethality and in zebrafish leading to morphological defects and failure to produce red blood cells. Embryonic lethality was rescued through the supplementation of exogenous heme (223). Interestingly, another study in *C. elegans* suggests ABCC5 as an exporter of vitamin B12 by showing rescue of embryonic lethality by supplying exogenous vitamin B12 (239). Interestingly, a study in *D. melanogaster* showed that the knockout of the resident heme exporter CG4562 could be alleviated by the expression of ABCC5. Therefore, suggesting ABCC5 is the mammalian equivalent of CG4562 (240). Investigations in mice propose that ABCC5, along with ABCC12, may participate in regulating male reproductive functions and mitochondrial sufficiency. In their study, double-knockout mice for MRP5 and MRP9 exhibited significant male reproductive deficits, implicating

MRP5 in mitochondrial function and sperm physiology (224). This suggests that MRP5 may have diverse physiological roles beyond its suggested function as a heme transporter.

Several other substrates have been proposed for ABCC5, including folates and polyglutamated folates, as demonstrated in vesicle studies using HEK293 cells (241). The kinetics of ABCC5 drug transport were also assessed using carboxydichlorofluorescein (CDCF). This investigation confirmed that transport was indeed ATP-dependent and glutathione-independent (242). A separate study on glutathione transport in astrocytes further affirmed that ABCC5 does not contribute to glutathione transport (243).

A study on ABCC5 KO mice observed the accumulation of a range of metabolic compounds, especially in the brain. Interestingly, these metabolites featured several compounds of similar structure, including N-acetylaspartylglutamate (NAAG) and its polyglutamated form, NAAG2, alongside β-citrylglutamic acid (BCG). Assays on vesicles further confirmed the transport of NAAG with a K_m of 3.5 mM. However, assays using HEK293 cells overexpressing ABCC5 exclusively identified BCG, its analogue BCG2, and N-acetylaspartate as substances exported by ABCC5, excluding NAAG (244). The discrepancies observed between native vesicular and recombinant whole-cell transport assays may arise from variations in ABCC5 expression levels. As previously mentioned, ABCC5 has been reported to localise in both the plasma membrane and intracellular compartments. Furthermore, the presence of other ABC transporters with broad substrate specificity adds complexity to assessments, making it challenging to definitively identify a single transporter responsible for substrate transport.

1.6.2 Structure

The absence of an X-ray crystal structure for ABCC5 has posed challenges in understanding its molecular architecture. The elucidation of the protein's structure is paramount for unravelling its functional mechanisms, substrate recognition, and drug-binding sites. Over the years, several researchers have modelled ABCC5, relying on homology with related proteins and utilising templates such as Sav1866 from *Staphylococcus aureus* and MsbA from *E. coli* (245; 195). Early structural analyses looked at hydropathy profiles and highlighted distinctive features of ABCC5, such as a unique membrane topology and variations in the amino-terminal region compared to other MRP family members (198). An initial structure of ABCC5 based on homology with the bacterial ABC transporter Sav1866 was constructed that suggested two potential cGMP binding sites (246). This structure was compared to the well-characterised P-glycoprotein (ABCB1). Notably, identified differences included amino acid charge distributions and substrate translocation chamber properties, underscoring the importance of understanding the structural basis of substrate specificity (195).

Another study evaluated proposed binding site residues by also using the crystal structure of ABCB1. This validation reinforced the significance of conserved amino acid residues, such as Ile306, Ile340, Phe343, Phe728, and Val982, in forming a substrate translocation pore (245). Subsequent investigations focused on identifying novel cGMP efflux inhibitors through virtual ligand screening. Utilising a homology model based on the *Mus musculus* ABCB1 crystal structure, potent ABCC5 inhibitors with salicylic acid moieties were identified and key interactions with amino acids like Lys448 and Gln190 were highlighted (232). Another group constructed multiple ABCC5 models based on five different ABC transporter crystal structures. These models were ranked according to structural

quality, providing a comprehensive approach to addressing the uncertainties associated with the previously predicted binding site residues and confirming the proposed binding site residues (247).

The structure of ABCC5, like that of other transporters, undergoes various post-translational modifications, including but not limited to phosphorylation, ubiquitylation, and glycosylation. **Figure 1.5** details these modifications and highlights the specific domains that are modified. However, the functional roles of these modifications in ABCC5 remain poorly understood, necessitating further research.

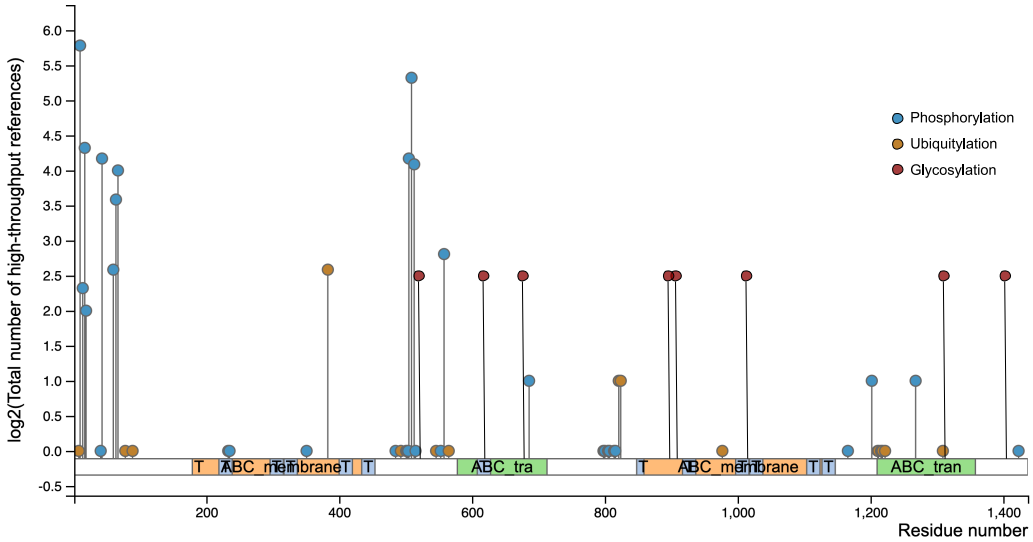

Figure 1.5: Post-translational modifications ABCC5. Phosphorylation and ubiquitylation sites were exported from PhosphoSite. The y-axis describes the number of records that ascribed this modification using proteomic discovery mass spectrometry. The graph was supplemented with data for glycosylation sites from UniProt and the y-axis scale does not apply to glycosylation data points.

In summary, the development of ABCC5 structural modelling has advanced from initial observations of its distinctive membrane topology to more sophisticated homology models based on related ABC transporters. However, to date, no re-

search group has successfully characterised the structure of ABCC5 through X-ray crystallography. Interestingly, the advancements in AlphaFold AI software have enabled more accurate structure predictions than previously achieved with homology modelling software. The prediction of the human ABCC5 structure is shown in **Figure 1.6** (248). The AlphaFold structure is colour-coded according to the confidence score achieved by AlphaFold. The structural areas predicted with high confidence are coloured in dark and light blue and areas with low confidence are coloured in yellow and orange.

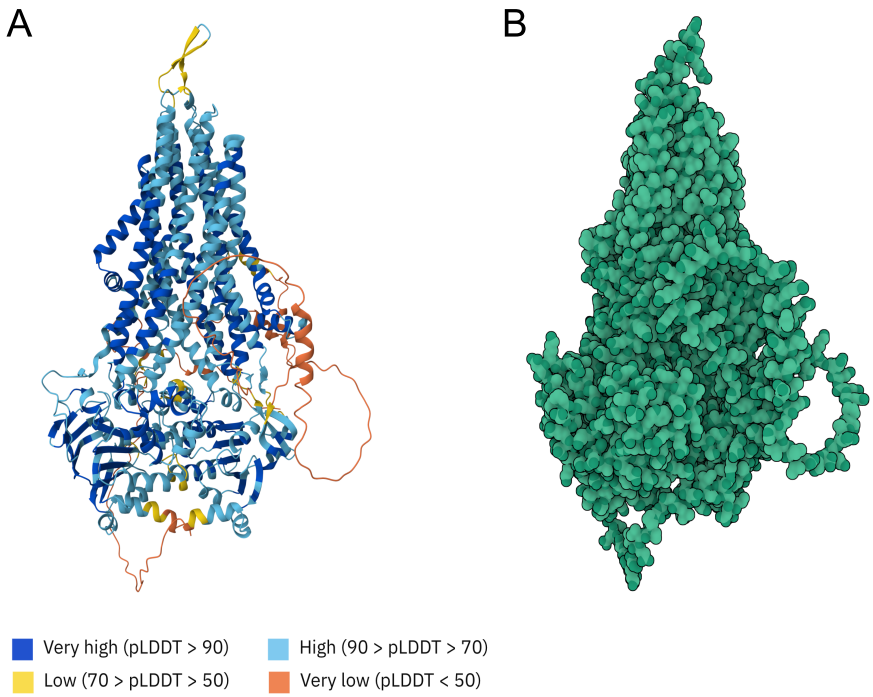

Figure 1.6: Human ABCC5 AlphaFold structure. **A** Human ABCC5 structure with highlighted structural elements according to per-residue model confidence score (pLDDT) predictions of AlphaFold that range between 0 and 100. **B** Illustrative volume depiction of human ABCC5 AlphaFold structure.Adapted from the https://alphafold.ebi.ac.uk/entry/O15440

1.6.3 Paralogues ABCC11 and ABCC12

ABCC11 and ABCC12 are recognised as paralogues of the ABCC5 gene, with their origin traced back to a duplication event as determined through phylogenetic analysis (249). ABCC11, also recognised as MRP8 or ATP-binding cassette subfamily C member 11, is situated on chromosome 16q12.1, encoding a protein with 1714 amino acids and a molecular weight of around 190 kDa (250; 249). It is expressed in human tissues, including the liver, lung, kidney, and various tumours (251; 252). It is noteworthy that ABCC11 lacks a counterpart in mice (253). Functionally, ABCC11 serves as an efflux pump for cyclic nucleotides (cAMP and cGMP) (205; 254). Computational models have identified potential binding sites for cGMP and the anti-cancer drug 5-fluoro-2'-deoxyuridine-5'-monophosphate on ABCC11 (255). Additionally, the transporter provides resistance to nucleotide analogues and fluoropyrimidines (256) and transports various substances, including glucuronidated and sulfated steroids, bile acids, and leukotriene C4 (257; 251). ABCC11 has been associated with breast cancer, where elevated expression correlates with aggressive subtypes and reduced disease-free survival (258; 87). The functional single nucleotide polymorphism rs17822931 in ABCC11 is linked to breast cancer risk in the Japanese population (259; 260). The SNP 538G>A (rs17822931) is also connected with earwax type and an increased breast cancer risk (261; 262). Moreover, ABCC11 has been identified in various cancer cell lines, including those from the lung, colon, prostate, ovary, and pancreas (263; 252). Studies suggest associations between ABCC11 expression and resistance to chemotherapeutic agents in leukaemia (263), osteosarcoma (264), and hepatocellular carcinoma (265). The expression of ABCC11 is associated with the duration of the disease-free interval of colorectal cancer patients (266). Additionally, ABCC11 has been implicated in conferring pemetrexed resistance in

lung cancer (267) and acquired resistance to alectinib in ALK-rearranged lung cancer (268).

ABCC12, also recognised as MRP9 or ATP-binding cassette subfamily C member 12, is situated on chromosome 16p13.1 and encodes a 1547 amino acid protein weighing approximately 170 kDa (252). ABCC12 exhibits tissue-specific expression patterns, with transcripts found at diminished levels in the testes, ovaries, and the prostate. Conversely, its presence is notably absent or expressed weakly in various other tissues, such as the pancreas (269). ABCC12 displays its highest expression in the testes, exclusively localised within the seminiferous tubules in both humans and mice (253; 270).

Additionally, noteworthy findings indicate ABCC12's presence in breast cancer, where it exhibits heightened expression compared to normal breast tissues, encoding two transcripts of varying sizes (271). Moreover, the presence of DNA copy number aberrations in ABCC12 is linked to the response to neoadjuvant chemotherapy in breast tumours (272). In hepatocellular carcinoma, ABCC12 expression is significantly elevated (265) and similarly, in basal cell carcinoma, it undergoes substantial up-regulation (273).

ABCC12 plays a role in drug resistance, specifically in the efflux of protease inhibitors. Despite the effectiveness of atazanavir, lopinavir, and ritonavir in overcoming resistance in cells that overexpress specific transporters, cells overexpressing ABCC12 exhibit a moderate level of resistance (274). Recent research has established a connection between ABCC12 and idiopathic chronic cholestasis. In this context, deleterious variants of ABCC12 are implicated in the loss of intrahepatic bile ducts (275). Further investigations into ABCC12 in model organisms, such as zebrafish and lower vertebrates, indicate its conserved role in metazoan heme homeostasis (223). Notably, ABCC12 has been suggested to compensate for the function of ABCC5 (224).

1.7 ABCC5 in Cancer

The ABC transporter family holds a crucial role in cellular detoxification and drug resistance, with ABCC5 standing out as a member consistently found to be overexpressed in a spectrum of cancer types. Notably, the association between ABCC5 and breast cancer has been extensively researched compared to many other cancer types. A study revealed the overexpression of ABCC5 in breast cancer bone metastasis compared to primary tumours, also linking this overexpression to the bone-metastatic potential of breast cancer cell lines (276). Further, a risk SNP (rs4148579) in an intronic region of ABCC5 influenced the response to neoadjuvant cytotoxic therapy in breast cancer (277). While, a pharmacogenetic analysis of breast cancer patients identified associations between specific ABCC5 genetic variants - namely, the ABCC5 g.+7161G>A (rs1533682) and ABCC5 g.-1679T>A polymorphisms and the pharmacokinetics of both doxorubicin and doxorubicinol (278). Interestingly, ABCC5 expression does not only seem to influence doxorubicin but also pemetrexed as ABCC5 expression significantly influenced pemetrexed sensitivity in breast cancer cells, both in vitro and in vivo. The study observed a correlation between ABCC5 overexpression and larger tumour volumes in mice (279). Subsequently, a separate study addressed this challenge by treating breast cancer cells with elevated ABCC5 expression using liposomal pemetrexed which enhanced drug accumulation (280).

Several other cancers are also associated with higher expression of ABCC5. In both lung adenocarcinoma and non-small cell lung cancer, ABCC5 is upregulated (281; 282). Additionally, ABCC5 has been linked to drug resistance, specifically demonstrating resistance to gemcitabine and cisplatin in non-small cell lung cancer (281; 283). Research on pancreatic adenocarcinoma cell lines also suggests that ABCC5 upregulation is linked to exposure to gemcitabine, influencing

resistance. Notably, ABCC5 exhibits higher expression in pancreatic adenocarcinoma cell lines with elevated IC_{50} values for gemcitabine compared to those with lower IC_{50} values (284). In Capan-2 pancreatic cancer cells, ABCC5 expression increases with higher concentrations of gemcitabine (285), further emphasising the association between ABCC5 and gemcitabine. Additionally, elevated ABCC5 expression was confirmed in human pancreatic carcinoma tissue compared to normal pancreatic tissue (269).

An investigation into pancreatic cancer stem cells revealed that the downregulation of RNA Polymerase II-Associated Factor 1 resulted in the decreased expression of various known stem cell genes, along with genes associated with metastasis, including ABCC5 (286). In two studies involving larynx cancer cells, an enrichment of stem cell markers was observed alongside the upregulation of ABCC5 as cells developed resistance to 5-fluorouracil (287). Additionally, the acquisition of paclitaxel resistance in these cells led to a similar upregulation of both stem cell markers and ABCC5 (287). Moreover, transcriptomic data indicates the prognostic significance of ABCC5 and its association with reduced overall survival in gastric cancer, especially within HER2-positive subgroups (288). In osteosarcoma, genetic variations in ABCC5, particularly the rs939338 SNP, are associated with elevated expression and poorer progression-free survival in patients (289; 290). Expanding the scope to breast cancer, GDF-15 levels correlate with metastasis and poor prognosis in breast cancer. GDF-15 mRNA showed a significant positive association with stemness and drug resistance markers (ABCC5, OCT4, SOX2, FOXM1).

ABCC5 is connected to the transcription factor FOXM1 across various cancer types. In nasopharyngeal carcinoma cells and cervical cancer cells, ABCC5 overexpression is associated with paclitaxel resistance, driven by the transcription factor FOXM1. FOXM1 binds to the ABCC5 promoter, modulating its expression

(291; 292). Notably, specific splicing variants are differentially (abcc5-1 /abcc5-2) influenced by FOXM1 (291). While, in head and neck squamous cell carcinoma, alternative splicing of ABCC5 is linked to lower overall survival (293). ABCC5 is markedly upregulated in breast cancer tissue, and expression is even higher in triple-negative breast cancer (294). In colorectal cancer cells, the recently identified miR-361 emerges as a novel regulator of chemosensitivity, enhancing susceptibility to 5-fluorouracil. This effect was partly attributed to the modulation of the FOXM1-ABCC5/10 pathway. Notably, the direct targeting of FOXM1 by miR-361 resulted in increased cytotoxicity of 5-FU upon its knockdown in resistant CRC cells (295).

In addition to FOXM1's transcriptional regulation of ABCC5, emerging evidence from various cancer studies suggests the presence of an additional regulatory mechanism - the miR-128-Bmi-1-ABCC5 axis. Decreased miR-128 levels in breast tumour-initiating cells (BT-IC) contribute to chemotherapy resistance by upregulating the expression of Bmi-1 and ABCC5. The introduction of miR-128 into BT-ICs mitigates Bmi-1 and ABCC5 levels, thereby enhancing sensitivity to doxorubicin. Notably, clinical analysis reveals that diminished miR-128 in breast tumour tissues correlates with insufficient responses to chemotherapy and diminished patient survival (296). Consistent findings extend to ovarian cancer, where miR-128 treatment results in reduced expression of Bmi-1 and ABCC5, leading to elevated cisplatin levels (297). Further research highlights the pivotal role of SLC34A2 in inducing doxorubicin resistance through the SLC34A2-Bmi1-ABCC5 signalling pathway, emphasising ABCC5 as a direct transcriptional target of Bmi1, as affirmed by chromatin immunoprecipitation (298). Corroborating the existence of the miR-128-Bmi-1-ABCC5 axis, a study on lung cancer stem cells demonstrates that BRM270 elevates miR-128 levels while concurrently reducing BMI-1, ABCC-5, E2F3, and c-MET in the presence of endostatin (299).

A recent study on hepatocellular carcinoma (HCC) cells, identified ABCC5 as a crucial regulator and therapeutic target for sorafenib resistance. Elevated ABCC5, associated with poor prognosis in sorafenib-resistant HCC cells, inhibits ferroptosis by enhancing glutathione production. Down-regulating ABCC5 reduces sorafenib resistance, highlighting its role in regulating ferroptosis in HCC cells (300). In conclusion, ABCC5's participation in various cancers emphasises its diverse roles in drug resistance, and prognosis, and as a potential therapeutic target. ABCC5's overexpression is consistently linked to multidrug resistance and increased cell survival and proliferation. The intricate regulatory networks influencing ABCC5 expression, its genetic variations, and its association with multiple cellular processes underscore the necessity for further research to unveil its role in cancer biology.

1.8 ABCC5 in Prostate Cancer

PCa represents a complex and heterogeneous disease, demanding a nuanced understanding of its molecular intricacies for effective therapeutic intervention. In recent years, ABCC5 has emerged as an interesting player in the progression and metastasis of PCa. Studies showed that ABCC5 expression was higher in PCa tissue than in normal tissue (301; 302). Moreover, a very recent study suggested ABCC5 as an independent prognostic factor for overall survival in PCa patients (303). As seen in **Figure 1.7**, a survival analysis using a Kaplan-Meier plot was extracted from a large dataset to evaluate the impact of ABCC5 expression levels on PCa patient survival (304). The plot highlights that high ABCC5 expression is significantly associated with reduced overall survival of PCa patients indicated by a Hazard Ratio of 3.35 when compared to the ABCC5 low expression cohort. This describes that the likelihood of death is more than 3 times higher when the

gene expression of ABCC5 is high. This is displayed by the two curves separating distinctively which implies that patients with high expression of ABCC5 die faster of PCa than their low expression counterparts.

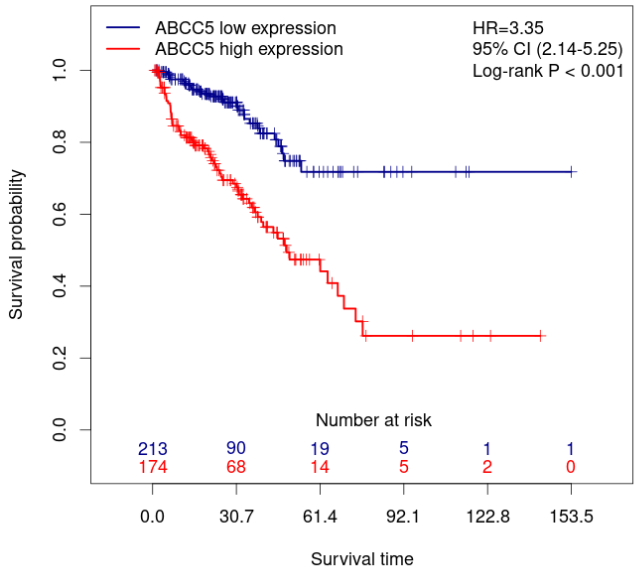

Figure 1.7: Kaplan-Meier Plot illustrating the impact of ABCC5 expression on PCa patient survival. High ABCC5 expression linked to a Hazard Ratio of 3.35. X-axis describes the number of patients alive according to survival time in months. Adapted from (304).

Further, large transcriptomic profiling across various stages of PCa, encompassing over 2000 profiles, revealed a significant association between ABCC5 expression and progression to late-stage metastasis (304). Additionally, another study proposed ABCC5 as a potential diagnostic marker for metastatic PCa (305). Interestingly, a polymorphism in ABCC5 was specifically linked to reduced overall survival and poor prognosis in castration-resistant PCa, emphasising the role of ABCC5 in progressed PCa (306). **Figure 1.8** highlights the mRNA expression levels of ABCC5 across different Gleason scores PCa and it becomes apparent

that ABCC5 expression increases with the Gleason score that represents progression of the disease (307).

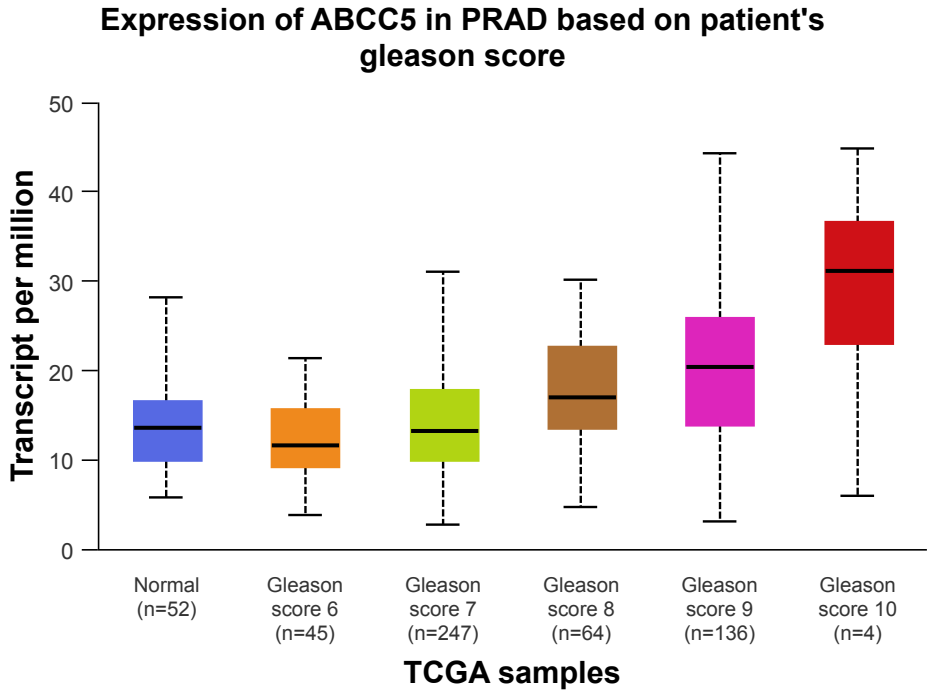

Figure 1.8: Expression of ABCC5 mRNA based on patient's Gleason score. Adapted from https://ualcan.path.uab.edu/cgi-bin/TCGAExResultNew2.pl?genenam=ABCC5&ctype=PRAD.

Other studies have linked ABCC5 overexpression to unfavourable tumour grading and shortened recurrence-free survival in PCa (308; 309; 301). ABCC5 promotes the proliferation, migration, and invasion of PCa cells in vitro and in vivo (310; 311; 301). Nevertheless, one study found that ABCC5 levels were not significantly different between tumour and normal groups and ABCC5 did not exhibit an association with PCa recurrence (312). Other investigations tried to understand the regulatory mechanisms of ABCC5 in PCa progression. ABCC5 was downregulated in advanced PCa upon activation of the androgen pathway (313). Furthermore, bioinformatics analysis suggested CDK1 as a downstream target molecule

of ABCC5. Experimental validation illustrated ABCC5's ability to prevent CDK1 degradation, thereby activating the AR signalling pathway. Inhibiting CDK1 exhibited the potential to suppress tumour growth and influenced enzalutamide sensitivity (311). ABCC5 depletion resensitised enzalutamide-resistant cells in another study, supporting the findings of the previous study and the involvement of ABCC5 in enzalutamide resistance (310). ABCC5 was also implicated in conferring resistance to doxorubicin in PCa cells (314). ABCC5 is known to be modulated by the microRNAs (miRNA) Let-7c and miR-516a-3p, which directly target ABCC5 and cause miRNA-mediated degradation. Notably, downregulation of miRNA Let-7c and miR-516a-3p in PCa cell lines resulted in upregulation of ABCC5 and increased invasiveness of the cells (315; 301). In summary, the cumulative evidence highlights the pivotal role of ABCC5 in various aspects of PCa progression. Elevated ABCC5 expression in PCa tissues, especially in advanced stages and metastasis, aligns with its association with unfavourable tumour grading and shortened recurrence-free survival. Studies underscore ABCC5 as a potential prognostic factor, with high expression significantly correlating with reduced overall survival in PCa patients. In conclusion, the evidence positions ABCC5 not only as a potential diagnostic marker and prognostic factor but also as a promising therapeutic target in PCa. A comprehensive understanding of its regulatory mechanisms and functional implications is imperative for advancing our knowledge of PCa progression and predicting worse outcomes for patients. Ultimately, targeting ABCC5 could lead to the development of effective therapeutic interventions, emphasising the critical need for additional research into the role of ABCC5 in PCa biology.

1.9 Summary and Hypothesis

Advanced prostate cancer (PCa) treatment remains a significant challenge, necessitating the identification of novel drug targets and therapeutic strategies to enhance patient outcomes. Recent studies have shed light on the role of ABCC5 in PCa, revealing its overexpression in aggressive tumours and its association with unfavourable clinical outcomes, including shortened recurrence-free survival and reduced overall survival. These findings highlight the clinical relevance of ABCC5 and underscore its potential as a diagnostic marker and therapeutic target in PCa. Despite these associations, the precise mechanisms by which ABCC5 contributes to PCa progression remain unclear. This thesis aims to elucidate these mechanisms by investigating ABCC5's role in cellular processes relevant to cancer progression, including proliferation, migration, invasion, and drug resistance. By exploring the regulatory networks and signalling pathways influenced by ABCC5, this study seeks to provide a comprehensive understanding of its functional implications in PCa biology.

I In **Chapter 3**, I delve into unravelling the role of ABCC5 in cancer biology through an extensive analysis of large transcriptomic datasets. The aims of this chapter encompassed investigating co-expressed genes with ABCC5, analysing their functional associations and pathways, and assessing potential structural features of ABCC5 through homology modelling.

II In **Chapter 4**, I look into the exploration of genes positively correlated with ABCC5 in prostate adenocarcinoma, building upon the outcomes of Chapter 3. Through computational analysis, I identified genes associated with ABCC5 and investigated their functional roles and pathways in the context of prostate adenocarcinoma.

III In **Chapter 5**, I focus on elucidating the potential protein interactors of ABCC5 and their implications in PCa by constructing a protein interaction network centred around ABCC5. Several highlighted proteins relate to pathways relevant to proliferation, apoptosis, and mitochondrial function.

IV In **Chapter 6**, I aim to identify and validate an anti-ABCC5 antibody for detecting ABCC5 expression across various methodologies.

This thesis highlights the significant role of ABCC5 in the progression of PCa, emphasising its potential involvement in epigenomic processes and expanding hypotheses regarding its role in mitochondrial functions.

2 | Material and Methods

2.1 Computational Analysis

2.1.1 Meta-analysis of ABCC5 Correlated Genes

The RNA-sequencing data from The Cancer Genome Atlas (TCGA) pan-cancer datasets was used for this meta-analysis. In the first step, genes which positively correlate with ABCC5 expression and their respective Pearson correlation coefficient were downloaded across 31 cancer types from the UALCAN database (316; 317). The datasets were split into three groups according to the expression level of ABCC5 in the tumour tissue in comparison to normal tissue.

Overexpression of ABCC5 in Tumour Tissue

Bladder urothelial carcinoma (BLCA), breast invasive carcinoma (BRCA), cervical squamous cell carcinoma (CESC), cholangiocarcinoma (CHOL), head and neck squamous cell carcinoma (HNSC), kidney chromophobe (KICH), kidney renal papillary cell carcinoma (KIRP), liver hepatocellular carcinoma (LIHC), lung adenocarcinoma (LUAD), lung squamous cell carcinoma (LUSC), prostate adenocarcinoma (PRAD), pheochromocytoma and paraganglioma (PCPG), rectum adenocarcinoma (READ), sarcoma (SARC), and skin cutaneous melanoma (SKCM).

Underexpression of ABCC5 in Tumour Tissue

Colon adenocarcinoma (COAD), oesophageal carcinoma (ESCA), glioblastoma multiforme (GBM), kidney renal clear cell carcinoma (KIRC), pancreatic adenocarcinoma (PAAD), thyroid carcinoma (THCA) and thymoma (THYM).

Undetermined expression of ABCC5 in healthy tissue in comparison to tumour tissue

Adrenocortical carcinoma (ACC), lymphoid neoplasm diffuse large B-cell lymphoma (DLBC), brain lower grade glioma (LGG), ovarian serous cystadenocarcinoma (OV), mesothelioma (MESO), acute myeloid leukemia (AML), testis germ cell tumours (TGCT), uterine carcinosarcoma (UCS) and uveal melanoma (UVM).

In the next step, the number of datasets each gene appeared in was quantified (**Figure 2.1**) and the mean Pearson correlation of each gene with ABCC5 was calculated as seen in **Figure 2.2**. This resulted in 12692 unique genes across all datasets. A threshold was introduced so genes that showed a Pearson correlation coefficient of equal to or greater than 0.5 with ABCC5 and that occurred in at least 10 datasets were included. Each group was then analysed separately and heatmaps were generated for the genes in the overexpressed and underexpressed datasets which had a mean Pearson correlation coefficient > 0.5 and occurred in more than half of the datasets within the group. All figures and analysis were created in R.

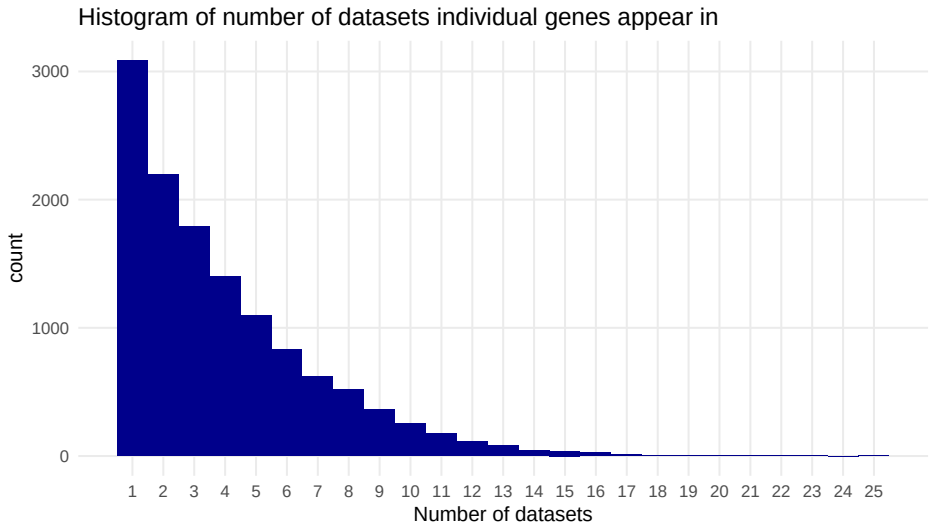

Figure 2.1: Histogram of number of datasets individual genes appear in.

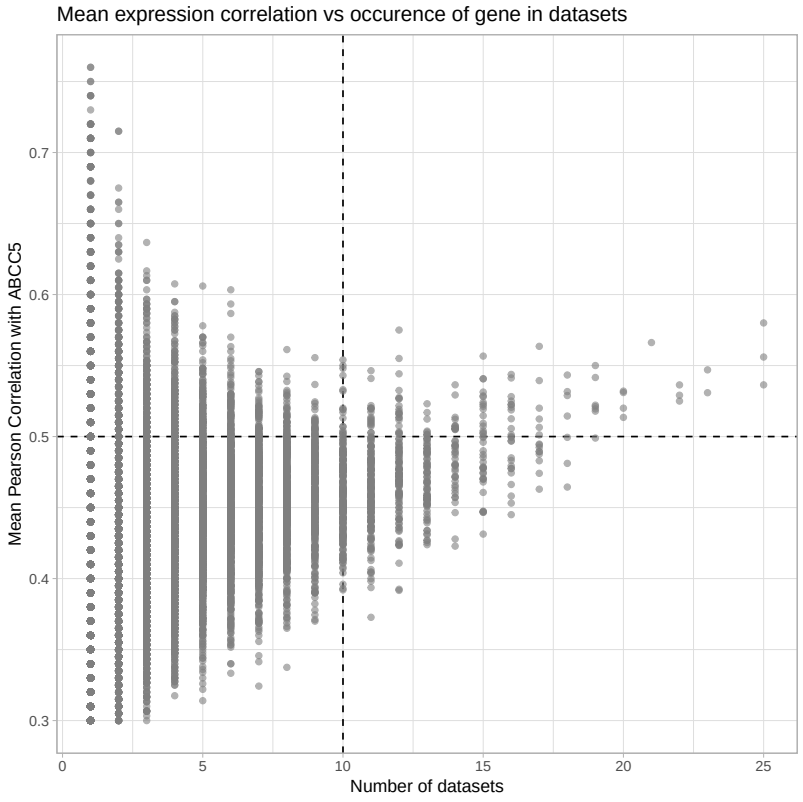

Figure 2.2: Meta-analysis on genes that correlate with ABCC5 from TCGA datasets. Occurrence against mean Pearson correlation for all genes in all datasets.

2.1.2 Metascape Pathway and Process Enrichment

For the comprehensive examination of gene lists associated with the all-cancer and prostate cancer (PCa) datasets, a comparative pathway and process enrichment analysis using the Metascape tool was conducted (318). The custom ontology analysis was performed with the following parameters: GO Molecular Functions, Reactome Gene Sets, GO Biological Processes, and GO Cellular Components. The entire genome's gene set served as the background for enrichment. Enriched terms meeting the criteria of a p-value value < 0.01, a minimum count of 3, and an enrichment factor > 1.5 (the ratio between observed and expected counts) were systematically identified. Subsequently, these terms were organised into clusters based on similarities in their membership. The default clustering settings were applied, considering terms with a similarity greater than 0.3 as belonging to the same cluster. Within each cluster, the most statistically significant term was selected to represent the entire cluster. For the analysis of the PCa dataset the following ontology sources were used: GO Biological Processes, GO Cellular Components, GO Molecular Functions, Reactome Gene Sets, oncogenic signatures and transcription factor targets. For the enrichment analysis, the same parameters as above were utilised. In the network analysis, terms with a similarity exceeding 0.3 were connected through edges. A constraint was applied to select terms with the best p-values from each of the 20 clusters, ensuring that no more than 15 terms were included per cluster.

2.1.3 REVIGO GO Term Enrichment Analysis

The gene lists were submitted to an analysis using g:Profiler to uncover the functional roles, associated pathways, and other relevant information (319). Subsequently, the results were visualised using REVIGO (320), wherein cluster rep-

resentatives that remained after redundancy reduction were positioned in a two-dimensional space. The colour-coded data points depicted distinct GO terms, offering insights into the functional associations of genes correlated with ABCC5 across various cancer types. Other visualisations showing GO term enrichment were created using R.

2.1.4 Homology Modelling with DALI

The initial step in the approach involved obtaining the predicted structure of ABCC5 generated by the AlphaFold algorithm (248). This model served as the foundation for the subsequent homology modelling analysis. The DALI (Distance-matrix Alignment) server (321) stands as an important tool in the field of structural bioinformatics for identifying structurally related proteins within the Protein Data Bank (PDB). The AlphaFold-predicted ABCC5 structure was submitted to the DALI server. Upon obtaining the DALI results, the dataset was screened for interesting hits. Subsequently, following the identification of promising hits from the DALI server results, the next stage of the investigation entailed a comprehensive sequence alignment utilising Clustal Omega. The results obtained from both the DALI server and the Clustal Omega sequence alignment were analysed, providing a foundation for subsequent investigations into the structural and functional implications of the identified homologous proteins concerning ABCC5.

2.1.5 Gene Promoter Motif Analysis

For the gene promoter motif analysis, the RSAT tool (322) was used to retrieve EnsEMBL sequences (18.09.2023). Specifically, sequences up to 2kb upstream of the genes within the ABC transporter cluster (blue) were extracted. Subsequently, the extracted sequences underwent analysis within the MEME Suite (https://meme-suite.org/meme/index.html). The SEA tool (Bai-

ley & Grant, 2021) within the MEME suite was used for further investigation. Following the completion of the analysis, the output files from SEA were reviewed and the results were interpreted considering e-values, and p-values. This involved selecting motifs specifically associated with ABCC5, excluding other transcription factors unrelated to ABCC5. An e-value threshold of log e-value 0.67 was applied for the discovery of significant motifs. To visually represent the sequence score for each motif for every protein, a heatmap was generated in Prism.

2.1.6 Protein-Protein Interaction Network Construction

The first step in generating a Protein-Protein Interaction (PPI) network for ABCC5 included analysing the literature and mining databases for proteins associated with or interacting with ABCC5. Proteins reported to be associated with ABCC5 were extracted from the databases listed in **Table 2.1**.

Table 2.1: Databases used for PPI Network.

Database	**Access**
Mentha Database (323)	17.02.2021
String Database (324)	17.02.2021
Proteomics DB (325; 326; 327)	17.02.2021
PSICQUIC (328)	03.02.2021
BioGrid (329)	03.02.2021
Integrated Interactions Database (330)	18.02.2021

Based on this data set of 76 proteins, a PPI network was constructed in the String Network Search Tool using String (Version 11; accessed 26.02.21). The following settings were used; complete STRING network, confidence lines, active interaction sources: textmining, neighbourhood, experiments, gene fusions, databases,

co-expression, co-occurrence, minimum required interaction score: high confidence of 0.700. The protein-protein network extracted from this analysis was supplemented with additional data from PDB, KEGG, and Genecards to identify the main cell compartments of the previously identified proteins within the network. In the second analysis, the data set of 76 proteins was imported into Cytoscape (Version 3.8.2) (331) using stringApp (332) with high confidence 0.700. Clustering was performed using the Markov clustering tool in the clusterMaker2 Cytoscape app. Clusters consisting of a single node were removed from the network. An overview of the entire analysis is shown in **Figure 2.3**.

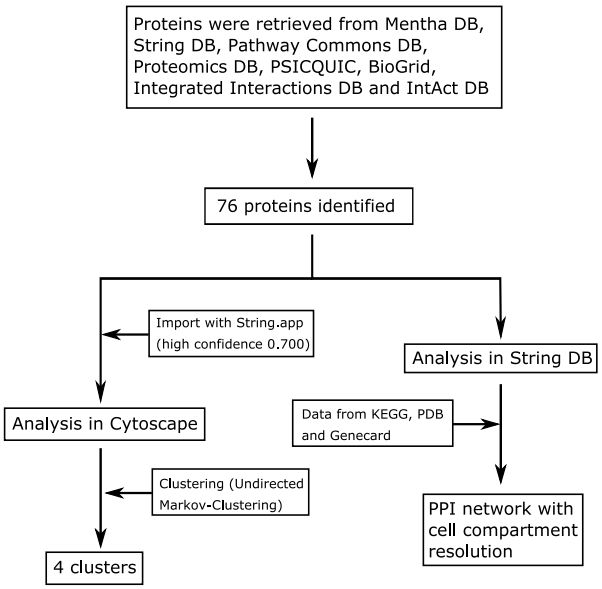

Figure 2.3: Protein-protein interaction analysis workflow.

2.2 Mice Work

2.2.1 Mice

All animal studies in this project were conducted under the animal care and ethical review committee of the University of Oxford following the Animal Scientific Procedures Act of 1986. Male Abcc5 knockout mice (Abcc5$^{-/-}$) and wild-type littermate controls were used for experiments. The Abcc5 knockout mice (Abcc5$^{-/-}$) line was generated by deleting 372 nucleotides within exon 13 by CRISPR/Cas9 technology. The removed area encodes the cytosolic part of nucleotide-binding domain 1 (NBD1). To generate Abcc5$^{-/-}$ mice and wild-type littermate controls, heterozygous mice were backcrossed. Animals were housed divided by genotype and sex, generally in groups of at least three mice per cage (unless specified otherwise). Mice were kept under standard conditions of light/dark cycle 12:12, 21 ± 2°C, humidity $55\% \pm 10\%$ and fed on standard chow.

2.2.2 Tissue Isolation

Mice were killed by cervical dislocation or carbon dioxide, and tissues were harvested and processed according to the relevant downstream application.

2.2.3 Histology and Cryosectioning

Freshly isolated tissue samples were fixed in 4 % paraformaldehyde (PFA) overnight and then immersed in a 30 % sucrose solution for 24 h. After cryoprotection, the samples were embedded in tissue Freezing Media (Thermo Fisher) and then flash-frozen in isopentane at -150°C. Frozen blocks of prostate tissue were cryosectioned at 15 μm thickness using a cryostat (Bright OTF5000, Bright Instruments, UK) and sections placed on glass slides or floated in phosphate-buffered saline

(PBS) in a 24-well dish.

2.2.4 Immunofluorescence of Cryosections or Floating Sections

For immunofluorescence of cryosections or floating sections, the sample was washed with PBS and subsequently blocked and permeabilised with Blocking and Permeabilisation solution (BPS) for 1 h. Samples were incubated with primary antibodies diluted in BPS overnight at $4°$C, washed with PBS and incubated with secondary antibodies diluted in BPS for 1 h at RT. Subsequently, the floating samples were placed on a slide and all samples were mounted with mounting media (ProLong Gold, Invitrogen) and sealed. The slides were dried at room temperature and then kept at $4°$C. Images were acquired with the Axiovert 2 (Zeiss) or the EVOS M5000 (Thermo Fisher) microscope.

2.3 RNA/DNA and Protein

2.3.1 Plasmid DNA Purification

Glycerol stocks containing transformed bacteria were used for DNA purification. A sterile filter tip was placed into the glycerol stock and transferred to a tube containing 1 mL of LB medium without antibiotics. The mixture was incubated for 4 h at 37°C and 300 rpm before streaking onto LB agar plates containing ampicillin (100 mg/mL) or kanamycin (50 mg/mL) depending on the plasmid. Successfully transformed colonies were selected and cultured in 10 mL LB supplemented with the respective antibiotic at 37°C overnight. The starter culture was then diluted in 250 mL of selective LB medium and grown for 16 h at 37°C, whilst shaking. The following day, the bacterial cells were harvested by centrifugation (15000 x g; 15 mins; 4°C) and DNA purification was carried out using the QIAGEN® Plasmid Maxiprep Kit, according to the manufacturer's instructions. Purified DNA was quantified using the NanoDrop Spectrophotometer (Thermo Fisher) and stored at -20°C. All the plasmids used are listed in **Table 2.2**.

Table 2.2: Plasmids.

Insert	Selection
hpSF-CMV-ABCC5	Ampicillin
hpSF-CMV-ABCC5-GFP	Kanamycin

2.3.2 Reverse Transcription and qPCR

Total RNA was extracted using the High Pure RNA Isolation Kit (Roche) according to the manufacturer's protocol. RNA was quantified using the NanoDrop 2000-c Spectrophotometer (New Brunswick) and then reverse transcribed into

cDNA using the RevertAid First Strand cDNA Synthesis Kit (Thermo Scientific) as per manufacturer's protocol for Oligo(d)T18 first-strand cDNA synthesis. The samples were diluted at 1:20 in RNAse/DNAse-free water and stored at -20°C. Gene expression was assessed by quantitative real-time PCR (qRT-PCR) using FastStart SYBR Green Master Mix (2x) according to the supplier's instructions and monitored using the 7500 Fast Real-Time System (Applied Biosystems). Each sample was analysed in triplicate and the mRNA levels normalised to β-actin. All qRT-PCR primer sequences are listed in **Table 2.3**.

Table 2.3: Human Primers.

Gene ID	**Forward Primer**	**Reverse Primer**
Beta-actin	AGAGCTACGAGCTGC CTGAC	AGCACTGTGTTGGCG TACAG
ABCC5	TGCTCCGCCACTGTA AGATTC	ATCGGAGCCTAGAAC CGTGT
ABCC11 new	AGTATGATGCTGCCT TGA	GGTGAGGTAGGAGAA CAG
ABCC11 old	CCACTCTGTGTGGCA AAGAA	AGTTGGGCACCCAGT ATGTC
ABCC12	CATAGGGCCGGTGAT TCTCAT	TAGTTGATGGCCCAG GCAAG
CASP6	CGATGTGCCAGTCA TTCCTT	CTCTAAGGAGGAGCC ATATTTTC
CASP7	CAGGGGGTTGAGGAT TCAGC	GAACGCCCATACCTG TCACT

Continued on next page

Table 2.3 – continued from previous page

Gene ID	Forward Primer	Reverse Primer
CASP8	TTCTGCCTACAGGGT CATGC	TCAAGGCTGCTGCTT CTCTC
DMTF1	CTGCTTCCTCCATCC TGGTATTTTT	GTCTATTTCATCCGC TTCTAGACAA
ESR1	ATGACCCTCCACACC AAAGCAT	ATCTTGAGCTGCGGA CGGTT
hpSF-CMV-ABCC5	CAGCGTATCTCTCTG GCTCG	AGCACGGTCTTGGA CTTCAG
MDM4	GGAGCTGCCGTAAGT TTTACC	AACATTTCACCTTGC GCACC
NRF1	GCTGATGAAGACTCG CCTTCT	TACATGAGGCCGTTT CCGTTT
PARP1	AAGCCCTAAAGGCTC AGAACG	ACCATGCCATCAGCT ACTCGGT
PRDM15	TAAGCAGGGCAAGGT CATCC	TGGACTCAAAGGGAC CGAAC
PTK2	ACTTGGACGATGTAT TGGA	AGGATTCTCTGTGAT GACTC
SESN2	CTCATCACCAAGGAA CACATC	CTCTGTTCACTAGGG GGTGTAG
SHMT2	AGTCTATGCCCTATA AGCTCAACCC	GCCGGAAAAGTCGA GCAGT

Continued on next page

Table 2.3 – continued from previous page

Gene ID	Forward Primer	Reverse Primer
SUPT7L	TGTTCTTCGTGCTCC TTTCGGTA	GGTATCTCTCCCCAG TATCTTTGC
TAF11	CAGGAAGTAAGATCC TGGCCT	ACTCTCGAGCTCGCC TT
TRIM52	GTGCAGGAGTACCAG AAGATAGG	ATCGGGCTTTGCAGA ACACT
ZBTB43	CGGCAGAGAGGATAT CTTGGG	TCACAAATCTTGTTC GGTGCTGC
ZNF75A	AAGCTGGCCGAGTGC TTTTA	CTGAGGGTCCAAGTA CGCAG
ZNF169	CTTCTGGACCTTTGT CCAGCTCA	GCACAGAAAACCCAC ACTACAAA
ZNF182	GCCAGGCTTTGTAAC GGTCT	GGGCAGGTCACTGTG TCTC
ZNF224	GATCGAATTAGGGGA AAAGGGG	AAGCAGAATTGTGCC AAGACAG
ZNF250	GGCCAAGCTGACCTT CGAG	TGGATCCTGGAAGTC CCAATG
ZNF471	AAGTCATGCCCCAGG TCTTT	ACTCGTCATCTCCCA AGGCT
ZXDC	TAGCGTTTGGCCCTT TGTGT	AACAGTGACAGAGAA ACCCTCAG

2.3.3 Protein Sample Preparation and Measurement

The cells were disrupted using RIPA buffer, which consisted of 150 mM NaCl, 50 mM Tris-HCl at pH 8.0, 1 % IGEPAL, 0.2 % sodium deoxycholate, and 0.1 % sodium dodecyl sulphate (SDS). To ensure protein stability, the RIPA lysis buffer was freshly supplemented with Protease Inhibitor Cocktail (PIC) cOmplete, EDTA-free (cat.no.: 11873580001, Roche) according to the manufacturer's instructions. The PIC tablets were dissolved in 1 mL of ultrapure water to create a 50x stock solution. For cells in 24-well plates, lysis was performed directly in the plate on ice using 60 μL of RIPA buffer supplemented with PIC, and incubated for 10 min. After lysis, cells were detached either by pipette tip (for 24-well plates) or cell scraper, and transferred to pre-chilled Eppendorf tubes. The samples were then centrifuged at 17,200 x g, 4°C for 15 min to remove nuclei and cellular debris, and the resulting clear cell lysate was collected into a fresh pre-chilled Eppendorf tube and stored at -80°C until further analysis. Total protein in whole-cell lysates of LNCaP and PC-3 cells and whole tissue lysates of mouse prostate were quantified by BCA (Bicinchoninic Acid) Protein Assay (Pierce™ BCA Protein Assay Kit - Thermo Fisher Scientific) according to manufacturer's protocol. Briefly, 10 μL of known concentrations of bovine serum albumin (BSA) and lysates (neat and diluted) were prepared in a transparent 96-well plate. A freshly prepared BCA working solution was added (30 μL per well), and the plate was incubated for 30 min at 37°C and subsequently read at 562 nm using a plate reader (ClarioStarPLUS, BMG Labtech, Germany). Lysate samples were stored at -80°C until Western blot analysis.

2.3.4 SDS-PAGE and Western Blot

For SDS-PAGE samples were prepared as follows: 14 μL of cell lysate mixed with 5 μL of NuPAGE™ LDS Sample Buffer (4X) (Thermo Fisher) and 1 μL of reducing agent - 20x Dithiothreitol (DTT, Sigma). Samples were heated at $65°$C for 10 min and cooled down on ice. 20 μL of the sample (20 μg of total protein) was loaded onto Tris-Glycine gels (Novex Wedge Well, Invitrogen) or 8 % polyacrylamide gel (self-made) and run at 120-150V in Running buffer for 1 h. Protein transfer was performed either using the iBlot 2 (Thermo Fisher) according to the manufacturer's protocol or the Tetra Blotting Module (BioRad). The membrane was blocked for 1 h at room temperature with blocking solution (5 % milk or 5 % BSA) and probed with primary antibody (**Table 2.4**) overnight at $4°$C in blocking solution. For detection by chemiluminescence, the membrane was washed and incubated with HRP-conjugated secondary antibody for 2 h at RT. The reagent system by Amersham ECL Select Western Blotting Detection Reagent (GE Healthcare) was used to detect the signal on X-ray films (Amersham Hyperfilm ECL, GE Healthcare) with standard developing and fixing reagents. For detection by near-infrared fluorescence, the membrane was washed and incubated with an IRDye® 800CW secondary antibody. The signal was visualised at 800nm and at 700nm with the LI-COR Odyssey Fc Imager (LI-COR Biosciences). The different secondary antibodies used are listed in **Table 2.5**.

Table 2.4: List of Primary Antibodies used for Western Blotting.

Primary Antibodies	**Product Code**	**Immunogen Sequence**
MRP5 (rabbit, pAb)	Thermo Fisher PA583701	SPGYRSVRERTSTSGT HRDREDSKFRRTRPL ECQDALETAARAEGL SLDASMHSQLRILDE EHPKGKYHHGLSAL KPIRTTSKHQHPVDN AGLFSCMTFSWLSSL ARVAHKKGELSMED VWSLSKHESSDVNC RRLERL
MRP5 (rabbit, pAb)	Thermo Fisher PA5102678	A synthesized peptide derived from human ABCC5, corresponding to a region within N-terminal amino acids
MRP5, E-4 (mouse, mAb, IgG_2b)	Santa Cruz sc-390797	specific for an epitope mapping between amino acids 13-46 of MRP5 of mouse origin
MRP5 (rabbit, pAb)	Abcam ab180724	Synthetic peptide corresponding to Human MRP5

Continued on next page

Table 2.4 – continued from previous page

Primary Antibodies	**Product Code**	**Immunogen Sequence**
MRP5, P-20 (goat, pAb	Santa Cruz sc-5781	
PSM, F-2 (mouse, mAb, $IgG_1\kappa$)	Santa Cruz sc-514444	raised against amino acids 568-627 of PSM of human origin
FOXM1, G-5 (mouse, mAb, $IgG_2b\kappa$)	Santa Cruz sc-376471	specific for an epitope mapping between amino acids 734-763 at the C-terminus of FOXM1 of human origin
FOXM1, A-11 (mouse, mAb, $IgG_2a\kappa$)	Santa Cruz sc-271746	amino acids 31-150 mapping near the N-terminus of PDE5A of human origin
α-tubulin (rabbit, pAb)	Abcam ab4074	
PARP-1, F-2 (mouse, mAb, $IgG_2a\kappa$)	Santa Cruz sc-8007	amino acids 764-1014 mapping at the C-terminus of PARP of human origin

Table 2.5: List of Secondary Antibodies used for Western Blotting.

Secondary Antibodies	**Product Code**
Donkey Anti-Rabbit IgG (H+L) Alexa Fluor 568	Abcam ab175692
Donkey anti-Rabbit IgG (H+L) HRP	Thermo Fisher SA1-200
Donkey anti-Mouse IgG (H+L) Alexa Fluor 568	Abcam ab175700
Donkey anti-Goat IgG HRP	Promega V8051
Donkey anti-Goat IgG (H+L) Alexa Fluor 568	Invitrogen A11057
m-IgG$kappa$ BP-FITC	Santa Cruz sc-516140
m-IgG$kappa$ BP-HRP	Santa Cruz sc-516102
IRDye® 800CW Donkey anti-Rabbit IgG	LI-COR 926-32213
IRDye® 800CW Donkey anti-Mouse IgG	LI-COR 926-32212

2.4 Prostate Cancer Cell Work

2.4.1 Cell Culture

All PCa cell lines used in this project (**Table 2.6**) were purchased from ATCC. LNCaP cells were maintained in ATCC modification medium RPMI-1640 (Gibco®, Invitrogen) and PC-3 cells in Ham's F-12K (Kaighn's) (Gibco®, Invitrogen). The mouse model L cell line cells (GLUTag cells) were cultured in low glucose Dulbecco's Modified Eagles Medium (DMEM) (Gibco®, 31885). All media was supplemented with 10 % heat-inactivated foetal bovine serum (FBS, Sigma). FBS was heat-inactivated in-house by placing the bottle in the water bath at $56°C$ for 40 min. Cells were passaged with trypsin-EDTA (0.05 %) after rinsing with Dulbecco's phosphate-buffered saline (DPBS), no calcium, no magnesium. Cells were kept at $37°C$ with 5 % CO_2 and were discarded past passage 25.

Table 2.6: Overview of the characteristics of the PCa cell lines (333; 334; 335).

	LNCaP	**PC-3**
Site of Origin	Lymph node	Bone
Androgen Receptor Expression	Mutant (T877A mutation in the AR coding sequence that gives it a promiscuous binding affinity to a range of steroid compounds)	-
Androgen Stimulation	Increases growth	No effect
Doubling time	~ 60 h	~ 33 h
PTEN status	-/-	-/-
PSA mRNA/ protein	+	-
PSMA expression	+	-
Other	-	transferrin receptor; more characteristic of neuroendocrine/small cell carcinoma than adenocarcinoma

2.4.2 ABCC5 Knockdown

LNCaP and PC-3 cells were seeded at $2x10^6$ cells/well in a 12-well plate (Corning) and at $1x10^5$ cells/well in a 96-well plate (Corning). The cells were kept in

culture medium overnight and transfected with either negative control siRNA or a combination of siRNA targeting ABCC5 (ID: s19555; 4392420, Ambion) and siRNA targeting ABCC5 pool (Dharmacon). The siRNA complex was prepared according to the manufacturer's protocol with Lipofectamine RNAiMAX reagent (Thermo Fisher). The final concentration of negative control and ABCC5 siRNA was 25 nM per well, and the cells were incubated for 24-72 h at 37°C with 5 % CO_2 depending on the experiment. Knockdown efficiency was assessed by qPCR and Western blot analysis.

Table 2.7: siRNA Sequences.

Target Gene ID		**Target Sequences**
ABCC5 siRNA (hu) (Ambion)	F	GCAGAAGACTAGAGAGACTTT
	R	AGTCTCTCTAGTCTTCTGCAG
ON-TARGETplus Human ABCC5 Dharmacon		GAACUCGACCGUUGGAAUG
		CGACAUAGGAAAAGAGUAU
		GCACAGAGACCGUGAAGAU
		GCAGAAGACUAGAGAGACU
ON-TARGETplus Non-targeting Pool Dharmacon		UGGUUUACAUGUCGACUAA
		UGGUUUACAUGUUGUGUGA
		UGGUUUACAUGUUUUCUGA
		UGGUUUACAUGUUUUCCUA

2.4.3 ABCC5 Overexpression

To overexpress ABCC5 in cell culture, LNCaP and PC-3 cells were seeded at 10 x 10^4 cells/well and transfected with 0.2 μg of plasmid per well using the TransIT®-LT1 Transfection Reagent (Mirus). The negative control well was transfected with the empty plasmid construct whilst the positive control was either transfected with

pSF-ABCC5 or pSF-ABCC5-GFP. The cells were incubated with the plasmid for at least 24 h before subsequent experiments were performed.

2.4.4 Immunofluorescence in Cell Culture

For immunofluorescence detection of protein expression in PCa cell lines, LNCaP (5 x 10^5 cells/well) and PC-3 (5 x 10^5 cells/well) cells were seeded onto sterile coverslips coated with poly-l-lysine in 12-well plates or LNCaP (10 x 10^4 cells/well) and PC-3 (10 x 10^4 cells/well) cells were seeded onto sterile 8-well LabTeks (Nunc™ LabTek™, Thermo Fisher). After 24 h, cells were briefly washed with PBS and fixed/permeabilised with either 100 % methanol or 100 % acetone for 5 min at -20°C or fixed with 4 % PFA for 10 min at RT and permeabilised with 0.01 % Triton-X for 10 min at RT. The coverslips/slides were washed twice with PBS before being subjected to blocking with 3 % BSA and 10 % donkey serum at RT for 1 h. Following three additional washes, the cells were incubated with primary antibody at 4°C, overnight. The following day, the coverslips/slides were washed and incubated with secondary antibody for 1 h at RT, shielded from light. Finally, after three additional PBS washes, the coverslips/slides were mounted with mounting media (ProLong Gold, Invitrogen) and sealed. Images were acquired with Axiovert 2 (Zeiss) or the EVOS M5000 (Thermo Fisher) or the Leica DM6000B (Leica Microsystems) microscope.

2.4.5 Colony Formation Assay

LNCaP or PC-3 cells were counted and seeded at 2x10^6 cells/well in a 12-well plate for knockdown or overexpression of ABCC5 (as described previously). The treated cells were harvested after 48 h (knockdown) or 72 h (overexpression) and subsequently replated at 2,000 cells/well in a 6-well plate to assess their colony formation ability. The plates were placed in the incubator and left for 7 days to

ensure sufficient colony formation. For fixation, the cells were carefully washed with PBS and then incubated with 3 mL of 100 % ice-cold methanol at RT for 20 min. Subsequently, the cells were stained with 1 mL of crystal violet solution (0.5 % w/v crystal violet) at RT for 30 min. The staining solution was carefully removed and the dishes were washed three times with tap water. The plates were dried at RT and recorded with a scanner (Epson). The scans were automatically analysed with a Fiji software plugin that was optimised for colony formation analysis (336).

2.4.6 Cell Migration Assay

LNCaP or PC-3 cells were counted and seeded at $2x10^6$ cells/well in a 12-well plate for knockdown or overexpression of ABCC5 (as described previously). The treated cells were harvested after 48 h (knockdown) or 72 h (overexpression) and the cells were centrifuged for 5 min at 1000 rpm to remove the trypsin and media. The cells were diluted in serum free media and added to the full media equilibrated Transwell (Sarstedt) inserts which were placed in 24-well plates. About 1 mL of full media was added to the lower compartment and the cells were left for 24 h to migrate. The next day, 100% ice-cold methanol was added to the lower compartment to fix and permeabilise the cells. The wells were washed with PBS and the inserts were placed in 1 mL crystal violet solution (0.5 % w/v crystal violet) and incubated for 30 min. The inserts were washed with ddH_2O and the upper side of the Transwell insert was wiped with cotton swabs. The filters were left to dry overnight and the membranes were removed using razor blades. The membranes were placed on glass slides and imaged with a stereo microscope. Images were analysed using Fiji.

2.4.7 Caspase Assay

LNCaP and PC-3 cells were seeded at 5x10^4 per well in a 96-well plate. Knockdown and overexpression were performed as previously described and the assay was commenced after 48 h (knockdown) and 72 h (overexpression). The caspase assay was performed according to the manufacturer's instructions of the Promega Caspase-Glo™ 3/7 Assay Kit and the Promega Caspase-Glo™ 9 Assay Kit (Promega). Briefly, reagents were equilibrated to RT and 100 μl of Caspase-Glo® 3/7 Reagent / Caspase-Glo® 9 Reagent were added to each well. The plate was covered and mixed using a plate shaker at 300 rpm for 1 min. The plate was incubated for 30 min at RT and measured every 30 min for 3 h with a plate reader (CLARIOstar Plus, BMG Labtech).

2.5 Data Analysis

Processing raw data was performed using Microsoft Excel (Microsoft, WA, USA) and then imported to Prism 9 (GraphPad Software, USA) for statistical analysis and graph plotting. Microscopy images were analysed using FIJI software (337).

2.6 Reagents

Table 2.8: Solutions and Buffers.

Solutions/Buffers	**Reagents**
Running Buffer	900 mL ddH_2O, 100 mL 10x Transfer Buffer, 10 mL 10 % SDS
Transfer Buffer (10x, pH 8.3)	Glycine 1.92 M, Tris-HCl 250 mM
TBS (10x, pH 7.6)	24 g of Trizma-Base, 88 g of NaCl in 1 L of ddH_2O
TBS-T	900 mL ddH_2O, 100 mL 10x TBS, 0.1 % Tween-20
RIPA Buffer	150 mM NaCl, 50 mM Tris-HCl (pH 8.8), 1 % IGEPAL, 0.5 % (w/v) Deoxycholic Acid
Blocking Solution WB	5 % of non-fat powder milk in TBS-T
Running Gel Buffer	1.5 M Tris-HCl (pH 8.8)
Stacking Gel Buffer	0.5 M Tris-HCl (pH6.8)
Blocking and Permeabilization	3 % BSA, 10 % donkey serum, 1 % Triton X-100, 0.02 % NaN3

Slide Coating Solution	5 g Gelatin, 0.5 g of $CrK(SO_4)2$ in 1 L of ddH_2O
Poly-l-lysine Solution	10 % of 0.1 % poly-l-lysine solution (P8920 Sigma) in ddH_2O
Crystal Violet Staining Solution (0.5 %)	0.5 g crystal violet powder in 80 mL distilled H_2O and 20 mL methanol

3 | Decoding Cancer Gene Networks and ABCC5's Potential Functions

3.1 Introduction

3.1.1 Meta-analysis TCGA Dataset

Cancer research has changed significantly over the last two decades, and this development can be attributed to the emergence of high-throughput molecular profiling technologies and the utilisation of extensive genomic datasets (338). The Cancer Genome Atlas (TCGA, https://tcga-data.nci.nih.gov/tcga/) project is an essential cancer research resource which was initiated in 2005 between the National Cancer Institute (NCI) and the National Human Genome Research Institute (NHGRI) (339). This collaboration resulted in a comprehensive database that characterises over 20,000 primary cancers across 33 cancer types. The data offer information about genomic, transcriptomic and proteomic aspects, allowing for the identification of shared characteristics and distinctive features among different cancer types. Furthermore, the data also includes important clinical annotations such as patient demographics, treatment regimens, and survival outcomes. This enables the correlation of molecular alterations with clinical variables and outcomes (The Cancer Genome Atlas Program (TCGA) - NCI, 2022). The TCGA data is categorised into three levels, with level 1 and level 2 data containing sensitive information like raw DNA-sequencing data, while level 3 data is publicly accessible and provides high-level summaries of gene expression (340). In the course of this research, the TCGA dataset was leveraged to discover new insights into the role of ABCC5 in cancer.

3.1.2 Functional Prediction via Homologous Proteins

Understanding the three-dimensional (3D) architecture of proteins is essential to delineate their functions and mechanisms (341). Predicting the 3D structure of a protein, especially when data from X-ray crystallography or NMR spectroscopy is unavailable, is challenging (342). Homology modelling, also known as comparative modelling, is a computational technique that aims to identify homologous proteins, which share common evolutionary ancestry and can be used to make predictions about the function, structure, and properties of target proteins (343). This method relies on the assumption that proteins with a similar sequence or structure are likely to perform similar functions. The first approach relies on the amino acid sequence of the target protein and initiates the modelling process by identifying a suitable template protein with a known structure, which is typically driven by sequence alignment tools such as BLAST or HMMER (344; 345). This approach is especially valuable when high sequence similarity between the target and template exists (346).

In contrast, the second method identifies homologous proteins based on similar 3D conformation with the target protein. To perform this type of analysis, having the structure of the target protein or a predicted structure is essential. This structural comparison often uncovers distant homology that is frequently overlooked in sequence-based comparisons (347). One such tool, the Distance-matrix Alignment for Structural Homology (DALI) server, has emerged as an important resource for exploring the functions of proteins by comparing their 3D structures (348; 83). Through the recent development of the neural network AlphaFold, the prediction of protein structures close to experimental accuracy has been enabled and an increasing number of protein structures are available including the predicted structure of ABCC5 (248). To gain a deeper understanding of ABCC5,

given the limited availability of experimental data, we employed functional prediction through structural homology modelling. This approach allowed us to explore potential connections between ABCC5 and the pathways previously identified in the TCGA dataset.

3.1.3 Aims

1. Investigate positively correlated co-expressed genes with ABCC5 in the TCGA dataset to understand the role of ABCC5 in cancer.

2. Examine the most promising correlated genes for ABCC5 and analyse their functional associations and pathways through gene ontology analysis.

3. Assess whether the involvement of pathways varies depending on ABCC5 expression levels, and identify indicators of differential pathways based on low or high ABCC5 expression.

4. Transfer initial findings and pathway associations to potential ABCC5 structural features by employing functional prediction via structural homologous modelling.

3.2 Results

3.2.1 Meta-analysis of Genes Correlating with ABCC5 from TCGA Datasets

The understanding of ABCC5's involvement in cancer is generally limited and typically does not extend beyond the observation that increased ABCC5 expression correlates with worse outcomes in different cancer types. The initial goal of this chapter was to perform a meta-analysis using transcriptomic data from the TCGA pan-cancer datasets to gain insights into the role of ABCC5. As outlined in **Figure 3.1 A**, genes that exhibited a positive correlation with ABCC5 expression and their respective Pearson correlation coefficients were retrieved across 31 different cancer types from the UALCAN database (316; 317). This analysis predominantly looks at genes that report a positive correlation with ABCC5 expression. This focus resulted from the observation that almost all datasets lacked genes with a negative correlation to ABCC5. The analysis identified 12,692 distinct genes that exhibited varying associations with ABCC5 across the 31 cancer datasets. Notably, most of these genes were observed in only 1-2 datasets, and genes with the highest average Pearson correlation were present in a relatively limited number of datasets as seen in **Figure 3.1 B**. The findings were refined to 137 genes by setting a threshold that genes had to be present in at least 10 different types of cancer and have at least a Pearson correlation coefficient of 0.5 with ABCC5. To further explore the potential functions associated with these 137 genes, we conducted a Gene Ontology (GO) term analysis. This analysis aimed to identify the most frequently associated biological functions and processes with ABCC5 through its correlated genes. The GO analysis revealed the most prevalent terms for molecular function, biological process, and cellular compartment. In the

molecular function category, we observed several highly significant terms, including DNA binding, Small Ubiquitin-like Modifier (SUMO)-specific endopeptidase activity, and ubiquitin-like protein-specific endopeptidase activity, among others.

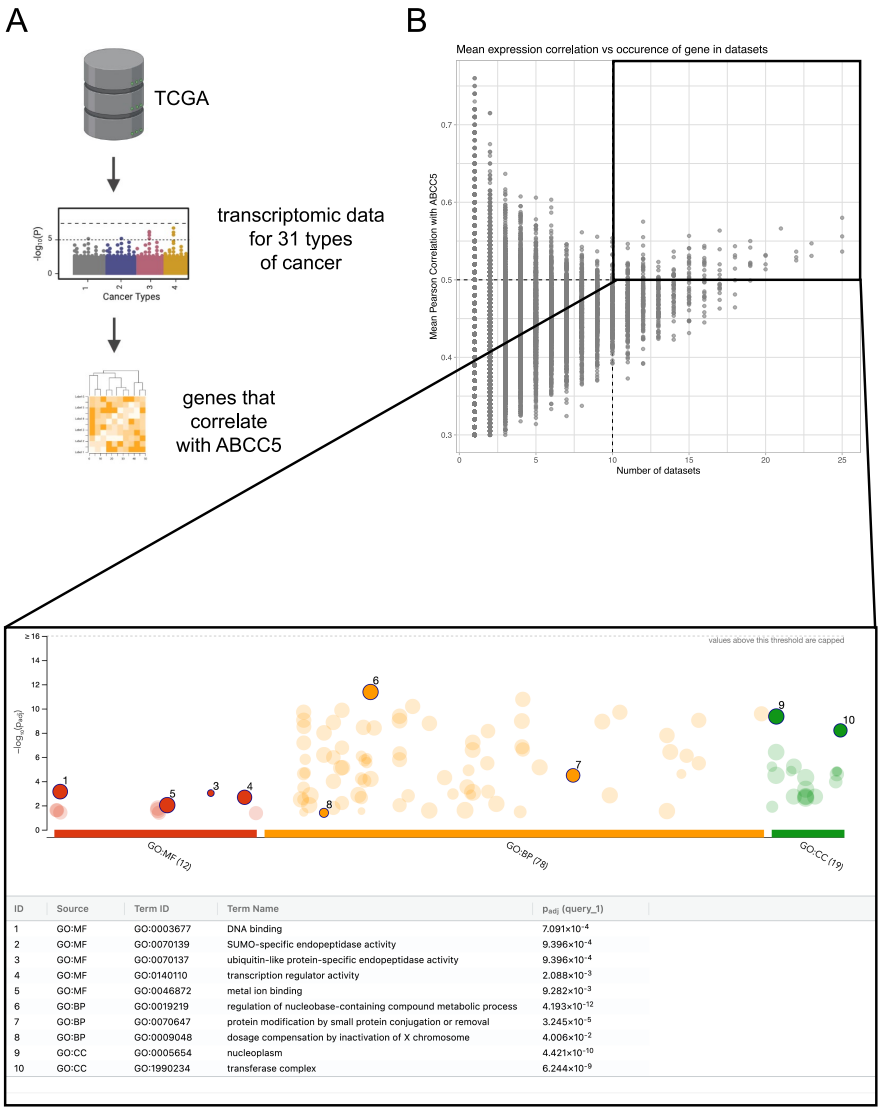

ID	Source	Term ID	Term Name	p_{adj} (query_1)
1	GO:MF	GO:0003677	DNA binding	7.091×10^{-4}
2	GO:MF	GO:0070139	SUMO-specific endopeptidase activity	9.396×10^{-4}
3	GO:MF	GO:0070137	ubiquitin-like protein-specific endopeptidase activity	9.396×10^{-4}
4	GO:MF	GO:0140110	transcription regulator activity	2.088×10^{-3}
5	GO:MF	GO:0046872	metal ion binding	9.282×10^{-3}
6	GO:BP	GO:0019219	regulation of nucleobase-containing compound metabolic process	4.193×10^{-12}
7	GO:BP	GO:0070647	protein modification by small protein conjugation or removal	3.245×10^{-5}
8	GO:BP	GO:0009048	dosage compensation by inactivation of X chromosome	4.006×10^{-2}
9	GO:CC	GO:0005654	nucleoplasm	4.421×10^{-10}
10	GO:CC	GO:1990234	transferase complex	6.244×10^{-9}

Figure 3.1: Meta-analysis of genes correlating with ABCC5 from TCGA datasets. **A)** Scatter plot illustrating the relationship between gene occurrence and mean Pearson correlation for all genes across all datasets. Created with BioRender.com. **B)** An overview of g:Profiler analysis for genes positively correlated with ABCC5 across all cancers, highlighting the significant GO terms.

In the biological processes category, notable terms included the regulation of nucleobase-containing compound metabolic processes, as well as processes related to protein modification, conjugation, or removal. Regarding cellular compartments, the most significant terms included the nucleoplasm and the transferase complex. To gain a deeper understanding, the respective terms for molecular function, biological process and cellular compartments were plotted separately as the initial analysis only highlighted the top terms. Therefore, to allow the identification of specific clusters the GO terms were analysed using the REVIGO tool. REVIGO reduces lists of GO terms by clustering similar terms together and by selecting representative terms for each cluster based on p-value and logsize. The colour (p-value) is a measure of the significance of the GO term in the analysis and darker colours refer to lower p-values. The point size (logsize value) represents the size of the GO term and relates to the number of genes that are associated with that term. As shown in **Figure 3.2**, the scatterplot visually represents the molecular function GO terms that exhibited statistically significant correlations with ABCC5. Upon examining the results, it becomes evident that the associated terms can be grouped into three overarching themes. The first theme encompasses terms related to cation, ion, and metal ion binding. The second theme includes terms associated with the regulation of transcription, such as DNA binding and transcription regulator activity. Finally, the third theme involves activity related to endopeptidases.

As shown in **Figure 3.3**, the scatterplot provides a visual representation of the biological process GO terms associated with ABCC5. Although a diverse range of terms is apparent, discernible clusters emerge. The most notable cluster encompasses processes involving histone modification, chromatin organisation, protein acylation, and modification by small protein conjugation or removal. Another cluster concerns the positive regulation of DNA-templated transcription. While

other terms are more widely dispersed, they can still be categorised under various facets of metabolic processes, including the involvement of nitrogen and cellular aromatic compounds.

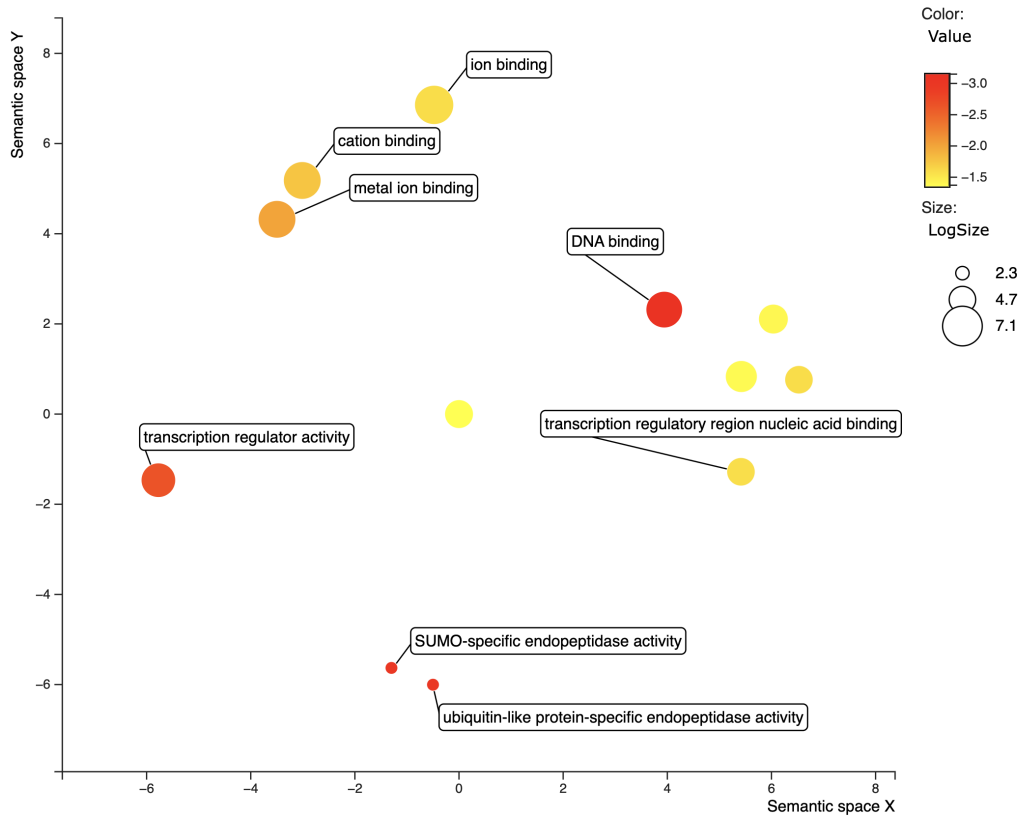

Figure 3.2: Scatterplot of GO terms for molecular function correlated with ABCC5 in multiple cancers. The most statistically significant points include the GO molecular function term. Colour (Value) reflects significance, with darker colours indicating higher statistical relevance. Size (LogSize) represents term extent, with larger points denoting associations with more genes, using logarithmic scaling for clarity.

As shown in **Figure 3.4**, the scatterplot shows the cellular compartment GO terms of the genes that displayed statistically significant correlations with ABCC5. Upon closer examination of the results, it becomes evident that, from a top-level perspective, the most significant cellular locations of the genes are intracellular or-

ganelles and the nucleus. Additionally, specific intracellular functional complexes such as the histone acetyltransferase complex, catalytic complex, and intracellular protein-containing complex are highlighted.

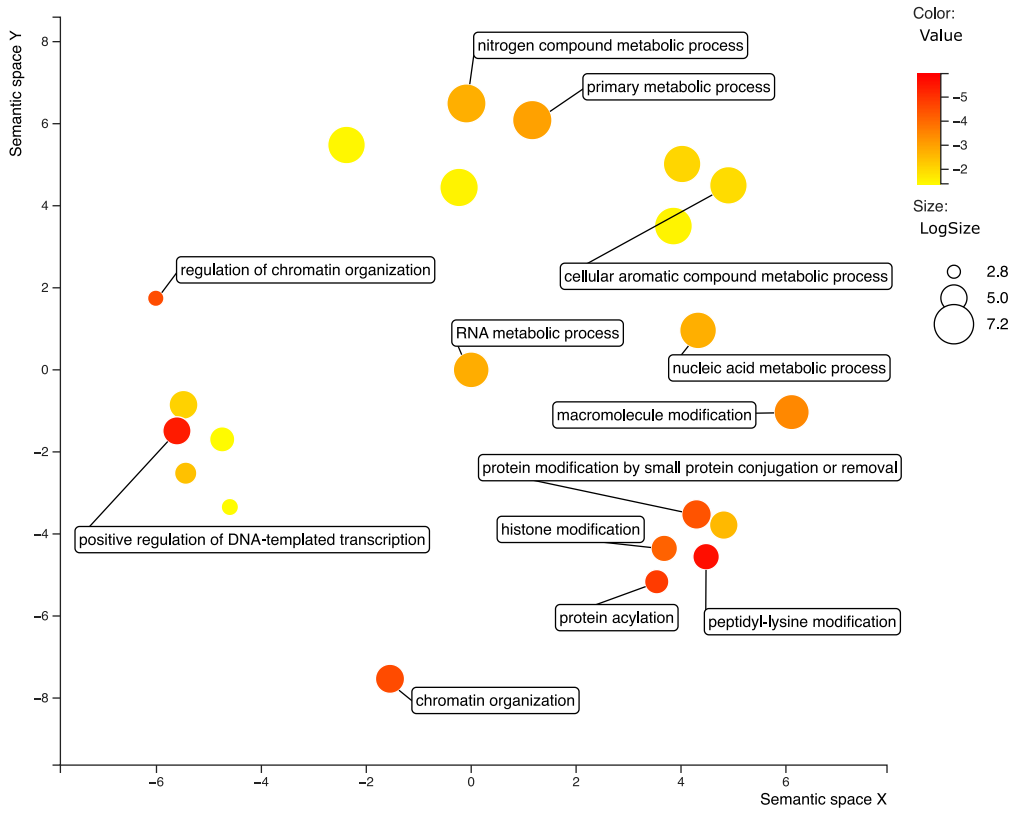

Figure 3.3: Scatterplot of GO terms for biological process correlated with ABCC5 in multiple cancers. The most statistically significant points include the GO biological function term. Colour (Value) reflects significance, with darker colours indicating higher statistical relevance. Size (LogSize) represents term extent, with larger points denoting associations with more genes, using logarithmic scaling for clarity.

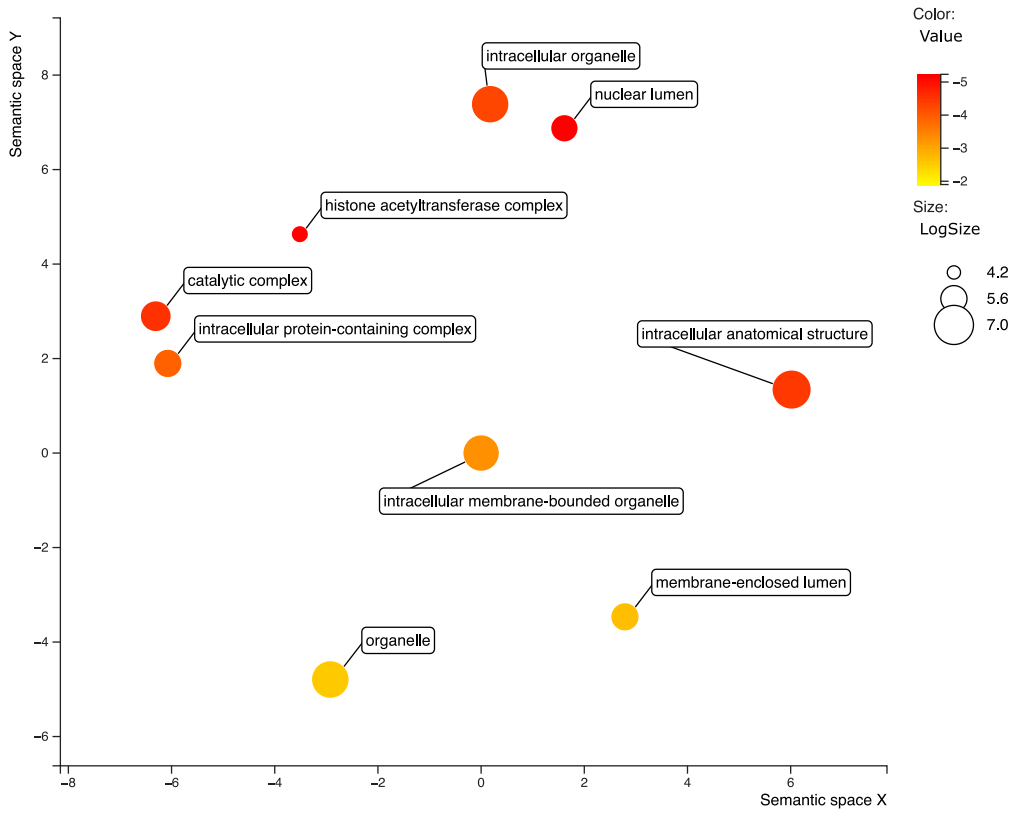

Figure 3.4: Scatterplot of GO terms for cellular compartment correlated with ABCC5 in multiple cancers. The most statistically significant points include the GO cellular compartment term. Colour (Value) reflects significance, with darker colours indicating higher statistical relevance. Size (LogSize) represents term extent, with larger points denoting associations with more genes, using logarithmic scaling for clarity.

3.2.2 ABCC5 Gene Expression Dependent Analysis

In this section, the dataset was stratified into three distinct groups based on the levels of *ABCC5* expression in tumour tissue compared to healthy tissue across the different cancer types as seen in **Figure 3.5**.

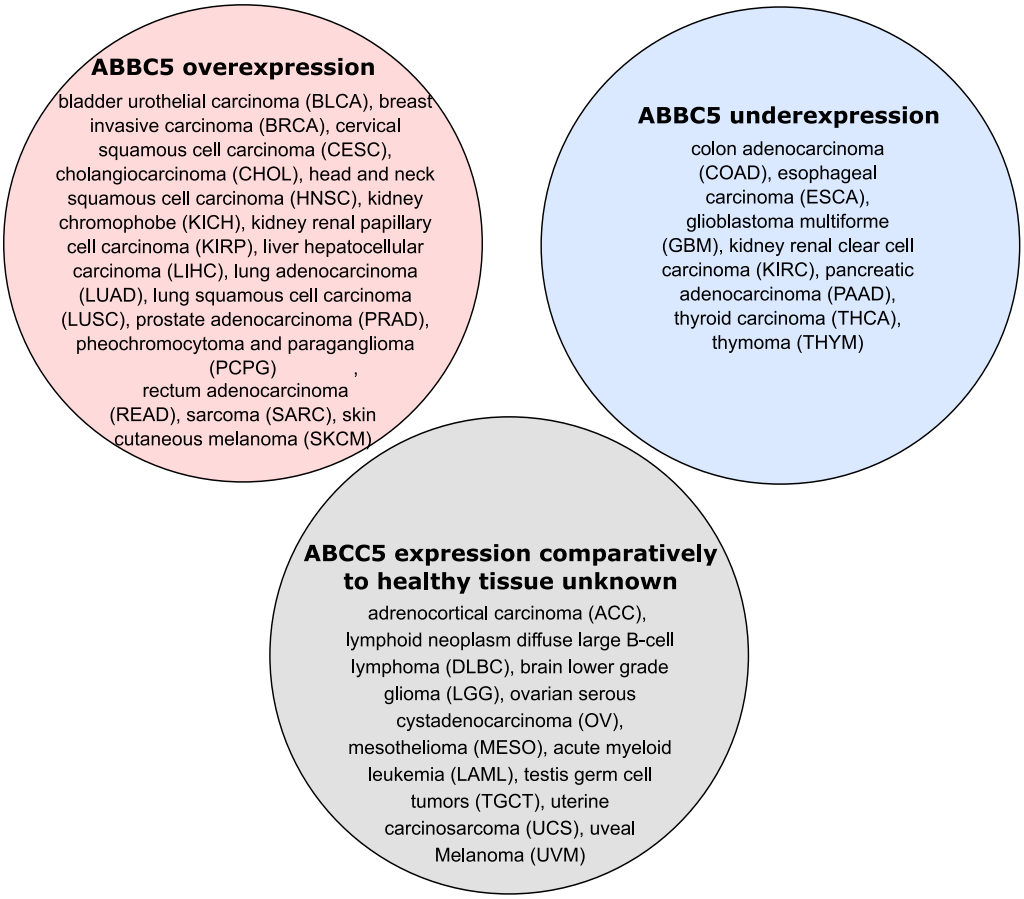

Figure 3.5: Venn diagram illustrating the distribution of cancer types according to *ABCC5* expression status in tumour and healthy tissue. Red: *ABCC5* overexpression in tumour tissue compared to healthy tissue; Blue: *ABCC5* underexpression in tumour tissue compared to healthy tissue; Grey: Uncharacterised expression status of *ABCC5* in tumour compared healthy tissue due to the absence of healthy tissue data.

Initially, the analysis considered the 12,692 genes identified in the first analysis, as depicted in **Figure 3.6 A**. This diagram effectively highlights the distinct and overlapping genes that positively correlate with *ABCC5* expression across the three groupings that depend on the relative expression of *ABCC5* in tumour compared to healthy tissue. Notably, it is intriguing to observe that the overexpression group comprises 1434 unique genes, while the underexpression group contains

980 unique genes. The majority of genes are shared across all three datasets, with 754 genes being shared specifically between the overexpression and underexpression datasets. It is worth noting that *ABCC5* overexpression is prevalent in approximately two-thirds of the cancer types with recorded comparative *ABCC5* expression levels.

Before further analysis, the Venn diagram gene data was reduced using the previous thresholds: genes that are present in at least 10 different cancer types and have a Pearson correlation coefficient of 0.5 or higher with *ABCC5*. Subsequently, heatmaps were created for both the overexpression and underexpression datasets, using the 137 genes that were most commonly observed across different cancer types as seen in **Figure 3.6 B** and **C**. It is intriguing to observe a consistent correlation between *ABCC5* and several genes across the over-and underexpression dataset. Notably, *DVL3* and *SENP5* show this correlation across both datasets and a wide spectrum of cancer types. Additionally, we find significant overlap in the expression patterns of *LOC220729*, *SLC25A36* and *VPS8*, across the datasets. The heatmap for the overexpression dataset (**Figure 3.6 B**) reveals that several genes, namely *DVL3*, *LSG1*, *MFN1*, *SENP2*, *SENP5*, *VPS8* and *TBL1XR1*, are consistently overexpressed across the majority of cancer types. Prostate adenocarcinoma (PRAD) specifically shares significant gene correlation overlap with head and neck squamous cell carcinoma (HNSC), sarcoma (SARC), liver hepatocellular carcinoma (LIHC), and exhibits similar patterns with rectum adenocarcinoma (READ). Equally, the most notable genes in the underexpression dataset (**Figure 3.6 C**) shared across all cancer types are *DVL3*, *SENP5*, *SLC25A36* and *VPS8*. Moreover, all the genes in the underexpression dataset are found in glioblastoma multiforme (GBM), colon adenocarcinoma (COAD), and pancreatic adenocarcinoma (PAAD).

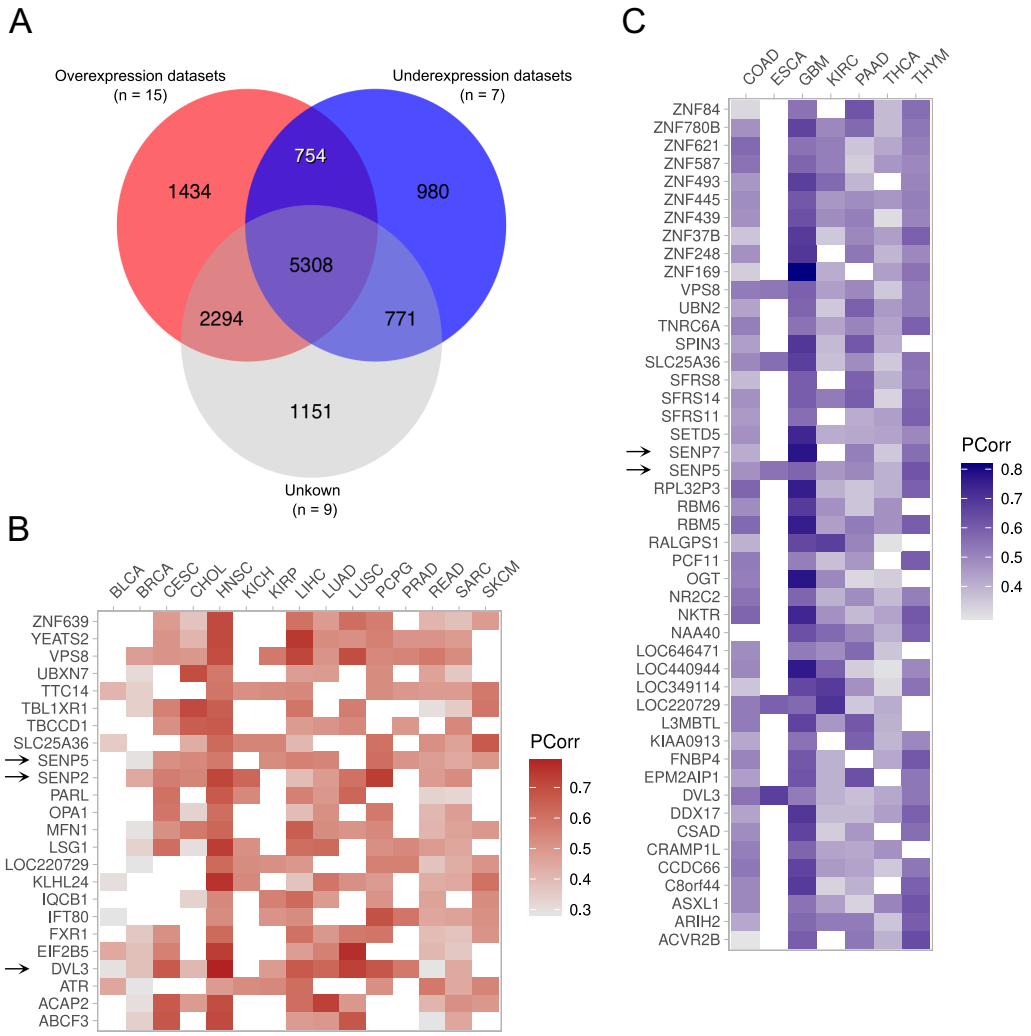

Figure 3.6: *ABCC5* expression-dependent gene clustering in tumour and healthy tissue reveals distinct molecular signatures. **A)** Venn diagram illustrating the gene overlap between three groups based on *ABCC5* expression in tumour versus healthy tissue. The groups comprise high expression of *ABCC5* in tumour tissue versus healthy tissue (overexpression dataset) (n=15), low *ABCC5* expression in tumour tissue versus healthy tissue (underexpression dataset) (n=7), and uncharacterised expression status of *ABCC5* in tumour compared healthy tissue due to the absence of healthy tissue data (unknown) (n=9). **B)** Heatmaps depicting the shortlisted genes in overexpression dataset. Heatmap represents Pearson correlation coefficient levels, with rows denoting genes and columns denoting individual cancer data based on cancer type (n=15). **C)** Heatmaps depicting the shortlisted genes in underexpression dataset. Heatmap represents Pearson correlation coefficient levels, with rows denoting genes and columns denoting individual cancer data based on cancer type (n=7).

Functional pathway analysis was conducted using the gene lists from the respective heatmaps to determine the significantly enriched GO terms. All of the genes displayed in the heatmaps fulfilled the previously used threshold so they were used for this analysis. The colour intensity of the bars in **Figure 3.7** represents the adjusted p-values of the enrichment, with darker colours indicating higher significance. **Figure 3.7 A** highlights the GO terms associated with the overexpression dataset, which primarily involve molecular function pathways related to endopeptidases and organelle/mitochondrial fusion. However, in **Figure 3.7 B**, which shows the underexpression dataset, a broader range of GO terms is observed. Notably, there are significant differences in the GO terms between the two datasets. The underexpression dataset features numerous terms related to transcription processes, spanning from transcription regulator activity to RNA polymerase II regulation. Additionally, this dataset includes biological process terms like RNA metabolic processes, nitrogen compound metabolic processes, and various biosynthetic processes. An interesting finding is that the GO terms "ubiquitin-like protein-specific endopeptidase activity" and "SUMO-specific endopeptidase activity" are the only terms shared between the overexpression and underexpression datasets. These findings reveal familiar terms as previously discovered. However, it is intriguing that underexpression of ABCC5 in cancer correlates with pathways related to transcription, while overexpression relates to fusion processes. Both datasets include SENP proteins that relate to the endopeptidase pathway, which was further investigated in the next section.

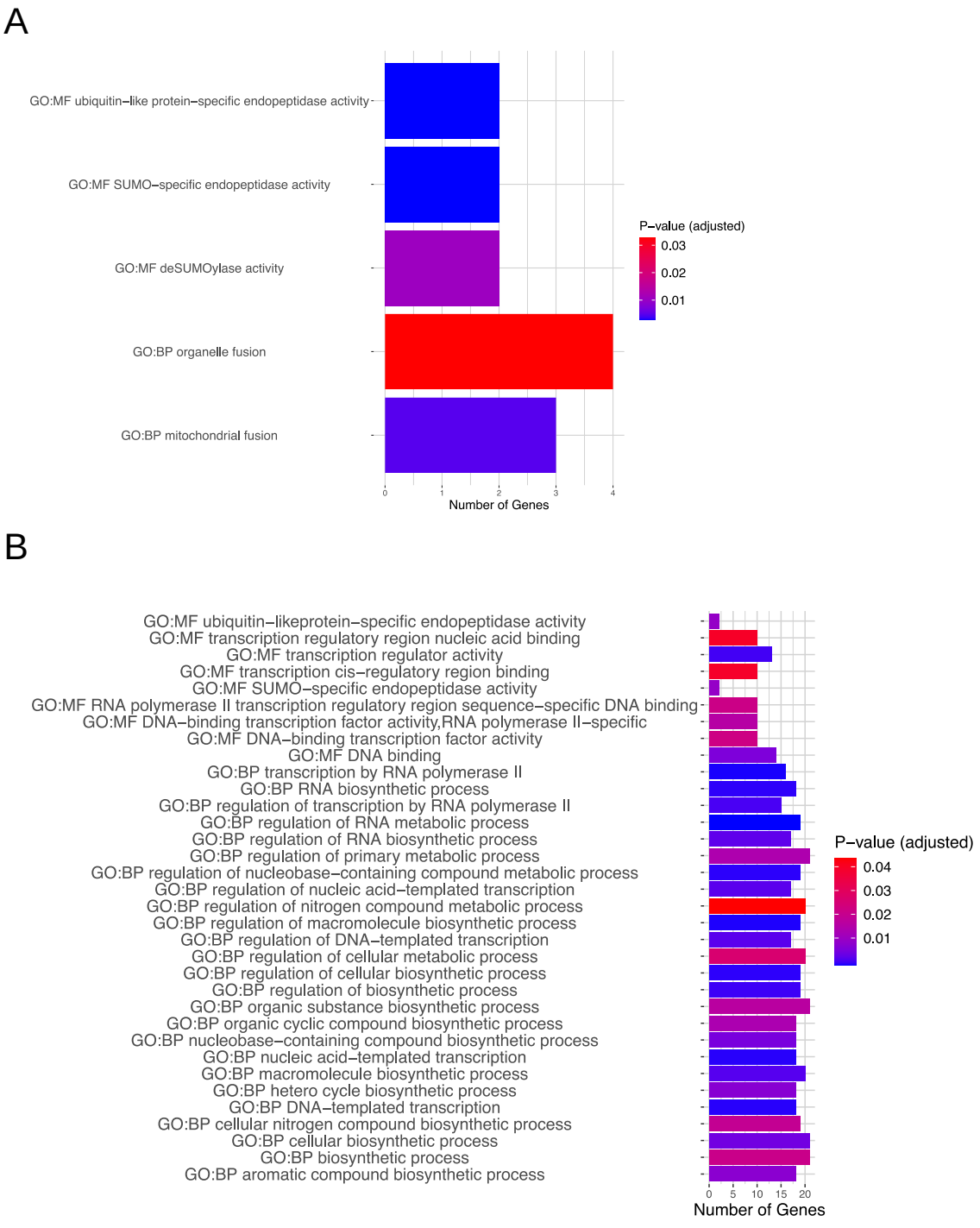

Figure 3.7: Functional Pathway Analysis **A)**Enriched Gene Ontology (GO) terms for genes positively correlated with ABCC5 in ABCC5-overexpressing cancer tissues **B)** Enriched GO terms for genes negatively correlated with ABCC5 in ABCC5 underexpressing cancer tissues.

3.2.3 Functional Prediction via Homologous Proteins

3.2.3.1 DALI Server Modelling against PDB Database

In the preceding section, our computational analysis unveiled pathways linked to a substantial number of genes that exhibit positive correlation with *ABCC5* expression. Consequently, it was of interest to explore whether the structural characteristics of ABCC5 could provide insights regarding its association with the identified GO functions. An important aspect of this idea is that the N-terminus of ABCC5 exhibits a distinctive length and composition, setting it apart from ABCC11, ABCC12, and other ABC transporters. To address this, the AlphaFold-predicted structure of ABCC5 was submitted to the DALI server, as shown in **Figure 3.8 A**, aiming to harness homologous proteins to identify structural features and their potential functionality. The results listed several human ABC transporters among the top hits, as one would anticipate due to the conserved nature of the nucleotide-binding domains (NBD) and the transmembrane structure of ABC transporters. Consequently, the results were refined to exclude close matches from the human ABC transporter family, thus directing the focus towards more distantly related homologous proteins.

The analysis yielded intriguing findings, revealing a diverse range of structurally similar proteins with enzymatic functions. In **Appendix A Figure A.1**, a sequence alignment is presented, highlighting the significance of a conserved catalytic cysteine residue across most of these proteins. The proteins in this study include exodeoxyribonuclease (E8PLM2), endopeptidase La (C9DRU9), bacteriocin-type signal sequence-containing protein (A3DCU2), excinuclease ABC subunit UvrA (Q0X0A9), excinuclease ABC subunit A (Q9RYW8), and nuclease SbcCD (P13458). This observation highlights a fascinating structural overlap between proteins possessing enzymatic functions and the N-terminus of ABCC5. Besides the cysteine

discovery, the amino acid alignment of the N-terminus showed relatively low similarity between the proteins.

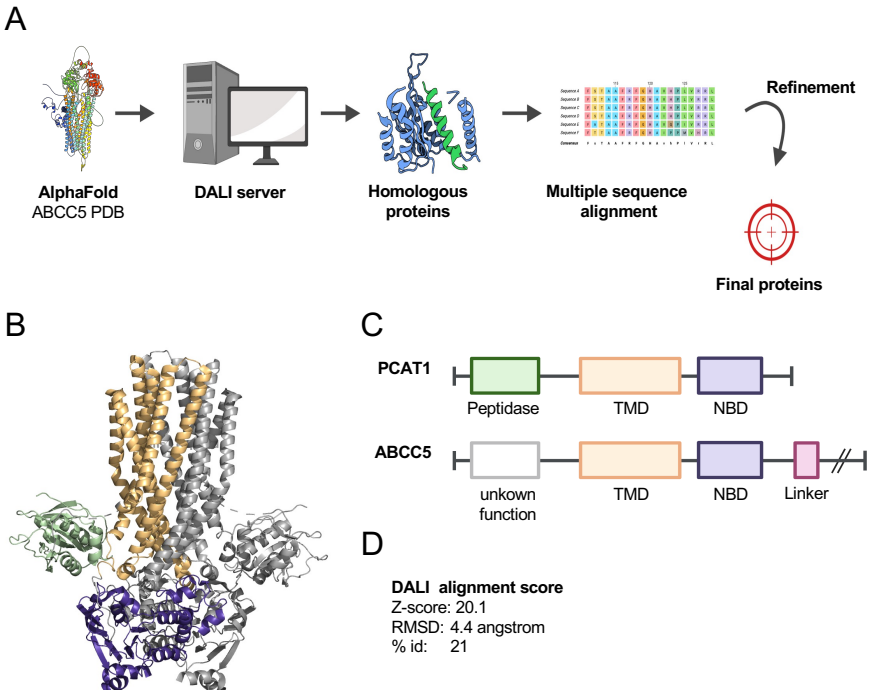

Figure 3.8: Comparative analysis of homologous proteins to ABCC5 for functional inference. **A)** Overview of the workflow employed to identify homologous proteins to ABCC5. The process involved refining the candidate proteins through multiple sequence alignment, ultimately leading to the selection of target proteins for further investigation. **B)** Structure of a highly promising homologous protein, PCAT1. **C)** Graphical comparison of key domain alignment between PCAT1 and ABCC5. **D)** Scores extracted from the DALI server alignment of ABCC5 and PCAT1. The scores include z-score, Root Mean Square Deviation (RMSD), and sequence identity. Z-score: amount of standard deviations a data point is from the mean. RMSD: average distance between corresponding data points in two sets. %ID: percentage of structural identity or similarity between a protein structure and another structure. Created with BioRender.com

The in-depth analysis highlighted another protein, peptidase-containing ATP-binding cassette (ABC) transporter 1 (PCAT1), as a promising candidate **Figure 3.8 B**. The protein showed the highest values across all match evalua-

tion scores including a sequence identity score of 21% and a z-score of 20.1. Peptidase-containing ABC transporters are a group of membrane proteins found in bacteria that are involved in the transport of peptides and peptide-like molecules across cell membranes (349; 350). These ABC transporters contain a peptidase domain in the cytoplasm which can cleave the transported peptides into smaller fragments, which are then transported into the cell (351). In the analysis, a significant alignment was observed between the N-terminus of ABCC5 and the peptidase domain located at the initial part of PCAT1's N-terminus as seen in **Figure 3.8 C**. After discovering the striking resemblance between the N-termini of PCAT1 and ABCC5, a comprehensive sequence alignment analysis was conducted. In **Figure 3.9**, we assessed whether the essential catalytic residues are identical in both proteins. The peptidase function is modulated through a catalytic triad consisting of residues C21, H99, and D115 (352). Interestingly, just as in the previous alignment, the key catalytic cysteine is identical between the two proteins. While there are differences relating to PCAT1 position H99 and D115. When examining the binding site residues one can observe that there is an identical glycine while the other two binding site residue differ between ABCC5 and PCAT1.

3.2.3.2 Alignment of ABCC5 and PCAT1

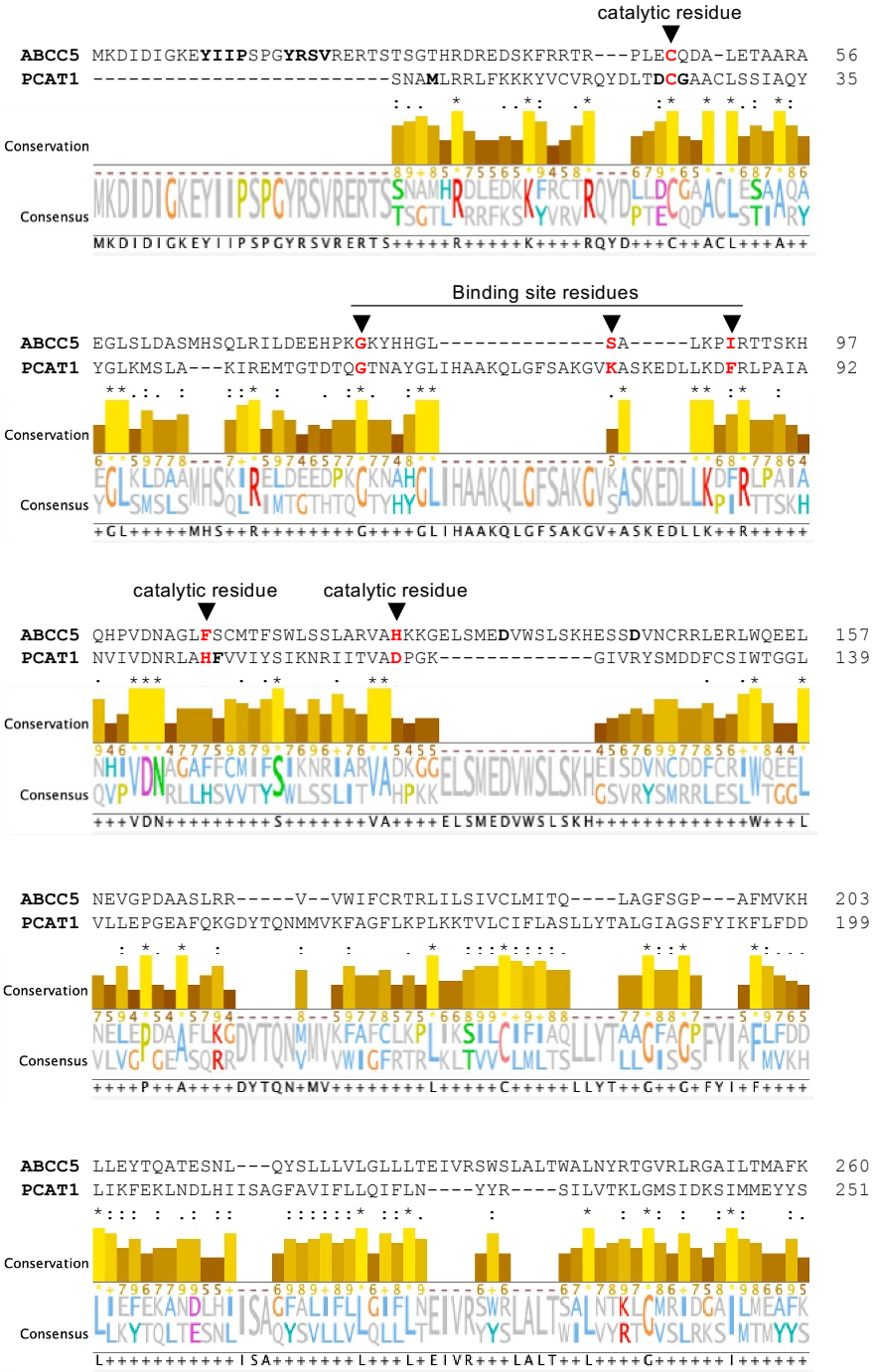

Figure 3.9: Sequence alignment of PCAT1 (PDB: 7T54_1) and ABCC5 with Clustal Omega. Relevant sequence elements are highlighted.

3.2.3.3 DALI Server Modelling against AlphaFold Database

To better understand the relationship between ABCC5 and distantly homologous proteins, an alternative analysis method was employed. This method involved investigating homologies by utilising AlphaFold's structural database instead of relying on screening against the established structures in the PDB database. The prior discovery involving PCAT1 emphasised the importance of exploring the alignment between ABCC5 and distantly related proteins within the bacterial family. As a result, another structural alignment analysis was conducted against *E. coli* AlphaFold structural database to identify potential novel alignments. This investigative approach led to interesting results in which two ATP-binding permease proteins, CYDC and CYDD, ranked among the top three hits. The resulting z-scores obtained were significant, especially when compared to self-alignment or alignment with human ABCC11 and ABCC12 as seen in **Table 3.1**. In the case of CYDC and CYDD, these two ATP-binding permease proteins form a heterodimer to enable transport of substrates relevant in the heme pathway (353). This data provides valuable insights into the potential relationships between ABCC5 and these bacterial proteins.

Table 3.1: Homology modelling hits of ABCC5 against human and *E. coli* AlphaFold structural database. LALI (Lateral Alignment Index): An index that quantifies the similarity between two protein structures by aligning them laterally. NRes (Number of Residues): The count of amino acid or nucleotide building blocks in a biological sequence.

Human ABCC5 against *E. coli* AlphaFold database						
Chain	**Z-score**	**rmsd**	**lali**	**nres**	**%id**	**PDB Description**
essr-A	31.5	3.9	563	573	19	ECOLI:AF-P23886-F1 ATP-BINDING/PERMEASE PROTEIN CYDC
etpc-A	31.4	5.4	497	582	23	ECOLI:AF-P60752-F1 ATP-DEPENDENT LIPID A-CORE FLIPPASE
etv6-A	30.6	3.3	569	588	17	ECOLI:AF-P29018-F1 ATP-BINDING/PERMEASE PROTEIN CYDD
Human ABCC5 against human AlphaFold database						
Chain	**Z-score**	**rmsd**	**lali**	**nres**	**%id**	**PDB Description**
e7l9-A	51.4	0.0	1436	1437	100	HUMAN:AF-O15440-F1 MRP5
fa2p-A	44.6	2.8	1283	1359	46	HUMAN:AF-Q96J65-F1 ABCC12
e8h6-A	43.5	2.5	1242	1382	42	HUMAN:AF-Q96J66-F1 ABCC12

Given the structural similarity observed between ABCC11 and ABCC12, the investigation was extended to assess whether a structural search would yield analogous hits for these two proteins when subjected to screening against the *E. coli*

AlphaFold database. This additional step was included to ascertain the specificity of the hits and that we did not observe generic matches applicable to structurally similar proteins to ABCC5. **Appendix A Table A.1** clearly illustrates that the screening results for ABCC5 are unique to ABCC5, with distinct outcomes observed for its paralogues. Therefore, in the next step the three top hits of the E. coli screen as seen in **Table 3.1** were analysed. Interestingly, the second most similar protein msbA requires a copper motif for its functionality which ABCC5 does not contain hence, msbA was not followed upon in greater detail (354). The subsequent analysis focused on the leading candidate, CydC, which exhibited the highest z-score. A structural alignment for CydD was omitted because both CydC and CydD align with the same structural aspect of ABCC5. Consequently, CydC was chosen for modelling due to its better structural compatibility. **Appendix A Figure A.2** shows the structural alignment between CydC and ABCC5, showcasing the similarity between their structural features which focuses on the transmembrane and NBD regions. Additionally, we also did a sequence alignment to look at important functional residue overlaps which is shown in **Figure 3.10**. The functionally important residues of CydC are highlighted in red in the alignment. Important residues that have been shown in molecular dynamic simulations to interact with heme include K3, K7, R77 R81, H85, R136 (355) and it is apparent that ABCC5 does not overlap within those areas. However, it has to be considered that structural alignment does not necessarily equal sequence similarities.

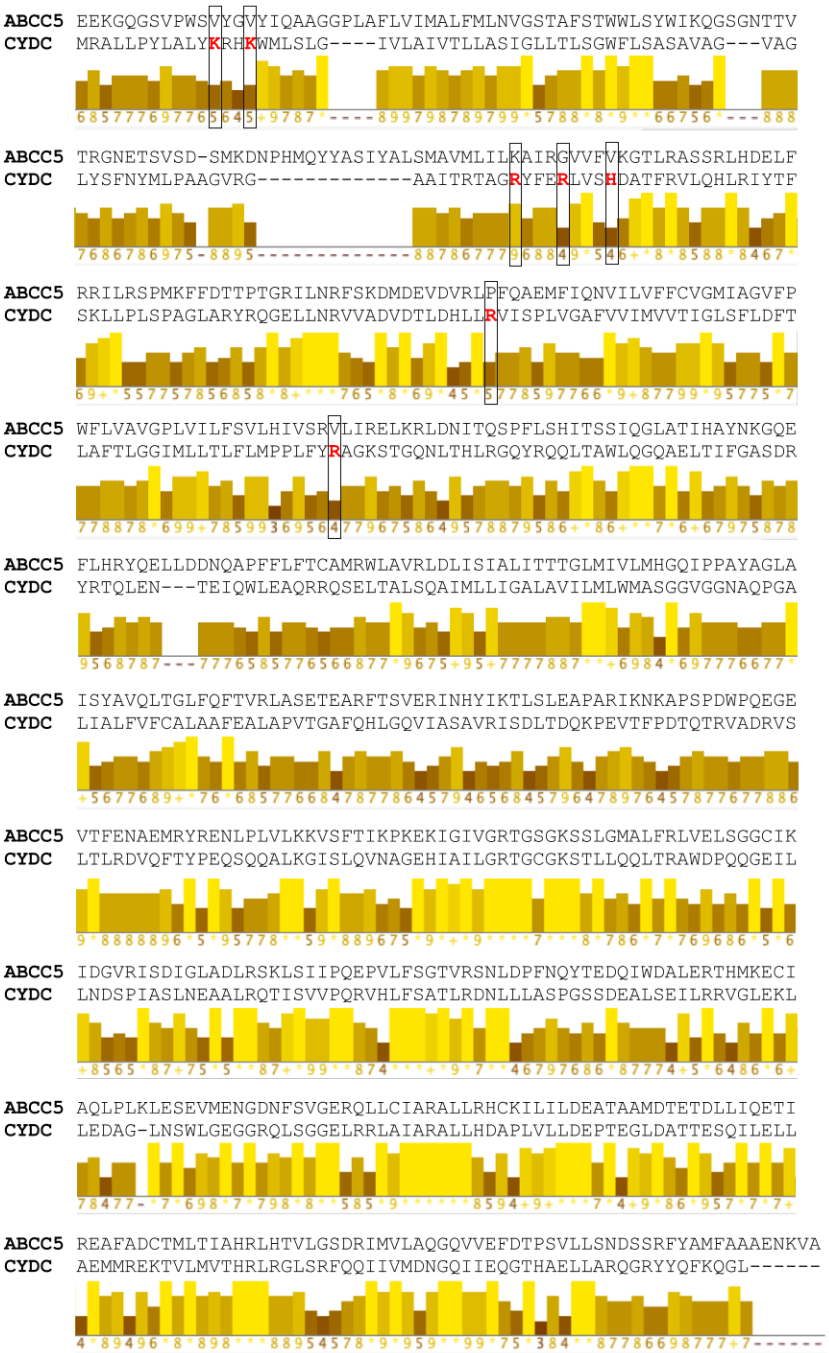

Figure 3.10: Sequence alignment between ABCC5 (human) and CydC (*E. coli*) (PDB: essr). Important heme coordinating residues are highlighted in red.

3.3 Discussion

3.3.1 ABCC5's Connection to the SUMO-specific Endopeptidase Pathway

The SUMO-specific endopeptidase pathway involves a group of enzymes and proteins that regulate the post-translational modification of proteins with Small Ubiquitin-like Modifier (SUMO) proteins (356). The SUMO-specific enzymes E1, E2, and E3 are responsible for catalysing the process of SUMOylation which entails attaching SUMO proteins to target proteins. On the other side of this pathway, Sentrin/SUMO-specific proteases (SENP) are in charge of deconjugating these SUMO-protein complexes (357). The SENPs are categorised into three families based on their substrate preferences. SENP1 and SENP2 are primarily located in the nucleus and deconjugate any of the SUMO isoforms, including SUMO-1, -2, and -3 (358; 359). Meanwhile, SENP3 and SENP5 preferably cleave SUMO-2/3 and localise to the nucleolus (360; 361). SENP6 and SENP7 also prefer SUMO-2/3 as substrates. Notably, they vary in their structure by having an additional loop within their catalytic domain and mainly locate to the nucleoplasm (362; 363).

SENPs cleave the isopeptide bond formed between the glycine residue of SUMO and the lysine side chain of target proteins by recognising a Gly-Gly motif (362; 364). The SUMO-specific endopeptidase pathway has shown significant relevance in the analysis of genes positively correlated with ABCC5. Notably, interesting findings show the correlation of specific SENPs with ABCC5 expression in different tumour scenarios. Specifically, SENP2 and SENP5 exhibited correlations with ABCC5 expression in tumours where ABCC5 was overexpressed (**Fig. 5.4**). On the other hand, SENP5 and SENP7 were correlated with ABCC5 ex-

pression in tumours where ABCC5 was underexpressed (**Fig. 5.4**). Remarkably, SENP5 demonstrated a correlation with ABCC5 across both datasets.

SUMOylation is a reversible modification which can modify the function, localisation, or stability of the target protein, and it plays a crucial role in various cellular processes, including gene expression, chromatin remodelling, DNA repair, and cell cycle regulation (365; 366; 367). The GO molecular function terms identified, including transcription factor activity, DNA binding, and RNA Polymerase II activity, closely correspond to the cellular pathways in which SENPs play a crucial role. Furthermore, SUMOylation can block the dimerisation of FOXM1 which is a transcription factor that peaks during the G2 and M phase of the cell cycle (368). It is particularly noteworthy that FOXM1 also functions as a transcription factor for ABCC5, adding another layer of complexity which could suggest a role of ABCC5 in the cell cycle (291). Interestingly, SENP5 is essential for cell cycle progression during mitosis and cytokinesis, and the removal of SENP5 resulted in inhibition of cell proliferation (360).

During the process of mitosis, SENP5 relocates to the mitochondria and deSUMOylation of mitochondrial proteins is essential for mitochondrial fragmentation (369). It is intriguing to observe that, in the overexpression dataset, GO-terms related to mitochondrial fusion and organelle fusion are noted. This could suggest a potential link between SENP5's relocation during mitosis and its role in regulating mitochondrial dynamics. The overexpression dataset also reported the protein MFN1 which is a key protein in mitochondrial fusion, and it has been shown that SUMOylation of MFN1 alters mitochondrial localisation (370; 371). Therefore, GO terms reported for both datasets can be related to the involvement of SENPs; however, it is unclear how exactly ABCC5 relates to SENPs. Several types of cancer have increased activity of SUMOylation and deSUMOylation which could be caused by their enhanced metabolic requirements (372). SENP1 expression cor-

relates with the aggressiveness and proliferation potential in breast and prostate cancer (373; 374). Meanwhile, overexpression of SENP3 is associated with enhanced differentiation in oral squamous cell carcinoma (375). SENP5 overexpression promotes tumorigenesis in hepatocellular carcinoma and differentiation in oral squamous cell carcinoma (376; 377). In conclusion, further investigation is essential to uncover the details of the connection between ABCC5 and the SUMO-specific endopeptidase pathway. However, a noteworthy observation is that the expression of SENPs is closely associated with ABCC5 expression in a significant proportion of the cancers within the TCGA database. This correlation suggests a potential interplay between these elements and highlights the relevance of exploring this relationship in the context of cancer biology.

3.3.2 Does ABCC5 have a Potential Enzymatic Function?

Remarkably, following the initial association of ABCC5 with the SUMO-specific endopeptidase pathway, structural homology modelling raised the intriguing possibility of a peptidase function within the N-terminus of ABCC5. Notably, the N-terminus sequence of ABCC5 stands out as distinctive when compared to ABCC11 and ABCC12, which lack a portion of the initial segment. The preservation of the primary catalytic cysteine, not only between PCAT1 and ABCC5 but also among several other enzymes identified in the analysis, is an intriguing observation. This shared characteristic strongly suggests that ABCC5 likely possesses some form of enzymatic functionality. PCAT1 contains an entire peptidase domain and belongs to the C39 family which are bacteriocin-processing peptidases (349; 350). Binding of the leader peptide to PCAT1 induces conformational changes, enabling specific protease activity which is inhibited by ATP hydrolysis (378). Post-processing, these changes guide the peptide into the translocation pathway. Unlike conventional ABC transporters, the substrate binding of PCAT1

doesn't trigger ATP hydrolysis, leading to reduced ATPase activity and promoting substrate translocation (379; 378).

To understand whether ABCC5 could have similar peptide functionality, similarities between the important functional residues were investigated. In the context of the catalytic residues 2 and 3, we observe notable differences, with phenylalanine substituting for histidine and histidine replacing aspartic acid. While the presence of a second histidine in position 3 might compensate for the absence of histidine in position 2, the structural impact of phenylalanine is significant. The aromatic ring structure can introduce substantial structural changes, thereby influencing the shape and chemical properties of the catalytic site (380). Histidine as well as aspartic acid can act as proton donors or acceptors in enzymatic reactions hence alterations can have a significant impact (381; 382). There are also variations in the binding site residues between ABCC5 and PCAT1 (**Fig. 3.9**). Although the first residue is identical, the replacement of lysine with serine at Residue 2 introduces a smaller, uncharged amino acid. This substitution raises the possibility of altering the electrostatic interactions and hydrogen bonding capabilities within the binding site. The replacement of isoleucine with phenylalanine at Residue 3 introduces a larger, aromatic side chain. This might lead to changes in the shape and hydrophobic properties of the binding pocket, which could impact substrate binding affinity (380). These complex alterations suggest that the binding site has evolved to potentially interact with a different substrate or ligand.

Such differences are not uncommon in the field of homology modelling as evolution can result in changes in amino acid sequences. Given the highlighted terms from the initial GO term analysis, it's particularly intriguing to note the pathways associated with histone modification, chromatin organisation, protein acylation, and modification through small protein conjugation or removal at the biological process level. Additionally, the presence of terms like catalytic complex and his-

tone acetyltransferase complex further accentuates this connection. Consequently, exploring the option of whether ABCC5 is involved in a catalytic complex related to the mentioned biological process could provide an interesting avenue. Further, it would be interesting to see whether certain amino acid residues in the N-terminus of ABCC5 overlap with functional entities in the mentioned pathways. Ultimately, from a functional standpoint, it's challenging to conclude without experimental data or more detailed structural information. To confirm the function of the N-terminus of ABCC5, experimental studies and more comprehensive structural analyses are necessary.

3.3.3 ABCC5 Involvement in Heme Transport

Following the initial identification of PCAT1, a bacterial protein, we conducted a comprehensive examination of the *E. coli* Alphafold structural database. Unexpectedly, our structural homology modelling reported a structural alignment between ABCC5 and the ATP-binding permease proteins CydC and CydD. Both, CydC and CydD exhibit a high level of sequence similarity and form the heterodimeric CydDC complex (383). The CydDC complex is essential for the assembly of cytochrome bd which is a triheme oxidase (384). The substrates and exact mechanism however have been a matter of debate and contradicting research. Initially, the CydDC complex was thought to be the only glutathione (GSH) and cysteine exporter in *E. coli* (385). Then a study suggested that ATP hydrolysis is modulated by heme while some even suggested that CydDC transports heme (386). However, other studies suggested that the main function is the maintenance of reduced-state cytoplasmic-L-cysteine (387), whilst a further study suggested that CydDC can export GSH but is not the only exporter of GSH (388).
Two recent studies were able to confirm that CydDC can transport heme through a series of cryo-EM structures across the translocation process. This data was fur-

ther supplemented with extensive molecular dynamic simulations (355; 389). The DALI alignment shows that the structural elements of ABCC5 align with the structural elements of CydC and CydD. This discovery is particularly intriguing, as it suggests a potential link between ABCC5 and heme transport. However, structural alignment alone is not sufficient to conclude that ABCC5 has a similar function to CydDC. Generally, there is high sequence similarity on the amino acid level between the proteins, but not necessarily for the residues involved in heme transport. Notably, previous research on ABCC5 has already hinted at the possibility of its involvement in heme transport. Studies in *C. elegans* proposed ABCC5 acts as a heme transporter as ABCC5 KO resulted in heme deficiency and embryonic lethality as the organism requires external heme for survival (223; 390).
However, another study reported that *C. elegans* depends on both vitamin B12 and heme for survival and the high concentrations used in the previous experiments increased membrane permeability, therefore allowing both heme and vitamin B12 to pass through. The study showed that vitamin B12 injections at physiological concentrations were able to rescue embryonic lethality and that ABCC5 KO prevented the rescue, hence, proposing ABCC5 as a vitamin B12 transporter (239). A study in *D. melanogaster* showed that transfection with human ABCC5 was able to rescue lethality based on heme accumulation upon CG4562 knockdown and proposed CG4562 as the functional counterpart of ABCC5 (240). A recent study in mice was able to show that loss of ABCC5 and its paralogue ABCC12 resulted in altered mitochondrial homeostasis and defective sperm. The study proposed the defective heme transport as the reason but also acknowledged that other substrates could be responsible (224). Ultimately, this highlights the current debate around the substrates of ABCC5 and its physiological role. Further experiments, specifically mutagenesis studies, will be necessary to delineate whether heme could be transported by ABCC5 and which residues would be responsible

for binding heme.

3.4 Summary and Limitations

This chapter has unveiled a previously unknown connection of ABCC5 to the SUMO-specific endopeptidase pathway across different types of cancer. Further investigation is necessary to understand the precise relationship between ABCC5 and the SUMO-specific endopeptidase pathway. However, the strong correlation between the expression of SENPs and ABCC5 in cancer cases from the TCGA database indicates an intriguing interplay between these elements, emphasising the importance of exploring this relationship in the context of cancer biology. While our analysis has found links, it's important to note that our findings come from just one large database. This database may have its limitations like data biases and varying data quality. However, due to the lack of alternatives at this scale, it serves as a valuable starting point.

While our results identified this correlation, there is no mechanistic insight into how these relationships function at the molecular level. More in-depth research is needed to understand the underlying mechanisms that should include initial studies utilising qPCR and western blot. While this was an interesting finding, it became even more intriguing to observe the similarity between the peptidase domain in PCAT1 and the N-terminus of ABCC5. In summary, the structural similarity and the high DALI server hit with PCAT1 are promising indicators that the N-terminus of ABCC5 might have some functional significance. However, these findings should be viewed as a starting point for further investigation. The upcoming chapter will centre on investigating ABCC5's role in prostate cancer, with a primary objective of assessing the significance of the findings presented in this chapter and unearthing any novel discoveries. Additionally, we will delve

deeper into key topics introduced earlier in this chapter, specifically examining the pathways related to histone modification and protein acylation and their potential relationship with ABCC5, which have been touched upon but not yet comprehensively discussed.

4 | Exploring Co-Expressed Genes of ABCC5 in Human Prostate Cancer: Discovering Diverse Functional Pathways and Potential Transcription Factors

4.1 Introduction

4.1.1 Preclinical Challenges Investigating Prostate Cancer

Prostate cancer cell lines

Prostate cancer (PCa) is challenging to study due to its high prevalence, heterogeneity, and clinical course that ranges from indolent to highly aggressive forms (391; 392). Specifically, conducting research on PCa in the laboratory is difficult regarding the selection of suitable models (393). Due to the mentioned disease heterogeneity and progressiveness across different stages, it has proven very difficult to develop new PCa models from human or mouse tissue as the models often grow poorly and inconsistently <(394; 395). PCa cell lines are classified based on diverse characteristics, including their site of origin, histopathology, and androgen dependency status, while considering additional factors like genetic mutations such as TP53, PTEN and androgen receptor (AR), drug sensitivity, and metastatic potential (396; 397; 28). The majority of PCa preclinical studies are conducted with LNCaP and PC-3 cells but more than 30 PCa cell lines have been established (398; 399; 400). This study utilised LNCaP and PC-3 cells to investigate the role of ABCC5 in PCa as seen in **Figure 4.1 A**. The colour scheme used in this figure is used throughout this thesis and labels LNCaP results in or-

ange and PC-3 results in blue. LNCaP cells were established from a biopsy of a metastatic PCa lesion of a supraclavicular lymph node of a white male. The cells are androgen-sensitive, express mutated ARs which have an enhanced steroid-binding capacity, and prostate-specific antigen (PSA) (401; 402). Considering the popularity of LNCaP cells several derivatives have been established to investigate tumour progression and androgen response (403). In contrast, PC-3 cells were isolated from lumbar vertebra PCa metastasis of a 62-year-old white male and are androgen-independent (404). The characteristics of PC-3 cells are those of poorly-differentiated adenocarcinoma and they are an adequate model of the most aggressive forms of PCa (405). LNCaP and PC-3 cells were chosen for our investigation of ABCC5 in PCa, as high ABCC5 expression is known to be associated with advanced/metastatic PCa, as shown in **Chapter 1**. Therefore, these cell lines were deemed to be the most appropriate models for delving into the precise mechanisms involved. **Figure 4.1 B** presents the transcriptomic analysis of patient samples from various PCa stages, categorised based on their proliferation and androgen receptor status (307). The transcriptomic profiles of LNCaP (orange) and PC-3 cells (blue) were added to assess how they compare with patient samples. Other commonly used cell lines include DU145, which, similar to PC-3, is androgen-independent (406). Additionally, 22RV1 and VCaP cells present altered androgen receptor states, making them valuable for investigating androgen signalling (407; 408). For the study of early-stage PCa, researchers typically use RWPE-1 cells, derived from benign hyperplastic prostate tissue (409).

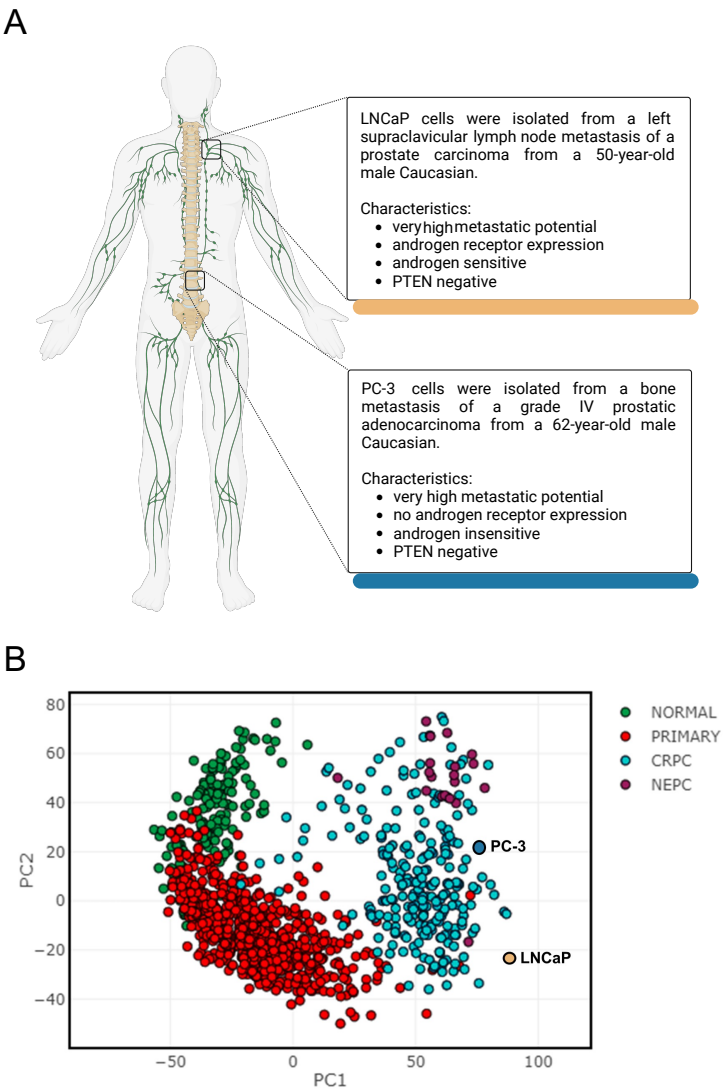

Figure 4.1: Overview of the prostate cancer (PCa) cell line characteristics used in this study. **A)** Site of origin of the respective PCa cell lines and their characteristics regarding molecular markers of PCa (333). Created with BioRender.com **B)** Principal component analysis (PCA) of pan-prostate cancer transcriptomes obtained from human studies of normal (green), primary (red), castration-resistant (CRPC, cyan), and neuroendocrine PCa (NEPC, purple). PC1 correlates with enhanced proliferation, whilst PC2 negatively correlates with canonical androgen receptor (AR) signalling. The transcriptome profiles of LNCaP (orange) and PC-3 cells (blue) were placed accordingly. Adapted from https://www.pcaprofiler.com/.

Prostate Cancer Mouse Models

Unlike some other types of cancer, PCa does not spontaneously develop in mice, which necessitates the development of mouse models that can recapitulate key aspects of human PCa (410). Genetically Engineered Mice (GEM) were developed to reflect different aspects of PCa development. The first models included the TRAMP and LADY models which were based on the expression of viral oncogenes. Both models are limited by the speed and type of tumour development as they rapidly develop neuroendocrine PCa which is not reflective of the majority of human metastatic disease (411). Enhanced models were developed by employing approaches like inducing Myc overexpression and utilising knockout mice for pivotal genes such as PTEN, Nkx3.1, and TP53. These strategies better emulate the genetic characteristics of human PCa (412; 413; 414; 415). Modelling the spontaneous development of bone metastasis is a significant obstacle when researching PCa in GEM (416), and although some models have been developed, this remains challenging. Xenograft models, on the other hand, avoid the need for GEM. Instead, they use human PCa cell lines or patient-derived xenografts , which are transplanted into immunocompromised mice (417; 418). This approach allows researchers to work with actual human tumour cells, which offer insights into the effects of potential therapeutic agents on human PCa (419; 420). However, there are limitations such as the absence of a functional immune system in the host mice which makes it challenging to assess the interplay with the immune system. The graft can also lose tumour heterogeneity and the stromal tumour environment can be replaced with mouse cells, removing an important layer of the microenvironment (421; 420).

4.1.2 Transcriptional Regulation

Transcription factors (TF) play a crucial role in controlling gene expression by their unique capacity to identify specific DNA sequence patterns located in regulatory regions, referred to as cis-elements (422; 423). The regulation of gene expression involves a complex interaction among cis-regulatory components, including core promoters, elements close to promoters, and various distant cis-regulatory modules (424; 425). These regulatory elements include enhancers, which are capable of acting across extensive genomic distances, and silencers, which repress gene activity (426; 427). Insulators are another crucial element; they prevent inappropriate interactions between chromatin domains (428). Tethering elements facilitate long-range enhancer-promoter interactions and promote fast gene activation (429). TF activity is influenced by the organisational state of the chromatin and post-translational modifications such as methylation and acetylation (430). Some TFs even influence the remodelling of chromatin to get access to binding sites (431). TFs comprise diverse families such as homeobox proteins, zinc finger proteins, and basic helix-loop-helix factors, each with unique features, mechanisms of action, and roles in gene regulation (432). FOXM1 has been shown to regulate ABCC5 expression in cervical cancer and nasopharyngeal cancer (291; 292). Other studies also showed FOXM1 involvement in the regulation of ABCC10 (433) and ABCC4 (434). FOXM1, a TF in the Fox family, plays a crucial role in regulating cell cycle progression, cell division, chromosome stability, and apoptosis during G1/S and G2/M phases (435; 436). Apart from FOXM1, no other TFs have been definitively associated with ABCC5.

4.1.3 Aims

1. Identify genes that are positively correlated with ABCC5 in prostate adenocarcinoma and compare results to the outcomes of **Chapter 3**.

2. Explore functional roles and associated pathways of prostate cancer-associated genes.

3. Validate experimental model cell lines for gene expression studies.

4. Conduct functional investigations to determine if genes associated with the GO term transcription factor regulation correlate with ABCC5 expression levels.

4.2 Results

4.2.1 Prostate Cancer Analysis with ABCC5

In the preceding chapter, we conducted a comprehensive analysis of theThe Cancer Genome Atlas (TCGA) dataset, seeking genes that exhibited a positive correlation with *ABCC5* expression across 31 different cancer types. Building upon this foundation, this chapter focuses on PCa. We selected PCa as our target for several compelling reasons. First and foremost, studies revealed a strong association between ABCC5 and PCa, specifically metastatic PCa (1). Furthermore, initial research showed promising results and there happens to be a noticeable gap in the existing body of research concerning the fundamental function and pathways that ABCC5 is involved in. The limited exploration of these aspects presents an exciting opportunity to make a significant contribution. Therefore, genes that displayed a positive correlation with *ABCC5* expression, along with their corresponding Pearson correlation coefficients, were downloaded from TCGA, specifically for prostate adenocarcinoma. This initial data retrieval provided us with a dataset comprising 3551 distinct genes. We further refined this dataset by focusing exclusively on genes exhibiting a Pearson correlation coefficient of 0.5 or higher which resulted in 85 genes. As seen in **Figure 4.2**, the gene list was subjected to an analysis using g:Profiler to characterise the molecular mechanisms of the genes, to identify associated pathways via gene ontology (GO) term annotations, and to make comparisons with the findings presented in **Chapter 3**.

Genes were enriched in many types of biological functions, including GO molecular function (MF), biological process (BP), and cellular compartment (CC) as seen in **Figure 4.2**. Terms associated with the list of 85 genes are displayed in colour, while non-significant terms linked to genes with a Pearson correlation co-

efficient below 0.5 are rendered opaque. In **Figure 4.3 A**, we delved into the connection between gene lists extracted from the all-cancer dataset and the PCa dataset. The visual representation circularly arranges the genes, with identical genes being linked by purple curves, while blue curves connect genes that exhibit enrichment in common GO terms.

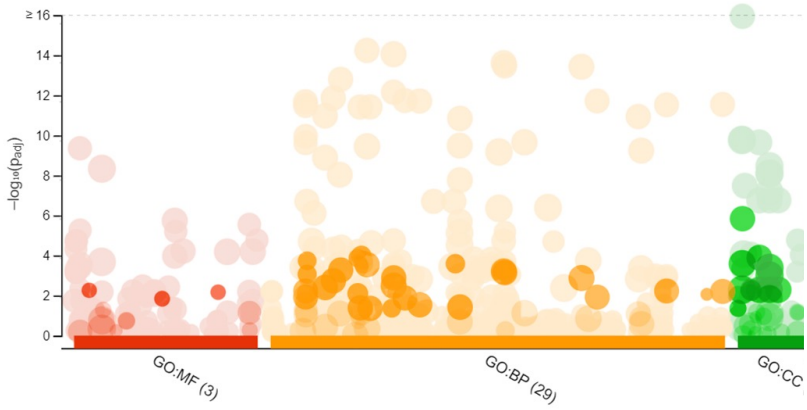

Figure 4.2: Functional analysis of positively correlated genes with ABCC5 in prostate adenocarcinoma using g:Profiler. An overview of g:Profiler analysis for genes positively correlated with ABCC5 in prostate adenocarcinoma, highlighting significant pathways corresponding to genes with a Pearson correlation coefficient $\geq$ 0.5. GO molecular function (GO:MF); GO biological process (GO:BP); GO cellular component (GO:CC).

Interestingly, both datasets share 25 identical genes, however, the majority of genes between the datasets differ. Nevertheless, it's noteworthy that a significant number of genes in both datasets are linked to the same GO terms, highlighting a degree of shared functional characteristics. In **Figure 4.3 B**, the top 20 enrichment clusters for both the all-cancer and PCa datasets are presented. This visualisation offers valuable insights into the shared characteristics and disparities between these two cancer datasets. Notably, out of the 18 clusters identified in the all-cancer dataset, PCa shares only 8 clusters, with RNA splicing and chromatin

organisation exhibiting high significance in this shared subset.

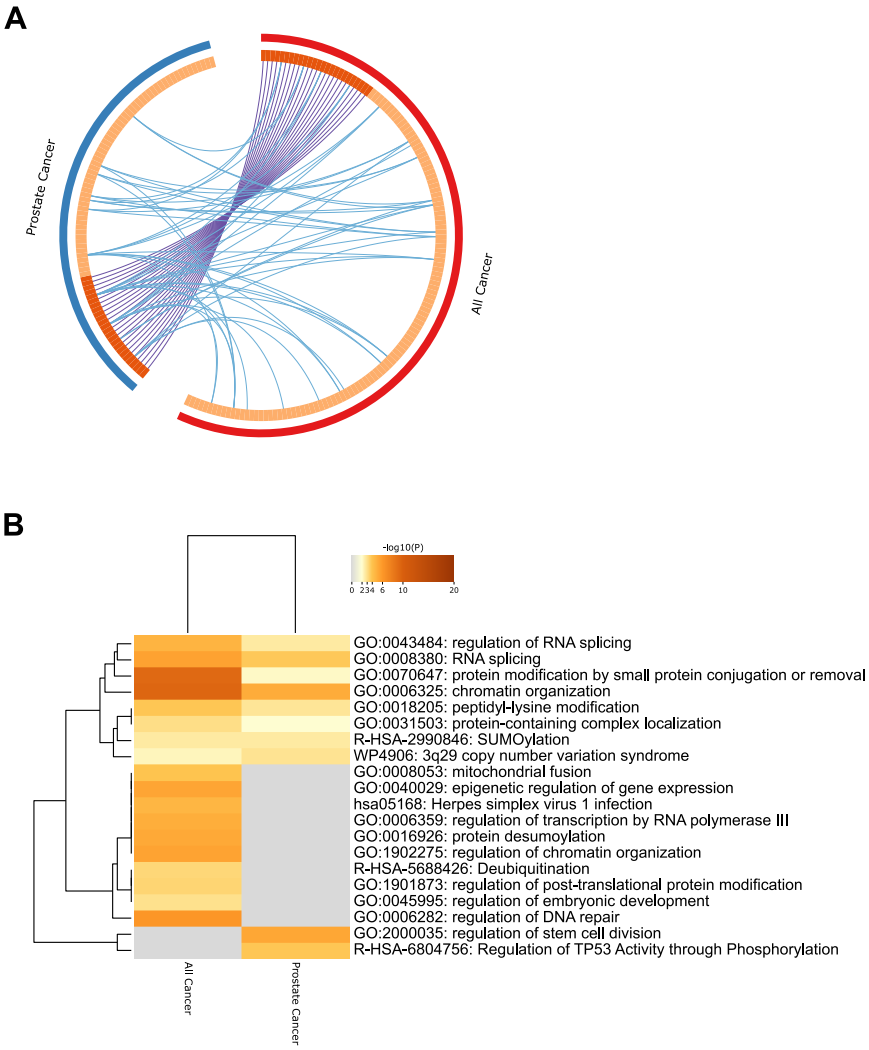

Figure 4.3: Meta-analysis results based on all-cancer and PCa datasets. **A)** Overlap between all-cancer and PCa gene lists. Purple curves connect identical genes, while blue curves link genes that share enrichment in the same GO terms. The inner circle represents the genes, with dark orange indicating genes appearing in the all cancer and PCa dataset and light orange signifying genes unique to the respective dataset-specific list. **B)** Heatmap highlighting the top enrichment clusters for the all-cancer and PCa dataset. The colour scale represents statistical significance and gray indicates no statistical significance.

Additionally, PCa features two distinct clusters that are exclusively enriched in this dataset, namely the regulation of stem cell division and the regulation of TP53 activity through phosphorylation. These unique clusters are among the top four most significant clusters for PCa in this analysis, alongside the previously mentioned RNA splicing and chromatin organisation clusters. Therefore, these specific clusters likely represent processes associated with unique dynamics within the context of PCa. The following analysis provides a more detailed examination of PCa and its associated pathways, focusing on the identification of the top enriched GO and REACTOME terms from the 85-gene list specific to PCa. The results reveal a comprehensive list of 14 distinct groups, as illustrated in **Figure 4.4**.

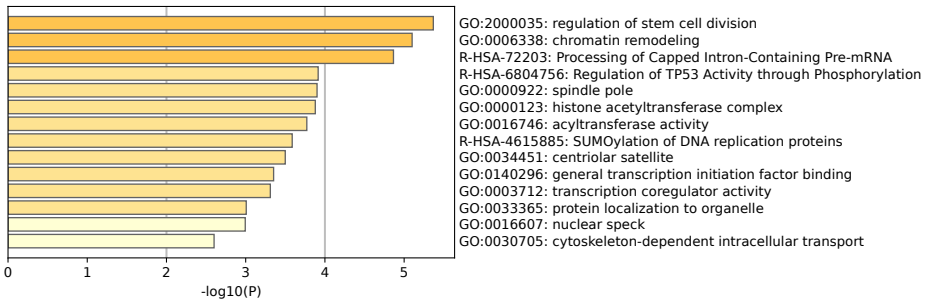

Figure 4.4: Top non-redundant enriched terms for positively correlated genes with *ABCC5* in PCa, colour-coded by p-values. Colour intensity reflects the p-value of the given term and the colour coding is the same as in **Figure 4.3 B**.

In our previous heatmap comparison to the all-cancer dataset, it was evident that the regulation of stem cell division is a unique feature specific to PCa. Additionally, this analysis highlights that this unique regulation of stem cell division is the most significantly enriched term from our gene list. Equally notable, the fourth most significant term exclusively relates to PCa, focusing on the regulation of TP53 activity through phosphorylation. Several highly ranked terms are associated with chromatin remodelling and histone modification. Especially, the

previously discovered role of SUMOylation, as outlined in **Chapter 3**, is further elucidated, particularly in the context of PCa, where it specifically involves the SUMOylation of DNA replication proteins. To better understand the interconnections between these groups and to determine the number of links and terms associated with each cluster, we have visually represented this data in a network analysis in **Figure 4.5**.

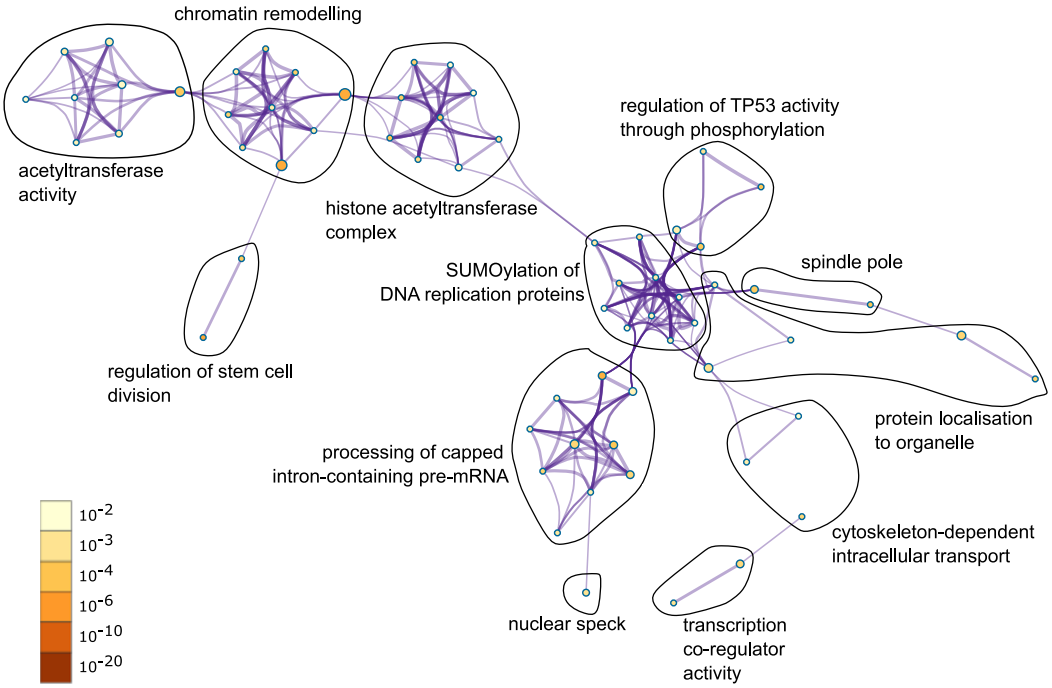

Figure 4.5: Enhanced visualization of metascape enrichment network showing intra-cluster and inter-cluster connections among enriched terms. Cluster annotations represented by color coding, with terms exhibiting greater gene presence highlighted by more significant p-values. Cluster labels were added manually.

The network arrangement highlights the presence of two primary clusters of interconnected groups. The first cluster includes groups such as acetyltransferase activity, chromatin remodelling, histone acetyltransferase complex, and the regulation of stem cell division. In contrast, the second cluster is centred around

functions like SUMOylation of DNA replication proteins, the regulation of TP53 activity through phosphorylation, and the processing of capped intron-containing pre-mRNA. To facilitate further analysis, the terms were grouped according to their association with GO BP, MF, CC, or REACTOME pathways. These groups were then analysed via clustergrams, which highlight terms associated with the overall group term in the columns. Genes are arranged in rows, and the colour intensity reflects the significance of a gene's association with a particular subterm of that group. The initial clustergram analysis presented in **Figure 4.6** reveals the genes linked to the BP terms **A)** regulation of stem cell division and **B)** chromatin remodelling.

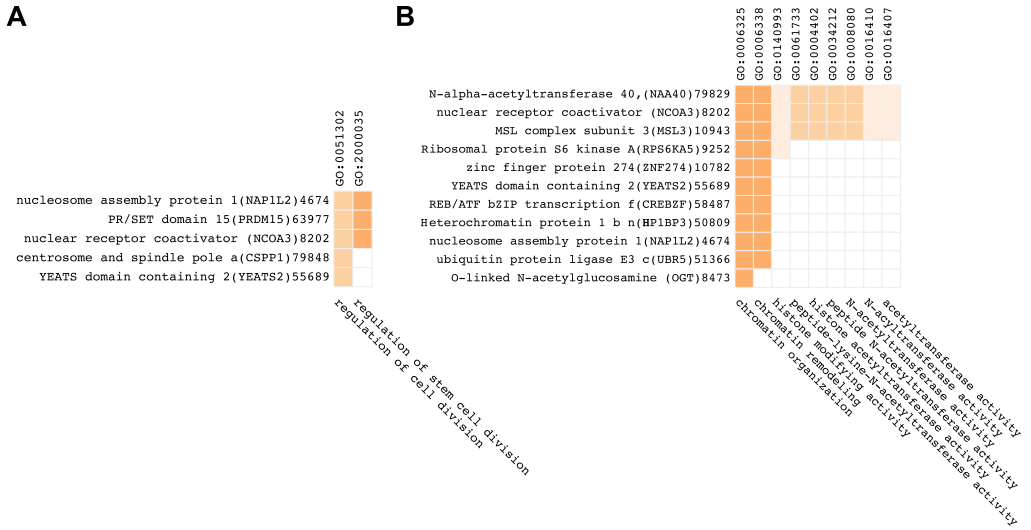

Figure 4.6: Clustergram analysis of the top two BP GO groups. **A)** Regulation of stem cell division and **B)** chromatin remodelling. Terms associated with the respective group are displayed as columns and genes as rows. Colour intensity reflects the p-value of the given term and the colour coding is the same as in **Figure 4.3 B**.

Within both datasets, three genes emerge as having relevance across all subterms of their respective groups. Specifically, for panel **A)**, these genes are *NAP1L2*, *PRDM15*, and *NCOA3*, while panel **B)** features *NAA40*, *NCOA3*, and *MSL3*. In-

terestingly, *NCOA3* overlaps between the two clusters and is an important transcriptional coactivator that has been implicated in pluripotency maintenance of stem cells in mice (437).

Figure 4.7 shows the top three REACTOME pathway cluster analyses for **A)** processing of capped intron-containing pre-mRNA, **B)** regulation of TP53 activity through phosphorylation and **C)** SUMOylation of DNA replication proteins. A substantial number of genes are linked to the processing of capped intron-containing pre-mRNA, and when examining all the graphs in this analysis, these genes consistently exhibit the most significant p-values (**Fig. 4.7 A**). The regulation of TP53 is intricately linked to the cell cycle, facilitating DNA repair (438). It's particularly fascinating to observe that the genes *TOPBP1*, *RFC4*, and *MDM4* consistently play a significant role within all sub-terms of category in (**Fig. 4.7 C**) which range from the cell cycle to TP53-specific terms. Within the group of (**Fig. 4.7 C**) focused on the SUMOylation of DNA replication proteins, the significance of genes associated with sub-terms within that group is notably lower when compared to **A** or **B**. Specifically, genes like *NUP85*, *NUP107*, *PIAS3*, and *SENP5* are of relevance in the SUMOylation subterms. Overall, it's worth pointing out that *NUP85*, *NUP107*, and *TAF11* are consistently present across all three REACTOME pathway groups.

The clustergram analysis presented in **Figure 4.8** reveals the genes linked to the GO CC terms **A)** spindle pole, **B)** histone acetyltransferase complex, and **C)** centriolar satellite. Spindle poles (centrosomes) are essential for organising microtubules during cell division and centriolar satellites are involved in the assembly and maintenance of centrosomes (439; 440). While, histone acetyltransferase complexes regulate gene expression (441). All of the mentioned GO CC terms are localised to the nucleus. As spindle pole and centriolar satellites are so closely involved in terms of their functionality in cell division, it is interesting to observe

that only two genes overlap between the two terms; *TBCCD1* and *CSPP1* (**Figure 4.8**). The most relevant genes in the category of the histone acetyltransferase complex are *MSL3*, *YEATS3*, *OGT* and *SUPT7L* (**Fig. 4.8 B**).

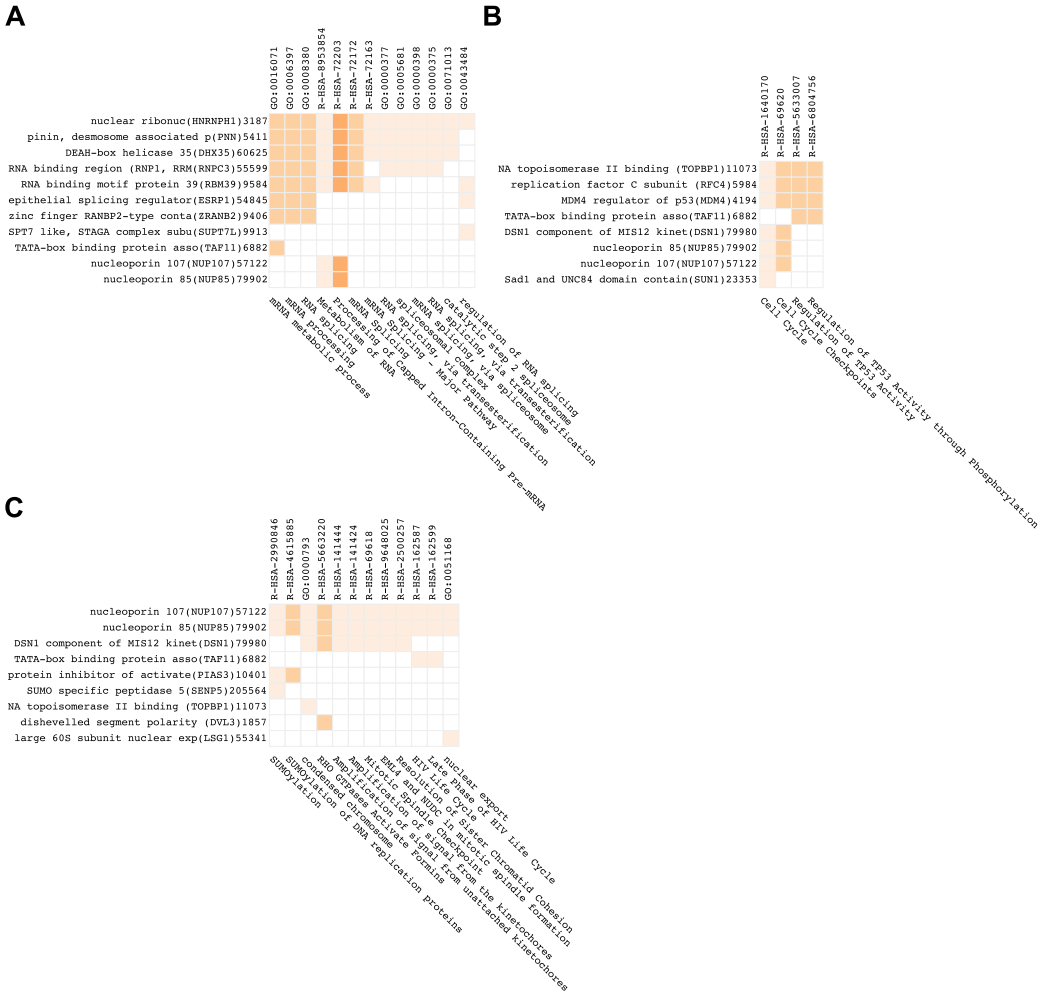

Figure 4.7: Clustergram analysis of the top three REACTOME pathway groups. **A)** Processing of capped intron-containing pre-mRNA, **B)** Regulation of TP53 activity through phosphorylation and **C)** SUMOylation of DNA replication proteins. Terms associated with the respective group are displayed as columns and genes as rows. Colour intensity reflects the p-value of the given term and the colour coding is the same as in **Figure 4.3 B**.

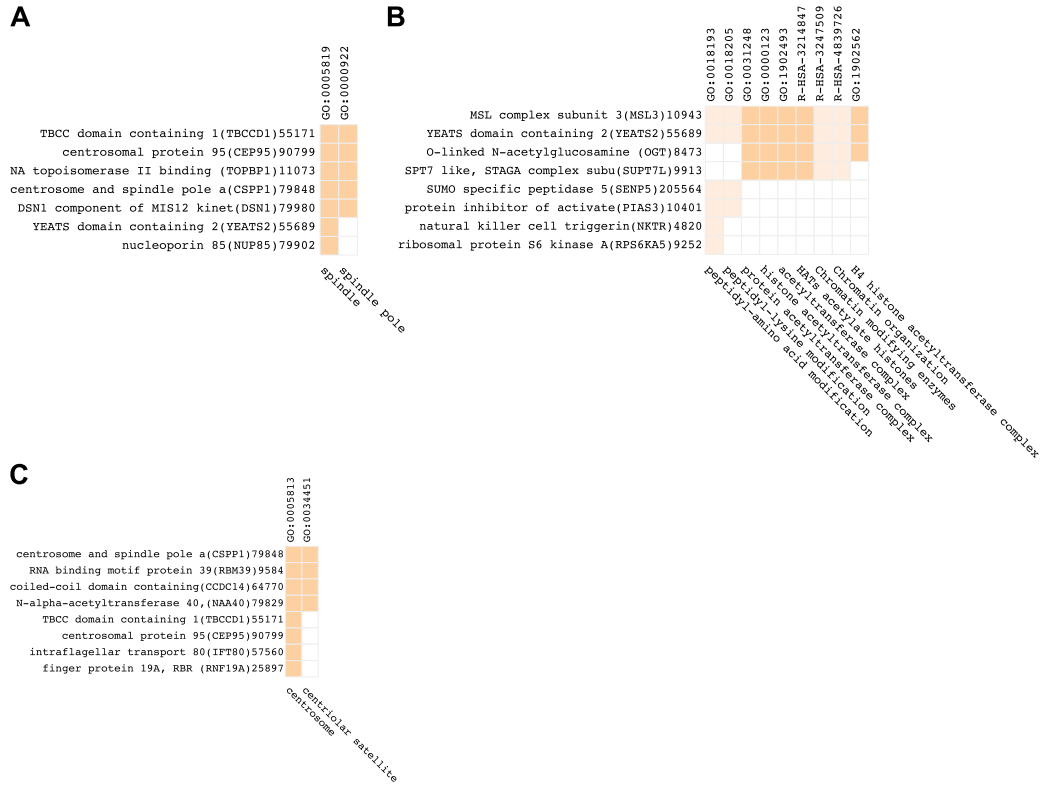

Figure 4.8: Clustergram analysis of the top three CC GO groups. **A)** Spindle pole, **B)** histone acetyltransferase complex and **C)** centriolar satellite. Terms associated with the respective group are displayed as columns and genes as rows. Colour intensity reflects the p-value of the given term and the colour coding is the same as in **Figure 4.3 B**.

In **Figure 4.9**, we can observe a cluster of genes associated with the GO MF term acetyltransferase activity. Among the most relevant genes in this category are *ARIH2*, *RNF19A*, *UBR5*, *TRIM52*, *PIAS3*, and *DM4*. Importantly, several of these genes are linked to multiple GO terms from previous cluster analyses, which further solidifies their involvement in specific biological pathways and functions. This analysis highlighted the enrichment of genes in pathways such as RNA splicing, chromatin organisation, and the regulation of stem cell division. Unique to PCa, significant clusters included the regulation of TP53 activity through phos-

phorylation and the SUMOylation of DNA replication proteins. Notably, genes like PRDM15, linked to stem cell division, and MDM4, associated with TP53 regulation, emerged as key findings. Additionally, the findings related to SENP genes align further with the initial insights from Chapter 3.

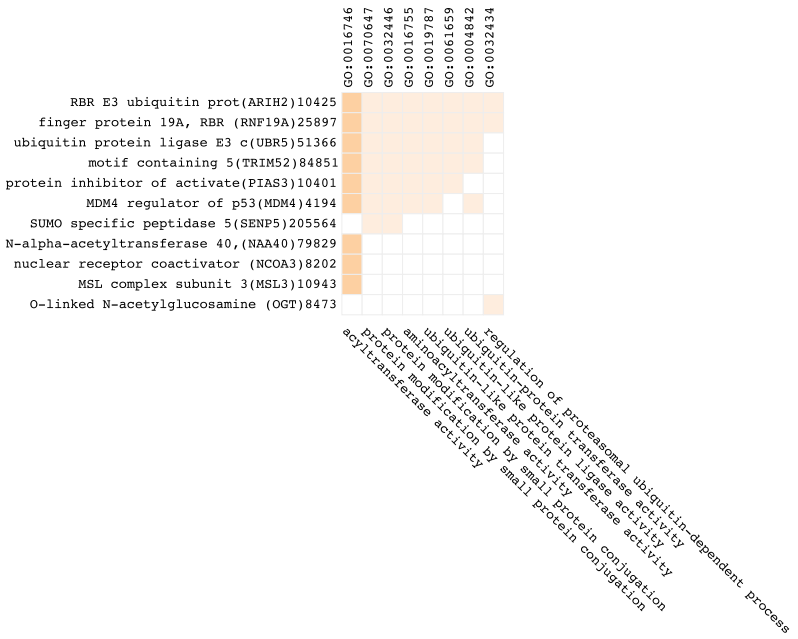

Figure 4.9: Clustergram analysis of the top MF GO group - acetyltransferase activity. Terms associated with the respective group are displayed as columns and genes as rows. Colour intensity reflects the p-value of the given term and the colour coding is the same as in **Figure 4.3 B**.

4.2.2 Transcription Factor Analysis

In this section, we now shift our focus exclusively to the GO MF terms linked to genes correlated with *ABCC5* in the context of PCa. As illustrated in **Figure 4.10 A**, several interesting terms were observed, including an expected cluster of terms encompassing histone-acetyltransferase activity, N-acetyltransferase activity, and acetyltransferase activity which were explored in more in-depth the previous section. Additionally, we also noted terms, such as binding, protein binding, and

transcription regulator activity. Given the manageable number of genes falling within the transcription regulator activity category (**Fig. 4.10 B**), the relative lack of knowledge surrounding the transcriptional regulation of *ABCC5*, and the fact that several of the genes in the list also appeared in the analysis of the previous section, it was decided to assess the genes associated with transcription regulator activity. The subsequent panel, as displayed in **Figure 4.10 C** and **D**, showcases the relationship between transcription regulator activity genes and the comprehensive dataset outlined in (**Chapter 3**), spanning 31 different cancer types. In **Figure 4.10 C**, a substantial representation of genes associated with the GO term transcription factor can be seen in the large dataset. **Figure 4.10 D**, on the other hand, underscores the selected genes from the list in **Fig. 4.10 B** across the entire dataset. Remarkably, a significant portion of these genes is relevant in multiple cancer types specifically *ZXDC*, *DMTF1*, *ZNF224* and *ZNF169*.

To delve deeper into this observation, a heatmap was generated as seen in **Figure 4.10 E**, which provides a detailed view of the data, illustrating the similarities and average Pearson correlation coefficients for each gene across all cancer types that express at least one gene of the list. Upon closer examination of the heatmap, it becomes evident that certain genes exhibit a higher degree of overlap in specific cancer types compared to others. Notably, adrenocortical carcinoma (ACC), colon adenocarcinoma (COAD), diffuse large B-cell lymphoma (DLBC), liver hepatocellular carcinoma (LIHC), and thyroid carcinoma (THCA) share a substantial number of genes with prostate adenocarcinoma (PRAD). Among these, DLBC demonstrates a particularly strong correlation with the genes associated with ABCC5 and closely mirrors the profile of PRAD. In contrast, bladder urothelial carcinoma (BLCA), breast invasive carcinoma (BRCA), esophageal carcinoma (ESCA), head and neck squamous cell carcinoma (HNSC), kidney chromophobe (KICH), and ovarian serous cystadenocarcinoma (OV) show minimal

gene overlap within the TF category with PRAD. Whether cancer types overexpress or underexpress ABCC5 in tumour versus healthy tissue did not affect the gene expression similarity to the profile of PCa.

A

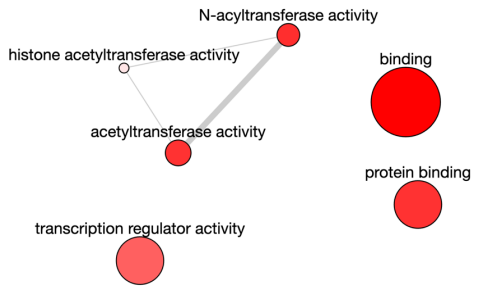

B

GO:MF	transcription regulator activity	(GO:0140110)
	DMTF1	ZXDC
	ZNF182	PIAS3
	ZBTB34	NCOA3
	ZBTB43	TAF11
	ZNF75A	CREBZF
	MDM4	PRDM15
	ZNF169	ZNF274
	TRIM52	ZNF250
	ZNF224	ZNF471
	ZNF449	SUPT7L

C

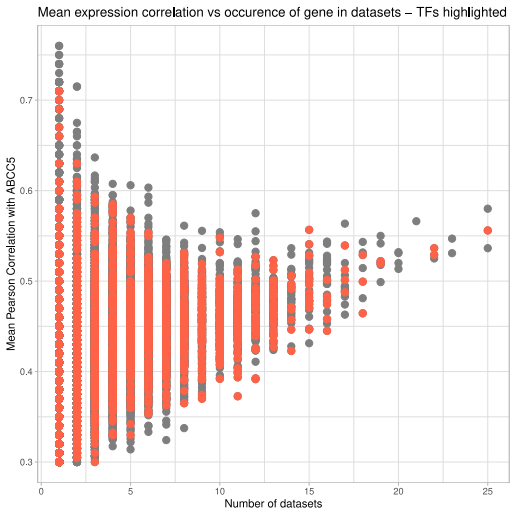

D

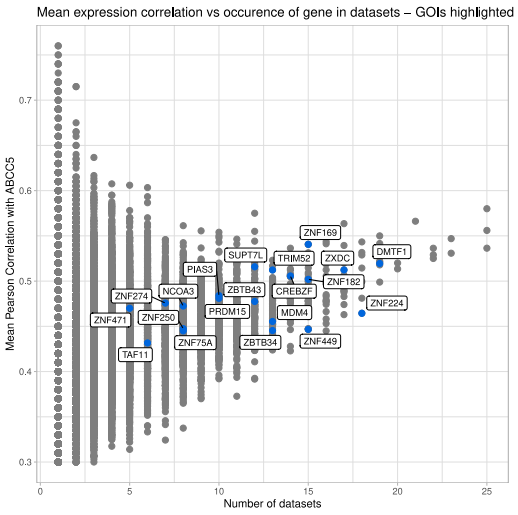

E

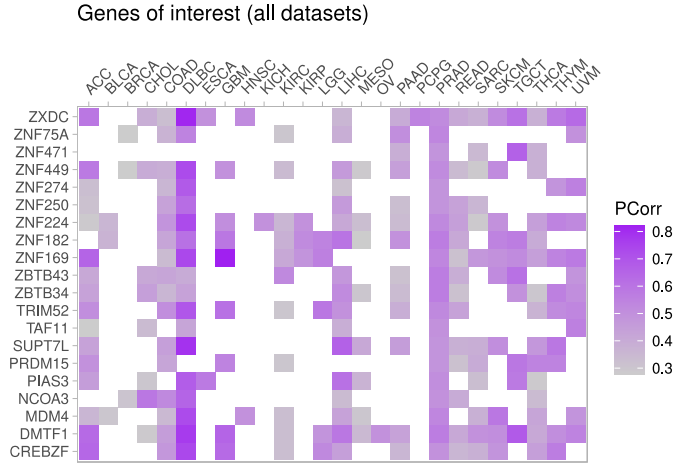

Figure 4.10: Visualisation of Gene Ontology Molecular Function (GO:MF) Enrichment and Correlation Analysis. **A)** Revigo visualisation of GO molecular function (GO:MF). The colour of each bubble corresponds to the provided Value for the respective GO Term in the dataset. The size of the bubble represents the LogSize value associated with the GO Term. **B)** Table displaying genes extracted from GO:MF category transcription regulator activity that correlate with ABCC5. **C)** Scatter plot depicting the relationship between gene occurrence and mean Pearson correlation for all genes. TFs are highlighted in red within this dataset. **D)** Scatter plot demonstrating the relationship between gene occurrence and mean Pearson correlation, with a focus on the genes identified in the previous figure under the Gene Ontology term: Molecular Function (GO:MF) transcription regulator activity. GOI = gene of interest. **E)** Heatmap showcasing the transcriptionally active genes from the list across diverse cancer datasets they appear in.

Ultimately, this computational analysis led to the identification of promising candidate genes that may play a role in the transcriptional regulation of *ABCC5* expression or other functions as examined in the previous section. To validate these findings, the next step involved performing successful *ABCC5* knockdown (KD) and overexpression (OE) experiments in both LNCaP and PC-3 cells.

4.2.3 ABCC5 Knockdown and Overexpression Validation

To be able to carry out experimental investigations on different aspects of ABCC5 in PCa, the expression of ABCC5 had to be confirmed in both LNCaP and PC-3 cells. Additionally, the ability to KD and overexpress ABCC5 in both cell lines was vital for our research. The data in **Figure 4.11** provides evidence for the expression of ABCC5 in both cell lines and an overview of the experimental results obtained from successful KD and OE of ABCC5 in LNCaP and PC-3 cells. A combination of techniques, including qPCR, western blot analysis, and fluorescent-tagged ABCC5 imaging, was used.

The effectiveness of the *ABCC5* KD was first assessed using qPCR. **Figure 4.11 A**

and **B** present the results for LNCaP cells, with the initial measurement of ABCC5 levels conducted at 24 h, 48 h, and 72 h post-KD to observe *ABCC5* levels over time. Notably, for LNCaP cells, the results were not statistically significant at these time points. Therefore, an additional earlier time point, as shown in **Fig. 4.11 A**, was assessed. Due to time constraints, only n=2 samples were analysed for this time point; however, it is evident that a reduction trend in *ABCC5* levels was observed in these samples. In contrast, **Figure 4.11 D** displays the results for PC-3 cells, where a significant KD was consistently observed across all three-time points. To validate the qPCR results and ascertain the success of KD in LNCaP cells, western blot analysis was conducted. **Figure 4.11 C** and *E* illustrate the analysis of ABCC5 post-KD at the same time points, using alpha-tubulin as a control. In both cell lines, successful KD was confirmed, as evidenced by a decrease in ABCC5 protein levels over time, with the lowest levels observed after 72 h in comparison to control.

To achieve ABCC5 overexpression, an expression vector containing ABCC5 was introduced into both cell lines. In **Figure 4.11 G**, a substantial increase in ABCC5 mRNA expression in LNCaP cells is evident, while **Fig. 4.11 F** demonstrates no changes when cells were transfected with an empty vector. Further validation is seen in **Fig. 4.11 H**, where images of LNCaP cells transfected with GFP-tagged ABCC5 confirm successful transfection at the protein level. The results of ABCC5 overexpression in PC-3 cells are presented in the panel below. In **Figure 4.11 J**, mRNA expression of ABCC5 is confirmed, while **Fig. 4.11 I** illustrates that levels remained consistent in the control experiment. Protein level overexpression in PC-3 cells is also verified in **Fig. 4.11 K**. In summary, our results indicate the successful establishment of KD and OE of ABCC5 in LNCaP and PC-3 cells.

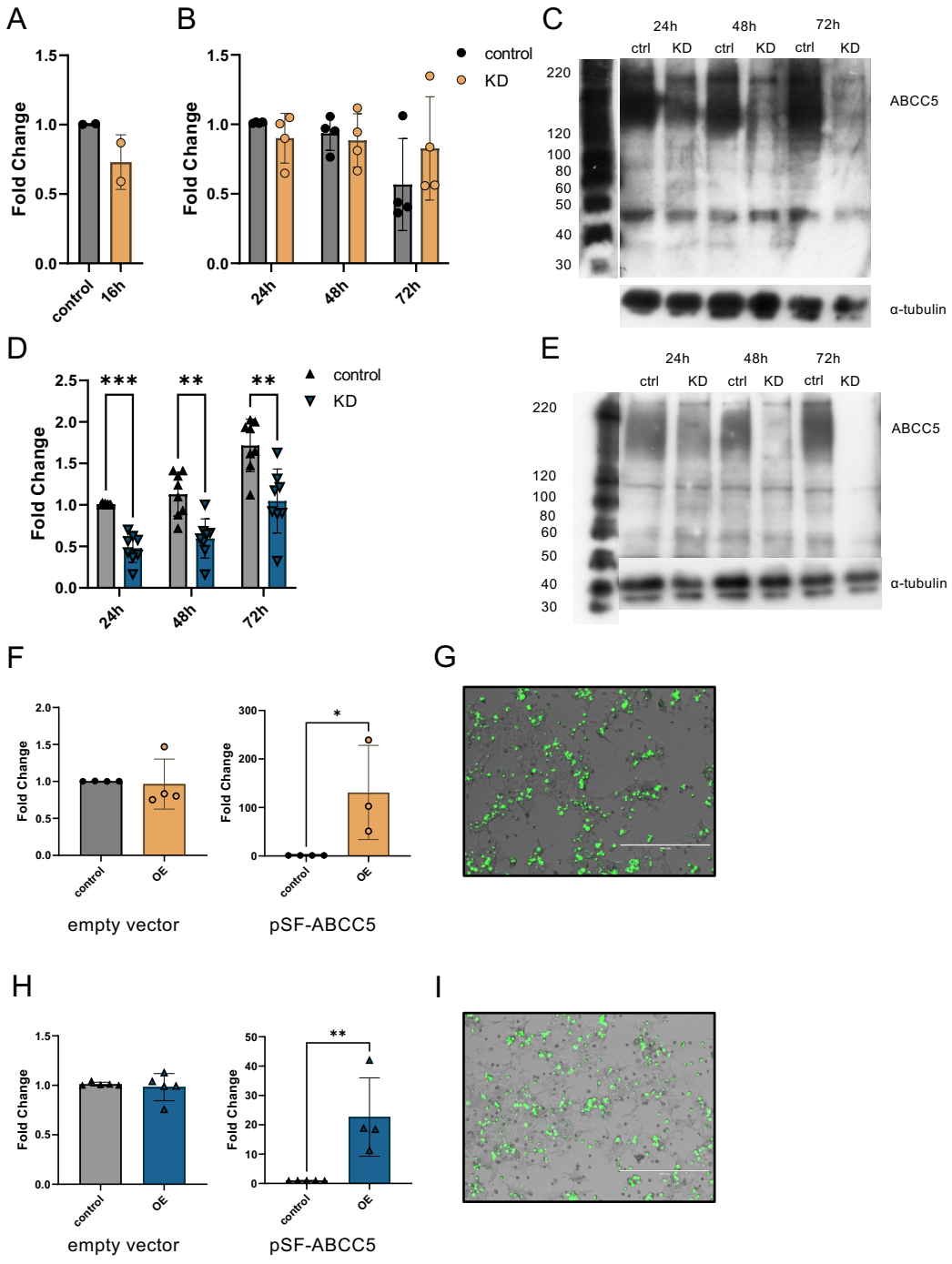
A
B
C
Fold Change
control
16h
24h
48h
72h
control
KD
ctrl
KD
ABCC5
α-tubulin
D
E
***
**
F
G
*
empty vector
pSF-ABCC5
OE
H
I

Figure 4.11: Validation of ABCC5 knockdown (KD) and overexpression (OE) in LNCaP (orange) and PC-3 cells (blue). **A)** Relative ABCC5 mRNA levels in LNCaP cells after 16 h of ABCC5 KD and **B)** 24 h, 48 h, and 72 h post-KD. **D)** Relative ABCC5 mRNA levels in PC-3 cells after 24 h, 48 h, and 72 h of ABCC5 KD. **C)** Western blot analysis of ABCC5 protein in LNCaP cells and **E)** PC-3 cells after 24 h, 48 h, and 72 h of ABCC5 KD. Representative blots from three experiments are shown. The molecular weight marker applies to the ABCC5 blot. Detection with antibody PA83701. **F)** Relative ABCC5 mRNA levels in LNCaP cells after transfection with empty vector and relative ABCC5 mRNA levels in LNCaP cells after transfection with pSF-ABCC5-GFP. **G)** Representative image of LNCaP cells transfected with pSF-ABCC5-GFP after 72 h. Detection with antibody ab13970. **H)** Relative ABCC5 mRNA levels in PC-3 cells after transfection with empty vector and relative ABCC5 mRNA levels in PC-3 cells after transfection with pSF-ABCC5-GFP. **I)** Representative image of PC-3 cells transfected with pSF-ABCC5-GFP after 72 h. Detection with antibody ab13970. Results are based on a sample size of n=4 and represented as mean $\pm$ standard deviation (SD). Statistical significance ($* \ P < 0.05$) was determined using 2-way ANOVA and Bonferroni's multiple comparisons.

4.2.4 Transcription Factor Assessment

Further, the previously identified genes that were associated with the GO MF term transcription factor were clustered into two groups. The first group comprises zinc finger transcription factors, including ZNF75A, ZNF169, ZNF182, ZNF224, ZNF250, ZNF471, ZBTZB43 and ZXDC. The second category consists of a diverse set of transcription factors and transcription-associated factors from various gene families, collectively labelled as other transcription factors, such as DMTF1, MDM4, PRDM15, SUPT7L, TAF11, and TRIM52. The potential correlation between ABCC5 KD and OE and the respective gene expression levels were assessed through qPCR. Please note that qPCR results are not available for all genes in the list (**Figure 4.10 B**), as obtaining specific primers proved to be challenging for some of the candidate genes.

4.2.4.1 Zinc Finger Transcription Factors

Zinc finger transcription factors are a class of regulatory proteins crucial for gene expression control (442). These proteins feature zinc ions coordinated by cysteine and histidine residues, allowing them to bind specifically to DNA sequences which permits precise targeting of genes (443).

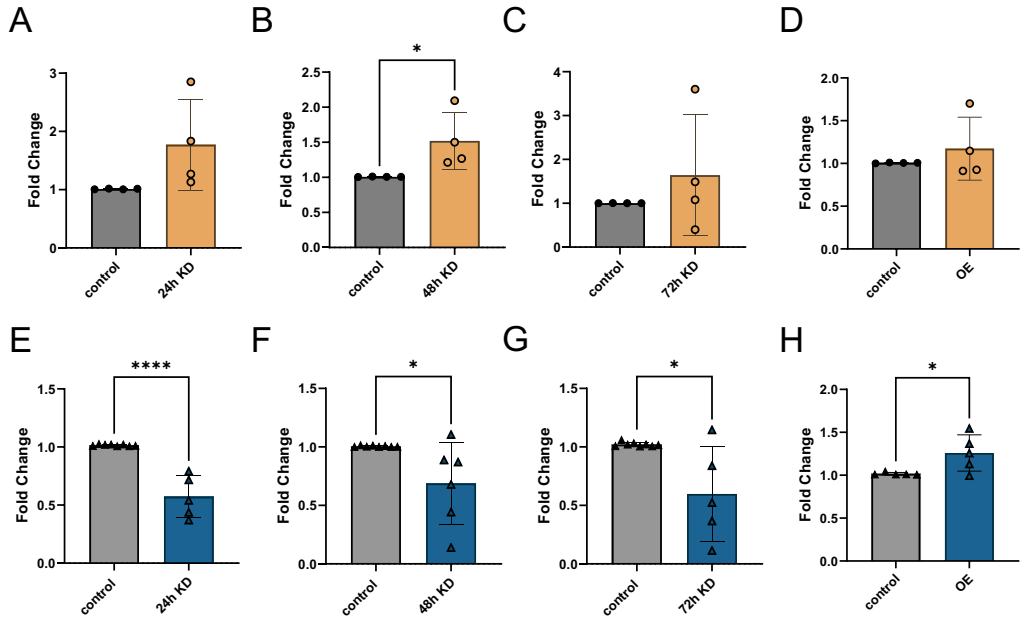

Figure 4.12: *ZNF75A* expression levels upon *ABCC5* knockdown (KD) and overexpression (OE). The relative *ZNF75A* mRNA levels in LNCaP cells (orange) and PC-3 cells (blue) are presented following *ABCC5* KD and OE. The mRNA levels were assessed at different time points: 24 h (**A**, **E**), 48 h (**B**, **F**), and 72 h (**C**, **G**) after *ABCC5* KD. Additionally, the relative mRNA levels of *ZNF75A* at 72 h (**D**, **H**) post-transfection with the ABCC5 plasmid in LNCaP and PC-3 cells, respectively, are depicted. The results, based on a sample size of n=4-8, are depicted as mean $\pm$ SD. Statistical significance (P-value * $<$0.05, **$<$0.01, *** $<$0.001) was determined using an unpaired two-tailed t-test.

As seen in **Figure 4.12**, *ZNF75A* expression exhibited a pronounced response to the KD and OE of *ABCC5* in PC-3 cells. Following a significant decrease within 24 h of KD, *ZNF75A* levels remained suppressed for up to 72 h post-KD. Accord-

ingly, the OE of ABCC5 led to increased levels of *ZNF75A* (**Fig. 4.12 H**). Interestingly, in LNCaP cells, we can observe the opposite trend despite significance only being observed at the 48 h timepoint after KD. Notably, OE also displayed an increasing trend in *ZNF75A* levels.

The analysis of expression levels of *ZNF169* (**Figure 4.13**) revealed an initial significant increase upon KD of ABCC5 in LNCaP cells which significantly reversed 72 h post-KD. While, inconsistent results are observed in PC-3 cells with significantly elevated *ZNF169* expression after 48 h of KD and in ABCC5 OE.

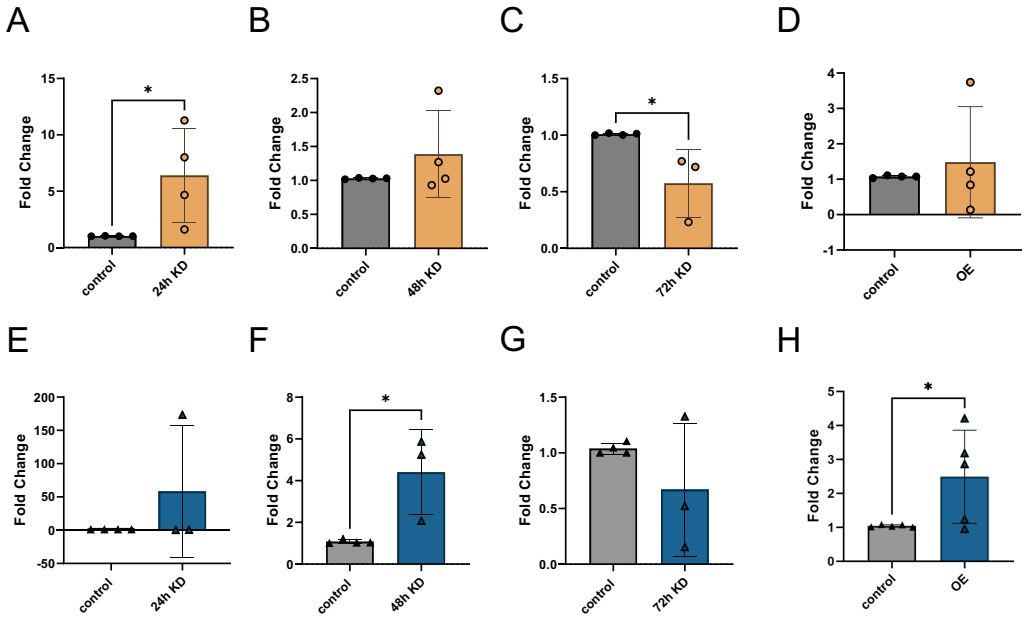

Figure 4.13: *ZNF169* expression levels upon *ABCC5* KD and OE. The relative *ZNF169* mRNA levels in LNCaP cells (orange) and PC-3 cells (blue) are presented following *ABCC5* KD and OE. The mRNA levels were assessed at different time points: 24 h (**A**, **E**), 48 h (**B**, **F**), and 72 h (**C**, **G**) after *ABCC5* KD. Additionally, the relative mRNA levels of *ZNF169* at 72 h (**D**, **H**) post-transfection with the ABCC5 plasmid in LNCaP and PC-3 cells, respectively, are depicted. The results, based on a sample size of n=4-8, are depicted as mean ± SD. Statistical significance (P-value * <0.05) was determined using an unpaired two-tailed t-test.

The KD of ABCC5 in LNCaP cells led to a significant upregulation of *ZNF182* expression after 24 h, and this increase continued albeit not significant after 48 h, as shown in (**Figure 4.14 A** and **B**. However, in PC-3 cells, the data from the KD showed considerable variability, and no discernible trends in *ZNF182* expression were observed. On the other hand, in the OE experiment for PC-3 cells, there was a notable and substantial increase in *ZNF182* expression (**Fig. 4.14 H**).

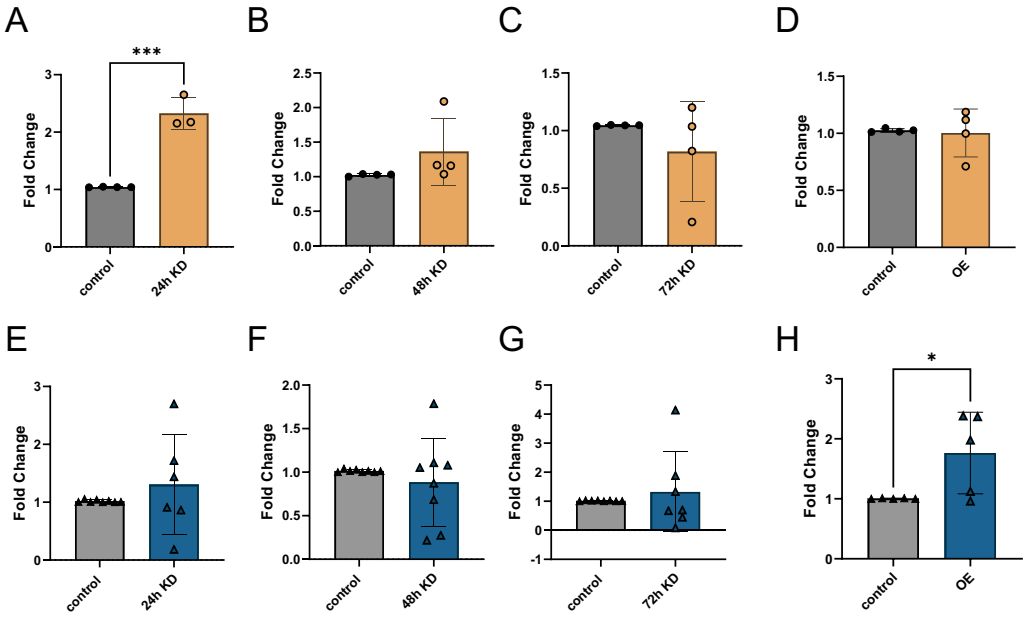

Figure 4.14: *ZNF182* expression levels upon *ABCC5* KD and OE. The relative *ZNF182* mRNA levels in LNCaP cells (orange) and PC-3 cells (blue) are presented following *ABCC5* KD and OE. The mRNA levels were assessed at different time points: 24 h (**A**, **E**), 48 h (**B**, **F**), and 72 h (**C**, **G**) after *ABCC5* KD. Additionally, the relative mRNA levels of *ZNF182* at 72 h (**D**, **H**) post-transfection with the ABCC5 plasmid in LNCaP and PC-3 cells, respectively, are depicted. The results, based on a sample size of n=4-8, are depicted as mean ± SD. Statistical significance (P-value * <0.05, **<0.01, *** <0.001) was determined using an unpaired two-tailed t-test.

In **Figure 4.15**, it is evident that the expression levels of *ZNF224* exhibited a notable progressive decrease across the 48 h and 72 h post-KD time points in LNCaP

cells. While OE in LNCaP cells demonstrated a trend towards increased *ZNF224* expression. Notably, in the case of PC-3 cells, no interesting trends or significant results were observed.

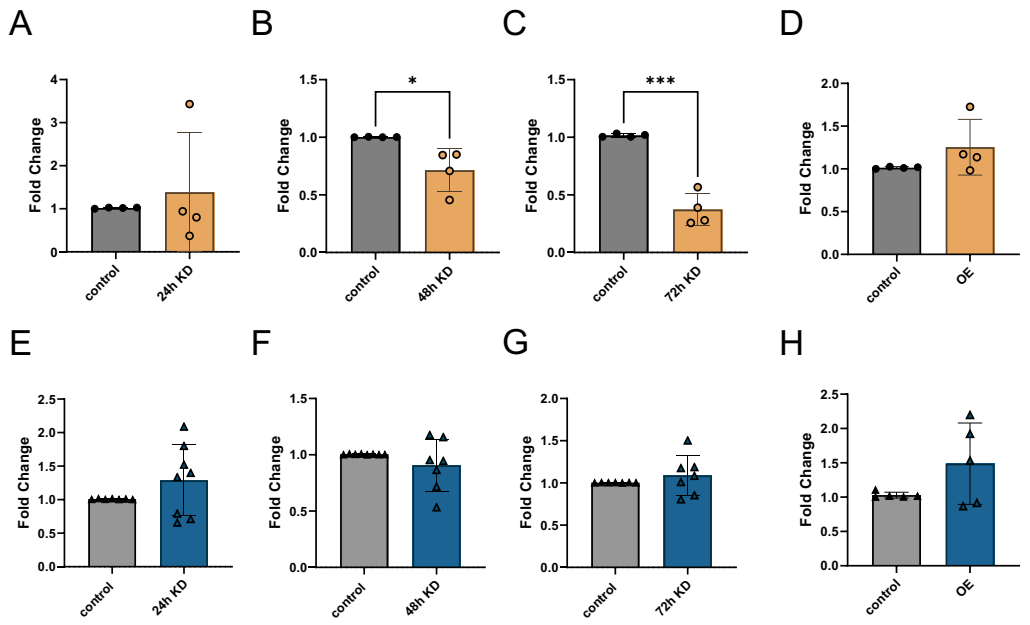

Figure 4.15: *ZNF224* expression levels upon *ABCC5* KD and OE. The relative *ZNF224* mRNA levels in LNCaP cells (orange) and PC-3 cells (blue) are presented following *ABCC5* KD and OE. The mRNA levels were assessed at different time points: 24 h (**A**, **E**), 48 h (**B**, **F**), and 72 h (**C**, **G**) after *ABCC5* KD. Additionally, the relative mRNA levels of *ZNF224* at 72 h (**D**, **H**) post-transfection with the ABCC5 plasmid in LNCaP and PC-3 cells, respectively, are depicted. The results, based on a sample size of n=4-8, are depicted as mean ± SD. Statistical significance (P-value * <0.05, **<0.01, *** <0.001) was determined using an unpaired two-tailed t-test.

The expression of *ZNF250* shows no significant changes upon KD or OE of ABCC5 in LNCaP cells (**Fig. 4.16**). In comparison, there is great variability in KD results in PC-3 but a significant slight increase in *ZNF250* in the OE results.

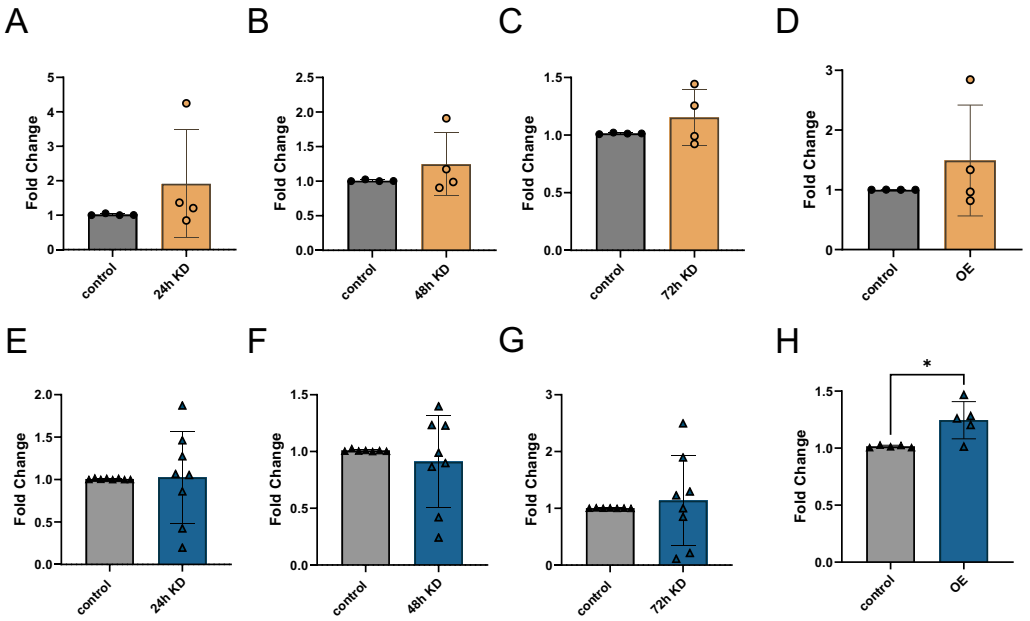

Figure 4.16: *ZNF250* expression levels upon *ABCC5* KD and OE. The relative *ZNF250* mRNA levels in LNCaP cells (orange) and PC-3 cells (blue) are presented following *ABCC5* KD and OE. The mRNA levels were assessed at different time points: 24 h (**A**, **E**), 48 h (**B**, **F**), and 72 h (**C**, **G**) after *ABCC5* KD. Additionally, the relative mRNA levels of *ZNF250* at 72 h (**D**, **H**) post-transfection with the ABCC5 plasmid in LNCaP and PC-3 cells, respectively, are depicted. The results, based on a sample size of n=4-8, are depicted as mean ± SD. Statistical significance (P-value * <0.05) was determined using an unpaired two-tailed t-test.

The findings for ZNF471 mirror those of ZNF250, as no significant alterations are evident in LNCaP cells (**Fig. 4.17**). However, in the context of *ABCC5* KD experiments, there is a modest non-significant increase in *ZNF471* expression after 24 h, and a noticeable positive trend is observed in the OE result, as depicted in **Figure 4.17**. In PC-3 cells, there is a notable and statistically significant decrease in *ZNF471* expression 48 h post-KD. Additionally, the OE experiments also exhibit a positive trend, although without reaching statistical significance.

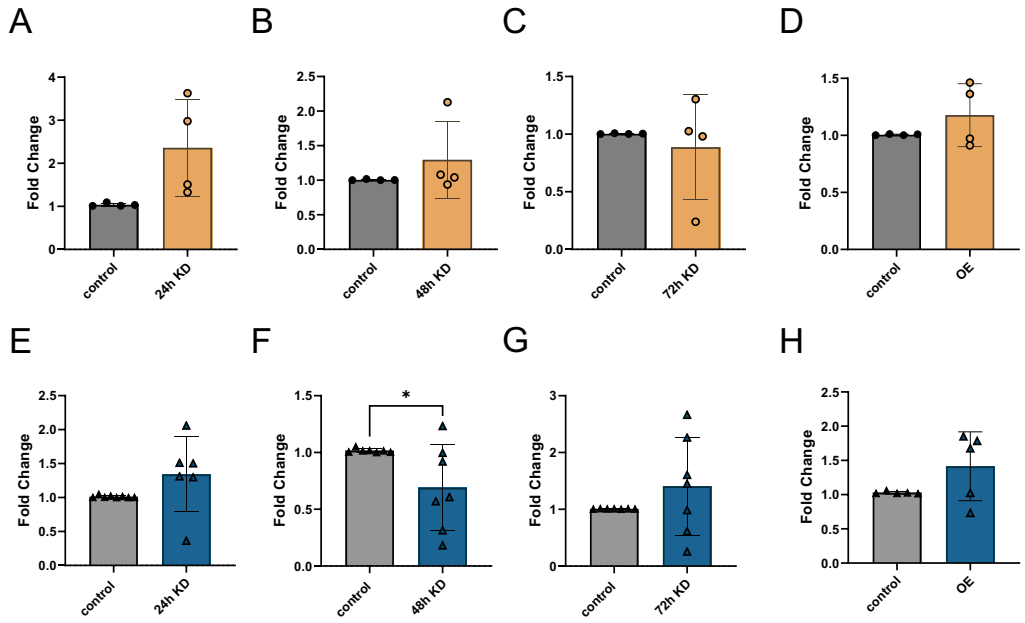

Figure 4.17: *ZNF471* expression levels upon *ABCC5* KD and OE. The relative *ZNF471* mRNA levels in LNCaP cells (orange) and PC-3 cells (blue) are presented following *ABCC5* KD and OE. The mRNA levels were assessed at different time points: 24 h (**A**, **E**), 48 h (**B**, **F**), and 72 h (**C**, **G**) after *ABCC5* KD. Additionally, the relative mRNA levels of *ZNF471* at 72 h (**D**, **H**) post-transfection with the ABCC5 plasmid in LNCaP and PC-3 cells, respectively, are depicted. The results, based on a sample size of n=4-8, are depicted as mean ± SD. Statistical significance (P-value * <0.05) was determined using an unpaired two-tailed t-test.

Zinc finger transcription factors containing a BTB domain, like ZBTB43, play pivotal roles in a diverse array of cellular processes. The BTB domain serves as a critical component for engaging in protein-protein interactions, allowing these factors to regulate genes by forming complexes and acting as transcriptional repressors (444). Interestingly, *ZBTB43* levels showed a substantial decrease at 48 h and 72 h following *ABCC5* KD in LNCaP cells, whereas *ZBTB43* expression remained consistent between control and OE in the OE experiment (**Figure 4.18**). Whilst, no significant changes are observed in *ZBTB43* levels in PC-3 cells.

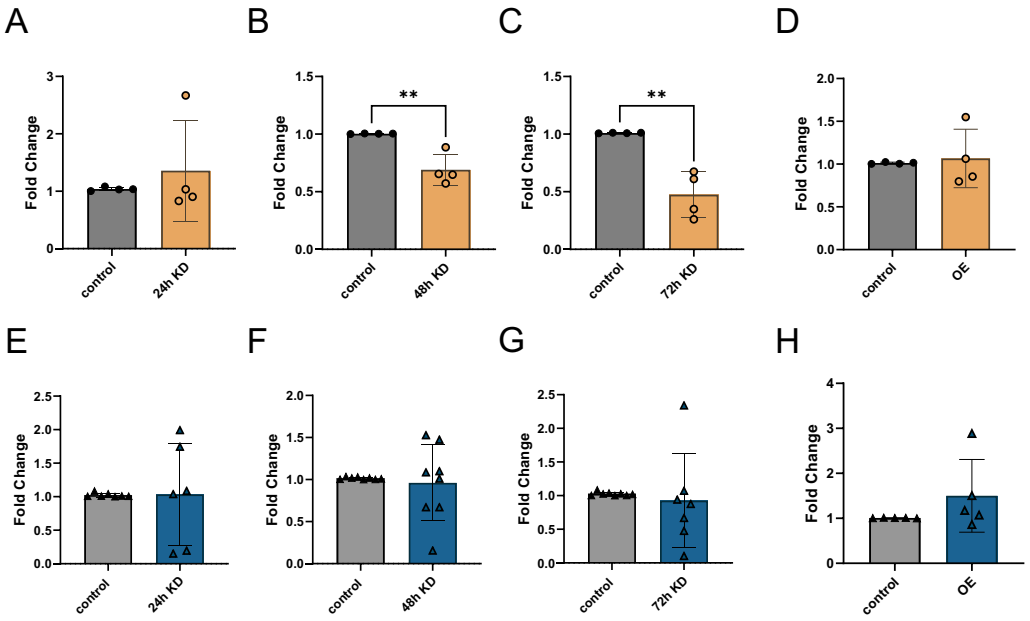

Figure 4.18: *ZBTB43* expression levels upon *ABCC5* KD and OE. The relative *ZBTB43* mRNA levels in LNCaP cells (orange) and PC-3 cells (blue) are presented following *ABCC5* KD and OE. The mRNA levels were assessed at different time points: 24 h (**A**, **E**), 48 h (**B**, **F**), and 72 h (**C**, **G**) after *ABCC5* KD. Additionally, the relative mRNA levels of *ZBTB43* at 72 h (**D**, **H**) post-transfection with the ABCC5 plasmid in LNCaP and PC-3 cells, respectively, are depicted. The results, based on a sample size of n=4-8, are depicted as mean ± SD. Statistical significance (P-value * <0.05, **<0.01) was determined using an unpaired two-tailed t-test.

Zinc finger, X-linked, duplicated family member C (ZXDC), is known to regulate the transcription of major histocompatibility complex class II genes in antigen-presenting cells, with potential roles in myeloid-specific gene expression regulation (445). Interestingly, no significant changes are observed in either *ABCC5* KD or OE across both cell lines (**Figure 4.19**).

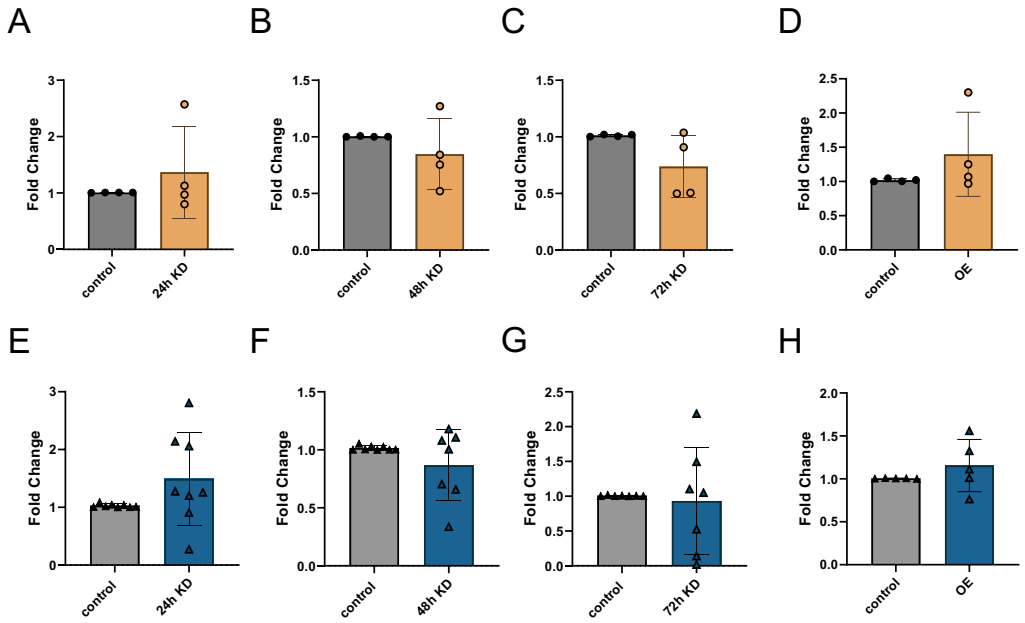

Figure 4.19: *ZXDC* expression levels upon *ABCC5* KD and OE. The relative *ZXDC* mRNA levels in LNCaP cells (orange) and PC-3 cells (blue) are presented following *ABCC5* KD and OE. The mRNA levels were assessed at different time points: 24 h (**A**, **E**), 48 h (**B**, **F**), and 72 h (**C**, **G**) after *ABCC5* KD. Additionally, the relative mRNA levels of *ZXDC* at 72 h (**D**, **H**) post-transfection with the ABCC5 plasmid in LNCaP and PC-3 cells, respectively, are depicted. The results, based on a sample size of n=4-8, are depicted as mean ± SD. Statistical significance was determined using an unpaired two-tailed t-test.

4.2.4.2 Other Transcription Factors

The cyclin D binding myb-like transcription factor 1 (DMTF1) is a TF that can promote p53/TP53-dependent growth arrest which is important in regulating cell cycle progression and cell proliferation (446). As seen in the top panel of (**Figure 4.20**), KD or OE of *ABCC5* do not influence the expression levels of *DMTF1* in LNCaP cells. However, in PC-3 cells, *DMTF1* levels decreased significantly 24 h and 72 h post-KD. While *DMTF1* demonstrates a slightly positive trend in the OE experiment (**Fig. 4.20 H**).

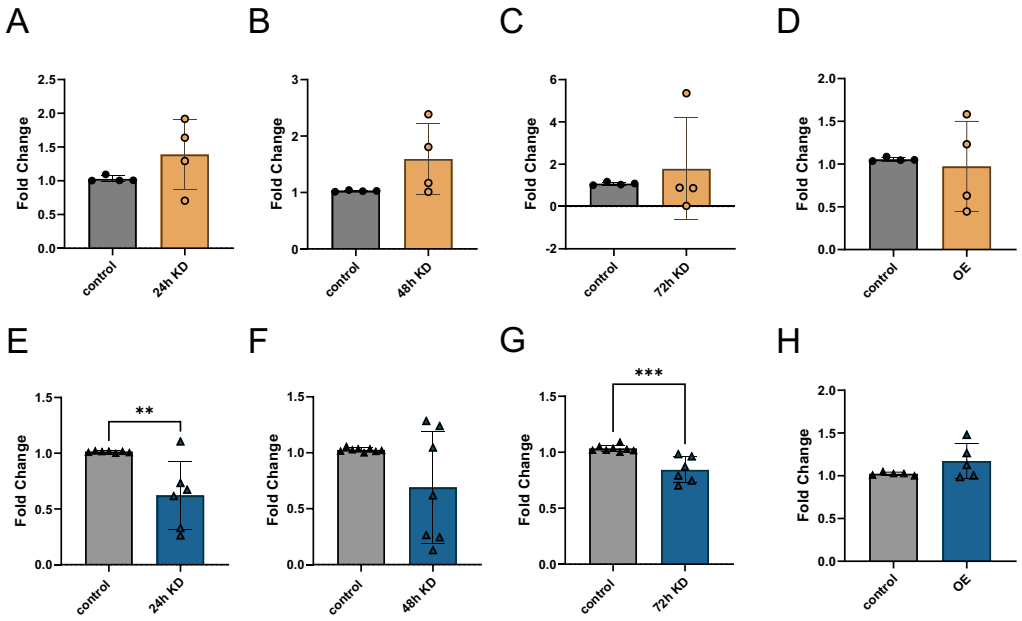

Figure 4.20: *DMTF1* expression levels upon *ABCC5* KD and OE. The relative *DMTF1* mRNA levels in LNCaP cells (orange) and PC-3 cells (blue) are presented following *ABCC5* KD and OE. The mRNA levels were assessed at different time points: 24 h (**A**, **E**), 48 h (**B**, **F**), and 72 h (**C**, **G**) after *ABCC5* KD. Additionally, the relative mRNA levels of *DMTF1* at 72 h (**D**, **H**) post-transfection with the ABCC5 plasmid in LNCaP and PC-3 cells, respectively, are depicted. The results, based on a sample size of n=4-8, are depicted as mean ± SD. Statistical significance (P-value * <0.05, **<0.01, *** <0.001) was determined using an unpaired two-tailed t-test.

The mouse double minute 4 (MDM4) plays a critical role in cancer by inhibiting the tumour suppressor protein p53, thus promoting cell survival and preventing apoptosis (447). Upon examining **Figure 4.21**, it becomes evident that there are no significant findings in the *ABCC5* KD experiments in both cell lines. However, intriguingly, the *ABCC5* OE experiments result in significantly increased *MDM4* levels in LNCaP and PC-3 cells.

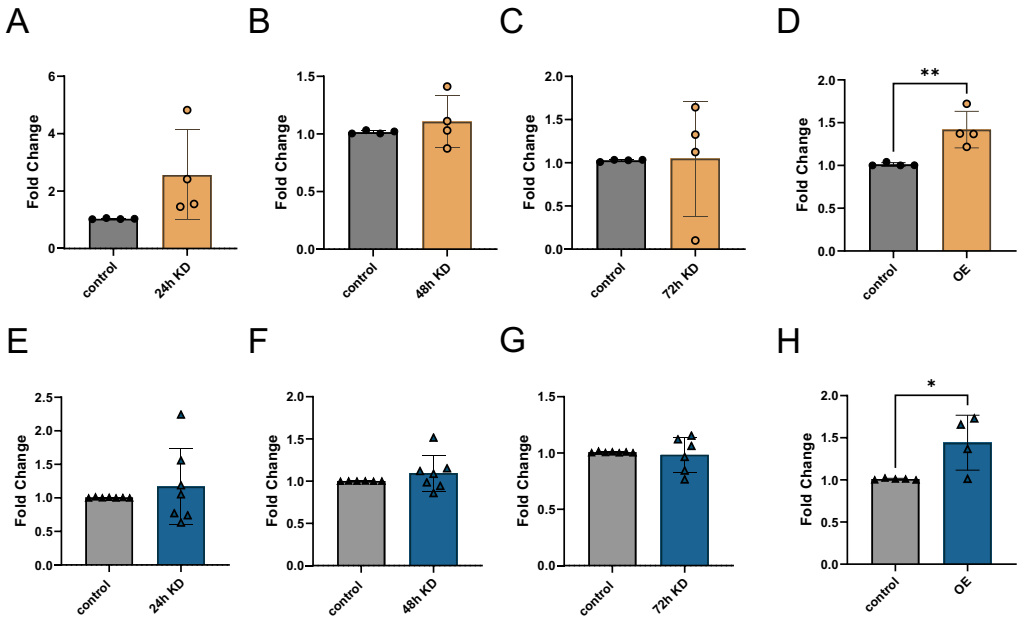

Figure 4.21: *MDM4* expression levels upon *ABCC5* KD and OE. The relative *MDM4* mRNA levels in LNCaP cells (orange) and PC-3 cells (blue) are presented following *ABCC5* KD and OE. The mRNA levels were assessed at different time points: 24 h (**A**, **E**), 48 h (**B**, **F**), and 72 h (**C**, **G**) after *ABCC5* KD. Additionally, the relative mRNA levels of *MDM4* at 72 h (**D**, **H**) post-transfection with the ABCC5 plasmid in LNCaP and PC-3 cells, respectively, are depicted. The results, based on a sample size of n=4-8, are depicted as mean ± SD. Statistical significance (P-value * <0.05, **<0.01) was determined using an unpaired two-tailed t-test.

Within the PRDI-BF1 and RIZ homology domain-containing (PRDM) family, PRDM15 stands out as a sequence-specific transcriptional regulator deeply involved in shaping cell identity and fate. In the context of cancer, PRDM15's impact is pronounced, as it orchestrates a transcriptional program that sustains the activity of the PI3K/AKT/mTOR pathway, underscoring its critical role in cancer-related dysregulation (448). As seen in **Figure 4.22**, the concentration of *PRDM15* increases after the KD of *ABCC5* in LNCaP cells after 24 h and 48 h of KD. However, in the OE experiment, there is no opposite trend; instead, it appears to exhibit a slight positive trend with increased *PRDM15* levels. Notably,

PRDM15 levels in PC-3 cells seem to remain largely unaffected by the experimental conditions (**Fig. 4.22**, lower panel).

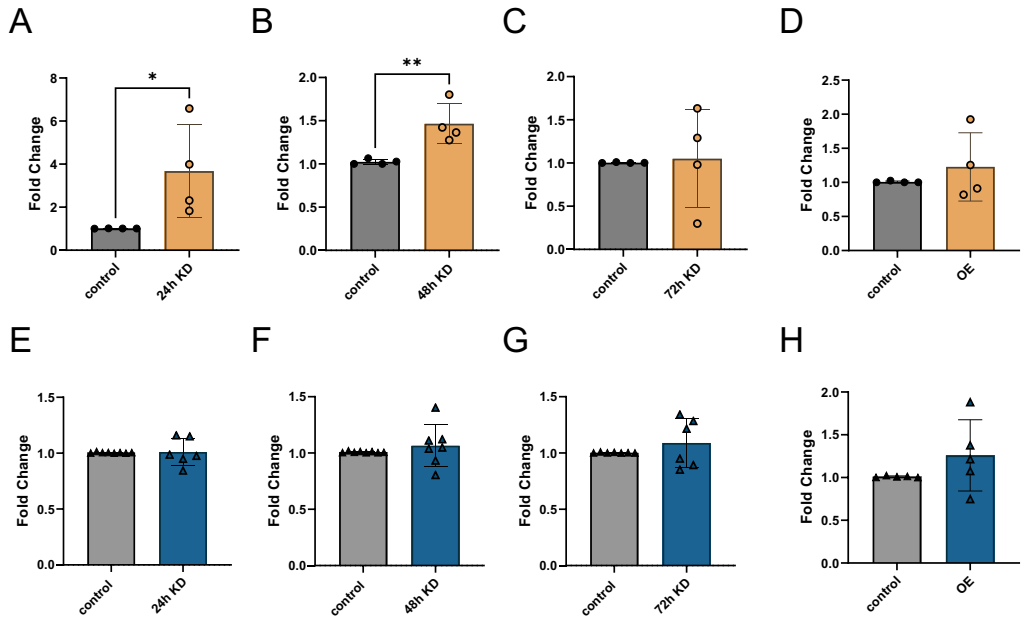

Figure 4.22: *PRDM15* expression levels upon *ABCC5* KD and OE. The relative *PRDM15* mRNA levels in LNCaP cells (orange) and PC-3 cells (blue) are presented following *ABCC5* KD and OE. The mRNA levels were assessed at different time points: 24 h (**A**, **E**), 48 h (**B**, **F**), and 72 h (**C**, **G**) after *ABCC5* KD. Additionally, the relative mRNA levels of *PRDM15* at 72 h (**D**, **H**) post-transfection with the ABCC5 plasmid in LNCaP and PC-3 cells, respectively, are depicted. The results, based on a sample size of n=4-8, are depicted as mean ± SD. Statistical significance (P-value * <0.05, **<0.01) was determined using an unpaired two-tailed t-test.

SUPT7L is a protein subunit of the human STAGA complex, a chromatin-modifying multiprotein complex known for its involvement in transcriptional regulation. This complex comprises SPT3, TAF9, and GCN5 acetyltransferase subunits, collectively contributing to epigenetic modifications essential for gene expression control (449). The **Figure 4.23** top panel, shows a gradual increase in *SUPT7L* expression following KD of *ABCC5*. Notably, the results obtained at the 24 h mark do not yet show a statistically significant change, but the significance becomes ev-

ident after 48 h. Furthermore, *SUPT7L* expression continues to exhibit a positive trend after 72 h in LNCaP cells. Meanwhile, the initial response in PC-3 cells is distinct. At 24 h post-KD, *SUPT7L* expression initially decreases, but then, it significantly increases around 72 h post-KD. In PC-3 cells, the OE experiments show a positive trend.

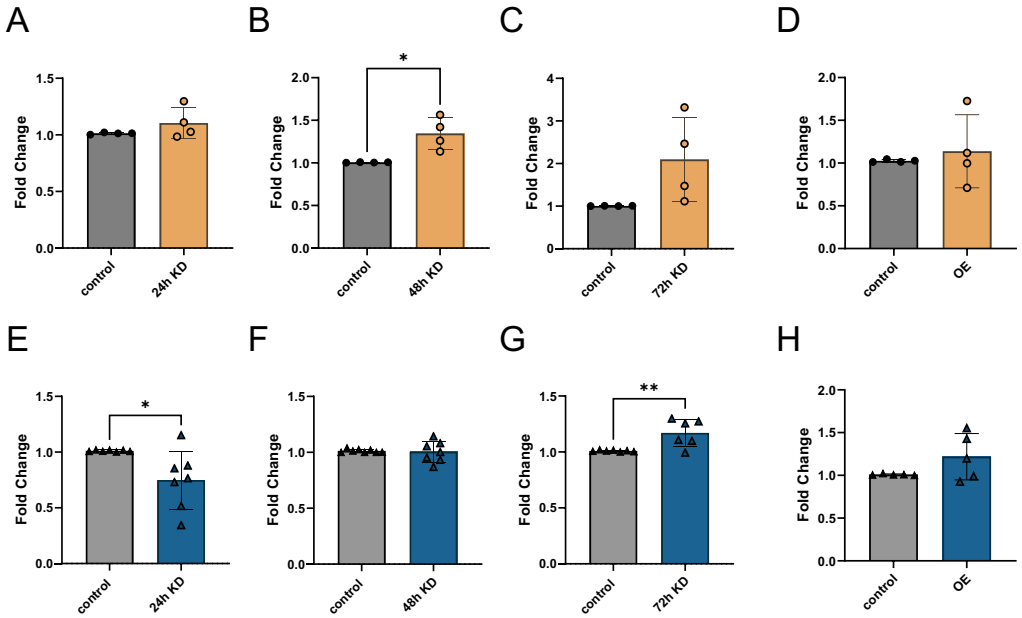

Figure 4.23: *SUPT7L* expression levels upon *ABCC5* KD and OE. The relative *SUPT7L* mRNA levels in LNCaP cells (orange) and PC-3 cells (blue) are presented following *ABCC5* KD and OE. The mRNA levels were assessed at different time points: 24 h (**A**, **E**), 48 h (**B**, **F**), and 72 h (**C**, **G**) after *ABCC5* KD. Additionally, the relative mRNA levels of *SUPT7L* at 72 h (**D**, **H**) post-transfection with the ABCC5 plasmid in LNCaP and PC-3 cells, respectively, are depicted. The results, based on a sample size of n=4-8, are depicted as mean ± SD. Statistical significance (P-value * <0.05, **<0.01) was determined using an unpaired two-tailed t-test.

TAF11, or TATA-box Binding Protein-Associated Factor 11, is a subunit of the general transcription factor TFIID. TFIID is a multi-protein complex that plays a crucial role in initiating the transcription of genes in eukaryotic organisms (450).

In LNCaP cells, we observed a positive trend in *TAF11* expression following the KD of *ABCC5*, with a significant increase after 48 h, as depicted in **Figure 4.24**. However, after 72 h, *TAF11* expression levels returned to a state similar to that of the control. Conversely, in PC-3 cells, expression of *TAF11* is significantly increased after 72 h post-KD and after OE of *ABCC5*.

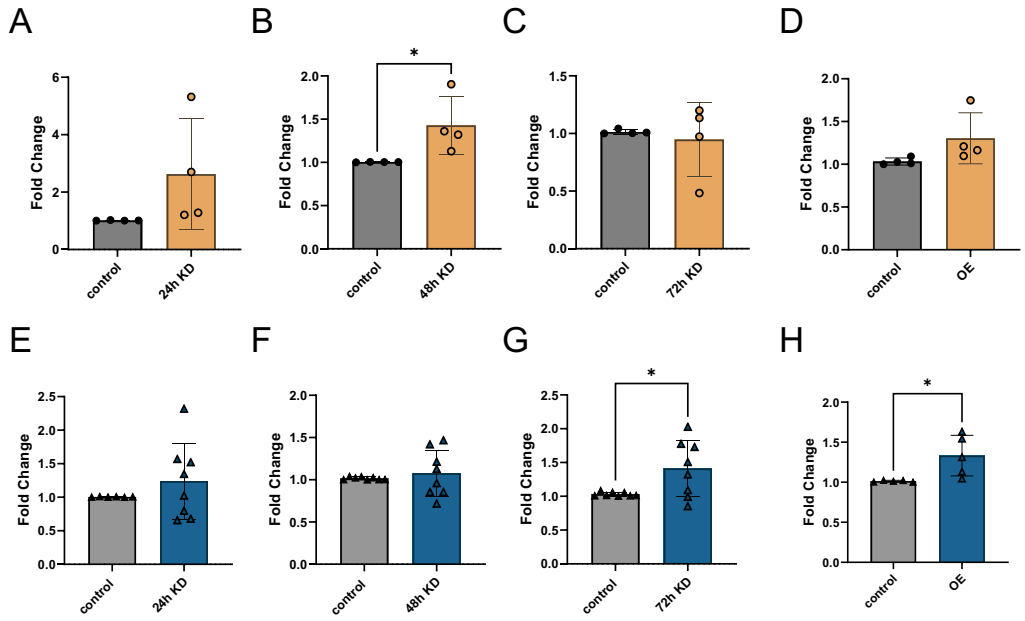

Figure 4.24: *TAF11* expression levels upon *ABCC5* KD and OE. The relative *TAF11* mRNA levels in LNCaP cells (orange) and PC-3 cells (blue) are presented following *ABCC5* KD and OE. The mRNA levels were assessed at different time points: 24 h (**A**, **E**), 48 h (**B**, **F**), and 72 h (**C**, **G**) after *ABCC5* KD. Additionally, the relative mRNA levels of *TAF11* at 72 h (**D**, **H**) post-transfection with the ABCC5 plasmid in LNCaP and PC-3 cells, respectively, are depicted. The results, based on a sample size of n=4-8, are depicted as mean ± SD. Statistical significance (P-value * <0.05) was determined using an unpaired two-tailed t-test.

TRIM52 is a member of the TRIM protein superfamily, which is known for its conserved motif architecture and its significant roles in both antiviral innate immunity regulation and cancer development. Notably, TRIM52 is associated with NF-κB activation (451). In LNCaP cells, TRIM52 expression increases signifi-

cantly 24 h post-KD and levels remain elevated up to the 48 h timepoint. Meanwhile, OE of *ABCC5* also leads to significantly increased expression of *TRIM52* (**Figure 4.25**, top panel). In PC-3 cells, KD of *ABCC5* does not change the expression levels of *TRIM52* while OE of *ABCC5* significantly increases *TRIM52* levels ((**Figure 4.25**, lower panel).

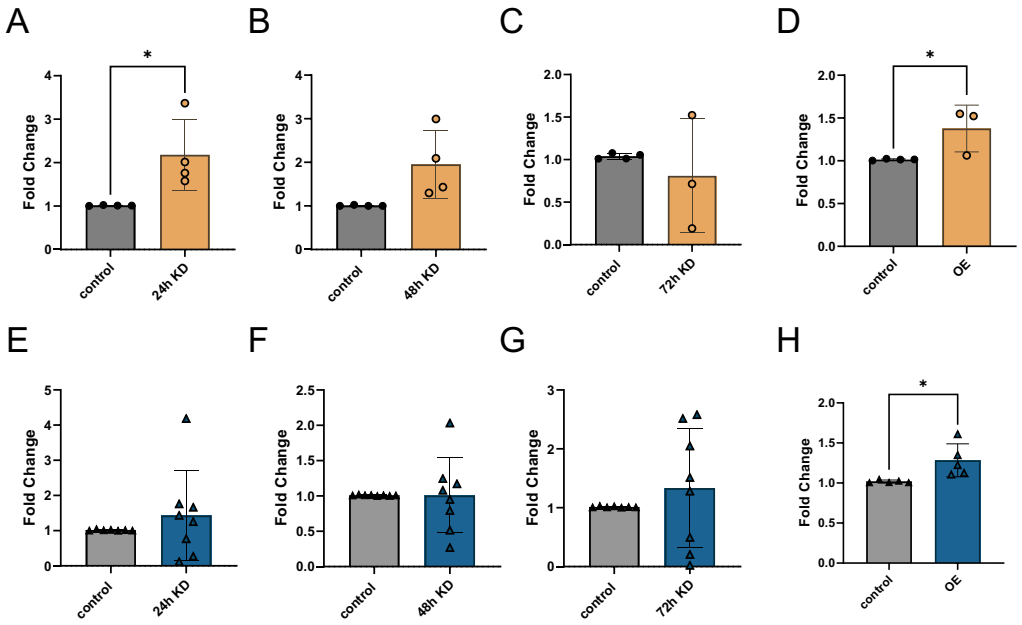

Figure 4.25: *TRIM52* expression levels upon *ABCC5* KD and OE. The relative *TRIM52* mRNA levels in LNCaP cells (orange) and PC-3 cells (blue) are presented following *ABCC5* KD and OE. The mRNA levels were assessed at different time points: 24 h (**A**, **E**), 48 h (**B**, **F**), and 72 h (**C**, **G**) after *ABCC5* KD. Additionally, the relative mRNA levels of *TRIM52* at 72 h (**D**, **H**) post-transfection with the ABCC5 plasmid in LNCaP and PC-3 cells, respectively, are depicted. The results, based on a sample size of n=4-8, are depicted as mean $\pm$ SD. Statistical significance (P-value * <0.05) was determined using an unpaired two-tailed t-test.

4.3 Discussion

In this chapter, a comprehensive analysis of ABCC5-associated gene expression patterns in PCa was conducted and a range of GO enrichment terms was identified that shed light on potential functional pathways influenced by ABCC5 in the context of PCa. While most of this discussion will focus on the findings specific to PCa, it is essential to recognise the broader context by incorporating results from the analysis of the all-cancer dataset. These shared and unique GO enrichment terms provide valuable insights into ABCC5's potential roles not only in PCa but also in cancer in general. In summary, four clusters have been identified, combining GO enrichment terms and qPCR gene results from both PCa and the all-cancer dataset. These clusters encompass chromatin regulation, cell division, transcriptional regulation, and protein modification and SUMOylation. Additionally, a specialised cluster was recognised to explore the TP53-related association unique to PCa.

Before delving into the specific clusters and detailed examination of the results, it is crucial to consider that there is a notable variation in the qPCR outcomes when comparing results from LNCaP and PC-3 cells, depending on the TF under investigation. This discrepancy implies that the two cell lines have distinct transcriptional profiles as shown in **Figure 4.1**. LNCaP and PC-3 cells originate from different types of PCa. As discussed in the introduction the cell lines have different origins which has profound implications for their gene expression patterns and a study found that more than 2000 genes are differentially expressed between the cell lines (452). PC-3 cells have adapted to the bone microenvironment, where they have evolved communication mechanisms via RNA with bone cells (453). Further, the bone environment can influence several metabolic pathways in PC-3 cells (454). In contrast, LNCaP cells, despite their metastatic ori-

gin, continue to exhibit gene expression patterns that closely resemble those of prostatic epithelium. They also maintain metabolic functions similar to those of the original prostate tissue (452). Moreover, there are several other distinctions between LNCaP and PC-3 cells. PC-3 cells are known to lack androgen receptor expression and are insensitive to androgen stimulation, while LNCaP cells retain androgen receptor expression and are androgen-sensitive (455; 402). Additionally, they possess dissimilar karyotypes, which may contribute to differences in their gene expression profiles (456). These variations in key molecular features significantly influence their responses to various experimental conditions, such as the impact of *ABCC5* KD and OE. Therefore, it is essential to consider this variation when interpreting the qPCR results. This distinction also opens the possibility of identifying genes specifically linked to ABCC5 across different stages of PCa and very much reflects the heterogeneity of PCa itself.

4.3.1 Chromatin Regulation Cluster

Several aspects of this chapter and the previous one, have consistently highlighted the significance of chromatin regulation. GO terms such as chromatin remodelling and histone acetyltransferase complex in the PCa dataset strongly indicate ABCC5's involvement in epigenetic control and chromatin dynamics. Notably, SUPT7L, linked to the histone acetyltransferase complex GO term, displayed varying responses to *ABCC5* KD in different cell lines. This suggests that SUPT7L may be part of the complex regulatory network involving ABCC5 and epigenetic processes. Further exploration of SUPT7L could yield valuable insights into how ABCC5 influences chromatin dynamics and gene expression, especially in cancer contexts.

The term SUMOylation of DNA replication proteins aligns with our initial findings in the previous chapter, shedding light on potential target processes of SUMOy-

lation. ABCC5's exact participation in this is unclear; however, this process has significant implications for DNA integrity and replication, which are pivotal in the context of PCa progression and metastasis (457). Significantly, chromatin organisation features in both datasets, while terms like regulation of chromatin organisation and epigenetic regulation of gene expression are in the all-cancer dataset. Both underscore the broader relevance of ABCC5's potential involvement in controlling gene expression through the involvement in chromatin organisation. Treating prostate cancer cells with histone deacetylase (HDAC) inhibitors has been demonstrated to attenuate androgen receptor signalling, leading to anti-proliferative and pro-apoptotic effects (458). Moreover, a study showed that HDAC inhibitors increased the expression of ABCC5 mRNA and protein in lung cancer and colorectal cancer cells (459). This increase in ABCC5 expression was also observed in pregnant rats who were administered valproic acid, an HDAC inhibitor (460). Interestingly, a bromodomain inhibitor resulted in decreased ABCC5 expression in triple-negative breast cancer cells and non-small lung cancer cells (461). Bromodomains recognise acetylated histones and regulate chromatin structure (462). These studies support the idea that there is a link between ABCC5 and chromatin organisation and regulation.

Furthermore, regulation of DNA repair is a GO term that implies ABCC5's possible association with DNA repair mechanisms in a pan-cancer context. DNA repair is a fundamental aspect of maintaining genomic stability, preventing mutations, and mitigating the risk of cancer development (463). A study examining cisplatin chemoresistance in non-small lung cancer cells showed that transcript abundances of ABCC5 and GTF2H2 correlated (283). GTF2H2 is a vital component of the TF IIH complex, which plays a central role in transcription initiation and DNA repair processes (464). Another study showed that a common long non-coding RNA (lncRNA) was identified as a regulator of ABCC5 and GSK3beta expres-

sion. LncRNAs are a class of RNA molecules longer than 200 nucleotides that do not encode proteins but instead play diverse roles in cellular processes including gene regulation (465). GSK3beta is a key player in cellular processes such as cell repair and DNA damage response (466). Interestingly, the co-occurrence of a significant number of *ABCC5*-positively correlated genes related to TF activity also suggests that ABCC5 may contribute to shaping the accessibility of DNA to TFs and thereby influence gene expression patterns. Despite initial studies suggesting a connection between ABCC5 and epigenetic regulation, as well as its involvement in DNA repair processes, further investigations and experimental validation are essential to substantiate and confirm this initial association.

4.3.2 Cell Division Cluster

Within the PCa dataset, the GO term regulation of stem cell division emerged as the most significant, implying a potential involvement of ABCC5 in orchestrating stem cell division within the context of PCa and potentially contributing to tumorigenesis (467). This term falls under the broader category of cell division, where the spindle pole and centriolar satellite are relevant. The spindle pole, or centrosome, organises microtubules and orchestrates the formation of the mitotic spindle, ensuring accurate chromosome segregation during cell division. Centriolar satellites, positioned near the centrosome, contribute to the regulation of centrosome duplication and maintenance (439; 440). Specifically, the genes NAP1L2, NCOA3, and PRDM15 are particularly noteworthy in the context of both the regulation of stem cell division and cell division. In the qPCR analysis, the observed increase in *PRDM15* expression upon *ABCC5* KD in LNCaP cells suggests a potential link between ABCC5 and the modulation of regulation of cell division and stem cell division. Interestingly, there is a decrease in *DMTF1* levels following *ABCC5* KD in PC-3 cells. DMTF1 is a tumour suppressor and

removal leads to the progression of the cell cycle (468). Additionally, the term regulation of embryonic development from the all-cancer dataset suggests a link to the term regulation of stem cell division as both encompass processes integral to the dynamic cellular changes during embryogenesis. This connection implies that ABCC5 may play a role in coordinating the regulation of stem cell division within the broader context of embryonic development, potentially influencing tissue differentiation and homeostasis.

A study in sea urchins showed that ABCC5 is essential for the development of the hindgut during embryogenesis and removal leads to gut defects (209). Another study confirmed the role of ABCC5 during gut development in sea urchins and showed that ABCC5 was restricted to the mesoderm (469). Both studies indicate a role of ABCC5 during embryonic development in sea urchins. Additionally, further studies show a connection between stem cells and ABCC5. The expression of ABCC5 in breast cancer stem cell-like cells exhibited a correlation with chemoresistance, and ABCC5 was identified as a direct target of the stem cell-related TF Bmi1 (298). In pancreatic cancer cells, stem cell features were found to be dependent on gene expression regulated by PAF1. The removal of PAF1 resulted in the downregulation of other genes associated with the regulation of stem cell features, including ABCC5 (286). The studies and our findings collectively suggest the involvement of ABCC5 in the modulation of stem cell features and embryonic development. However, to establish a definitive connection, additional research is necessary. The genes identified in this analysis provide an initial starting point for further analysis.

4.3.3 Transcription Regulation Cluster

The transcriptional regulation cluster is a very interesting category to investigate especially given that a significant proportion of *ABCC5*-positively correlated

genes are TFs or regulators in the all-cancer dataset. This aspect is also backed by the GO terms general transcription initiation factor binding and transcription coregulator activity in the prostate cancer dataset. This discussion has already explored qPCR results for various TF genes in previous sections. Now, our focus will be specifically on the results of zinc-finger TFs.

Differing responses in gene expression between the experimental groups in LNCaP and PC-3 cells are observed for *ZNF75A* and extend to other genes, including *ZNF169*, *ZNF182*, *ZNF224*, and *ZBTB43* which respond in LNCaP cells, whereas no alterations were noted in PC-3 cells. Particularly, in PC-3 cells, the downregulation of *ZNF75A* following *ABCC5* KD suggests a potential positive regulatory role of ABCC5 on *ZNF75A* expression, implying that ABCC5 may positively influence *ZNF75A*. Nonetheless, it's crucial to consider that this relationship might not be straightforward, as ABCC5 may participate in a regulatory pathway that indirectly impacts *ZNF75A* expression. Intriguingly, no significant impact on *ZNF75A* expression was observed in LNCaP cells. ZNF75A has been predicted to localise to the nucleus and be involved in the negative regulation of transcription by RNA polymerase II (470). *ABCC5* KD resulted in an upregulation of *ZNF169* and *ZNF182* expression in LNCaP cells, whereas *ZNF224* and *ZBTB43* exhibited a decrease following *ABCC5* KD in LNCaP Cells. Interestingly, apart from ZNF224, none of the other TFs have been specifically associated with cancer. ZNF224 has been identified as a regulator with a dual role in cell growth and resistance to apoptosis in cancer cells. The mechanism involves the downregulation of p53 among other tumour suppressors (471). These qPCR results collectively suggest that various zinc finger TFs are influenced by *ABCC5* levels, underscoring the potential role of ABCC5 in the regulation of transcriptional processes. Importantly, observed changes are predominantly associated with *ABCC5* KD and are not consistently reflected in overexpression results. Reasons for this

discrepancy include potential threshold levels in transcriptional regulation, where the amount of overexpressed ABCC5 may not reach the required threshold for observable changes in TFs (472). Additionally, feedback mechanisms activated during *ABCC5* KD may differ from those in overexpression, leading to distinct outcomes (473). Protein-protein interactions, critical in TF regulation, may not occur uniformly during ABCC5 OE, influencing TF expression differently than in KD situations (474). The temporal dynamics, saturation effects, and turnover rates of TFs could further contribute to the observed variations (475). Overall, some interesting candidate genes for additional experimental validation are highlighted.

4.3.4 Protein Modification and SUMOylation Cluster

In the previous chapter, the potential involvement of ABCC5 in SUMOylation was established. Building upon these findings, the current chapter not only reaffirms ABCC5's connection to SUMOylation but also presents a novel dimension by specifically associating it with the SUMOylation of DNA replication proteins in the prostate cancer dataset. PIAS3 is a particularly intriguing target due to its role as a SUMO E3 ligase, modifying various proteins, notably DNA-binding TFs (476). This insight complements the discussion of SENP proteins from the previous chapter. In the broader context of the all-cancer dataset, additional intriguing GO terms emerge, distinct from those observed in PCa. These include deubiquitination and protein desumoylation, offering a more comprehensive view of ABCC5's involvement in post-translational modification processes. While ABCC5 is connected to SUMOylation and deubiquitination, further investigations are necessary to elucidate the specific pathways and molecular mechanisms underlying these associations.

4.3.5 P53 Activity Regulation Cluster

A novel discovery specific to PCa was the identification of the GO term regulation of TP53 through phosphorylation, establishing a direct link between ABCC5 and the renowned tumour suppressor gene TP53 (477). The increased expression of *MDM4* upon *ABCC5* overexpression in both PC-3 and LNCaP cells provides valuable insights. MDM4, is a negative regulator of p53 and inhibits p53's tumour-suppressing functions (478). The association between ABCC5 and MDM4 suggests a potential role for ABCC5 in regulating TP53 activity through MDM4, contributing to the dysregulation of p53 in PCa cells. A study also showed that a metabolic switch to oxidative phosphorylation reduced the expression of ABCC5 in wild-type p53 cells while it increased the expression of ABCC5 in mutated p53 cells through the ERK5/MEF2 pathway (479). The precise connection between ABCC5 and TP53 remains unknown; however, MDM4 emerges as a promising avenue for further exploration of the link between ABCC5 and TP53.

4.4 Summary and Limitations

The exploration of the clusters collectively emphasises ABCC5's involvement in various cellular processes, particularly in gene regulation, post-translational modifications, genomic stability, and developmental processes. The presence of TFs among ABCC5-positively correlated genes in the all-cancer dataset suggests its pivotal role in orchestrating gene expression. While this study provides valuable insights into the role of ABCC5 in cancer biology and specifically PCa, it is crucial to acknowledge certain limitations.

First, the KD of ABCC5 was marginal at the RNA level and overall transient, raising questions about the actual impact of this change. The observed KD was approximately 50%, whereas the OE experiments resulted in a 50- to 100-fold increase in ABCC5 expression. This disparity likely induced significant cellular stress, which may have confounded the results. Given these limitations, a full CRISPR KO of ABCC5 might offer a more definitive approach to understanding which genes respond to the absence of ABCC5. A CRISPR KO would eliminate the gene, providing a clearer picture of the downstream effects and avoiding the transient nature of RNA-level changes observed in KD experiments. Additionally, the experimental approach would have benefitted from validation with a known transcription factor of ABCC5, such as FOXM1. Assessing whether ABCC5 KD or OE leads to changes in FOXM1 expression would provide a more targeted and reliable measure of the impact on gene regulation. Ultimately, the chosen experimental procedure to identify transcription factors was not ideal and other methods such as chromatin immunoprecipitation (ChIP), electrophoretic mobility shift assays (EMSA) or reporter gene assays should have been used.

Furthermore, computational methods inherently pose limitations, and the reliance on gene expression data emphasises the need for a comprehensive investigation

at the protein level. To gain a deeper understanding of observed effects, additional experiments such as ChIP assays and functional studies are suggested to confirm relationships between *ABCC5* and specific co-expressed genes, such as *DMTF1*, *PRDM15*, and *SUPT7L*. ABCC5's association with chromatin organisation and epigenetic regulation implies that it may impact the epigenetic landscape of cancer cells. Further research into the specific genes affected by ABCC5 in these processes and their relevance to cancer development is warranted. Furthermore, the interaction between ABCC5 and MDM4, a regulator of the p53 pathway, presents a promising avenue for additional research. Understanding how ABCC5 affects MDM4 and, consequently, p53 activity may provide insights into cancer progression, especially in prostate cancer. The next chapter investigates the role of ABCC5 in protein-protein interactions and seeks to identify shared pointers linking results from previous chapters. Additionally, the chapter explores various functional assays designed to assess how ABCC5 impacts cancer cell behaviour. This marks a shift from molecular insights to a more comprehensive understanding, trying to connect gene expression data to tangible outcomes influencing cancer progression.

5 | Proteome Studies Uncover ABCC5 Connections to Apoptosis and Mitochondrial Pathways

5.1 Introduction

5.1.1 Protein Co-Expression and Interaction Network Analysis

ABCC5 has been associated with various roles, with a primary focus on its involvement in drug resistance in cancer, as also observed for numerous ABC transporters (279; 291; 238). However, detailed mechanistic data on the role and involvement of ABCC5 in oncogenic pathways have so far been lacking. The complex biochemical and metabolic protein-protein interaction networks that are present in cells are necessary for the maintenance of homeostasis. These complex interactions are disrupted upon the development of cancer (480). Computational approaches that look at the information contained within protein-protein interaction networks (PPIs) have emerged as promising tools to shed light on the elusive roles of proteins in a cellular context (481; 482). Proteins which are involved in the same cellular pathways and processes often interact repeatedly and transiently (483; 484). More than 80% of proteins operate in complexes or across transient interactions which can be explored by looking at the connectivity patterns of proteins in PPI networks (485). Studying PPIs is crucial for deducing the functions of proteins within a cell as it enables us to predict the functionality of uncharacterised and orphan proteins based on their interactions with proteins whose functions are already known (486; 487).

5.1.2 Promoter Motif Analysis

Gene promoter analysis is a technique by which regulatory regions upstream of genes are analysed for specific DNA motifs that act as binding sites for transcription factors (488). When these motifs overlap between genes encoding distinct proteins, it can be a shared regulatory mechanism, hinting at their potential involvement in similar cellular pathways and functions (489; 490). A recent study showed that 95% of co-expressed genes shared regulatory elements (491). Discovering shared promoter motifs can provide clues about the biological functions of the clustered proteins. If the identified motifs are bound by specific transcription factors that are associated with a particular biological process or pathway, it may indicate that the transcribed proteins play roles in those processes (492; 493). This can help to determine the involvement of proteins and guide further experimental studies to investigate the functions of the proteins within the context of cellular pathways.

5.1.3 Cancer Hallmarks

The hallmarks of cancer encapsulated the fundamental characteristics of malignant cells and were first proposed about 20 years ago (494). Since then, the hallmarks have been expanded to include resistance to cell death, sustaining proliferative signalling, evading growth suppressors, replicative immortality, neovascularisation, invasion and metastasis, reprogramming cellular metabolism, and avoiding immune destruction (495). While all of these factors are relevant in prostate cancer (PCa), this chapter narrows its focus on sustaining proliferative signalling and resistance to cell death. In cancer, cellular proliferation is characterised by uncontrolled division and expansion of malignant cells (496). In PCa, this uncontrolled proliferation is primarily driven by the androgen receptor pathway (497).

Further, dysregulation of apoptosis permits the survival and proliferation of cancerous cells (498). Mitochondria are essential organelles responsible for energy production in cells through oxidative phosphorylation, but they also play a critical role in the regulation of apoptosis (499). Mitochondria release cytochrome c and other pro-apoptotic factors which trigger the intrinsic apoptosis pathway via caspase proteins (500).

5.1.4 Aims

1. Identify and characterise potential protein interactors of ABCC5 by screening databases and establishing a network of proteins that may interact with ABCC5.

2. Investigate potential regulatory similarities between ABCC5 and its potential interactors by looking at promoter motif similarities to differentiate whether shared regulatory elements suggest coordinated gene expression patterns.

3. Investigate the roles and functions of the identified proteins and evaluate if groups of them relate to certain pathways or metabolic processes.

4. Select the most promising candidates related to ABCC5 and PCa and conduct initial functional studies to establish their connection to ABCC5.

5.2 Results

5.2.1 Protein Interaction Network

In this chapter, the focus shifts from the RNA level to the protein level, thus advancing the exploration of ABCC5 and its potential role in cellular pathways and PCa. By examining potential protein interactors, the aim is to connect the findings at the RNA level with corresponding protein-level observations. Little is known about the potential interactions and regulatory mechanisms surrounding ABCC5. Therefore, protein databases were searched for reported and predicted ABCC5 interactor proteins to construct an extended PPI network. A network analysis was conducted using the STRING database (481; 482) as seen in **Figure 5.1**. The network consists of 76 nodes and 103 edges, with an average node degree of 2.71, indicating each protein interacts with approximately 2.71 others (501). The average local clustering coefficient is 0.444, revealing a dense network where proteins' interacting partners tend to interact with each other (502). Additionally, the PPI network showed a low enrichment p-value of $1.0e^{-16}$, therefore suggesting a low likelihood that these interactions occur by chance. The database retrieval that was conducted would naturally yield a network with ABCC5 at its core, given that all the proteins examined were either experimentally confirmed or proposed to interact with ABCC5.

The clustering analysis was performed using the String database to provide deeper insights into the interrelationships among the proteins. The primary objective was to identify and categorise distinct functional groups based on the interconnection patterns. Subsequently, this network (**Figure 5.1**) was supplemented with data that incorporates information about the main cellular compartments in which each protein is located, such as the nucleus, the plasma membrane, and the mito-

chondria. The largest group of proteins (12%) corresponds to transport and related processes while the remaining proteins are involved in metabolic and translational functions or cover a range of other diverse processes. A substantial portion of the co-expressed proteins shows localisation to the nucleus. Furthermore, a small fraction of the co-expressed proteins is found to be localised to the mitochondria. Interestingly, the network exhibited a natural tendency to segregate into three clusters. Therefore, the identified proteins were clustered by MCL clustering, which considered the interconnectivity between proteins reflected in the number of edges that connect them, to ascertain the presence of distinct groups within the network structure. To enhance the robustness of the analysis, clusters consisting of only one protein were excluded, resulting in a subset of 55 proteins that effectively formed three distinct clusters as seen in **Figure 5.2**. The proteins of the two main clusters (blue and red) were submitted for analysis by GProfiler to get the most significant and relevant Gene Ontology (GO) molecular function terms associated with these clusters.

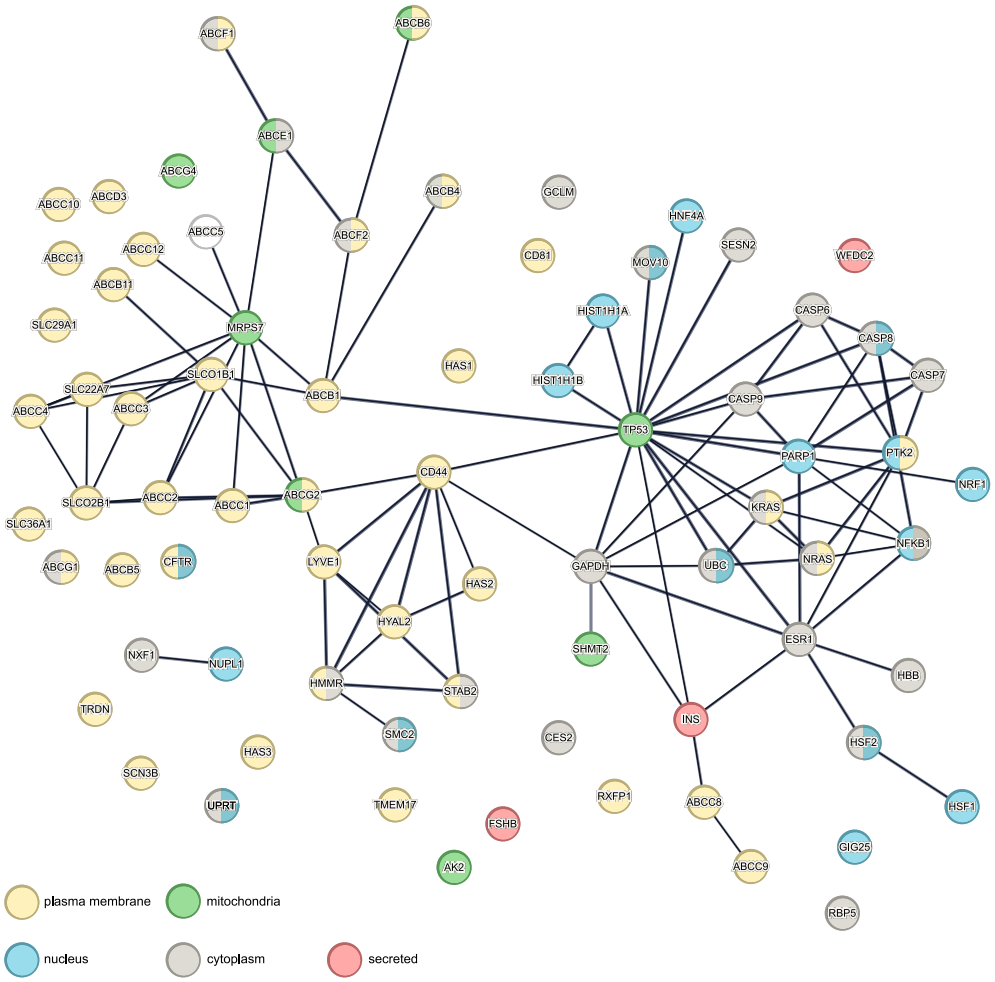

Figure 5.1: ABCC5-associated protein network. ABCC5-associated proteins were curated from various databases (**Chapter 2**) and visualised using String, with a high-confidence score threshold of 0.700. The resulting network comprises 76 nodes connected by 103 edges, yielding an average node degree of 2.71. The average local clustering coefficient is 0.444 and the enrichment p-value is $1.0e^{-16}$. The interaction network was supplemented with data on the subcellular protein location from the PDB, KEGG, and Genecards database.

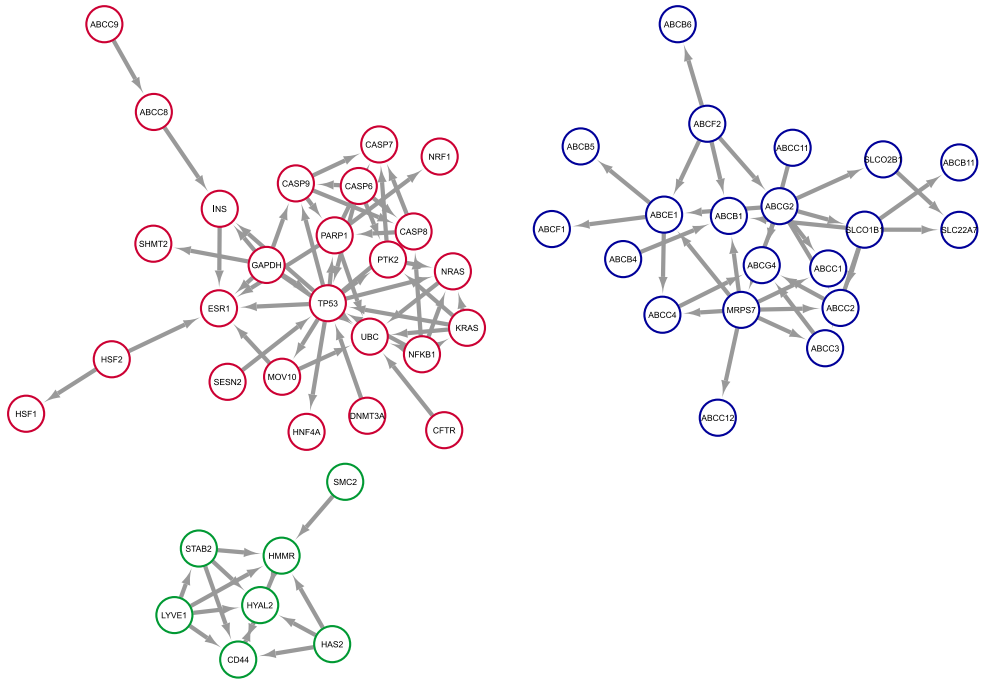

Figure 5.2: Clustering of proteins. The PPI network associated with ABCC5 exhibits a distinct clustering pattern, partitioning into four discernible clusters. The clustering analysis was executed using the MCL tool within the clusterMaker2 Cytoscape app, leveraging the network's edge connections to group nodes effectively. Clusters comprising only a single node have been omitted from display for clarity and conciseness.

Figure 5.3 highlights the associated GO terms per cluster according to the cluster colour. The analysis groups together semantically similar GO terms and selects representative terms for each cluster. The size of each bubble in the graph corresponds to the log p-value of the associated terms and their statistical significance. The blue cluster predominantly encompasses various types of ABC transporters, which is reflected by the GO terms relating to ATP-hydrolysis, ABC-type transporter activity, and lipid transporter activity. In the red cluster, a considerable degree of variability is observed in the associated molecular function terms. These terms span a wide spectrum of biological activities, including DNA-binding tran-

scription activator activity, chromatin binding, enzyme binding, protein complex binding, compound binding, and cysteine-endopeptidase activity linked to apoptosis. This diversity emphasises the varied molecular functions associated with the proteins in the red cluster.

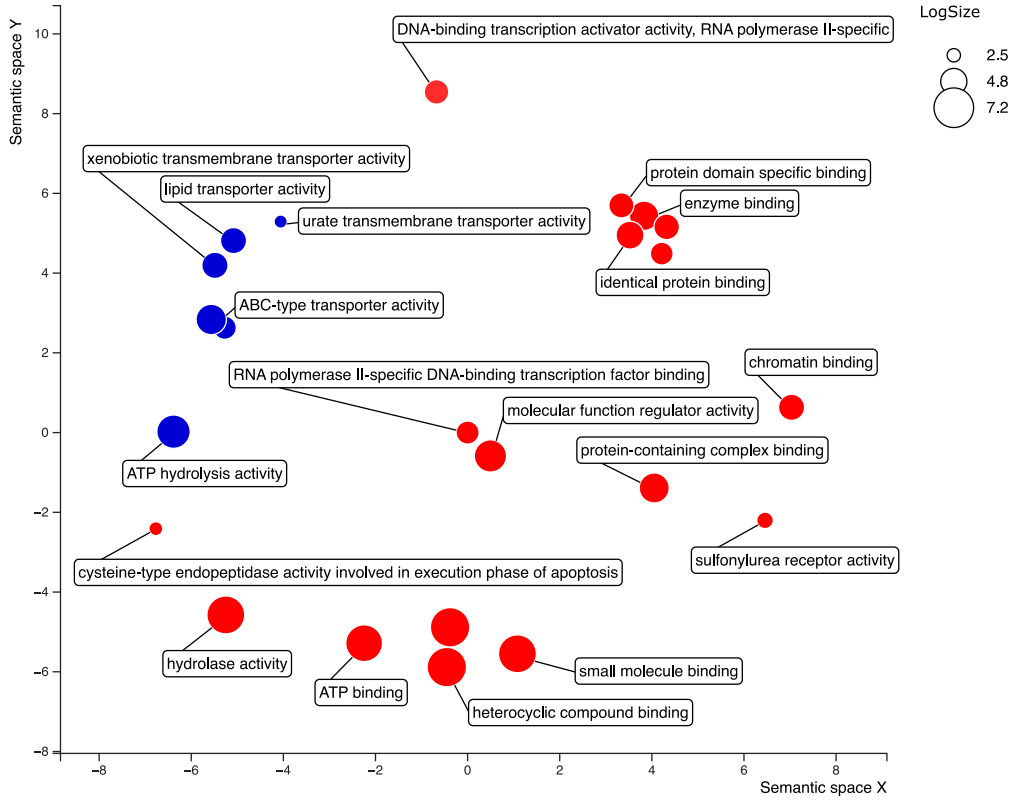

Figure 5.3: Scatterplot of GO terms for molecular function correlated with the proteins of Cluster 1 (red) and Cluster 2 (blue). The most statistically significant points include their respective GO molecular function term and redundant terms are not displayed. The size of the bubble correlates with the respective log p-value of the term.

A more detailed investigation of selected proteins within the red cluster involved looking into a meta-analysis that encompassed a comprehensive compilation of 1,488 transcriptomic profiles obtained from both benign and malignant prostate tissues, spanning various stages of cancer progression across multiple studies

(304). From this study, the co-expression values of the proteins and ABCC5 were extracted, and serine hydroxymethyltransferase 2 (SHMT2), protein tyrosine kinase 2 (PTK2), poly(ADP-ribose) polymerase 1 (PARP1), nuclear respiratory factor 1 (NRF1), estrogen receptor 1 (ESR1), caspase (CASP) 6, 7, and 8 (CASP6; CASP7; CASP8) were identified as particularly interesting candidates. These candidates were further assessed to determine if the observed correlation in gene expression translates to a protein-level relationship with ABCC5. Next, we also explored the potential relationship between the ABC-transporters in the blue cluster and ABCC5. This was accomplished by examining promoter motif similarities to establish if there were indications of coordinated expression between these transporters and ABCC5.

5.2.2 Transporter Proteins

5.2.2.1 Motif Analysis

In this section, we conducted a comprehensive analysis of the promoter motifs associated with the proteins in the blue cluster and ABCC5. Our hypothesis originated from the idea that co-expressed proteins may exhibit similar or overlapping patterns of binding site motifs within their gene promoter regions. To test this hypothesis, we obtained the respective promoter regions from Ensemble and utilised the SEA algorithm (503) to identify significant motif overlap. The analysis initially identified a total of 178 motifs across all the analysed gene promoters. To refine the results, the number of motifs was narrowed down by only considering motifs that were present in ABCC5, resulting in a reduced set of 39 motifs. These selected motifs were then evaluated based on their respective p-values, q-values, and e-values. Of particular importance was the e-value, as a lower e-value indicates that the observed motif overlap is less likely to have occurred randomly. In

essence, this process allowed us to focus on the 19 most relevant motifs for further analysis. **Figure 5.4** presents the results of this analysis in the form of a heatmap. This heatmap offers a comprehensive overview of the distribution of motifs within the blue cluster and ABCC5. The order of motifs in the heatmap is determined by their statistical significance, with the most significant motifs positioned at the top of the heatmap. **Table 5.1** provides more detailed information for each motif detailing the consensus sequence, name, and their respective p-value, e-value, and q-value scores.

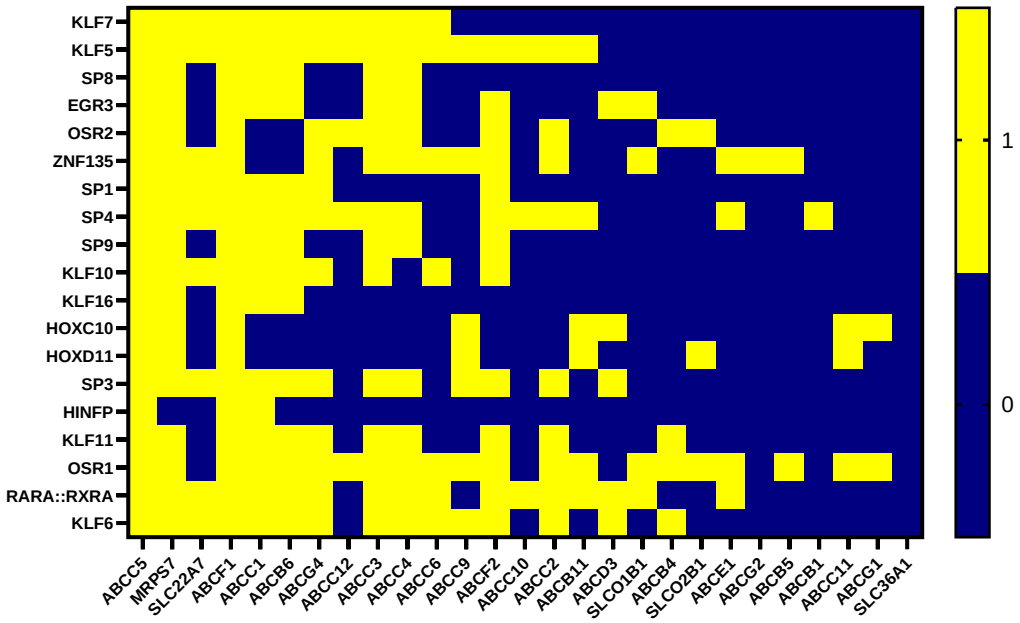

Figure 5.4: Binary heatmap of motif occurrence in transporter protein gene promoters. Each row represents a distinct motif, and each column depicts a promoter sequence of a transporter protein. Yellow squares signify the presence of motifs, whilst blue signifies motif absence.

Table 5.1: Enriched motifs in promoter sequences of submitted proteins. (P-value * <0.05, E-value * <0.05, Q-value * <0.05)

	Motif name	P-value	E-value	Q-value
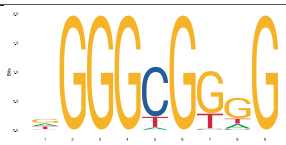	KLF7	$3.32e^{-6}$	$4.07e^{-3}$	$1.50e^{-3}$
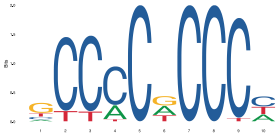	KLF5	$9.77e^{-6}$	$1.20e^{-2}$	$1.50e^{-3}$
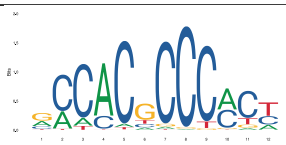	SP8	$1.60e^{-5}$	$1.97e^{-2}$	$1.50e^{-3}$
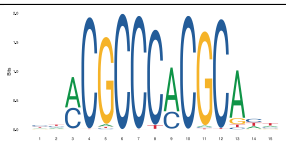	EGR3	$3.47e^{-5}$	$4.26e^{-2}$	$1.94e^{-3}$
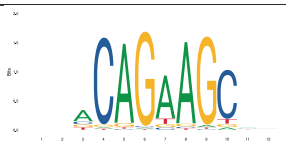	OSR2	$3.47e^{-5}$	$4.26e^{-2}$	$1.94e^{-3}$
	ZNF135	$4.14e^{-5}$	$5.08e^{-2}$	$1.94e^{-3}$
	SP1	$5.40e^{-5}$	$6.63e^{-2}$	$2.30e^{-3}$
	SP4	$7.46e^{-5}$	$9.15e^{-2}$	$2.48e^{-3}$

Continued on next page

Table 5.1 – continued from previous page

	Motif name	P-value	E-value	Q-value
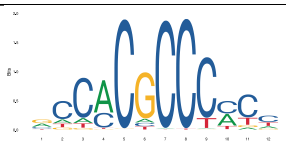	SP9	$1.30e^{-4}$	$1.59e^{-1}$	$2.74e^{-3}$
	KLF10	$2.23e^{-4}$	$2.74e^{-1}$	$3.64e^{-3}$
	KLF16	$2.26e^{-4}$	$2.77e^{-1}$	$3.64e^{-3}$
	HOXC10	$3.03e^{-4}$	$3.71e^{-1}$	$4.57e^{-3}$
	HOXD11	$3.03e^{-4}$	$3.71e^{-1}$	$4.57e^{-3}$
	SP3	$3.87e^{-4}$	$4.75e^{-1}$	$4.63e^{-3}$
	HINFP	$5.24e^{-4}$	$6.43e^{-1}$	$4.63e^{-3}$
	KLF11	$6.90e^{-4}$	$8.46e^{-1}$	$5.70e^{-3}$

Continued on next page

Table 5.1 – continued from previous page

	Motif name	P-value	E-value	Q-value
	OSR1	8.05e^{-4}	9.88e^{-1}	6.39e^{-3}
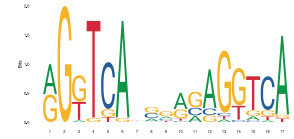	RARA-RXRA	1.29e^{-3}	1.58e^{0}	8.15e^{-3}
	KLF6	1.59e^{-3}	1.95e^{0}	9.43e^{-3}

Figure 5.5 offers insights into the extent of motif correspondence between these transporter gene promoters and the ABCC5 promoter. When analysing the graph, we can categorise the results into distinct groups based on the percentage of similarity observed in the promoter regions.

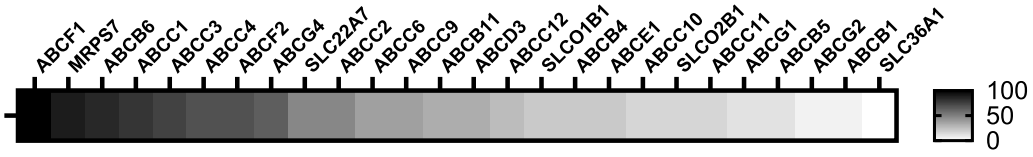

Figure 5.5: Motif overlap analysis. Percentage of shared promoter motifs between transporter proteins and ABCC5.

The first group demonstrates high similarity, ranging from 79% to 100%, which was observed in the promoter regions of ABCF1, MRPS7, ABCB6, and ABCC1. This group exhibits either an identical set of motifs or very high similarity among the motifs present. The second group displays moderate similarity, with values falling between 63% and 74%. Members of this group include ABCC3, ABCC4,

ABCF2, and ABCG4. The third group, characterised by partial similarity ranging from 26% to 47%, includes SLC22A7, ABCC2, ABCC6, ABCC9, ABCB11, ABCD3, and ABCC12. These genes exhibit some indicative overlap of motifs but also have a notable number of missing motifs when compared to the ABCC5 promoter. The final group demonstrates either no similarity (0%) or minimal similarity, up to 21%. Members of this group encompass SLCO1B1, ABCB4, ABCE1, ABCC10, SLCO2B1, ABCC1, ABCG1, ABCB5, ABCG2, ABCB1, and SLC36A1. Notably, the ABCC5 paralogs ABCC11 (16%) and ABCC12 (26%) exhibit very low scores in terms of promoter motif similarity.

This prompted a further look at the ABCC5 paralogues in the next section as diverging promoter motifs might elucidate differential roles in human pathways. **Figure 5.6** shows a more in-depth analysis of the results, with a specific focus on individual motifs and their associated Seq Scores. The Seq Score is important as it quantifies the similarity between these motifs, offering insights into their sequence-level identity. The Seq Scores in this analysis span a range from 5 to 17 for the selected 19 motifs, with a score of 0 indicating the absence of a motif. This detailed examination provides a nuanced perspective on the degree of motif similarity and presence within the dataset. Seq Scores of 5 are indicative of a substantial overlap in motif identity, which provides sufficient evidence to suggest the functionality of these motifs. Upon closer examination of the motifs, it becomes evident that certain motif families, such as the Krüppel-like factor (KLF) family and the Specificity Protein (SP) family, exhibit a higher frequency than other motif types. Notably, when these KLF motifs are present, fairly high Seq Scores are consistently observed across all members of the KLF family, including KLF5, KLF6, KLF7, KLF10, and KLF11. Overall, among the 19 identified promoter motifs, 16 belong to the class of CH2H2 zinc finger transcription factors with motifs belonging to the following families: the three-zinc finger Kruppel-related

family, factors with up to three adjacent zinc fingers, factors with more than three adjacent zinc fingers, and factors with multiple dispersed zinc fingers.

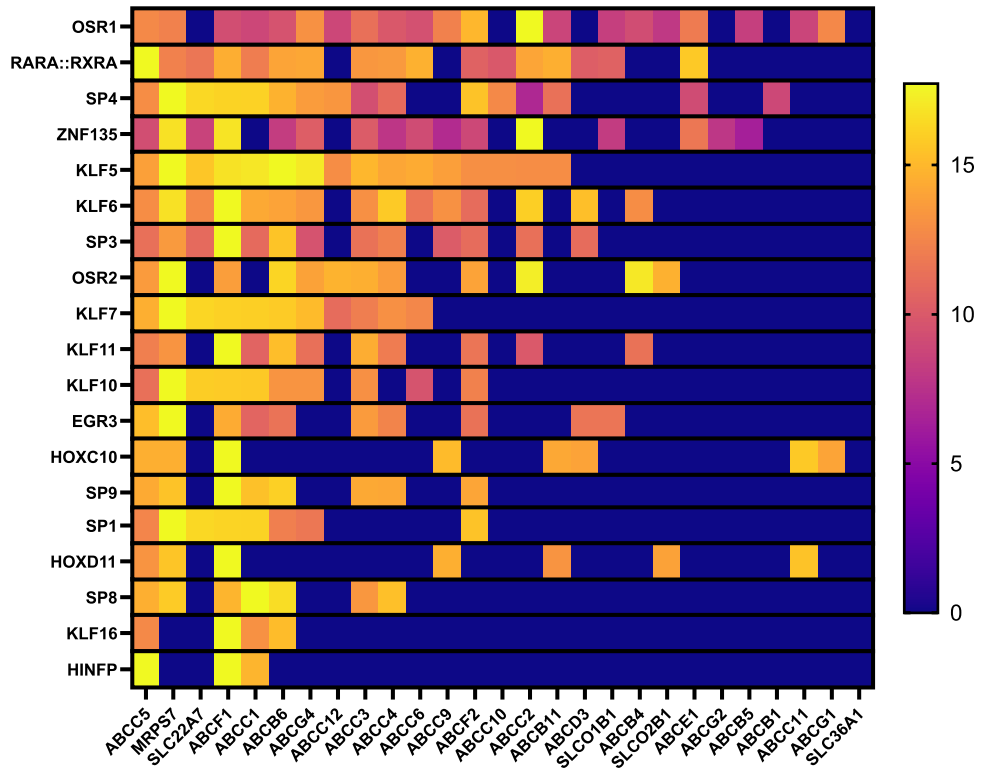

Figure 5.6: Heatmap of motif occurrence across promoter sequences of the transporter proteins. Colour intensity reflects Seq Scores, quantifying motif presence and match strength. The analysis is row-based, ensuring independent comparisons within each row, unadjusted for between-row comparisons.

In this analysis, we therefore successfully identified motifs that were shared among the protein cluster. Subsequently, the motifs were subjected to further analysis to uncover potential associations between the motifs and specific cellular pathways. To address this, the most significant associated GO terms across the motifs were identified. These terms encompassed three categories: molecular function (MF), biological process (BP), and cellular compartment (CC). **Figure 5.7** illustrates the most significant results in a 2D interaction map. The colour intensity in the fig-

ure signifies the relative percentage of overlap, which has been normalised to the highest motif overlap.

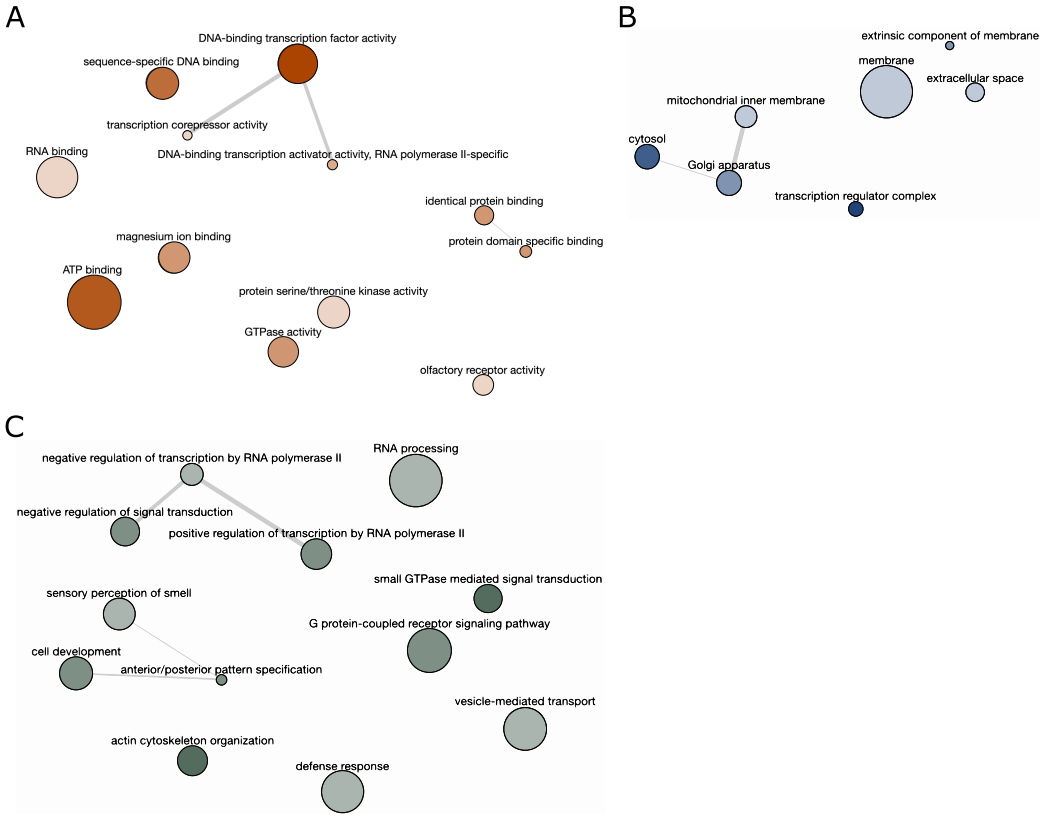

Figure 5.7: Mining consensus Gene Ontology (GO) terms from promoter motif analysis. Most significant GO terms are extracted from the top associated terms across all motifs. The terms were grouped by **A)** molecular function, **B)** cellular compartment, and **C)** biological process. The colour intensity reflects the prevalence of GO terms across motifs. The connection represents terms that belong to overarching common pathways while the bubble size represents the GO term statistical significance.

Interestingly, for MF, DNA-binding transcription factor activity and sequence-specific DNA binding are particularly prominent, as well as ATP binding. Motifs are also associated with magnesium ion binding, GTPase activity, and protein binding. In terms of cellular compartments, cytosol, the mitochondrial inner mem-

brane, and the Golgi apparatus are interesting findings. For BP, the most prominent terms are linked to signal transduction across multiple cellular domains. Furthermore, motifs were found to be associated with actin cytoskeleton organisation and cell development. The results highlight pathways and functions that are associated with the respective transcription factors that bind the promoter motifs.

5.2.2.2 Role of ABCC5 Paralogues

The results in the previous section prompted a more in-depth analysis of the relationship between ABCC5, ABCC11 and ABCC12. Therefore, we explored the relationship between ABCC5 and ABCC11 expression by qPCR analysis of ABCC11 mRNA levels in cells treated with siRNA targeting ABCC5 or overexpressing ABCC5. The results of this analysis are presented in **Figure 5.8**. As shown in **Fig. 5.8 C**, decrease of ABCC5 using siRNA led to a significant increase in ABCC11 mRNA levels after 72 h. Specifically, ABCC11 mRNA levels were increased by approximately 2-fold in LNCaP cells compared to control cells treated with non-targeting siRNA. On the contrary, overexpression of ABCC5 did not result in a change in ABCC11 mRNA levels. Interestingly, ABCC11 mRNA levels were reduced by 50% after 24 h of ABCC5 elimination in PC-3 cells, showing a reverse trend to the data in LNCaP cells. The initial decrease in PC-3 cells after 24h levels off at later time points, and there was no difference between treatment and control.

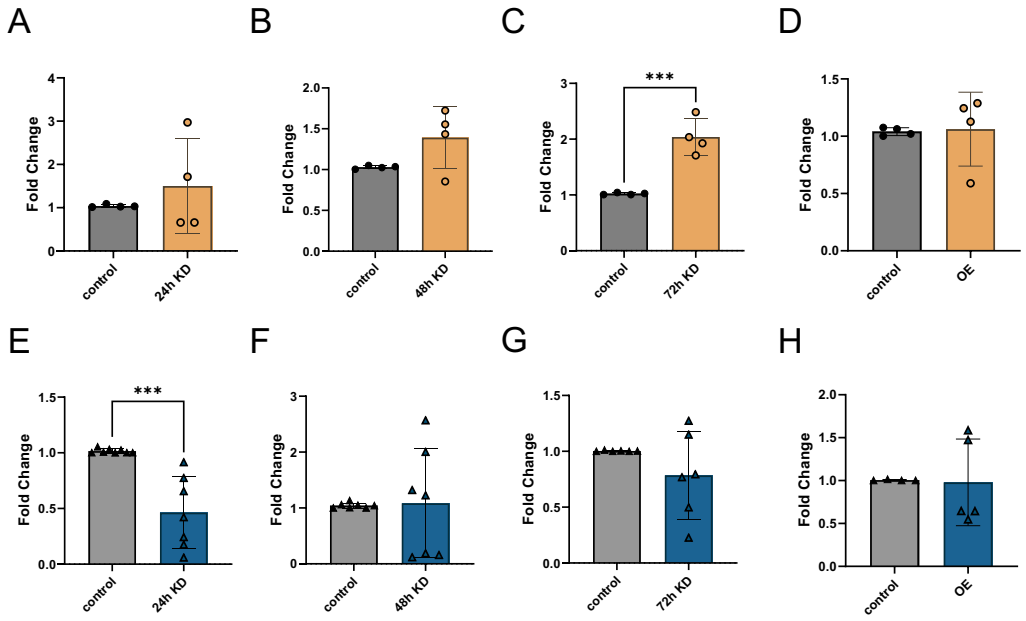

Figure 5.8: *ABCC11* expression levels upon *ABCC5* KD and OE. The relative *ABCC11* mRNA levels in LNCaP cells (orange) and PC-3 cells (blue) are presented following *ABCC5* KD and OE. The mRNA levels were assessed at different time points: 24 h (**A**, **E**), 48 h (**B**, **F**), and 72 h (**C**, **G**) after *ABCC5* KD. Additionally, the relative mRNA levels of *ABCC11* at 72 h (**D**, **H**) post-transfection with the ABCC5 plasmid in LNCaP and PC-3 cells, respectively, are depicted. The results, based on a sample size of n=4-8, are depicted as mean ± SD. Statistical significance (P-value $***$ <0.001) was determined using an unpaired two-tailed t-test.

Regarding the ABCC12 expression data, there is an initial decrease in ABCC12 mRNA after 24 h in LNCaP cells, as seen in **Figure 5.9 A**. However, a noticeable trend is observed, whereby the ABCC12 mRNA levels tend to return to control levels at later time points. In regards to the expression levels of ABCC12 in PC-3 cells, no discernible changes were observed following ABCC5 KD or OE. Ultimately, there is no clear correlation between ABCC5 and ABCC11 or ABCC12 according to the qPCR shown here.

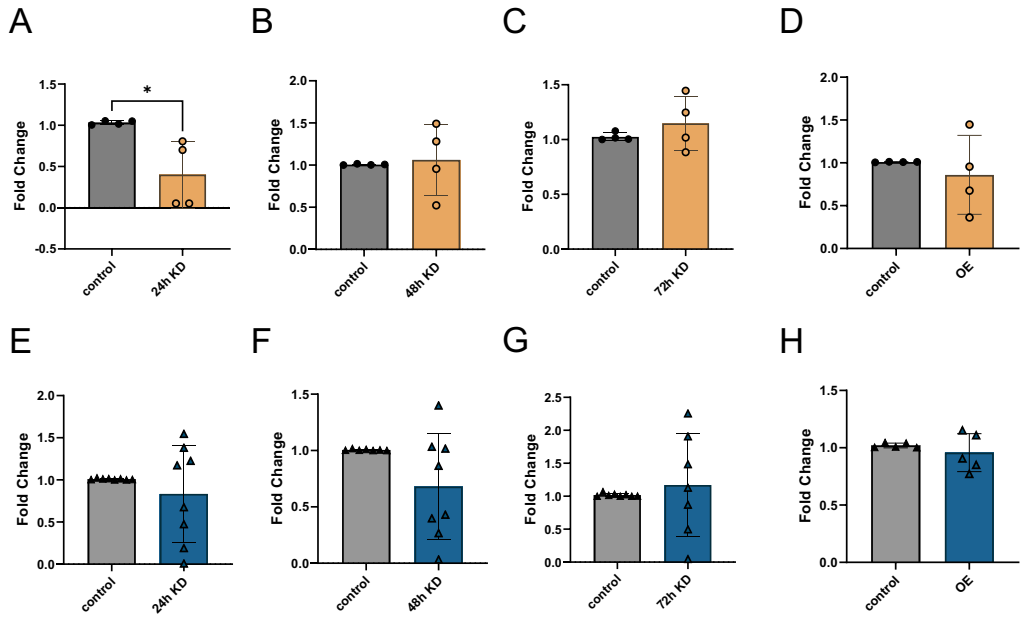

Figure 5.9: *ABCC12* expression levels upon *ABCC5* KD and OE. The relative *ABCC12* mRNA levels in LNCaP cells (orange) and PC-3 cells (blue) are presented following *ABCC5* KD and OE. The mRNA levels were assessed at different time points: 24 h (**A**, **E**), 48 h (**B**, **F**), and 72 h (**C**, **G**) after *ABCC5* KD. Additionally, the relative mRNA levels of *ABCC12* at 72 h (**D**, **H**) post-transfection with the ABCC5 plasmid in LNCaP and PC-3 cells, respectively, are depicted. The results, based on a sample size of n=4-8, are depicted as mean ± SD. Statistical significance (P-value * <0.05) was determined using an unpaired two-tailed t-test.

5.2.3 Cancer Pathway-Associated Proteins

The initial protein network clustering underscored the importance of proteins within the red cluster (**Figure 5.2**), particularly after integrating data from transcriptomic analyses of multiple PCa studies. These proteins were further classified into three groups based on their pathway involvement: sustaining proliferative signalling and replicative immortality, resistance to cell death, and metabolic involvement relevant in cancer development. In the following sections, we look into each category's proteins and their potential connection to ABCC5.

5.2.3.1 Sustaining Proliferative Signalling and Replicative Immortality

This section focuses on key candidates from the red cluster-NRF1, PARP1, PTK2, and ESR1 associated with sustaining proliferative signalling and replicative immortality in cancer. The gene expression response of these genes was measured following ABCC5 manipulation through knockdown (KD) or overexpression (OE) experiments, conducted in both LNCaP and PC-3 cells, consistent with previous chapters.

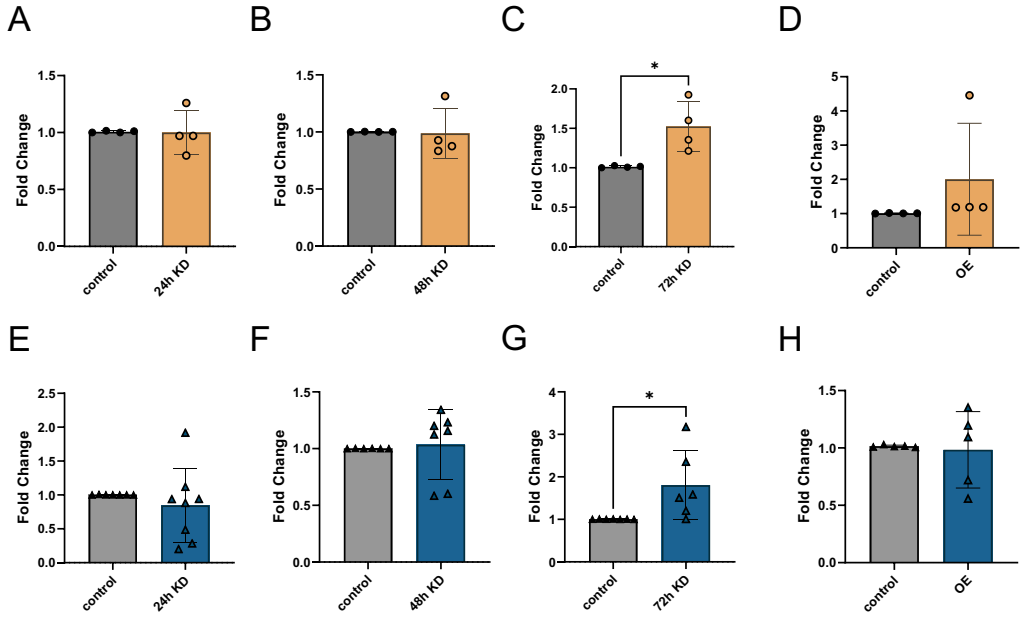

Figure 5.10: *NRF1* expression levels upon *ABCC5* KD and OE. The relative *NRF1* mRNA levels in LNCaP cells (orange) and PC-3 cells (blue) are presented following *ABCC5* KD and OE. The mRNA levels were assessed at different time points: 24 h (**A**, **E**), 48 h (**B**, **F**), and 72 h (**C**, **G**) after *ABCC5* KD. Additionally, the relative mRNA levels of *NRF1* at 72 h (**D**, **H**) post-transfection with the ABCC5 plasmid in LNCaP and PC-3 cells, respectively, are depicted. The results, based on a sample size of n=4-8, are depicted as mean ± SD. Statistical significance (P-value * <0.05) was determined using an unpaired two-tailed t-test.

As seen in **Figure 5.10-5.11-5.12**, *ABCC5* KD led to a significant increase in mRNA expression levels of *NRF1*, *PARP1*, and *PTK2* after 72 h of *ABCC5* KD

in LNCaP and PC-3 cells. The mRNA expression of *ESR1* was only significantly increased after 72 h in LNCaP cells but not in PC-3 cells as seen in **Figure 5.13**. The magnitude of the mRNA level alterations varied, with *NRF1* showing a 1.5-fold increase (**Fig. 5.10**), *PARP1* (**Fig. 5.11**) and *ESR1* (**Fig. 5.13**) displaying a 2-fold increase, and *PTK2* (**Fig. 5.12**) exhibiting a 3-fold increase in LNCaP cells. Notably, in PC-3 cells, the fold increases for *NRF1*, *PARP1*, and *PTK2* after 72 h of KD consistently remained below the levels observed in LNCaP cells.

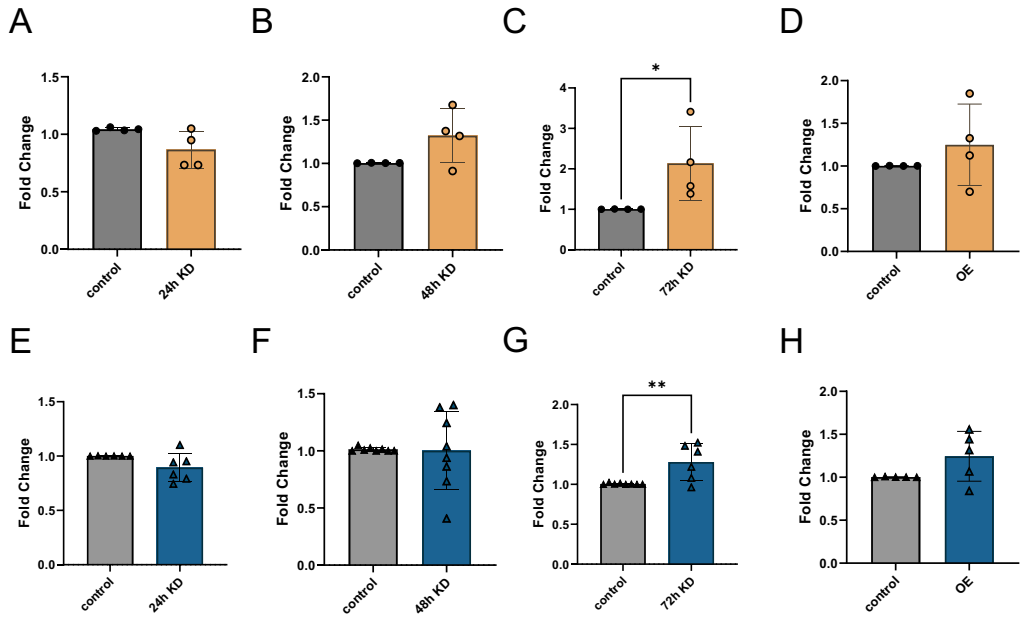

Figure 5.11: *PARP1* expression levels upon *ABCC5* KD and OE. The relative *PARP1* mRNA levels in LNCaP cells (orange) and PC-3 cells (blue) are presented following *ABCC5* KD and OE. The mRNA levels were assessed at different time points: 24 h (**A**, **E**), 48 h (**B**, **F**), and 72 h (**C**, **G**) after *ABCC5* KD. Additionally, the relative mRNA levels of *PARP1* at 72 h (**D**, **H**) post-transfection with the ABCC5 plasmid in LNCaP and PC-3 cells, respectively, are depicted. The results, based on a sample size of n=4-8, are depicted as mean ± SD. Statistical significance (P-value * <0.05, ** <0.01) was determined using an unpaired two-tailed t-test.

Interestingly, despite not being significantly elevated yet, mRNA levels of *PARP1*, *PTK2* and *ESR1* were already showing a positive trend after 48 h of *ABCC5* KD in

LNCaP cells. Conversely, *ABCC5* OE did not result in any significant changes in the expression levels of *NRF1*, *PARP1*, *PTK2* and *ESR1* compared to the control group in either LNCaP or PC-3 cells.

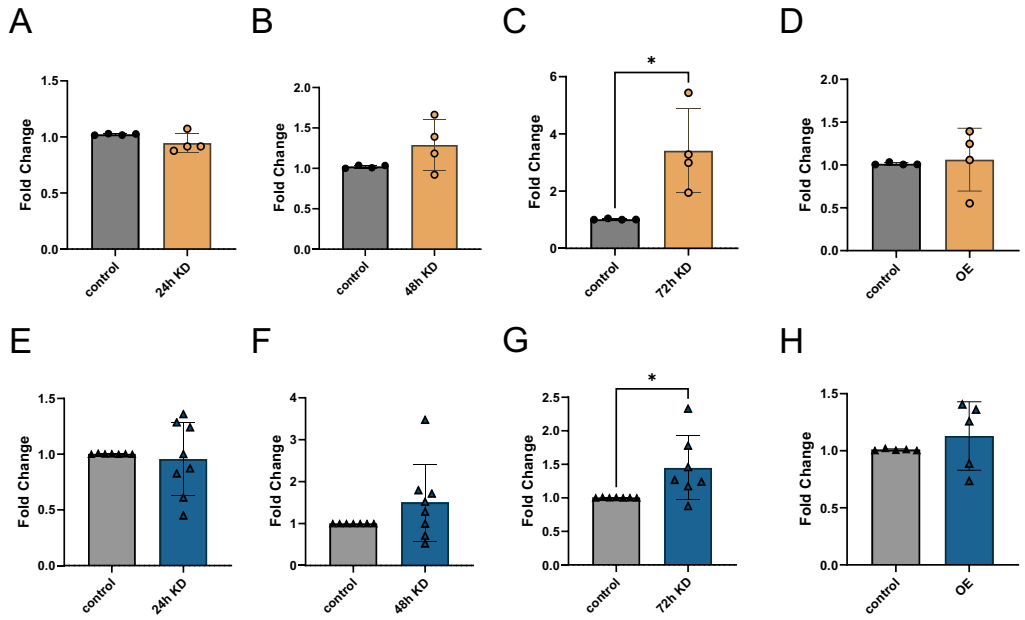

Figure 5.12: *PTK2* expression levels upon *ABCC5* KD and OE. The relative *PTK2* mRNA levels in LNCaP cells (orange) and PC-3 cells (blue) are presented following *ABCC5* KD and OE. The mRNA levels were assessed at different time points: 24 h (**A**, **E**), 48 h (**B**, **F**), and 72 h (**C**, **G**) after *ABCC5* KD. Additionally, the relative mRNA levels of *PTK2* at 72 h (**D**, **H**) post-transfection with the ABCC5 plasmid in LNCaP and PC-3 cells, respectively, are depicted. The results, based on a sample size of n=4-8, are depicted as mean ± SD. Statistical significance (P-value * <0.05) was determined using an unpaired two-tailed t-test.

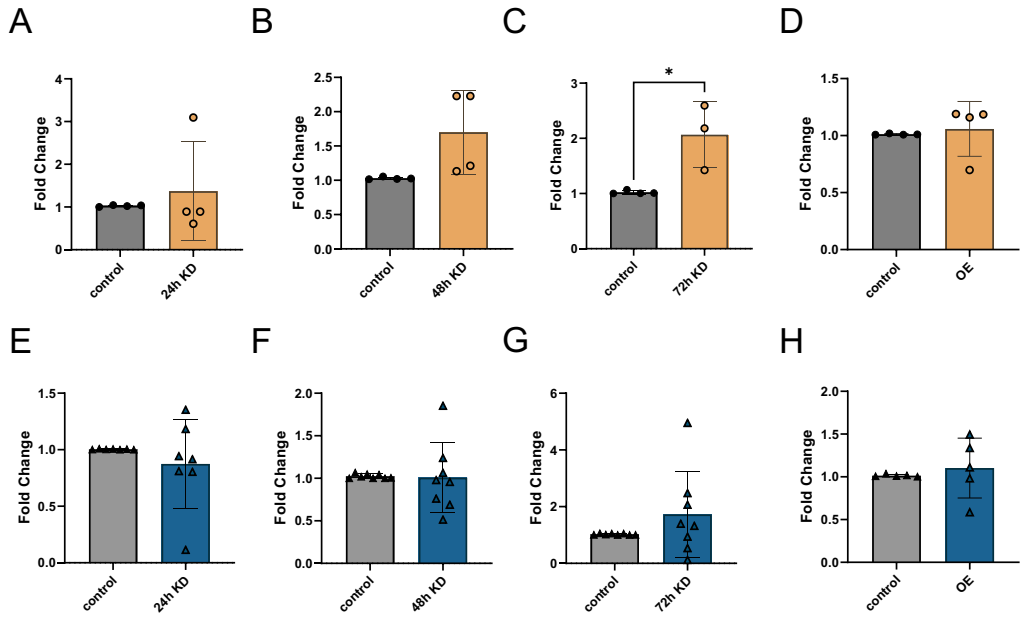

Figure 5.13: *ESR1* expression levels upon *ABCC5* KD and OE. The relative *ESR1* mRNA levels in LNCaP cells (orange) and PC-3 cells (blue) are presented following *ABCC5* KD and OE. The mRNA levels were assessed at different time points: 24 h (**A**, **E**), 48 h (**B**, **F**), and 72 h (**C**, **G**) after *ABCC5* KD. Additionally, the relative mRNA levels of *ESR1* at 72 h (**D**, **H**) post-transfection with the ABCC5 plasmid in LNCaP and PC-3 cells, respectively, are depicted. The results, based on a sample size of n=4-8, are depicted as mean ± SD. Statistical significance (P-value * <0.05) was determined using an unpaired two-tailed t-test.

The gene expression response of *NRF1*, *PARP1*, *PTK2* and *ESR1* upon manipulation of *ABCC5* gave initial hints on a potential role of *ABCC5* expression levels in cell proliferation. Therefore, in the next experiments the impact of *ABCC5* KD and OE on colony formation and cell migration in LNCaP and PC-3 cells was investigated. As seen in **Figure 5.14**, *ABCC5* KD resulted in an increase in colony formation compared to the control group in LNCaP cells. Conversely, *ABCC5* OE in LNCaP cells showed a trend towards decreasing colony formation, although this trend did not achieve statistical significance.

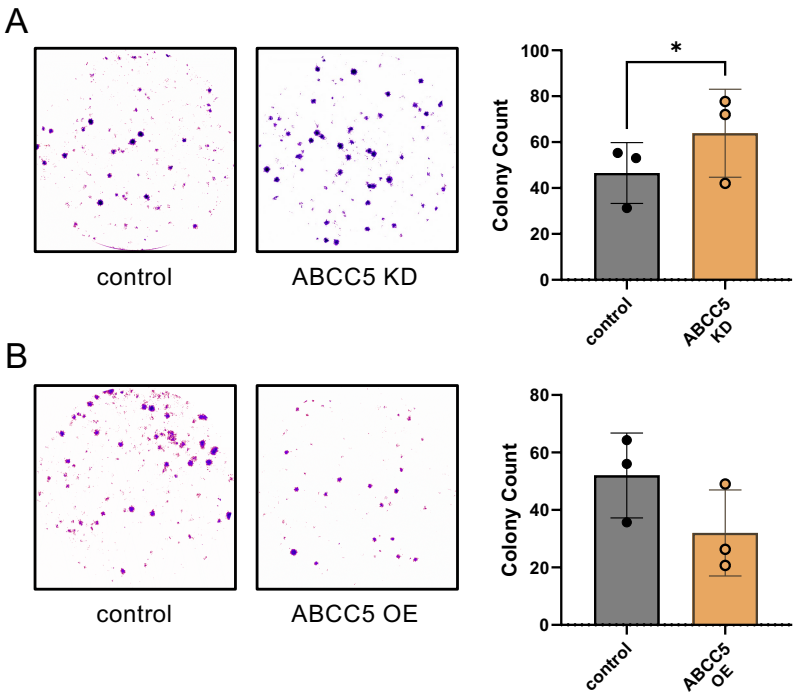

Figure 5.14: Impact of ABCC5 on colony formation in LNCaP cells. Representative images of colony formation in **A)** control and *ABCC5* KD and in **B)** control and *ABCC5* OE in LNCaP cells. The relative colony count is shown in the accompanying bar graph. Results are from n=3. Data are represented as mean ± SD. Statistical significance (P-value * <0.05) was determined using a paired two-tailed t-test.

In PC-3 cells, no significant differences in colony formation were observed across *ABCC5* KD and OE as seen in **Figure 5.15**.

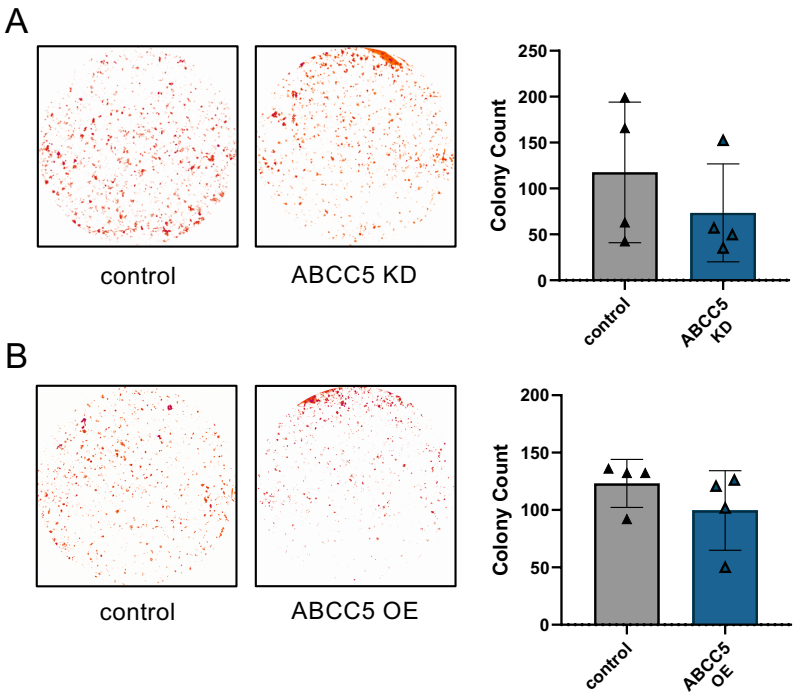

Figure 5.15: Impact of ABCC5 on colony formation in PC-3 cells. Representative images of colony formation in **A)** control and *ABCC5* KD and in **B)** control and *ABCC5* OE in PC-3 cells. The relative colony count is shown in the accompanying bar graph. Results are from n=3. Data are represented as mean ± SD. Statistical significance was determined using a paired two-tailed t-test.

The next experiment examined the number of cells migrating across a filter barrier towards a cell culture dish, based on ABCC5 expression. In **Figure 5.16**, *ABCC5* KD induced a significant increase in cell migration in LNCaP cells compared to the control group. However, *ABCC5* OE did not show any significant impact on cell migration.

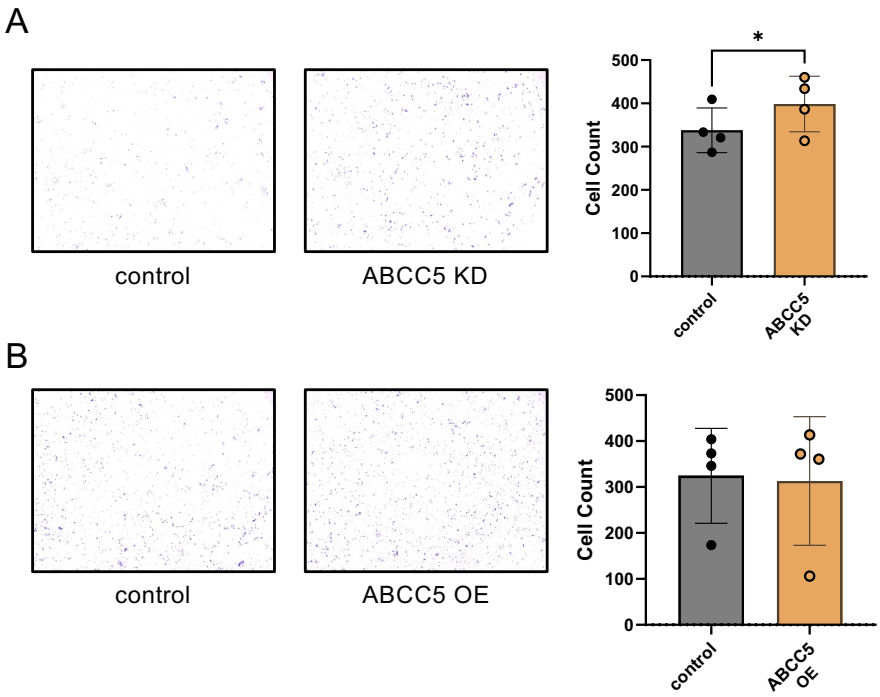

Figure 5.16: Impact of ABCC5 on LNCaP cell migration. Representative images of cell migration in **A)** control and *ABCC5* KD and in **B)** control and *ABCC5* OE in LNCaP cells. The relative migrated cell number is shown in the accompanying bar graph. The relative colony count is shown in the accompanying bar graph. Results are from n=3-4. Data are represented as mean ± SD. Statistical significance (P-value * <0.05) was determined using a paired two-tailed t-test.

In PC-3 cells, a slight decreasing trend is observed in the *ABCC5* KD group, although no significant difference is evident in *ABCC5* OE. It's important to note that the OE dataset includes only one experiment (**Figure 5.17**).

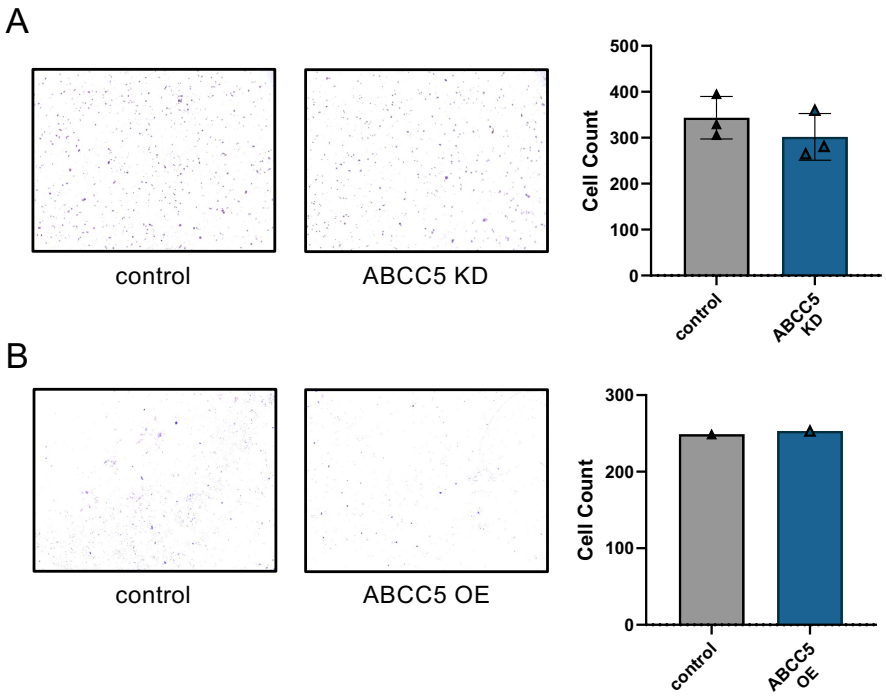

Figure 5.17: Impact of ABCC5 on PC-3 cell migration. Representative images of cell migration in **A)** control and *ABCC5* KD and in **B)** control and *ABCC5* OE in PC-3 cells. The relative The relative migrated cell number is shown in the accompanying bar graph. The relative colony count is shown in the accompanying bar graph. Results are from n=3 for **A)** and n=1 for **B)**. Data are represented as mean ± SD. Statistical significance was determined using a paired two-tailed t-test.

5.2.3.2 Resistance to Cell Death

In our initial network analysis, we identified CASP proteins as promising candidates for investigation. Caspases play a pivotal role in the regulation of apoptosis, a critical cellular pathway that can become dysregulated in cancer (498). In this section, our analysis primarily focuses on CASP6, CASP7, and CASP8, with later analyses also considering CASP3 and CASP9. These caspases are central players in the complex machinery governing cell death and survival processes (504). **Figure 5.18** reveals intriguing trends in *CASP6* expression when *ABCC5* is either

KD or OE. Notably, *CASP6* expression consistently increases as *ABCC5* concentration decreases in KD studies, with fold change ranging from approximately 1.75-fold after 48 h to approximately 2.25-fold after 72 h. Accordingly, *CASP6* expression is slightly decreased upon OE of *ABCC5*. However, this result is only observed in LNCaP cells and no discernible trend is observed in either KD or OE in PC-3 cells.

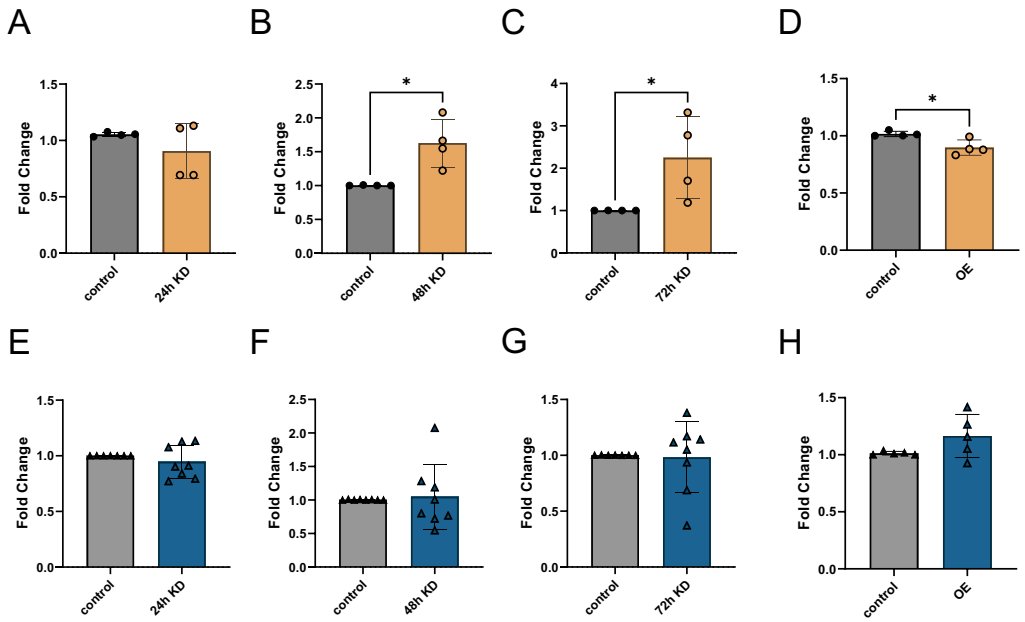

Figure 5.18: *CASP6* expression levels upon *ABCC5* KD and OE. The relative *CASP6* mRNA levels in LNCaP cells (orange) and PC-3 cells (blue) are presented following *ABCC5* KD and OE. The mRNA levels were assessed at different time points: 24 h (**A**, **E**), 48 h (**B**, **F**), and 72 h (**C**, **G**) after *ABCC5* KD. Additionally, the relative mRNA levels of *CASP6* at 72 h (**D**, **H**) post-transfection with the ABCC5 plasmid in LNCaP and PC-3 cells, respectively, are depicted. The results, based on a sample size of n=4-8, are depicted as mean ± SD. Statistical significance (P-value * <0.05) was determined using an unpaired two-tailed t-test.

Similar observations are made for *CASP7* expression in LNCaP cells, where a decrease in *ABCC5* expression correlates with increased *CASP7* levels as seen in **Figure 5.19**. Interestingly, in PC-3 cells, a statistical difference is noted in *CASP7*

expression after 72 h, which matches the observation in LNCaP cells. However, this pattern was not consistently observed at other time points.

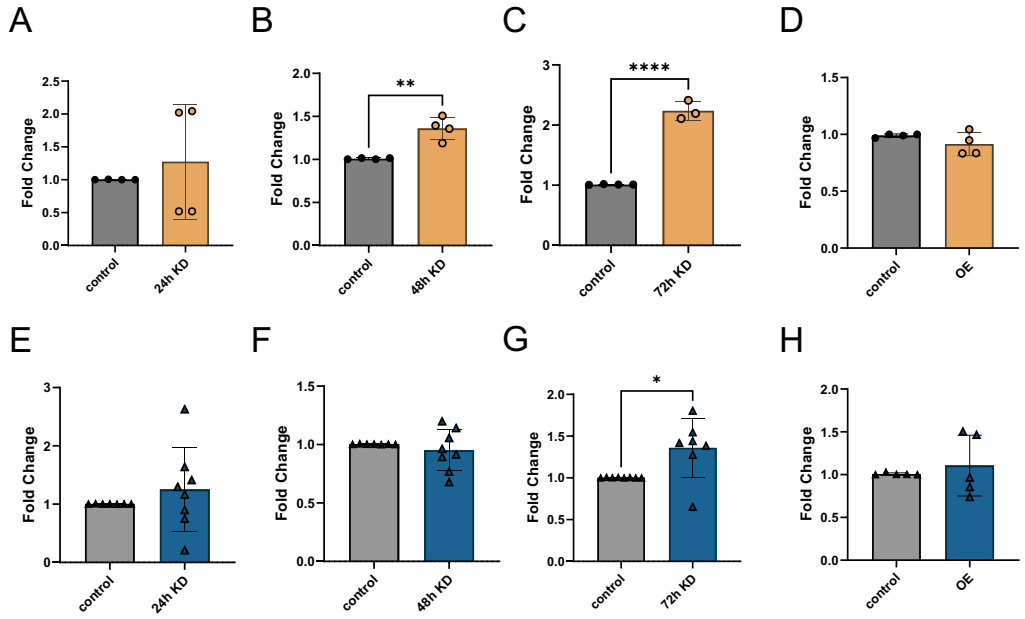

Figure 5.19: *CASP7* expression levels upon *ABCC5* KD and OE. The relative *CASP7* mRNA levels in LNCaP cells (orange) and PC-3 cells (blue) are presented following *ABCC5* KD and OE. The mRNA levels were assessed at different time points: 24 h (**A**, **E**), 48 h (**B**, **F**), and 72 h (**C**, **G**) after *ABCC5* KD. Additionally, the relative mRNA levels of *CASP7* at 72 h (**D**, **H**) post-transfection with the ABCC5 plasmid in LNCaP and PC-3 cells, respectively, are depicted. The results, based on a sample size of n=4-8, are depicted as mean ± SD. Statistical significance (P-value * <0.05, ** <0.01) was determined using an unpaired two-tailed t-test.

The results for *CASP8* expression in **Figure 5.20** mirror those observed for *CASP6* and *CASP7*, with a non-significant increase in *CASP8* expression after 48 h and a significant increase after 72 h in LNCaP cells. This inverse relationship is further supported by the OE dataset, which shows a significant reduction in *CASP8* expression. However, in the case of PC-3 cells, a similar pattern is only evident in the *CASP8* dataset at the 72 h time point, with no consistent trend observed in the OE dataset.

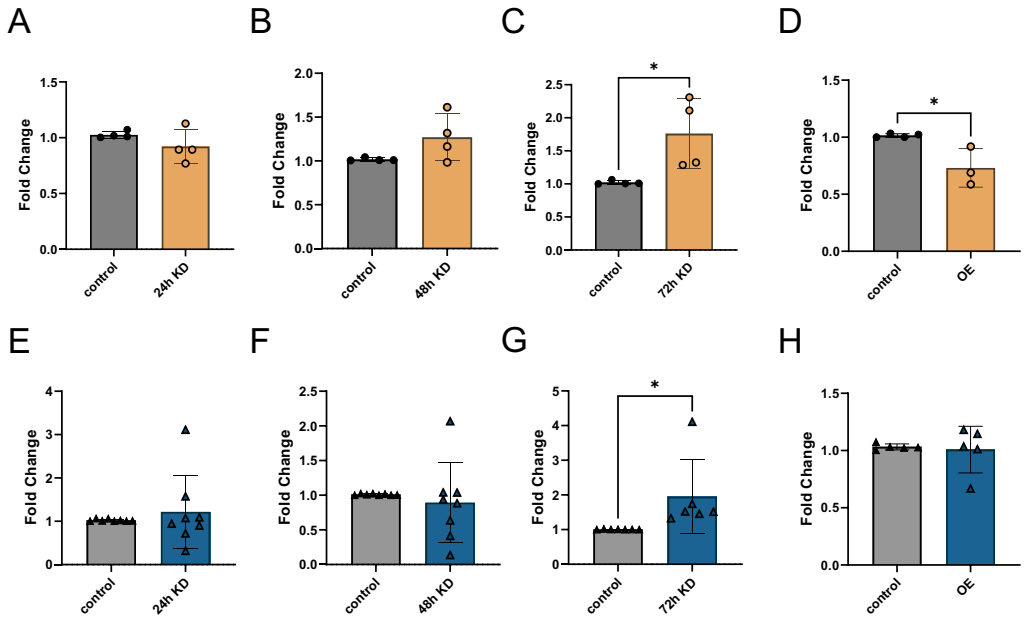

Figure 5.20: *CASP8* expression levels upon *ABCC5* KD and OE. The relative *CASP8* mRNA levels in LNCaP cells (orange) and PC-3 cells (blue) are presented following *ABCC5* KD and OE. The mRNA levels were assessed at different time points: 24 h (**A**, **E**), 48 h (**B**, **F**), and 72 h (**C**, **G**) after *ABCC5* KD. Additionally, the relative mRNA levels of *CASP8* at 72 h (**D**, **H**) post-transfection with the ABCC5 plasmid in LNCaP and PC-3 cells, respectively, are depicted. The results, based on a sample size of n=4-8, are depicted as mean ± SD. Statistical significance (P-value * <0.05) was determined using an unpaired two-tailed t-test.

To further explore the relationship between caspases and ABCC5, caspase activity studies in LNCaP and PC-3 cells were conducted. Notably, CASP 3/7 activity (**Figure 5.21**, **top row**) increased sharply upon OE of *ABCC5* in LNCaP cells. Interestingly, in PC-3 cells both KD and OE of *ABCC5* lead to significantly increased activity of CASP 3/7. Upon evaluating CASP 9 activity (**Figure 5.21**, **bottom row**), there were no significantly different activity levels following KD or OE of *ABCC5* in LNCaP cells. In contrast, in PC-3 cells, activity significantly decreased in both the KD and OE groups.

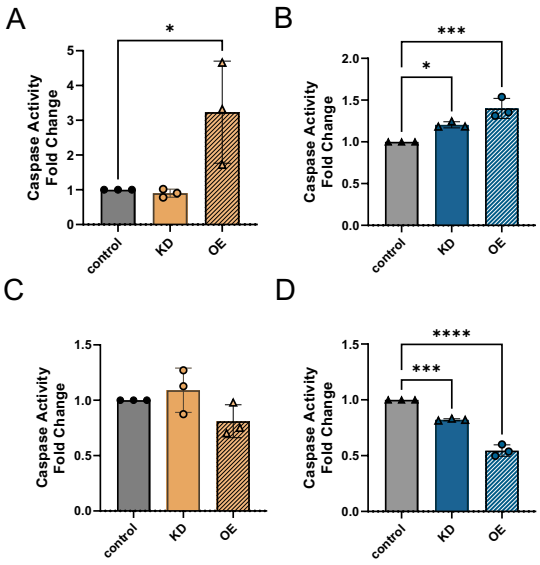

Figure 5.21: Caspase activity levels upon *ABCC5* KD and OE. Relative Casp 3/7 activity in **A)** LNCaP and **B)** PC-3 cells, respectively, after 72 h of *ABCC5* KD and OE. Relative Caspase 9 activity in **C)** LNCaP and **D)** PC-3 cells, respectively, after 72 h of *ABCC5* KD and OE. Results are from n=3. Data are represented as mean $\pm$ SD. Statistical significance (P-value * $<$0.05, ** $<$0.01, *** $<$0.001) was determined using one-way ANOVA.

5.2.3.3 Mitochondrial Involvement via SHMT2

In our investigation of the interplay between *ABCC5* and *SHMT2* gene expression, experiments in LNCaP and PC-3 cells as seen in **Figure 5.22** were completed. Upon *ABCC5* KD in LNCaP cells, a significant increase in *SHMT2* gene expression after 48 h, with a 1.5-fold upregulation, was detected. This upregulation became more pronounced after 72 h, reaching a 2-fold increase in *SHMT2* expression. Conversely, in the context of *ABCC5* OE, only a marginal reduction in *SHMT2* gene expression in LNCaP cells was observed. However, the same experimental setup conducted in PC-3 cells yielded did not yield significant results. In PC-3 cells, neither *ABCC5* KD nor OE led to any substantial changes in *SHMT2* gene expression levels at any of the time points investigated.

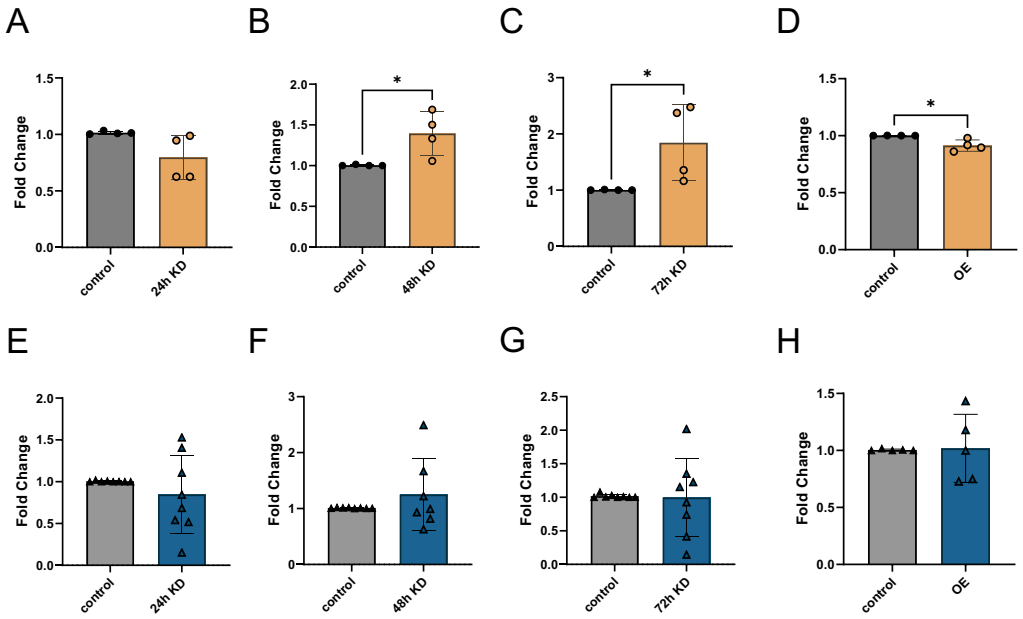

Figure 5.22: *SHMT2* expression levels upon *ABCC5* KD and OE. The relative *SHMT2* mRNA levels in LNCaP cells (orange) and PC-3 cells (blue) are presented following *ABCC5* KD and OE. The mRNA levels were assessed at different time points: 24 h (**A**, **E**), 48 h (**B**, **F**), and 72 h (**C**, **G**) after *ABCC5* KD. Additionally, the relative mRNA levels of *SHMT2* at 72 h (**D**, **H**) post-transfection with the ABCC5 plasmid in LNCaP and PC-3 cells, respectively, are depicted. The results, based on a sample size of n=4-8, are depicted as mean ± SD. Statistical significance (P-value * <0.05) was determined using an unpaired two-tailed t-test.

The initial observation of *SHMT2* expression changes following *ABCC5* KD and OE raised the question about the potential significance of SHMT2 in PCa. To get a better understanding data was extracted from the Pan Prostate Transcriptome Atlas (307) a valuable online resource known for its comprehensive gene expression data across PCa stages.

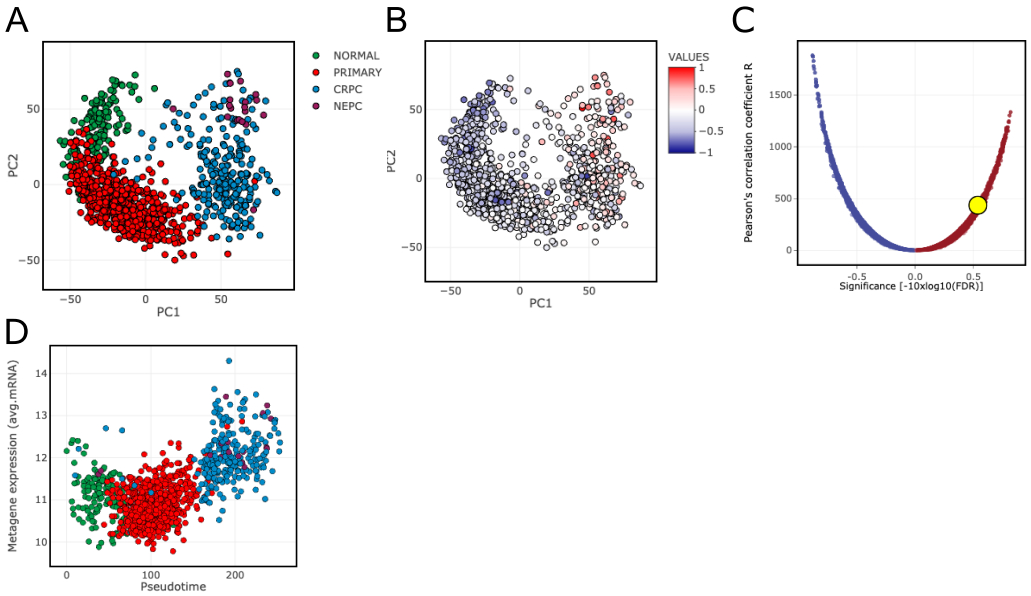

Figure 5.23: Relationship between SHMT2 expression and PCa stage. **A)** Principal component analysis (PCA) of pan-prostate cancer transcriptomes (307) obtained from the indicated studies of normal (shades of green), primary (shades of red), castration-resistant (CRPC, shades of blue), and neuroendocrine PCa (NEPC, shades of purple) **B)** Expression level change of SHMT2 dependent on PCa stage. **C)** Pearson's correlation coefficient and significance of SHMT2 correlation with disease progression in PCa - R:0.54, FDR: $2.2e^{-44}$. **D)** SHMT2 and ABCC5 mRNA correlated expression dependent on PCa stage.

Figure 5.23 A shows the principal component analysis (PCA) of the PCa datasets and highlights how the samples from distinct disease stages cluster in different localisations. This graph provides an overview of the content of the dataset itself. To examine the role of SHMT2 in PCa, expression levels across different disease stages were investigated. **Figure 5.23 B** illustrates these findings, with shades of blue indicating reduced *SHMT2* levels and shades of red indicating increased *SHMT2* levels. Notably, the analysis reveals a pronounced and statistically significant increase in *SHMT2* expression in the most advanced stages of PCa. **5.23 C** presents the pseudo line Pearson coefficient correlation, revealing an R-value of 0.54, indicative of a moderate positive correlation. Furthermore, the low false dis-

covery rate of $2.2e^{-44}$ signifies the statistical significance of this correlation. This analysis supports the notion that higher *SHMT2* expression is positively associated with more advanced stages of PCa. Additionally, it was of interest to look at the relationship between *SHMT2* and *ABCC5* expression levels across the different stages of PCa. **5.23 D** demonstrates an almost linear increase in mRNA levels of *ABCC5* and *SHMT2* as PCa stages progress.

5.3 Discussion

5.3.1 Exploring ABCC5 Interactors and Linking Gene Promoter Motifs to Prostate Cancer

The blue cluster shown in **Figure 5.2** predominantly comprises proteins from the ABC transporter family, along with some proteins from the solute carrier (SLC) transporter family. ABC transporters are involved in a wide range of cellular pathways and are responsible for the active transport of structurally diverse substrates across cellular membranes facilitated by ATP hydrolysis (505). The SLC transporters on the contrary facilitate passive diffusion of different metabolites such as amino acids, sugars, and ions (506). The clustering of these proteins was somewhat unexpected as these proteins have not previously been reported to have any interactions with each other. This has raised questions about potential common themes or interactions among members of these two transporter families, as well as their potential interactions with ABCC5. In multiple instances, interactions have been observed between ABC transporters and other proteins For example, ABCC8 and ABCC9 are well known to interact with potassium channels Kir6.1 and Kir6.2, forming channel complexes (166). Additionally, several ABC transporters, including CFTR, ABCA1, and ABCA7, possess PDZ-binding motifs that facilitate protein-protein interactions (507; 508). Notably, the ABCA1 transporter plays a crucial role in apoprotein-stimulated cholesterol efflux, which relies on a direct interaction between the apoprotein and the transporter (509).

To determine whether the proteins in the blue cluster are co-expressed with ABCC5 and may have potential PPIs, one possible approach is to examine the similarities in the gene promoter motifs. Co-expressed genes or genes belonging to similar pathways often exhibit coordinated motifs, indicating shared regulatory mecha-

nisms (489). These co-expressed genes are typically involved in related biological processes or pathways (490). For instance, a study demonstrated that co-expressed genes involved in myeloid cell differentiation tend to have a higher representation of overlapping motifs in their promoters (489). The most prevalent motif class identified in this study, present in the majority of analysed gene promoters, are the CH2H2 zinc finger factor motifs. CH2H2 motifs are bound by CH2H2 zinc finger transcription factors that can be divided into several families (510).

The CH2H2 zinc finger transcription factor family includes the Krüppel-like factor (KLF) subfamily and specificity protein (SP) transcription factor subfamily amongst others. These transcription factors are highly diverse and can regulate a wide range of genes and biological processes (511). CH2H2 zinc finger transcription factors are characterised by a zinc ion coordinated by two cysteine residues and two histidine residues, forming a structure that allows specific binding to DNA (512). Out of the 19 identified motifs shared by ABCC5 and the proteins in the blue cluster, six were found to belong to the KLF family, which plays a crucial role in cellular functions such as development, proliferation, and cell death (513). A study was also able to show that PCa clinical outcome is associated with different KLF mRNA levels (514).

The other large subfamily were SP transcription factors including SP1, SP3, SP4, SP8 and SP9. These proteins are known for their role in binding GC-rich DNA sequences and regulating the transcription of genes involved in cell growth, survival, and differentiation (515). Interestingly, there is growing evidence that the upregulation of SP1, SP3 and SP4 is associated with the transition of healthy cells towards cancerous cells (516). Specifically, SP1 has been identified as a negative prognostic marker of PCa, and a study found that G2 and S phase-expressed-1 protein upregulates the expression of SP1 in PCa cells which in turn activates the transcription of FOXM-1 (517). FOXM-1 has been shown to regulate the expres-

sion of ABCC5 in nasopharyngeal carcinoma (291). Therefore, it is reasonable to hypothesise about the interconnections among SP1, FOXM-1, and ABCC5, and how their upregulation may contribute to increased proliferation, as observed in the mentioned studies. On the contrary, the transcription factor EGR3 that was also detected is known as an important metastasis suppressor in PCa, and deletion of EGR3 is a key alteration reported in patient samples (518).

Several proteins have shown significant promoter motif overlap with the gene promoter region of ABCC5, indicating a degree of regulatory conservation. This suggests that these proteins may share common functional roles or participate in similar biological processes, and the expression of these proteins is coordinated within the spatial-temporal landscape of cell development. However, it is important to note that the same motifs could be differentially regulated and utilised depending on the cellular context (519). Notably, ABCF1 is the only gene promoter that shares all of the investigated motifs with the ABCC5 promoter. ABCF1, also known as ATP-binding cassette sub-family F member 1, plays a crucial role in the regulation of protein translation. It directly interacts with translation initiation factors, ribosomes, and various RNA-binding proteins (520). This suggests a potential functional link between ABCC5 and ABCF1 in the context of protein translation regulation. There was also a very significant motif overlap with MRPS7, ABCB6, ABCC1, and ABCC3. Interestingly, a study suggested ABCB6 and ABCC3 as predictors of PCa progression and the reduction of ABCC1 elevated chemosensitivity of LNCaP and PC-3 cell lines (312). Subsequently, a GO pathway analysis of the associated motifs was performed to provide a functional context for understanding why ABCF1, MRPS7, ABCB6, ABCC3 and ABCC1 might have clustered together in our initial analysis.

The analysis of MF GO terms revealed that the identified motifs are significantly associated with DNA-binding transcription factor activity and sequence-specific

DNA binding. This intriguing finding hints at a potential role in transcriptional regulation for the proteins linked to these motifs. Worth noting is that, to date, none of the proteins identified in this analysis have been associated with DNA-binding transcription factor activity and sequence-specific DNA binding roles. Additionally, ATP binding is another identified function, which confirms the validity of the data mining experiment, especially considering that the clustered proteins are predominantly ABC transporters. The presence of ATP binding in ABC proteins aligns with expectations, given their transport function is dependent on ATP hydrolysis. Furthermore, motifs associated with magnesium ion binding, GTPase activity, and protein binding suggest diverse molecular functions within the studied proteins across both clusters. Regarding cellular localisation, the association of motifs in the cytosol aligns with the expected intracellular distribution of ABC transporters. The motifs associated with the Golgi apparatus and mitochondrial inner membrane imply the potential roles of the identified candidate proteins in these subcellular compartments. MRPS7 is a mitochondrial ribosomal protein localised in the mitochondria and plays a crucial role in mitochondrial protein synthesis (521). While there is no known direct interaction between MRPS7 and ABCC5, a study showed the localisation of ABCC5 to mitochondrial-associated membranes (224).

In this initial analysis, several intriguing aspects of the clustered proteins were highlighted. Particularly noteworthy were the proteins ABCF1 and MRPS7, which exhibited a significant overlap with ABCC5 in gene promoter sequence motifs. Consequently, future research should explore potential connections between ABCC5 and these proteins from a more experimental perspective. At this stage, the study's scope and depth are insufficient to offer definitive mechanistic explanations for the findings reported here, underscoring the need for further research. Notably, it is fascinating to observe that several of the transcription factors present are linked

to PCa or have general associations with cancer progression or suppression. In summary, the network of proteins identified to interact with ABCC5 is immensely complex with a large number of diverse functions and cellular localisation and necessitates more targeted and comprehensive investigations of the gene expression network associated with ABCC5 function to fully elucidate its functional intricacies.

5.3.2 Potential Interrelationship between ABCC11 and ABCC5 in Prostate Cancer

My data revealed that there might be a compensatory mechanism between ABCC5 and the ABCC11 paralogue. Many genes in the mammalian genome have paralogues which are generated through gene duplication events (514). Due to the different chromosome localisation of ABCC5 (3q27.1) in comparison to ABCC11 and ABCC12, ABCC5 duplicated independently from its paralogues while ABCC11 and ABCC12 tandem duplicated on chromosome 16q12 (249). In LNCaP cells, ABCC5 KD resulted in up-regulation of ABCC11 RNA. Compensation between ABCC paralogues has previously been shown between ABCC5 and ABCC12 in testes tissue in which only double-knockout mice showed the expected phenotype (224). Other studies have also shown that paralogues can influence transcriptional regulation (522) or even suppress the expression of other paralogues (523). Accordingly, the KO or even KD of ABCC5 alone might not result in a clear phenotype if there is genetic compensation due to the existence of the functionally similar ABCC11 and ABCC12. Additionally, the motif analysis showed that there was a fairly low overlap of gene promoter motifs between ABCC5 and ABCC11 (16%) and ABCC12 (26%) in the context of this analysis.

Gene duplication events are a measure to increase biological diversity and often duplicated genes undergo functional divergence which leads to the preservation of

both gene copies (524). However, some duplicate genes also persist without functional divergence by maintaining functional redundancy. Interestingly, tandem duplicates share more genomic elements that regulate expression while sequence similarity declines depending on the distance to the duplication event (525). Often paralogues expand into divergent functions whilst also retaining overlapping functions. Ultimately, the protein can have paralogue-specific functions as well as being able to maintain functional redundancy (526; 527). In this case, ABCC5, ABCC11, and ABCC12 might have evolved to have distinct substrate specificities or tissue-specific expression patterns, preserving their functions in different contexts whilst still being able to compensate on a functional level for ABCC5. This would also explain the low overlap in gene promoter motifs which would enable differential regulation. A study of *Drosophila melanogaster* paralogues related to wing development demonstrated that paralogous genes can exhibit compensation in response to regulatory silencing of a paralogue promoter (528).

To substantiate the initial findings in this chapter, it is necessary to demonstrate the same outcomes at the protein level. Furthermore, KO cell models would have to be generated as studies of mice are limited by the absence of the ABCC11 gene in mice (253). Furthermore, this effect is only observed in LNCaP cells and not in PC-3 cells. Both cell lines are isolated from very different milieus as PC-3 cells are isolated from bone metastasis whilst LNCaP cells are isolated from lymph node metastasis which highly affects their gene expression profile (529). LNCaP cells retain more prostate cell-specific properties in their gene expression profile (452), whereas PC-3 cells highly adapt to the bone environment and show similar behaviour to osteoblasts (530). These differences between both cell lines might explain the difference in ABCC11 RNA expression upon KD of ABCC5. Interestingly, ABCC12 does not show the same up-regulation as ABCC11 and therefore the compensatory mechanism might be tissue-dependent. ABCC12 is

initially down-regulated after 24 h in LNCaP cells but recovers to regular levels shortly after. The initial downregulation of ABCC12 could be an off-target effect of the utilised siRNA which could target ABCC12 due to the sequence similarity with ABCC5.

5.3.3 Contradicting Results Regarding the Role of ABCC5 in Prostate Cancer Cell Proliferation and Related Proliferation Pathways

In the context of cancer biology, the ability to sustain proliferative signalling and bypass replicative senescence are key hallmarks of cancer development (531). This section looked into the role of ABCC5 in PCa cell proliferation. Intriguingly, our findings reveal an increase in both proliferation and migration of LNCaP cells under ABCC5 KD conditions however we did not see any changes in PC-3 cells. It is worth noting that contrasting results have been reported in other studies, which demonstrated that ABCC5 KD inhibited proliferation, migration, and invasion of LNCaP, PC-3 (301) and C4-2 cells (308; 311). The mentioned studies were also able to observe the opposite trend in ABCC5 OE with increased rates of proliferation and migration. Another study also showed that ABCC5 removal resulted in resensitising 22RV1 and C4-2B PCa cells to enzalutamide - an important treatment for castration-resistant PCa (532). One notable difference between these studies and our experimental procedures was the method of KD. The other studies utilised shRNA-mediated KD, while we employed siRNA-mediated KD. SiRNA-mediated KD offers rapid and specific suppression but is transient, while shRNA-mediated KD is stable and has reduced off-target effects but takes longer to establish (533). The studies did not specify the duration of their shRNA-mediated KD or the timing of secondary experiments, making it impossible to

rule out whether differences in results were influenced by cellular adaptation to the prolonged absence of ABCC5. The immediate increase in proliferation and migration following the siRNA-mediated decrease of ABCC5 in our experiments could potentially represent an adaptive short-term response by the cells. However, it is important to note that our results were collected at a single time point, preventing us from determining whether this effect might have stabilised or changed over time. From previous studies and our results, it is clear that ABCC5 does play a role in PCa cell proliferation and migration - exact pathways however are currently unknown.

The upregulation of PTK2 also known as focal adhesion kinase (FAK) upon *ABCC5* KD is consistent with the observed increase of PCa cell proliferation and migration upon *ABCC5* KD in LNCaP cells. FAK is a nonreceptor cytoplasmic tyrosine kinase (534) and is involved in the proliferation, migration, and invasion of cancer cells (535; 536). FAK is frequently overexpressed and overactive in several cancers including in PCa (537; 538). Therefore, it is interesting to see that KD of *ABCC5* seems to trigger increased expression of FAK. The mechanisms of upregulation of FAK are diverse and range from gene amplification, oncogenic transcription factors such as STAT3 and NF-κB, phosphorylation, growth factors, and integrin signalling to cancer pathways such as Ras-MAPK and PI3K-AKT (539; 540; 541). Thus, the connection between ABCC5 and FAK (PTK2) is unclear and warrants further investigation. Most likely, ABCC5 is connected to FAK via other proteins and modulators. estrogen receptor 1 (ESR1) is a well-known player in hormone-dependent cancers, including breast cancer (542).

However, the role of ESR1 in PCa remains a subject of ongoing debate, and its significance has not been firmly established (543; 544). Furthermore, it is worth noting that LNCaP cells have very low expression of estrogen receptors. This limitation makes them an inadequate model for studying estrogen receptors in the

context of PCa (543). Given this, the potential connection to ABCC5 may not be of significant interest for further investigation, as the current literature does not lend strong support to this line of inquiry, and LNCaP cells are not an adequate model for investigation.

PARP1 is an enzyme involved in DNA repair and the maintenance of genomic stability (545; 546). It plays a critical role in the recognition and repair of single-strand DNA breaks, contributing to genome integrity (547). Research in androgen receptor-expressing PCa cells revealed that PARP1 can enhance tumorigenic effects (548). Furthermore, a subsequent study showed that the activity of PARP1 increased as the PCa progressed to castration-resistant PCa (549). Therefore, the increase of PARP1 alongside an increase in proliferation and invasion in LNCaP cells is consistent with the current knowledge of the literature. Another study also showed that PARP1 KD reduced the growth and invasion capacity of PCa cells (550). More recently, PARP1 inhibitors have been approved by the US FDA for the treatment of metastatic castrate-resistant PCa in patients with specific DNA repair deficiencies (551). The direct link to ABCC5 is still missing but further research would be necessary to firmly establish that there is a link to PARP1 by replicating the results on the protein level.

NRF1 relates to proliferation on a more abstract level as it acts as a transcription factor (552). The functions relate to cellular homeostasis, mitochondrial biogenesis, heme biosynthesis, and the regulation of oxidative stress response (553; 554). NRF1 seems to have an oncogenic as well as tumour-suppressor function in PCa. One study showed that boosting NRF1 expression inhibited the spread of PCa by enhancing mitochondrial function (555) while another study indicated that NRF1 plays a role in the progression towards castration-resistant PCa (556). Ultimately, the role of NRF1 is not elucidated yet and more research is necessary. An interesting finding was that NRF1 is involved in the coordination of SHMT2 expres-

sion which was another protein within the same cluster that is highly relevant in mitochondrial metabolism (557; 558). Ultimately, this section has pinpointed intriguing targets that warrant further in-depth experimental validation before definitively concluding interactions between ABCC5 and these proteins or involvement in common pathways.

5.3.4 Is ABCC5 Connected to the Induction of Apoptosis via Caspase Activity?

Cell death is fundamental in the regular life cycle of a cell, however, this process is often dysregulated in cancer cells (498). In healthy cells, apoptosis is mediated by caspases which can be divided into initiator caspases and executioner caspases. Our experiments focussed on exploring CASP3, CASP6, CASP7, CASP8 and CASP9 of which CASP3, 6, and 7 belong to the executioner caspases and CASP8 and 9 to the initiator caspases (504). The gene expression data in LNCaP cells reveals significantly elevated levels of CASP6, CASP7, and CASP8 at various time points following ABCC5 KD. Additionally, OE data of CASP6 and CASP8 data also align with this trend. In contrast, the PC-3 data only show results after a 72 h KD for CASP7 and CASP8. These findings are particularly intriguing, as they underscore that both the initiator CASP8 and the executioner CASP3, CASP6, and CASP7 are responsive to the absence or OE of ABCC5. This result would lead us to conclude that the downregulation of ABCC5 initiates apoptosis mediated by caspases in PCa cells. However, to substantiate these findings, experiments were conducted to look at the ABCC5 KD and OE effect on protein levels.
Interestingly, ABCC5 OE in LNCaP cells led to an increase in CASP3 and CASP7 while both KD and OE caused an increase in CASP3 and 7 in PC-3 cells. The LNCaP Western Blot results did not align with the gene expression results while in PC-3 cells the KD Western Blot results align with gene expression results and

OE does not. The significant increase in executioner caspases observed in ABCC5 OE in both cell lines may be attributed to the elimination of cells that exhibit a significant OE of ABCC5, which is not in line with typical physiological levels. Similar results have previously been reported in the OE of β-Catenin in cell culture (559). ABCC5 is produced by ribosomes in the endoplasmic reticulum and cell death can be induced by endoplasmic stress of high protein production (560; 561). Nevertheless, this does not explain the lack of CASP 3/7 increase after ABCC5 KD in LNCaP cells.

Next, we looked at CASP9 which is the first initiator caspase in the intrinsic apoptosis pathway that leads to the activation of CASP3 and 7 by mitochondrial permeabilisation and the release of cytochrome C (562). Interestingly, no significant changes in mRNA were reported for LNCaP cells although there appears to be a trend to an increase in CASP9 gene expression after ABCC KD and a decrease in gene expression after ABCC5 OE. Meanwhile, in PC-3 cells both KD and OE of ABCC5 lead to a decrease in CASP9 gene expression. In comparison to CASP3/7, CASP9 belongs to the initiator caspases, and it is interesting to see the opposite response in terms of caspase activity in PC-3 cells when compared to LNCaP cells. Ultimately, the limitations of these assays have to be mentioned as these assays are end-of-point measurements with the risk of signal contamination by endogenous proteases or caspase inhibitors as well as off-target effects (563). Ultimately, the results on gene expression level and caspase activity level need to be supplemented with Western Blot data. Interestingly, melatonin-treated doxorubicin-resistant hepatocellular carcinoma cells showed a decrease of ABCC5 gene expression while the expression of CASP3 and 7 was upregulated (537; 538). Further, a drug resistance study on hepatocellular carcinoma showed an increase in ABCC5 expression while reporting a decrease in CASP3/7 (564). Both studies highlight that there might be a relevant connection between ABCC5 and caspase-

mediated apoptosis. Our results support the notion that there might be a connection between ABCC5 and caspase-mediated apoptosis; however, this needs to be substantiated with further studies on protein level to decipher the effect of ABCC5 on various caspases.

5.3.5 Is SHMT2 Potentially the Link Connecting ABCC5 to Mitochondrial Involvement?

The findings of this study have shed light on the differential effect of ABCC5 expression on SHMT2 in LNCaP and PC-3 cells, sparking intriguing questions about the significance of SHMT2 in PCa progression. The results demonstrate that the KD of ABCC5 in LNCaP cells leads to a significant upregulation of SHMT2 gene expression, while the OE of ABCC5 in the same cell line only results in marginal changes in SHMT2 levels. However, in PC-3 cells, neither ABCC5 KD nor OE has substantial effects on SHMT2 expression. As previously discussed in the introduction of **Chapter 4** and in earlier sections of this chapter, the differences between LNCaP and PC-3 cells are already acknowledged. These findings highlight a potential cell-type-specific nature of the ABCC5-SHMT2 relationship in PCa. This notion is supported when looking at the specificity of SHMT2 upregulation in castration-resistant PCa. PCa is a highly heterogeneous disease (391; 565) and SHMT2's role may vary depending on the subtype and molecular signature in progressed PCa.

SHMT exists as two isoenzymes with SHMT1 describing the cytosolic enzyme and SHMT2 the mitochondrial enzyme (566). SHMT2 is pivotal in mitochondrial metabolism by initiating the serine catabolic pathway, which facilitates the transfer of one-carbon units from serine to tetrahydrofolate (THF). This process leads to the production of glycine and 5,10-methylene-THF (567). The one-carbon pool is essential for several functions of the mitochondria and disruption leads to defi-

ciencies in the translation of mitochondrial proteins by loss of formyl methionyl-tRNAs and nucleotide synthesis (568). This impaired translation further impacts the assembly of Complex I (569) thus impairing oxidative phosphorylation in human cells (570).

The relevance of one-carbon units in cancer development was established fairly early by looking at blood-based cancers (571; 225). The high proliferation rate of cancer cells requires one-carbon units for nucleotide synthesis and metabolism (572; 573). The positive correlation observed between SHMT2 expression and disease progression in our results underscores the potential significance of SHMT2 in cancer particularly in PCa. It suggests that higher SHMT2 expression may be associated with more aggressive phenotypes. SHMT2 expression patterns in PCa were positively correlated with the sensitivity to platinum compounds (574; 575). Furthermore, it was shown that SHMT2 expression is upregulated upon IL-6 stimulation by the JAK2/STAT3 canonical pathway. This axis was shown to modulate the Warburg effect which is a hallmark of more aggressive PCa (576). Other results also reported that high expression of SHMT2 was associated with shorter disease-free survival in PCa patients (577). In contrast, one study showed the opposite of SHMT2 acting as a proliferation suppressor and negative regulator of aggressive PCa cell behaviour (532). Overall, more research is necessary to elucidate the interplay of SHMT2 in PCa; however, it will be of interest to see whether ABCC5 could be connected to SHMT2 beyond the initial results that are shown in this chapter.

Interestingly, a study showed that SHMT2 can act as an RNA-binding protein (RBP) (578) which are proteins relevant in regulating gene expression by stabilising, transporting, and controlling the translation of mRNA molecules within cells. They can either enhance or inhibit various aspects of mRNA function, influencing protein production and cellular processes (579). A study evaluated the interactome

by using UV crosslinking according to two protocols and reported that SHMT2 bound ABCC5, PARP-1, and ABCF1 mRNA among many others (578). These findings are intriguing, as they link ABCC5 to SHMT2 and the mitochondria as a cellular compartment. Moreover, a study previously discussed the compensatory mechanism of ABCC12 and ABCC5 also showed that ABCC5 was significantly expressed in mitochondrial-associated membranes (MAMs) in mice. They also reported that some of the most impacted pathways by the double knockout of ABCC5 and ABCC12 in mice were oxidative phosphorylation and mitochondrial dysfunction (224). This supports the notion of ABCC5 playing a potential role in the mitochondria or MAMs. However, current data is insufficient to be able to conclude a more precise mechanism. Potentially, SHMT2 could be responsible for shuttling ABCC5 mRNA into MAMs or the mitochondria, where the protein is then translated. The group that discovered the localisation of ABCC5 in MAMs didn't propose a mechanism for this process.

Furthermore, it is intriguing to observe that the mRNA of PARP-1 and ABCF1 is also bound by SHMT2. PARP-1 has been found to respond to ABCC5 expression levels, and ABCF1 is the sole protein exhibiting a 100% overlap with ABCC5 promoter motifs among the investigated proteins as discovered in this chapter. In summary, the findings suggest a complex relationship between ABCC5, SHMT2, and a potential mitochondrial localisation of ABCC5 in PCa. Further research is essential to unravel this intriguing connection and its implications in PCa biology.

5.4 Summary and Limitations

While this chapter provides novel insights into several proteins identified within the two gene clusters subjected to detailed analysis, it is important to consider several limitations. The results regarding the identification of specific motifs in gene promoters are predominantly based on computational and bioinformatic analyses. While these methods provide valuable insights, they are predictions and associations rather than experimentally validated interactions. Further, this was only an initial study and therefore the scope and depth of the results are limited. These results are insufficient to conclude potential mechanistic explanations of the findings and also only give some correlation but no evidence for causal relationships between the proteins or motifs. Future experiments should aim to validate whether there are direct interactions between the identified proteins or explore some of the most promising pathways of PCa through experimental assessment and the use of co-immunoprecipitation western blots could be a first step to ascertain if there is a physical vs functional interaction of the gene products.

Based on our findings, we can confidently conclude that ABCC5 plays a role in proliferation pathways within cancer cells to some extent. However, it is important to note that this study has certain limitations. The use of LNCaP cells, which represent only a specific PCa subtype, may restrict the universal applicability of the results. Additionally, the transient nature of the KD limits our understanding of longer-term consequences and how they might impact the expression of PTK2, ESR1, PARP-1, and NRF1 within the context of PCa. It is essential to acknowledge that this study highlights interesting targets for further investigation but does not provide underlying mechanisms. Replicating these initial results at the protein level is crucial to solidify these associations. In summary, this section lays a valuable foundation for exploring the potential role of ABCC5 and its interactions

with various proteins in the context of PCa cell proliferation.

The apoptosis study primarily relies on gene expression and CASP activity levels but lacks data at the protein level. While the data yielded promising results on the gene expression side, the CASP activity assay produced conflicting and challenging-to-interpret data. Therefore, expanding this line of investigation to include other assays, such as Western blot, becomes essential. Although it is encouraging that other studies have observed effects on CASP levels depending on *ABCC5* expression, this study should be interpreted with caution.

The discovery of a potential link between ABCC5 and SHMT2 is indeed intriguing and may provide valuable insights into the involvement of ABCC5 with mitochondria. However, it is important to acknowledge that the current findings are primarily based on gene expression experiments, and to strengthen the evidence, further validation at the protein level is essential. Specifically, assessing SHMT2 protein expression alterations following *ABCC5* KD and OE is necessary to confirm initial observations. While the discovery of SHMT2 binding to *ABCC5* mRNA is promising, the precise mechanism of this interaction and its functional consequences remain unexplored. Investigating this interplay will be crucial for a comprehensive understanding of their relationship.

To broaden the relevance of these findings, it is necessary to integrate them into the broader metabolic pathways connected to one-carbon metabolism, such as glycolysis and oxidative phosphorylation. Furthermore, it is essential to explore whether any signalling pathways involving SHMT2 and ABCC5 have been identified in PCa. In summary, while the initial findings are interesting, further investigations at the protein level, a deeper understanding of the SHMT2-ABCC5 interaction, and integration into broader metabolic pathways and signalling networks in PCa are essential for a more comprehensive understanding. This chapter has unveiled previously unreported association partners with ABCC5. Given the

available data, the next step in this research project will be a comprehensive exploration of ABCC5's involvement in apoptosis and its role in mitochondria, which appear to hold great promise. Future studies should aim to extrapolate from the existing findings by employing diverse experimental approaches to investigate the impact of ABCC5 protein expression on the candidate proteins identified.

6 | Antibody Validation for the Detection of ABCC5

6.1 Introduction

6.1.1 Antibody Testing and Validation

In the previous chapters, the identification of interesting interaction targets of ABCC5 through genetic network and interactome analyses has provided valuable insights into the possible physiological roles of ABCC5. However, to further our understanding, it is crucial to substantiate initial findings with data which includes successful visualisation of ABCC5. Protein-level detection requires the use of working antibodies that can specifically detect the target protein. The correct testing and validation of antibodies play a vital role in ascertaining target specificity and eliminating off-target protein recognition which yields false positive results - a huge problem in the field of ABC transporters where many proteins have very similar conserved domains and therefore similar amino-acid sequences (580; 581). It is well known that antibodies produced for immunoassays exhibit a certain affinity for their intended antigen but can also display varying affinity to other proteins, known as cross reactivity. The specificity and signal-to-noise ratio of an antibody in an immunoassay depends on the difference in affinity between the target antigen and other proteins (582). Therefore, stringent antibody validation is of great importance to determine antibody specificity. Unfortunately, often antibodies are only validated for certain tissues or cells, making it necessary for the end user to validate the antibodies with their preferred application, such as western blot, immunofluorescence (IF), immunohistochemistry (IHC), and tar-

get tissue before using them. ABCC5 protein detection faces challenges due to non-specific commercial antibodies. Many studies showing ABCC5 protein localisation lack proper controls and fail to confirm specificity using proper negative controls such as knockout (KO) tissue (200; 206).

6.1.2 Aims

1. Identify an anti-ABCC5 antibody capable of detecting ABCC5 expression using diverse methodologies, including western blot, IF, and IHC.

2. Validate the efficacy of the anti-ABCC5 antibody in both knockdown and overexpression studies in prostate cancer (PCa) cell lines.

3. Validate the efficacy of the anti-ABCC5 antibody using tissue from mice genetically lacking Abcc5, the ABCC5$^{-/-}$ mouse model.

4. Use the anti-ABCC5 antibody to detect and assess ABCC5 expression levels in human PCa samples across distinct stages, assessing ABCC5 involvement and potential implications in PCa.

6.2 Results

6.2.1 Screening of Commercial Antibodies

The primary objective of this study was to identify a functional anti-ABCC5 antibody suitable for western blotting, IF, and IHC assays. To achieve this, four different commercially available antibodies were obtained. After careful consideration, antibody sc-5781 was also included in the panel given its established track record in the lab for detecting ABCC5 in the mouse gut and GLUtag cells (Data Thesis M. Cyranka). **Table 6.1** shows the characteristics of each antibody and their binding site on ABCC5 and species specificity according to the manufacturer.

Table 6.1: Commercial antibody characteristics (ms=mouse, hu=human).

Antibody	**Epitope on ABCC5**	**Species Specificity**	**Manufacturer**
sc-390797	N-terminus	ms, hu	Santa Cruz
sc-5781	not stated	ms, hu	Santa Cruz (discontinued)
ab180724	not stated	ms, hu	Abcam
PA5-102678	N-terminus	ms, hu	Thermo Fisher
PA5-83701	N-terminus	hu	Thermo Fisher

6.2.1.1 Immunofluorescence

All five distinct anti-ABCC5 antibodies were assessed for their ability to detect ABCC5 in wild-type (WT) mouse prostate tissue, as well as in PCa cell lines LNCaP and PC-3. The expression of ABCC5 in PC-3 and LNCaP cells was confirmed by qPCR and western blot in **Chapter 4**. The expression of Abcc5 was

confirmed by qPCR for wildtype mouse prostate as seen in **Figure 6.1**.

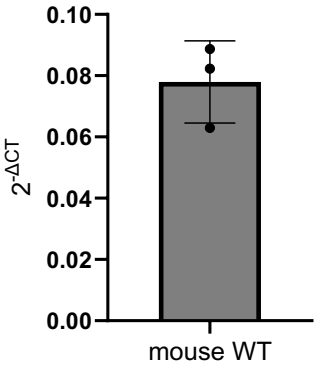

Figure 6.1: Relative expression of ABCC5 in wt mouse prostate compared to negative control. The results are from n=3. Data are represented as mean ± SD.

The initial staining of WT mouse prostate tissue was performed using the different commercial ABCC5 antibodies and compared to the control staining without primary antibody (**Figure 6.2**). Unfortunately, none of the antibodies tested exhibited a strong positive stain on the mouse prostate tissue, and a majority of the samples displayed some unspecific secondary antibody staining. To improve the staining quality and minimise unspecific secondary antibody staining, trials were conducted with the Visublock reagent (**Figure 6.3**). This led to a noticeable reduction in background staining. Consequently, the mouse prostate staining was repeated, incorporating the Visublock reagent into the protocol, and also increasing the antibody concentration as seen in **Figure 6.4**. Despite these efforts to reduce background staining, none of the tested antibodies showed promising results for staining ABCC5 in mouse prostate tissue. To confirm the efficacy of the staining protocol, tyrosine hydroxylase staining was used as a positive control (**Appendix 2 Figure A.3**).

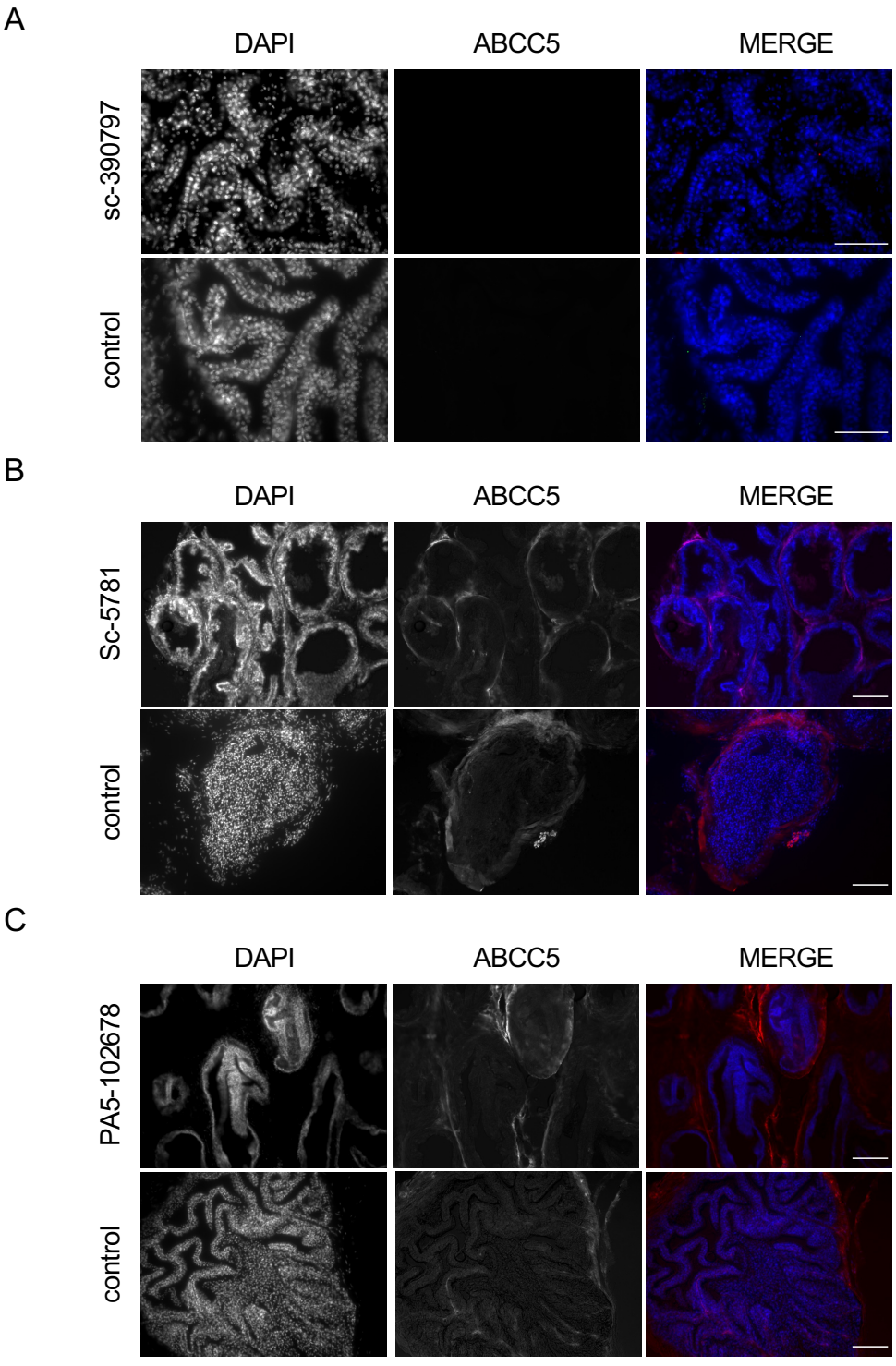
A
DAPI
ABCC5
MERGE
sc-390797
control
B
DAPI
ABCC5
MERGE
Sc-5781
control
C
DAPI
ABCC5
MERGE
PA5-102678
control

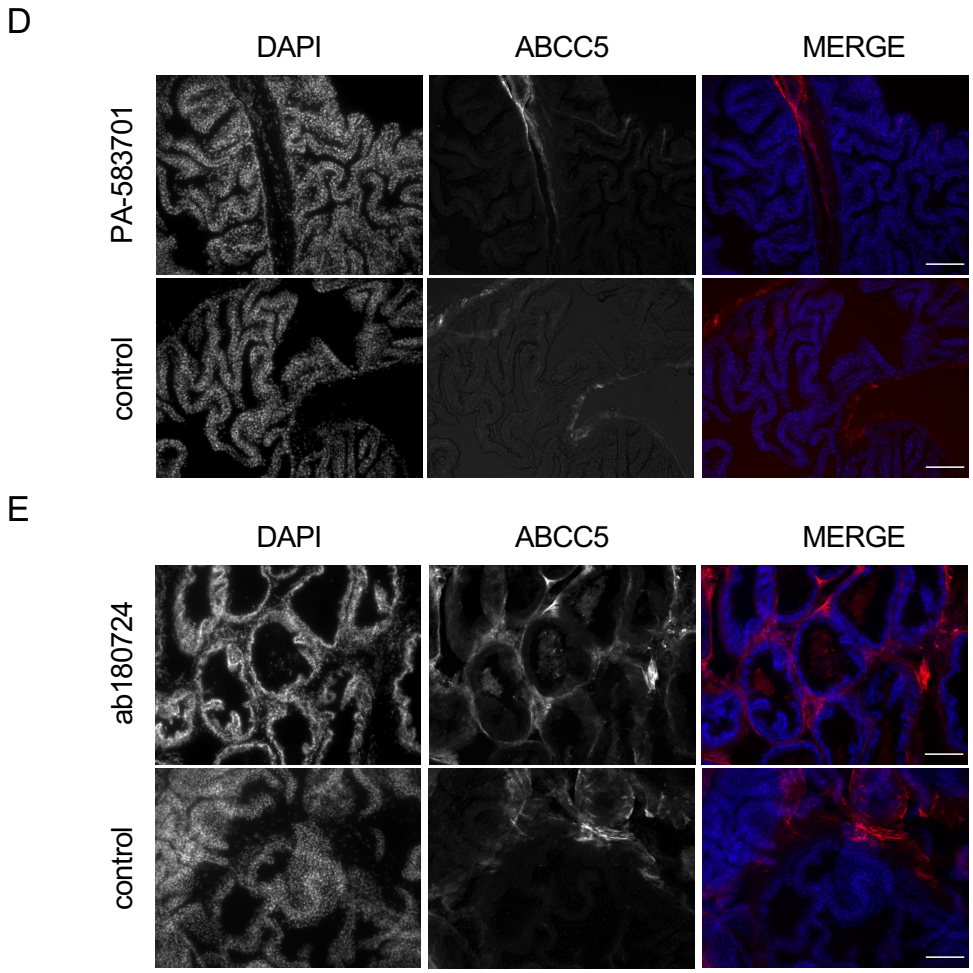

Figure 6.2: Staining of WT mouse prostate tissue with commercial anti-ABCC5 antibodies. Images of ABCC5 staining with **A)** sc-390797 **B)** sc-5781 **C)** ab180724 **D)** PA583701 **E)** PA5102678 of mouse prostate compared to no primary control (n=1). No Visublock reagent and antibody concentration at 1/250. The scale bar is 200 μm.

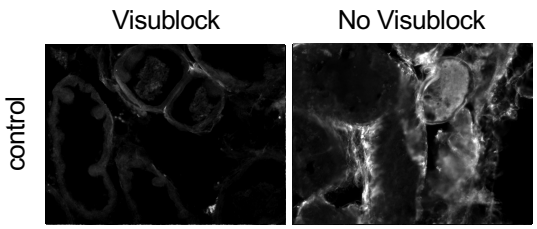

Figure 6.3: Optimisation of secondary antibody background staining with Visublock reagent.

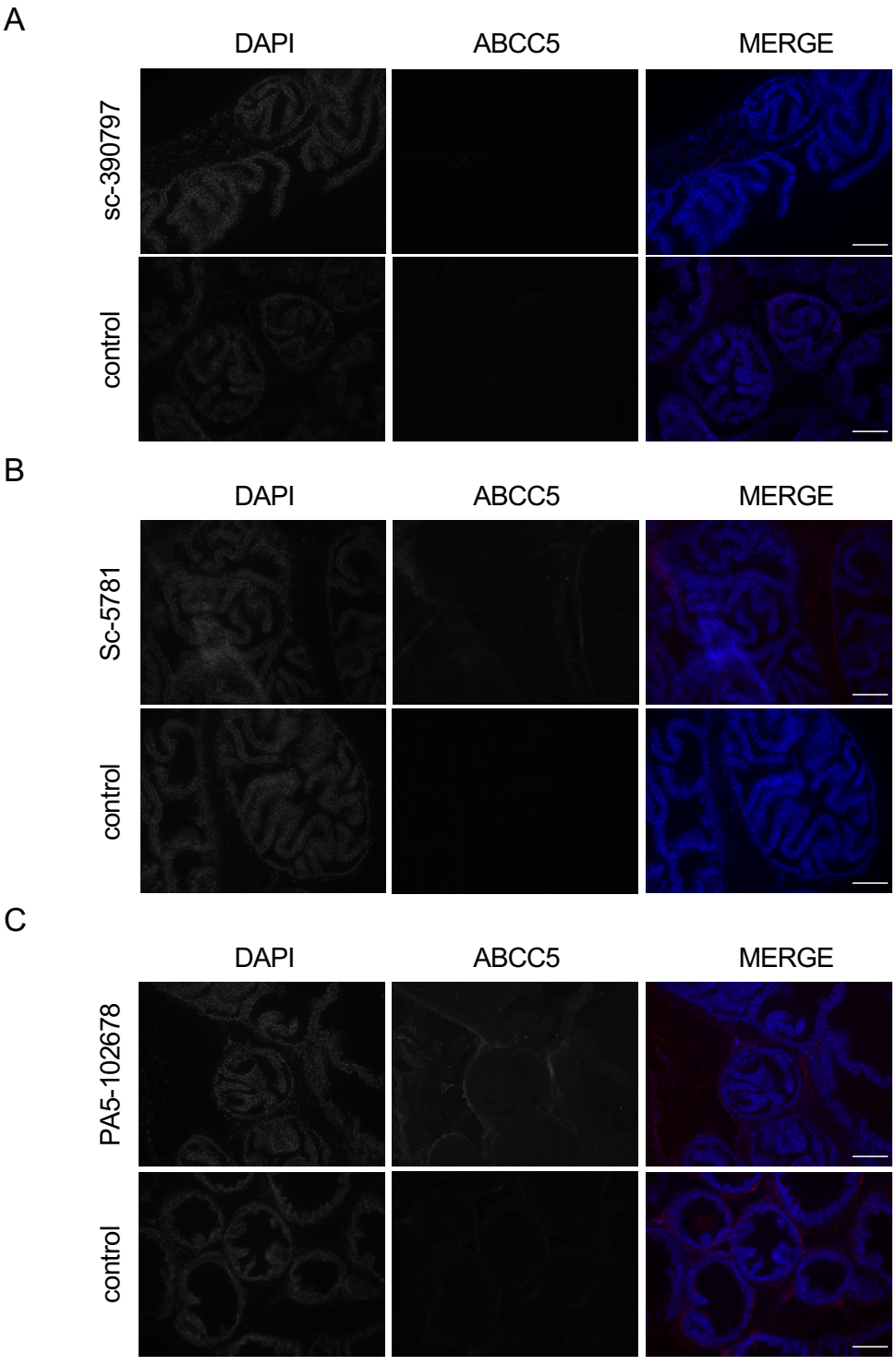
A
DAPI
ABCC5
MERGE
sc-390797
control
B
DAPI
ABCC5
MERGE
Sc-5781
control
C
DAPI
ABCC5
MERGE
PA5-102678
control

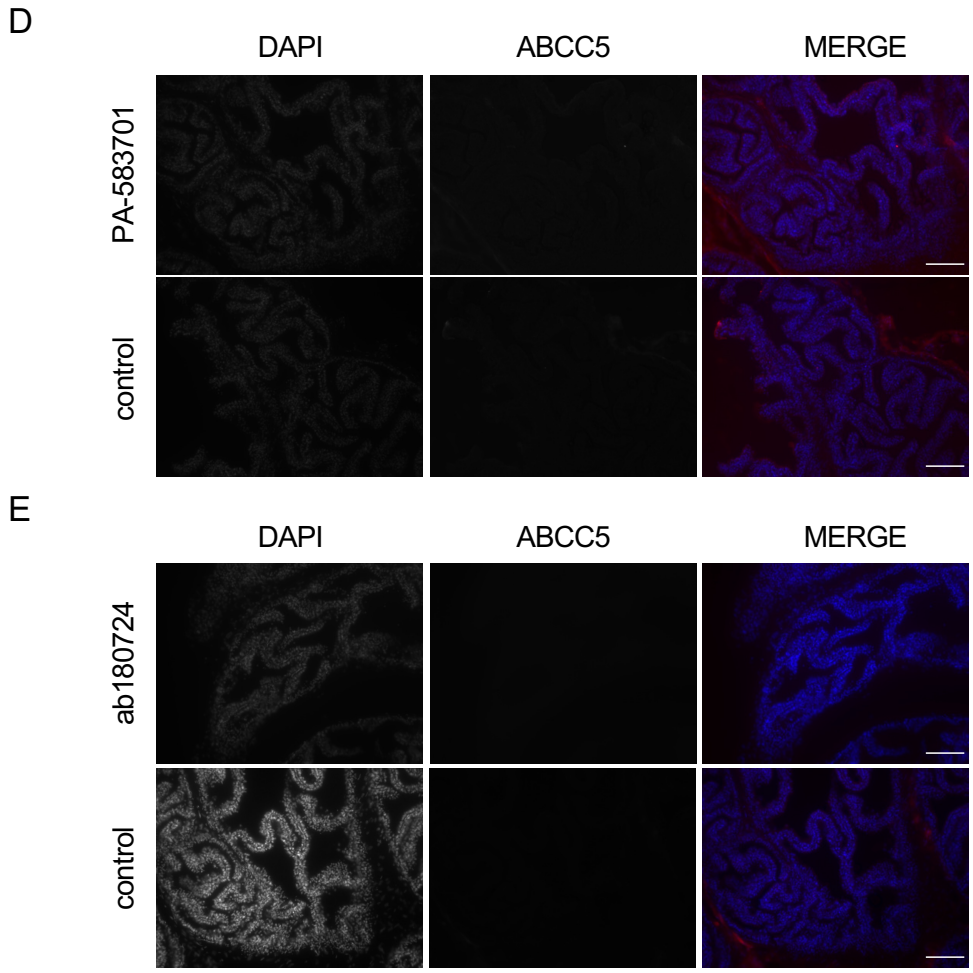

Figure 6.4: Staining of WT mouse prostate tissue with commercial anti-ABCC5 antibodies. Images of ABCC5 staining with **A)** sc-390797 **B)** sc-5781 **C)** ab180724 **D)** PA583701 **E)** PA5102678 of mouse prostate compared to no primary control (n=1). Visublock reagent and antibody concentration at 1/100. The scale bar is 200 μm.

Subsequently, the aforementioned antibodies were evaluated in PC-3 cells however, none of the antibodies yielded a positive staining outcome. **Appendix Figure 6.5** shows the staining with the highest concentration of antibody compared to the control stain without primary antibody in PC-3 cells. Different antibody concentrations (**Appendix Figure A.4**) were used to see if that would increase the

staining however there was no improvement observed.

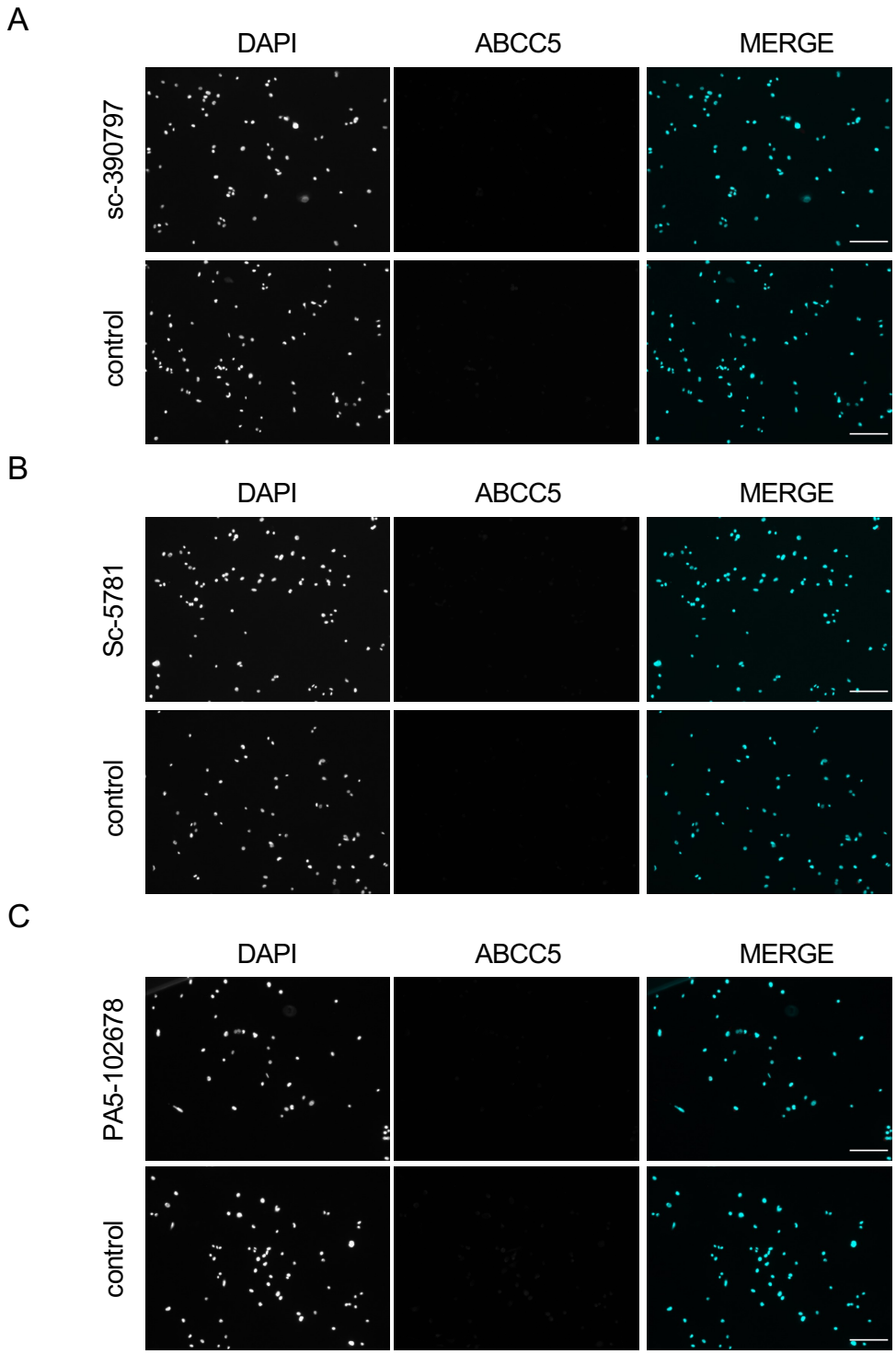

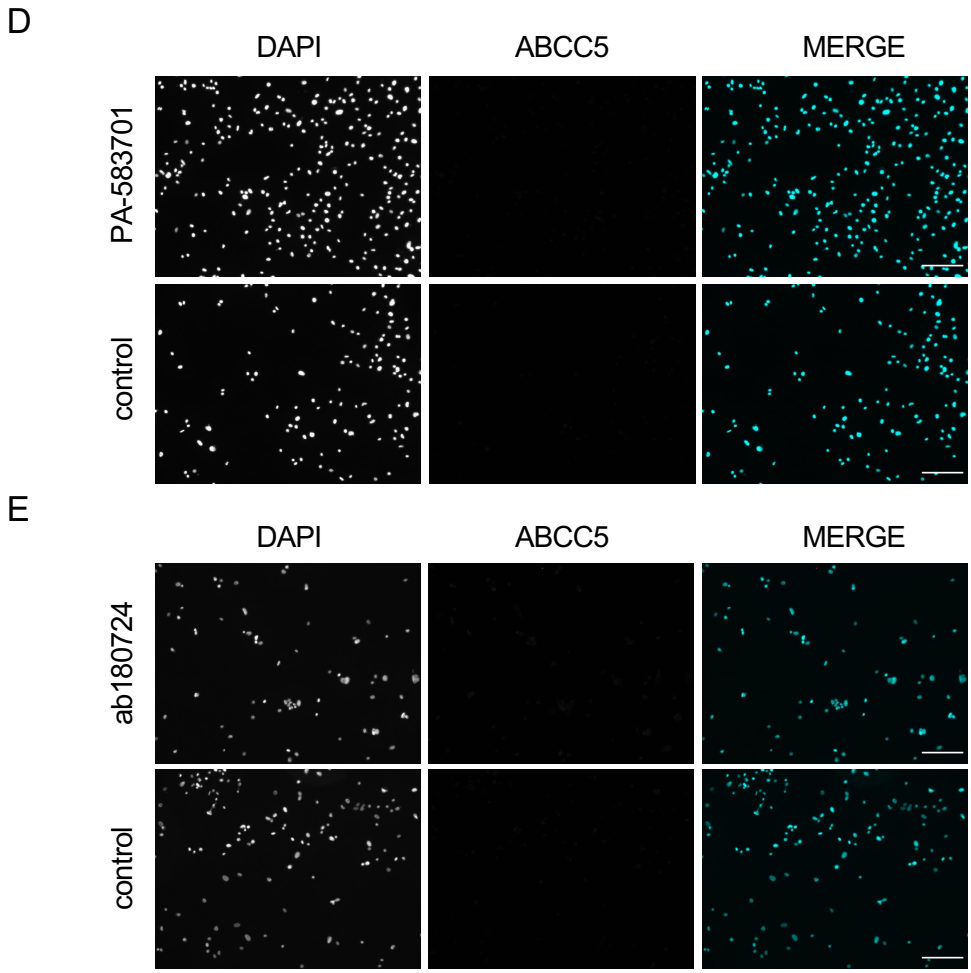

Figure 6.5: Staining of PC-3 cells with commercial anti-ABCC5 antibodies. Images of ABCC5 staining with **A)** sc-390797 **B)** sc-5781 **C)** ab180724 **D)** PA583701 **E)** PA5102678 of PC-3 cells compared to no primary control (n=1). Antibody concentration at 1/100. The scale bar is 200 μm.

6.2.1.2 Western Blot

After the initial immunofluorescence test, the same five antibodies were used to detect ABCC5 in mouse prostate tissue lysate as well as cell lysates from LNCaP, PC-3, and GLUTag cell lines using western blotting. GLUtag cells were selected as the cell line for the antibody validation experiments due to their routine usage in the laboratory, known ABCC5 expression, and the ability to reliably de-

tect ABCC5 with the sc-5781 antibody (Thesis G. Cyranka). Glutag cells are a type of enteroendocrine cell line derived from the mouse intestinal L-cell, commonly used in research to study gut hormone secretion and glucose metabolism (583). **Figure 6.6** shows the results after using chemiluminescence as the detection method and compares wet (**Fig. 6.6 A**) and semi-dry (**Fig. 6.6 B**) transfer. PA-583701 showed strong ABCC5 signal in both LNCaP and PC-3 cells whilst sc-5781 detected ABCC5 in GLUtag cells. In contrast, antibodies sc-39077 and PA5-102678, although indicated by the manufacturer to be capable of detecting both human and mouse ABCC5, showed no signal in any of the lysates. Notably, ab180724 exhibited highly promising results, showing signal presence in all four lysates. To further investigate the specificity of ab180724, an additional experiment was conducted on WT and KO ABCC5 tissue lysates as seen in **Figure 6.6 C**. Surprisingly, the same band was observed for both samples.

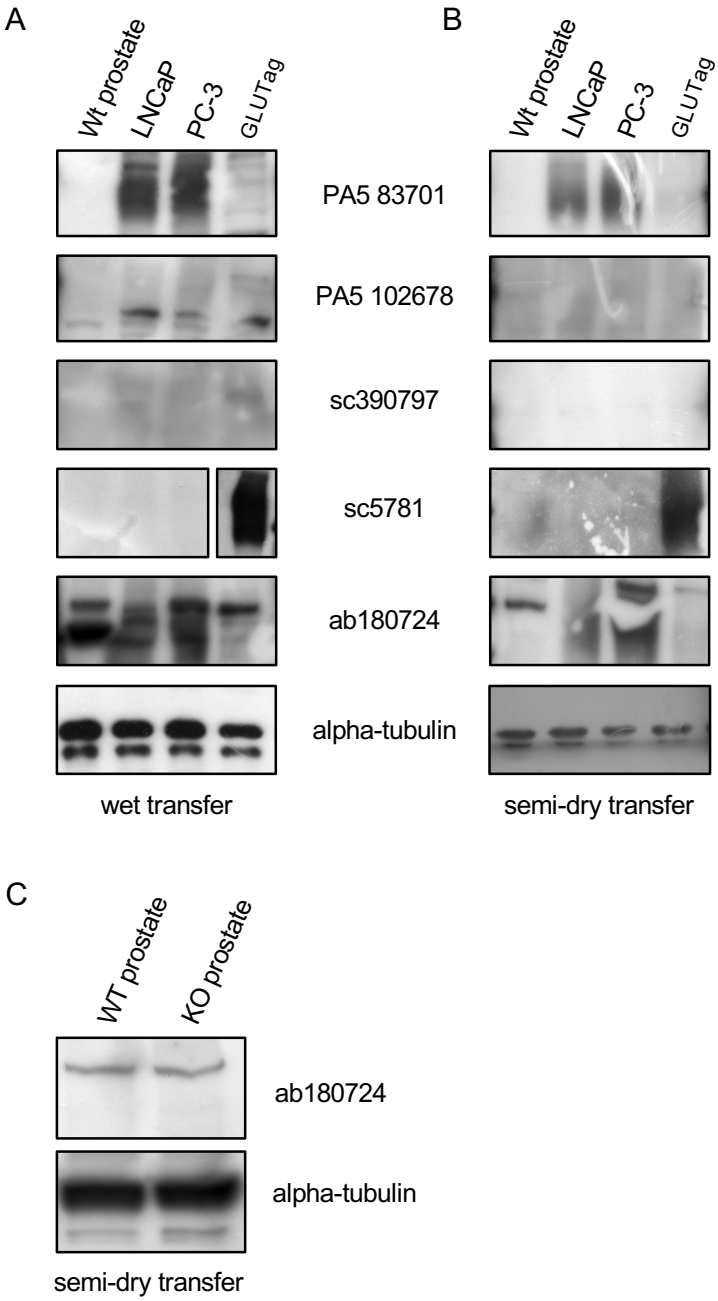
A
Wt prostate
LNCaP
PC-3
GLUTag
PA5 83701
PA5 102678
sc390797
sc5781
ab180724
alpha-tubulin
wet transfer
B
Wt prostate
LNCaP
PC-3
GLUTag
semi-dry transfer
C
WT prostate
KO prostate
ab180724
alpha-tubulin
semi-dry transfer

Figure 6.6: Anti-ABCC5 antibody testing. Western Blots showing ABCC5 expression of ABCC5 (185 kDa) **(A)** after wet transfer and **(B)** after semi-dry transfer. Antibodies were tested against GLUTag, LNCaP and PC-3 cell lysates and WT mouse lysate. **C)** Western blot showing ABCC5 expression comparing WT and KO mouse prostate lysate. Alpha-tubulin (50 kDa) was used as a loading control.

The reliable detection of ABCC5 proved to be method-dependent, with successful outcomes achieved primarily using western blotting. Ultimately, none of the antibodies yielded sufficient results. Therefore, we decided to design custom antibodies with Thermo Fisher.

6.2.2 Antibody Design

To successfully design antibodies against specific regions of ABCC5, it is crucial to accurately predict the transmembrane topology of the protein, identify its transmembrane helices, and predict its secondary structure elements. This information is essential to understand the structure-function relationship of the protein and to identify areas that are available for antibody targeting in a native environment, which is imperative for epitope recognition in IHC. Two widely used methods to analyse the properties of transmembrane proteins are the transmembrane protein topology predictor support vector machines (MEMSAT-SVM) and PSI blast-based secondary structure prediction (PSIPRED). MEMSAT-SVM was used to predict transmembrane helices as well as extracellular and cytosolic elements and PSIPRED was used to predict secondary structure elements, including alpha-helices and beta-sheets as seen in **Appendix 2 A.5**. By combining these two methods and receiving insight from Thermo Fisher, we were able to identify and agree on three antibody binding sites in ABCC5, as seen in **Figure 6.7**.

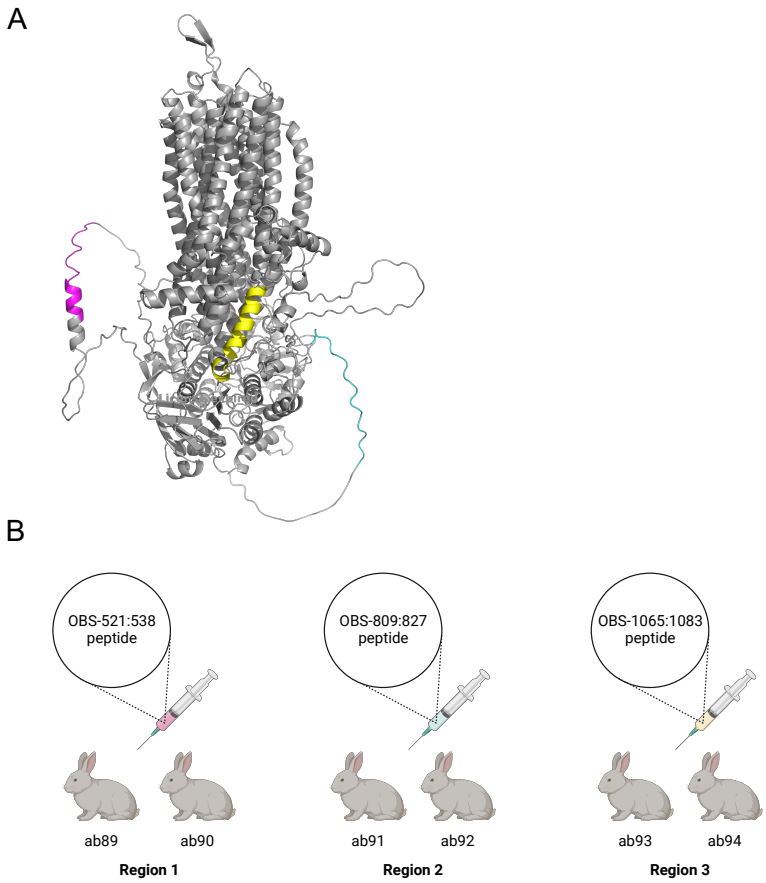

Name	Peptide	Position	Colour
OBS-521:538	RASRGKKEKVRQLQRTEH	521	Magenta
OBS-809:827	DKGPKTGSVKKEKAVKPEE	809	Cyan
OBS-1065:1083	HAYNKGQEFLHRYQELLDD	1065	Yellow

Figure 6.7: Antibody design. **A)** Truncated structure of human ABCC5 (Jumper et al., 2021). The highlighted structural elements refer to the target sequences of the designed antibodies. **B)** Overview of rabbit immunisation with the respective peptides and antibody nomenclature. Created with BioRender.com The table below summarises the peptide sequence, position, and name of the three target regions.

However, in the case of ABCC5, there are also two closely related paralogs ABCC11 and ABCC12 that share a significant portion of the sequence identity, as shown in **Figure 6.8**.

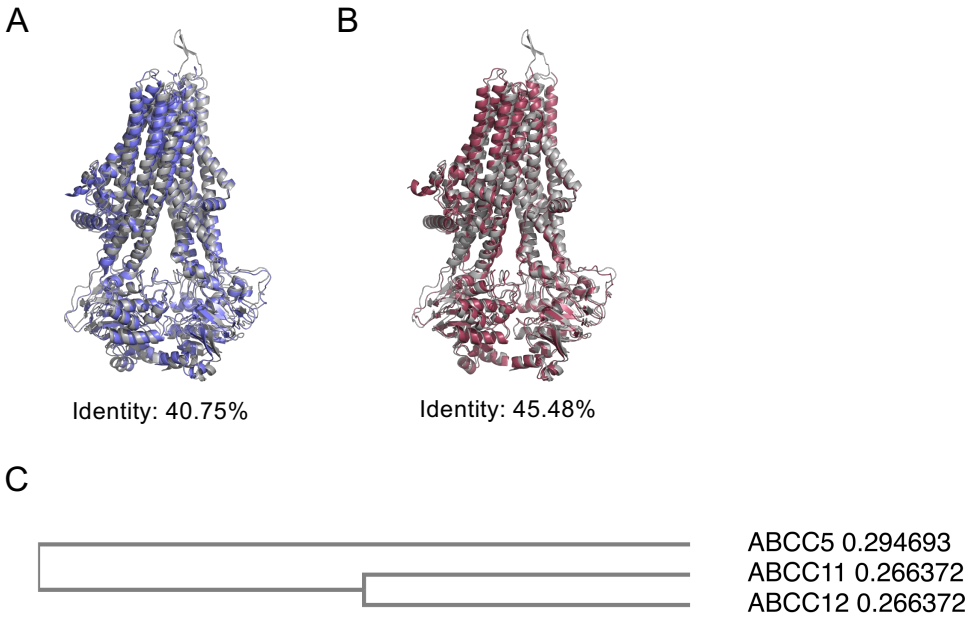

Figure 6.8: Structural alignment of ABCC5, ABCC11, and ABCC12. **A)** Side view of the structural alignment of ABCC5 (AlphaFold, grey) and ABCC11 (AlphaFold, blue). **B)** Side view of the structural alignment of ABCC5 (AlphaFold, grey) and ABCC12 (AlphaFold, maroon). The percent identity was determined by Clustal2.1. **C)** A cladogram was constructed after multiple sequence alignment of ABCC5, ABCC11 and ABCC12 using Clustal omega.

Therefore, it was essential to check whether ABCC11 and ABCC12 are expressed in the PCA cell lines LNCaP and PC-3 before evaluating whether there could be potential cross-reactivity. As seen in **Figure 6.9**, both ABCC11 and ABCC12 are expressed in LNCaP and PC-3 cells.

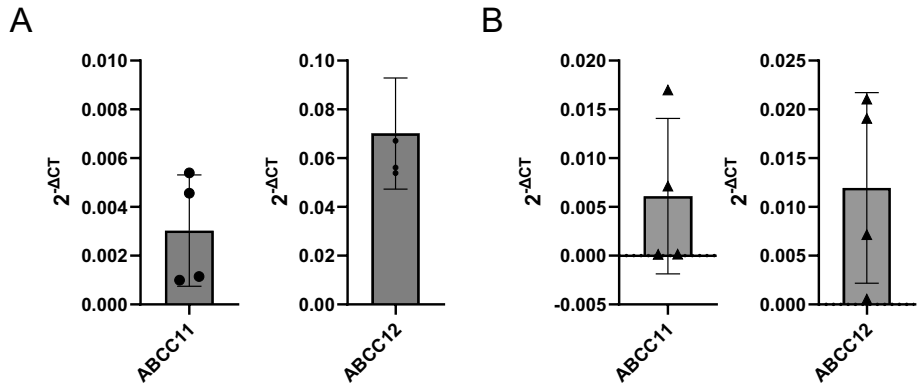

Figure 6.9: Relative expression of ABCC11 and ABCC12 in **A)** LNCaP and **B)** PC-3 cells in comparison to negative control. The results are from n=4. Data are represented as mean ± SD.

Concluding, antibodies designed against ABCC5 must consider potential cross-reactions with ABCC11 and ABCC12. To evaluate the potential for cross-reactivity, a multiple sequence alignment was conducted for the sequences which were determined in **Figure 6.7**. The sequences of ABCC5, ABCC11 and ABCC12 were aligned using Jalview and colour-coded according to their chemical properties. The similarity of the physicochemical properties was summarised by calculating the level of conservation below the alignment as seen in **Figure 6.10**. The alignment for OBS-1065:1083 (**Fig. 6.10 C**) shows very high conservation between ABCC5, ABCC11, and ABCC12, while the other two areas show less conservation in comparison. Hence, caution should be exercised when analysing the staining data of antibodies targeting region 3. Nevertheless, the three peptide sequences were synthesised and separately injected into two rabbits each to generate six polyclonal antibodies which was done by Thermo Fisher as outlined in **Figure 6.7 B**.

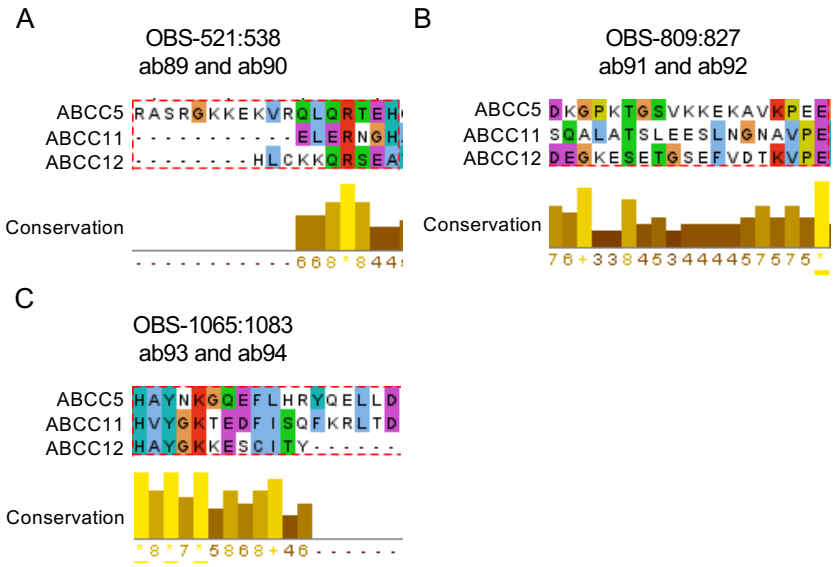

Figure 6.10: Alignment of the antibody target sequences of human ABCC5 with ABCC11 and ABCC12. Alignment and conservation of the peptide sequence which is targeted by **(A)** ab89 and ab90, **(B)** ab91 and ab92, **(C)** ab93 and ab94. The alignment was generated in Jalview using the clustal X default colouring scheme, which colours residues by their chemical properties. Conservation describes a numerical index that reflects the conservation of physicochemical properties per column.

6.2.3 Screening of Antibody Serum

Rabbits were injected with purified peptide antigen, boosted and the day 72 bleed collected. This initial bleed was used to evaluate whether the rabbits had produced a sufficient immune response to ABCC5 antigens. Therefore, antibody sera were tested on PC-3 cells compared to no primary control as seen in **Figure 6.11**. The assay produced positive results for all the sera tested, indicating that the antibodies in the sera had the potential to detect and quantify ABCC5. Additionally, fixative screening results determined that 100% methanol (MeOH) and 4% paraformaldehyde (PFA) are suitable before antibody labelling (data not shown). Immunoreactivity of the sera was also verified by indirect ELISA (Thermo Fisher). Upon confirmation of specificity, the antibodies were affinity column purified and their specificity was confirmed by indirect ELISA (data not shown). The purified antibodies were evaluated in the next section.

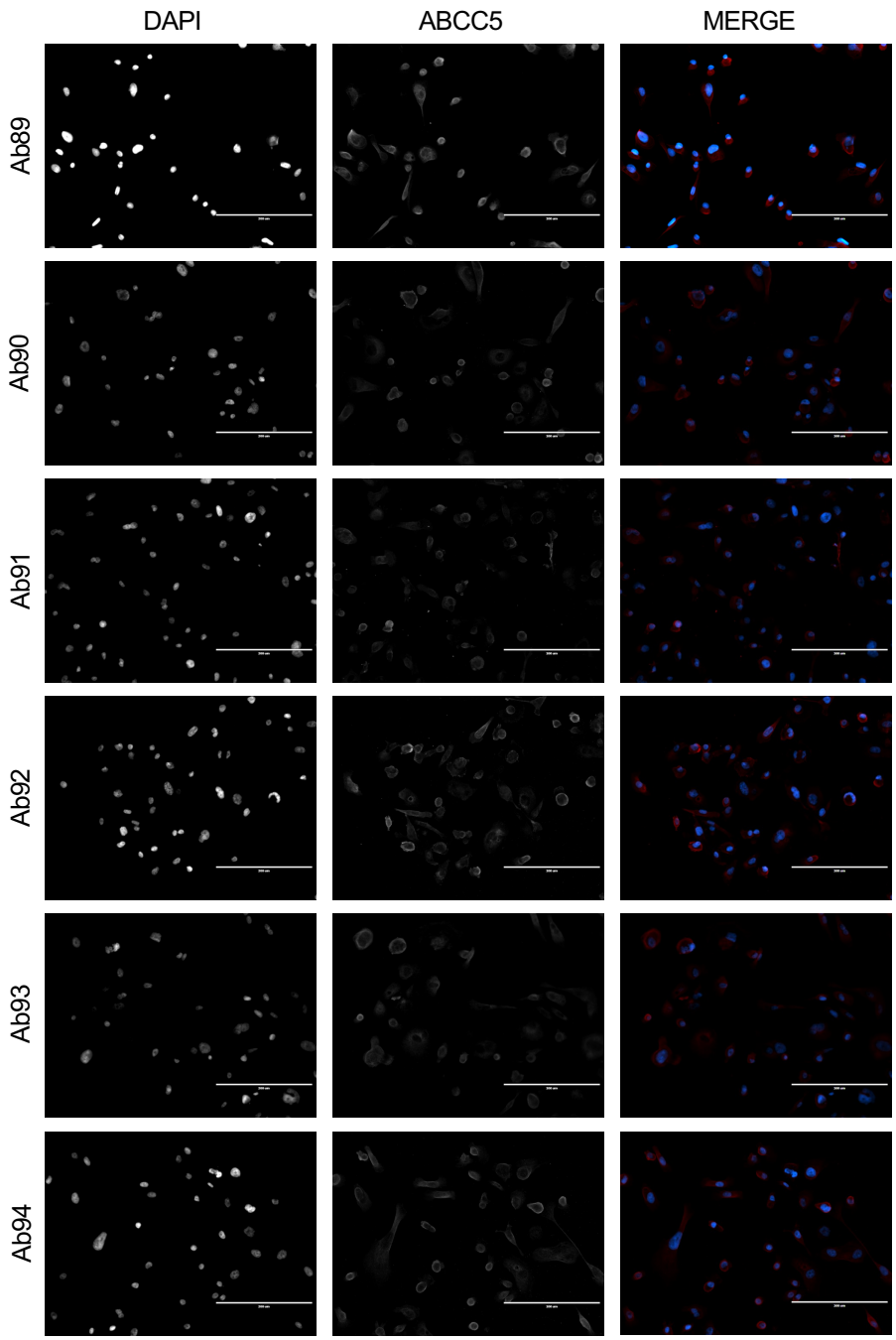
DAPI
ABCC5
MERGE
Ab89
Ab90
Ab91
Ab92
Ab93
Ab94

Figure 6.11: Screening of anti-ABCC5 serum. On day 72, the bleeds of the 6 rabbits were used to stain PC-3 cells for ABCC5. Rabbit 1 (ab89) and rabbit 2 (ab90) were immunised against OBS-521:538. Rabbit 3 (ab91) and rabbit 4 (ab92) were immunised against OBS-809:827. Rabbit 5 (ab93) and rabbit 6 (ab94) were immunised against OBS-1065:1083. Each antibody staining also has no primary control staining which is not shown. The scale bar is 200 μm.

6.2.4 Screening of Customised Antibodies

The primary objective of this section was to systematically evaluate and validate the efficacy of the customised antibodies in detecting ABCC5 across diverse applications, including western blot, IF, and IHC.

6.2.4.1 Immunofluorescence

Validation of ABCC5 Antibodies through Colocalisation Analysis with ABCC5-GFP

Performing colocalisation experiments using immunofluorescence staining on cells expressing the corresponding fluorescent-conjugated protein can help ensure that the antibody specifically binds to the intended target protein. Therefore, PC-3 cells were transfected with ABCC5 protein fused with green fluorescent protein (GFP) and stained with anti-ABCC5 antibody as seen in **Figure 6.12**. The colocalisation pattern of ab89-ab92 overlapped with ABCC5-GFP, and the antibodies also detected natively expressed ABCC5. Whereas, ab93 and ab94 did not detect ABCC5-GFP in all instances as highlighted by the white arrows and also failed to detect the transfected protein to the same staining intensity. Therefore, ab93 and ab94 were not used in the subsequent knockdown staining.

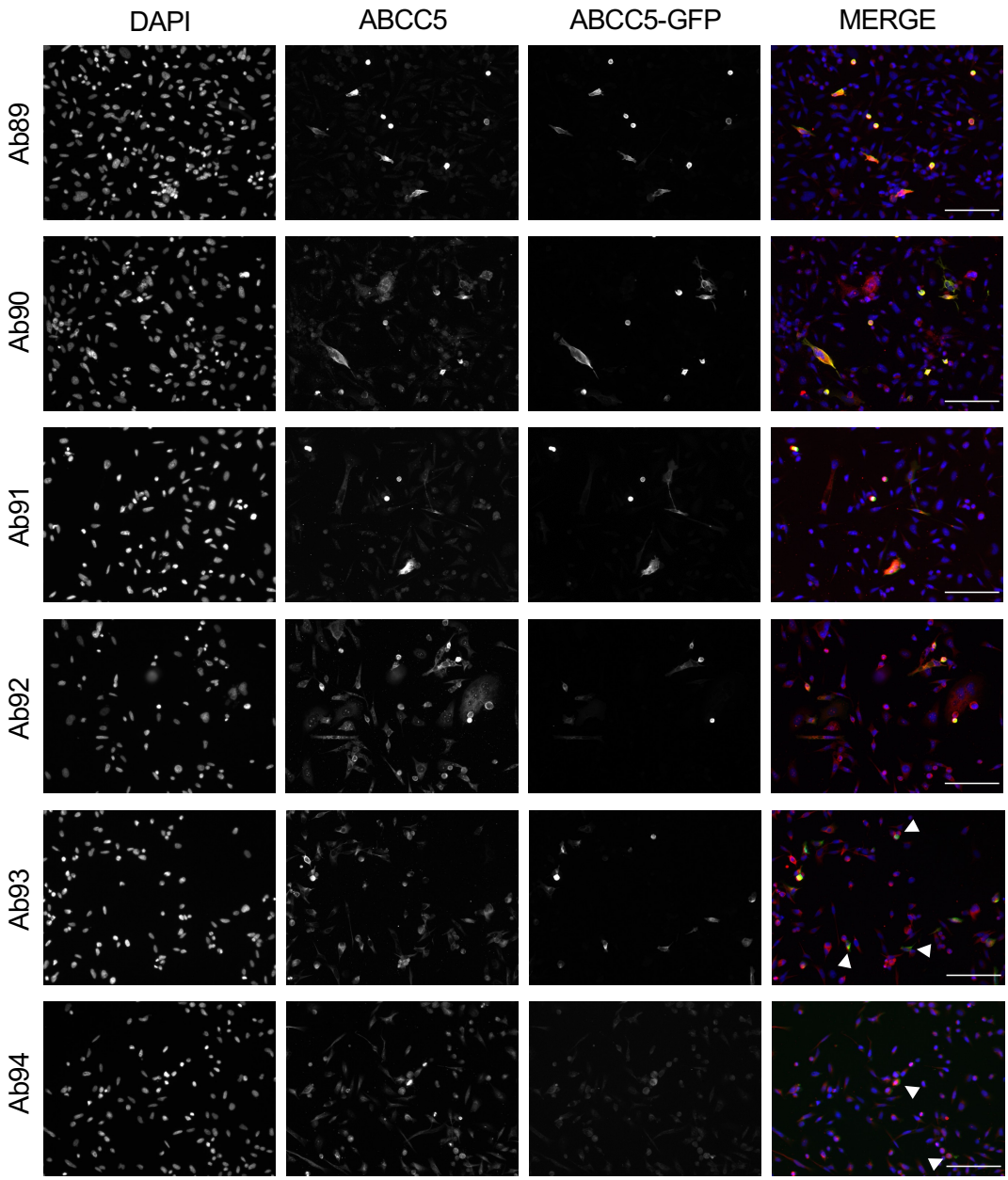

Figure 6.12: Colocalisation staining with ABCC5-GFP transfected PC-3 cells and anti-ABCC5 antibodies. Representative images are shown for each antibody (n=3). The scale bar is 300 μm.

Validation of ABCC5 Antibodies through ABCC5 Knockdown

In **Chapter 4**, siRNA-mediated knockdown of ABCC5 was confirmed by qPCR and western blot. Subsequently, the same method was used to evaluate anti-ABCC5 antibody specificity. The primary objective was to observe reduced ABCC5 detection in siRNA-treated samples compared to the control, indicating antibody specificity. **Figure 6.13** depicts the results obtained using ab89 and ab90 antibodies. While ab89 demonstrated the ability to detect the knockdown of ABCC5, its reliability was limited, showing inconsistencies across different experiments. Ab90 exhibited a more promising performance, showing a significant reduction in signal intensity in knockdown samples compared to the control. This signal reduction amounted to approximately 50%, which aligns with the qPCR-based knockdown achieved in **Chapter 4**. **Figure 6.14** showcases the staining outcomes of ab91 and ab92, where neither antibody demonstrated a discernible difference in signal detection between the control and KD. As previously stated, ab93 and ab94 were excluded from the KD experiment, as their previous performance with ABCC5-GFP staining showed off-target false positive results.

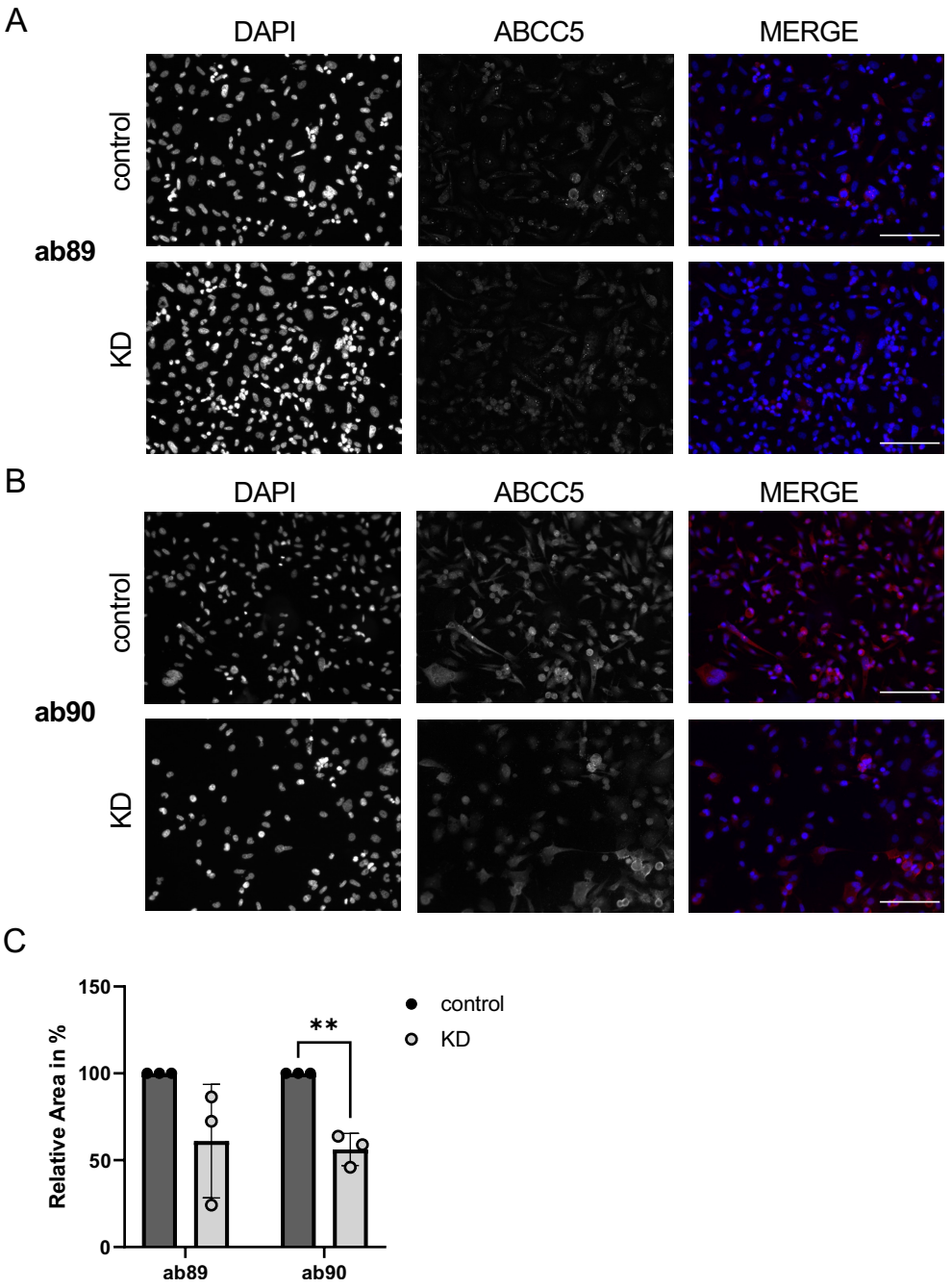

Figure 6.13: Detection of ABCC5 KD mediated by siRNA with immunofluorescence. PC-3 cells were stained with anti-ABCC5 antibody. Representative images of staining 72 h post-KD with **A)** ab89 and **B)** ab90. The scale bar is 300 μm. **C)** Quantification of the relative stained area expressed as a percentage compared to the control. The results are from n=3. Data are represented as mean $\pm$ SD. ** $<$0.01. The P-value is calculated using a two-tailed unpaired t-test.

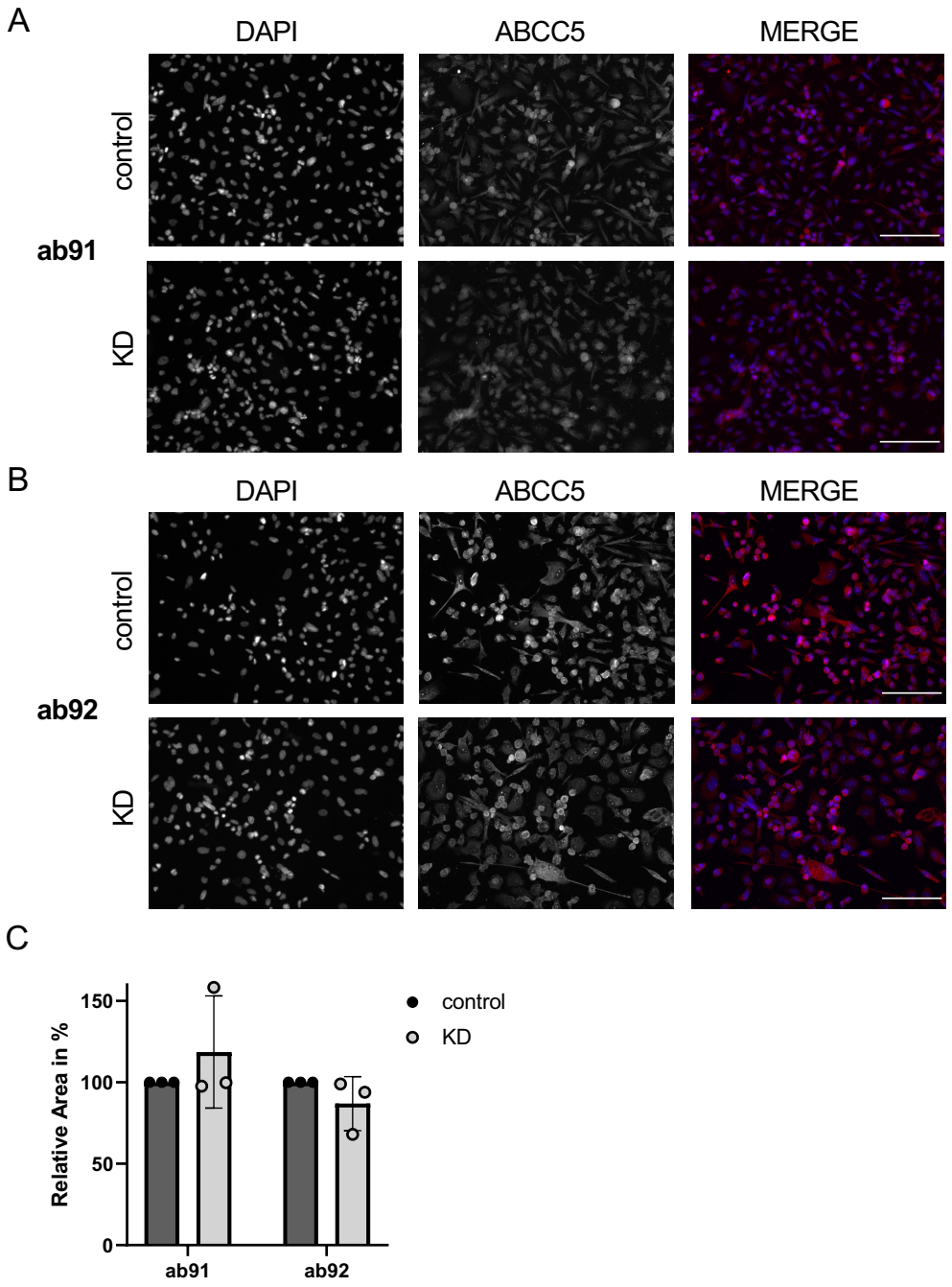

Figure 6.14: Detection of ABCC5 KD mediated by siRNA with immunofluorescence. PC-3 cells were stained with anti-ABCC5 antibody. Representative images of staining 72 h post-KD with **A)** ab91 and **B)** ab92. The scale bar is 300 μm. **C)** Quantification of the relative stained area expressed as a percentage compared to the control. The results are from n=3. Data are represented as mean $\pm$ SD. ** $<$0.01. The P-value is calculated using a two-tailed unpaired t-test.

Validation of anti-ABCC5 antibody in different cell lines

The primary goal of this study was to develop antibodies capable of detecting ABCC5 in both mouse and human samples. To thoroughly evaluate their potential, the two most promising antibodies, ab89 and ab90, were subjected to further testing to determine their effectiveness in various cell lines, including LNCaP, PC-3, HEK293, and GLUTag cells. These cell lines were chosen to represent diverse conditions, encompassing different tissue types, cancerous versus healthy tissue, and both mouse and human origins. Impressively, both antibodies exhibited discernible staining in each of the cell lines tested as seen in **Figure 6.15** and **Figure 6.16**.

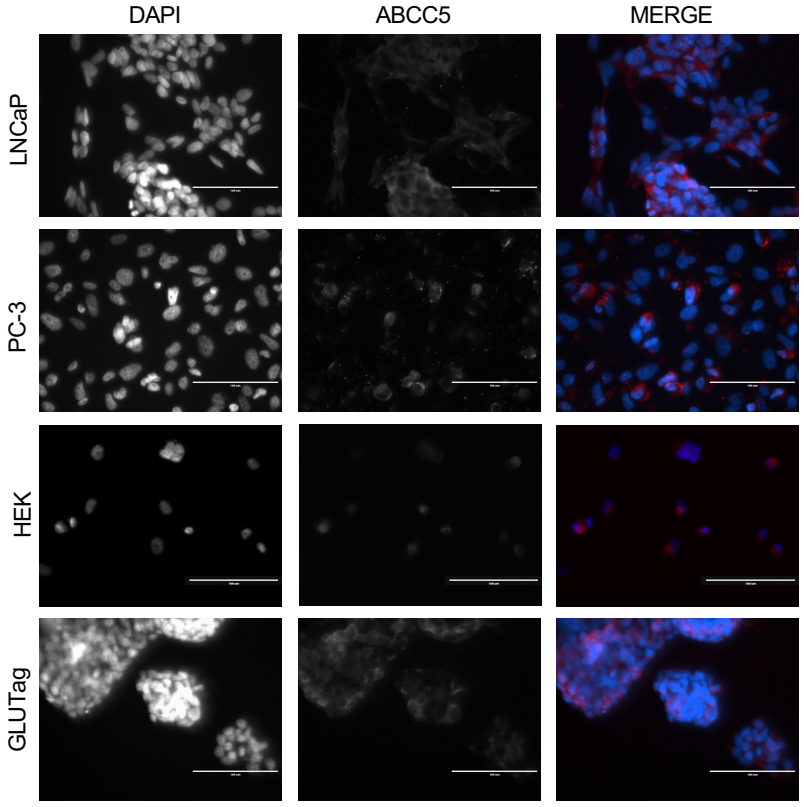

Figure 6.15: Staining of LNCaP, PC-3, HEK, and GLUTag cells with ab89 (n=1). The scale bar is 100 μm.

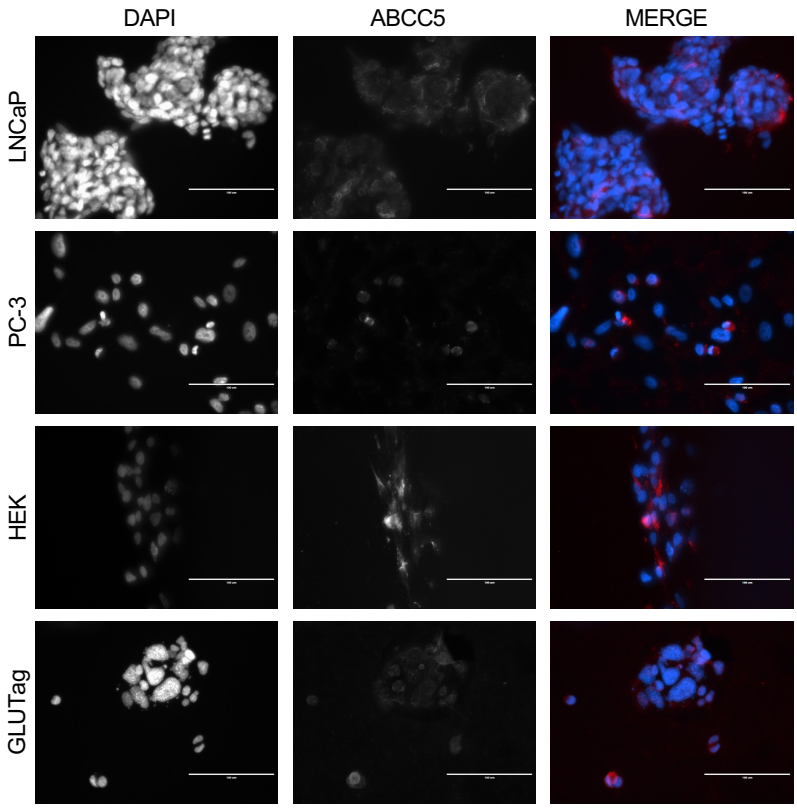

Figure 6.16: Staining of LNCaP, PC-3, HEK, and GLUTag cells with ab90 (n=1). The scale bar is 100 μm.

Validation of anti-ABCC5 antibody in ABCC5 KO mouse model

The evaluation of antibodies with mouse KO models is essential to ensure antibody specificity and to verify the results obtained from antibody-based experiments. Therefore, I used prostate sections from WT mice compared to Abcc5$^{-/-}$ KO mice generated by CRISPR/Cas9 to evaluate anti-ABCC5 antibodies. **Figure 6.17** presents the staining results of prostate tissue sections with ab89 and ab90 antibodies. Intriguingly, ab89 exhibited no discernible difference between WT and KO samples. On the contrary, ab90 displayed a substantial increase in signal intensity in the KO samples compared to WT. Interestingly, none of the customised antibodies displayed a reduction in staining intensity when subjected

to KO as compared to WT tissue (data not shown).

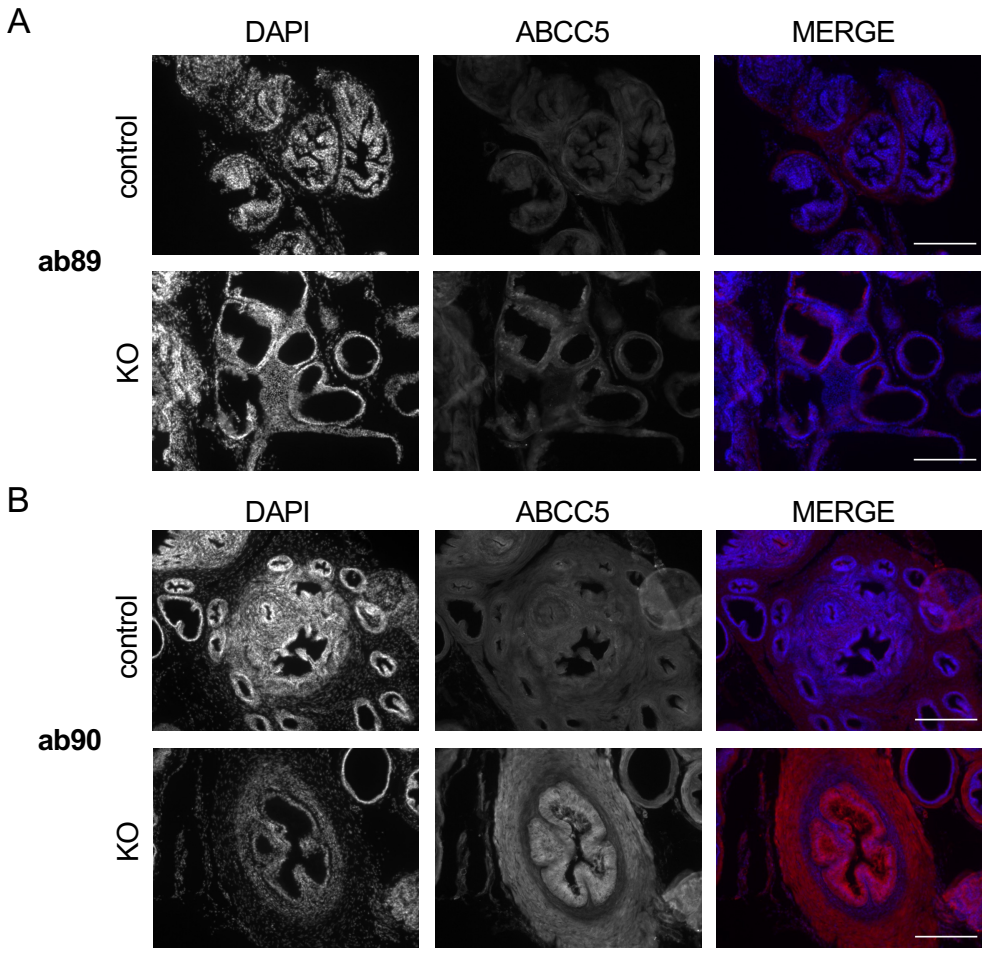

Figure 6.17: ABCC5 staining of WT and ABCC5 KO mouse prostate tissue. Representative images of **A)** ab89 and **B)** ab90 staining. The scale bar is 300 μm.

6.2.4.2 Western Blot

The anti-ABCC5 antibodies were assessed in LNCaP and PC-3 cells. Initially, all antibodies were subjected to screening in LNCaP and PC-3 cell lysates, with the most encouraging candidates selected from the data presented in **Figure 6.18 A** and then further assessed via KD and OE experiments. The results of this section were compared to the successful KD western blots of ABCC5 in **Chapter 4**. The

ability of ab92 to detect ABCC5 was examined in greater detail using LNCaP cells in **Fig. 6.18 B** and **C**, wherein a surprising finding was noted: the antibody demonstrated a lack of ability to detect ABCC5, as evidenced by the absence of any difference between control and KD in the knockdown experiment, as well as a similar lack of detection in the overexpression experiment. **Figure 6.18 D** shows the results for ab93, for which the KD experiment yielded no signal in PC-3 cells and the same level of expression in LNCaP cells after 72 hours, while the OE result was found to be the most promising, with a more pronounced staining intensity for overexpression.

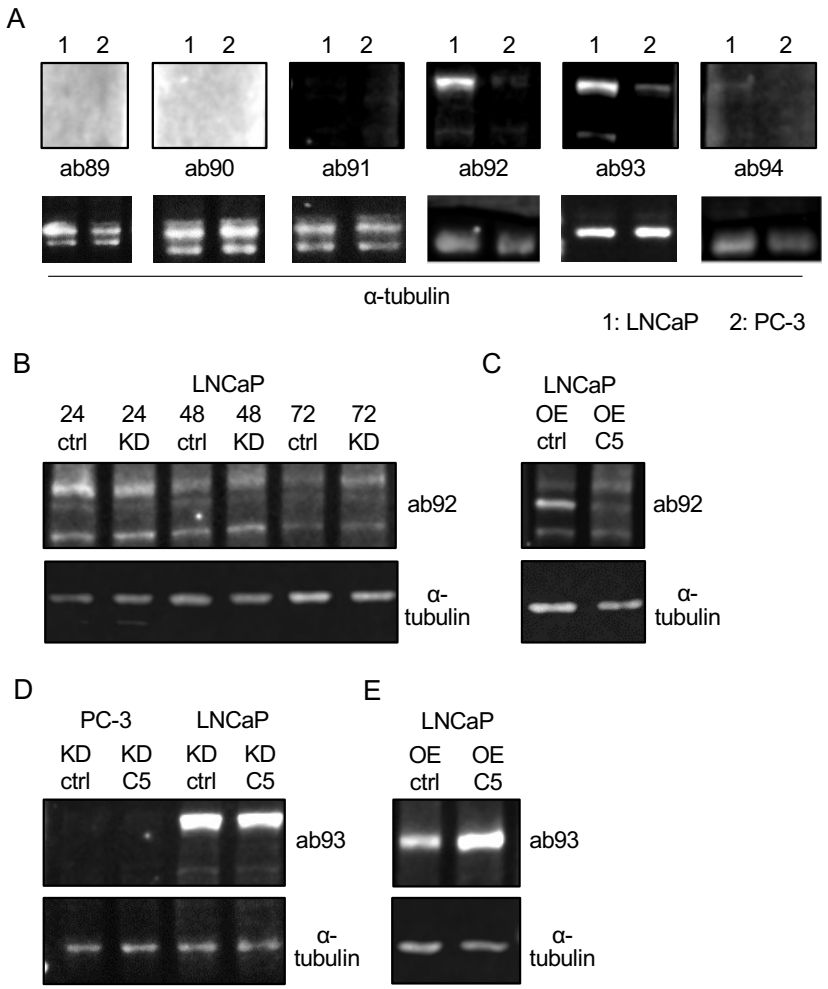

Figure 6.18: Western blot analysis for ABCC5 antibody specificity in LNCaP (1) and PC-3 (2) cells. **A)** Initial screen of LNCaP and PC-3 cell lysate with customised antibodies. **B)** Staining of untreated or ABCC5 siRNA-treated LNCaP cells at different time points with ab92. **C)** ABCC5 detection with ab92 in ABCC5 overexpressing or control LNCaP cells. **D)** Staining of untreated or ABCC5 siRNA-treated LNCaP and PC-3 cells after 72 h with ab93. **E)** ABCC5 detection with ab93 in ABCC5 overexpressing or control LNCaP cells. Knockdown (KD), overexpression (OE).

6.2.5 Custom Antibodies from the Borst Group

During our investigation into the customised antibodies, the laboratory group of Prof. Dr. P Borst generously provided us with their customised anti-ABCC5 antibodies. Following the acquisition of ambiguous results from our customised antibodies, I proceeded to evaluate the three antibodies designed by the Borst group.

6.2.5.1 Validation of ABCC5 Antibodies through Colocalisation Analysis with ABCC5-GFP

Here, ABCC5 was overexpressed in PC-3 cells using GFP as a reporter gene to test their ability to recognise and bind to ABCC5-GFP. Analysis of the resulting data, as presented in **Figure 6.19**, revealed the ability of all three antibodies to efficiently recognise and bind to ABCC5-GFP in PC-3 cells. Nevertheless, disparities in the fluorescence intensity and staining quality among the antibodies were observed. These findings imply that all three antibodies possess the potential to detect ABCC5 in PC-3 cells. However, MON9034 exhibited inferior staining results compared to the other two antibodies as highlighted by the white arrows. Specifically, MON9034 displayed a reduced antibody signal in the areas overlapping with ABCC5-GFP, despite demonstrating a strong overall signal. In light of these observations, MON9033 and MON9123 were deemed more promising candidates for downstream experimentation, including the knockdown study.

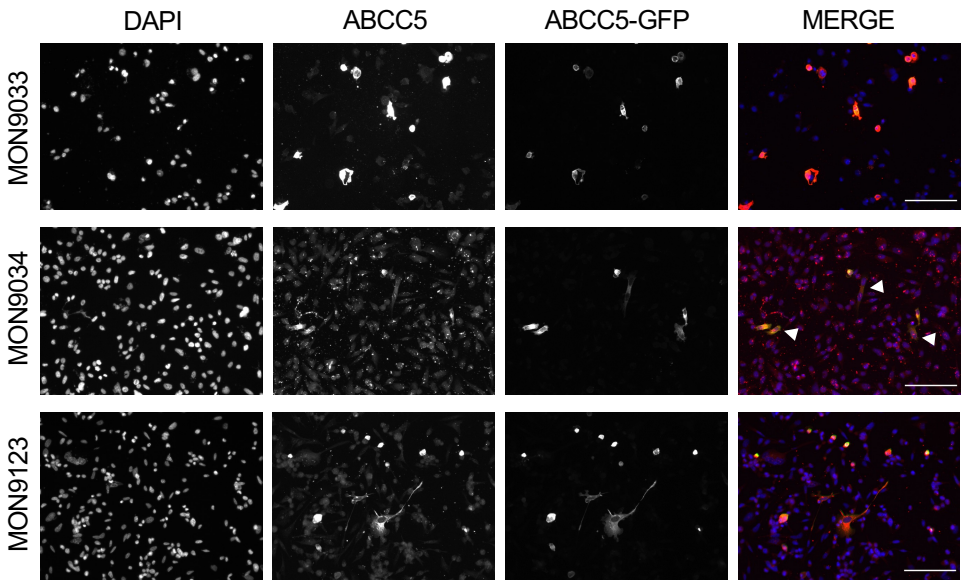

Figure 6.19: Colocalisation staining with overexpressed ABCC5-GFP in PC-3 cells and anti-ABCC5 antibodies. Representative images are shown for each antibody. The scale bar is 300 μm.

6.2.5.2 Validation of ABCC5 Antibodies through ABCC5 Knockdown

To assess the staining ability of MON9033 and MON9123, we performed staining experiments after ABCC5 KD for 72 h. The results presented in **Figure 6.20** revealed that MON9033 detected a reduction in the signal of approximately 50%, which aligns with the qPCR data obtained in Chapter 4. MON9123 demonstrated an even more significant reduction in staining signal, approximately 75%, in the KD samples which aligns more with the reduction shown in the western blot results in Chapter 4. In conclusion, the findings from this section underscore the potential of MON9123 as a robust antibody for detecting ABCC5 through immunofluorescence in cell lines. However, to thoroughly evaluate the antibody's performance, further testing on WT and knockdown prostate tissue sections is essential.

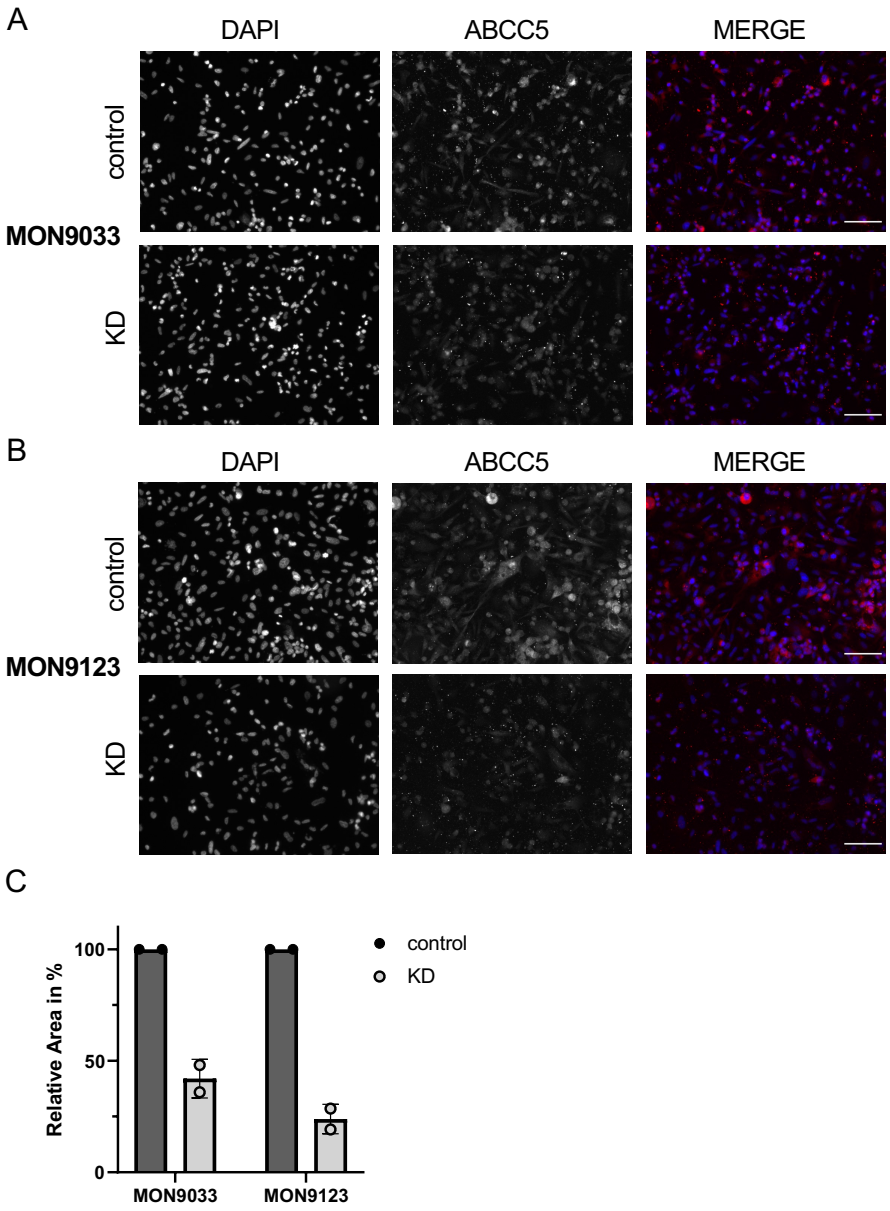

Figure 6.20: Detection of ABCC5 KD mediated by siRNA with immunofluorescence. PC-3 cells were stained with anti-ABCC5 antibody. Representative images of staining 72 h post-KD with **A)** MON9033 and **B)** MON9123. The scale bar is 200 μm. **C)** Quantification of the relative stained area expressed as a percentage compared to control. The results are from n=2. Data are represented as mean $\pm$ SD.

6.3 Discussion

6.3.1 Challenges in ABCC5 Detection: Overcoming Antibody Limitations

The results of the initial study of commercial antibodies yielded promising outcomes in western blot, with PA5-83701 displaying a strong signal specific to human ABCC5, as anticipated since it was the only antibody used that was designed exclusively for human ABCC5 detection. Ab180724 showed highly promising results, indicating signal presence in all four lysates. However, the observation of the same band in both KO and WT samples raised concerns about the antibody's specificity and the possibility of contamination or other interfering factors. The absence of disclosed information regarding the targeted region of ABCC5 further complicates the interpretation of these results. In conclusion, the commercial antibodies used in our study did not yield positive staining outcomes using IF for either mouse prostate tissue or human PCa cell lines. These results prompted our research group to pursue the development of custom antibodies, with a deliberate focus on targeting different regions of ABCC5. Most commonly used antibodies target either the N- or C-terminus of the protein. The C-terminal antibody is currently not available commercially but has been used extensively in the literature to stain human placenta, heart and pancreatic cancer tissue (200; 228; 269; 206). The majority of publications utilise the N-terminus of ABCC5 for visualisation in rat microglia, brain endothelial cells, renal and foetal tissue, and mouse prostate (584; 208; 224; 585; 223; 586; 587; 588).

Despite the overwhelming amount of literature showing the utilisation of the N-terminus, we decided to explore alternative regions for antibody targeting from the recognition that most commercial antibodies, which primarily targeted the N-

terminus of ABCC5, failed to deliver successful staining results for both mouse and human samples using IF in our experiments. By selecting these specific regions (**Figure 6.7**) for our custom antibody design, we aimed to create antibodies that would exhibit effective performance in both human and mouse samples, with the lowest probability of cross-reacting with ABCC11 or ABCC12. The evaluation of our customised antibodies revealed ab90 as the most promising candidate for detecting ABCC5 in both human and mouse samples. Whilst, ab89, ab91, ab92, ab93, and ab94 were not convincingly detecting ABCC5 across the different methods. **Figure 6.21**, highlights the different antibody binding sites on a schematic model of ABCC5 and highlights that the areas targeted have different functionality.

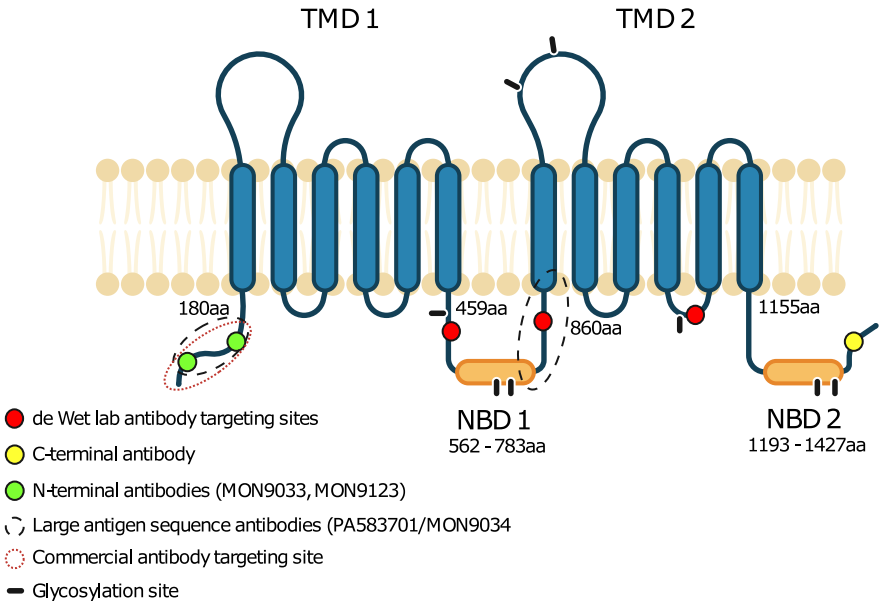

Figure 6.21: Schematic overview of ABCC5 and the respective antibody binding sites.Created with BioRender.com

Antibody target regions 1 and 2 are located within an unstructured loop region of

ABCC5 (**Figure 6.21**). Both regions have a per-residue confidence score below 50, indicating low confidence in their structural position (248). Therefore, it is very difficult to assess how this region behaves in the functioning transporter and whether the epitope is available or not. Region 1 (ab89, ab90) is closely located to the A-loop of ABCC5, which is a critical region involved in nucleotide binding through $\pi - \pi$ interactions and hydrogen bonding. This binding is essential for the subsequent hydrolysis of ATP (589). Region 2 (ab91, ab92) is located in the loop following NBD1 (248) which is utilised by ABCC5 for its dimerisation and hydrolysis of ATP (198). Hence, the question arises as to whether the selected areas are accessible for antibody binding depending on the conformational position of the protein during fixation.

Region 2 (ab91 and ab92) exhibited robust staining in the knockdown experiments, indicating that the antibody likely detects other proteins in addition to ABCC5. Similarly, antibodies ab93 and ab94 that target region 3 showed strong off-target staining in the OE staining and only limited ability to detect ABCC5. It is important to note that polyclonal antibodies are more prone to causing non-specific staining compared to monoclonal antibodies (590). The expression of ABCC11 and ABCC12 was confirmed for the PCa cell lines LNCaP and PC-3 however further studies into potential off-target binding necessitate assessing the expression levels of ABCC12 in mouse prostate. Intriguingly, ab90 also displayed an increase in signal in the Abcc5 KO tissue, which parallels the western blot result of ab180724. This observation raises questions regarding the KO model and warrants further investigation to understand the underlying factors contributing to this unexpected signal in the KO samples.

The western blot results with the customised antibodies failed to obtain staining of ABCC5. However, it is essential to consider the experimental conditions. It is worth noting that all experiments detailed in **Figure 6.18** utilised a LICOR detec-

tion system, while the working antibody described in **Chapter 4** was evaluated using ECL and film. This difference in detection methodologies may have contributed to the suboptimal results observed with the customised antibodies. To avoid overlooking any potential nuances and to gain a comprehensive understanding of the antibody performance, it is advisable to conduct further evaluations using the prior detection methodology (ECL and film). This approach will allow for a direct comparison of the customised antibodies with the working antibody from **Chapter 4** and allow a more informed conclusion about their effectiveness and suitability for ABCC5 detection.

An additional plausible explanation for the observed staining results of ab93 and ab94 could be attributed to the glycosylation of ABCC5, which may interfere with antibody binding. **Figure 6.21** illustrates that region 3 is located near glycosylation sites. This suggests that the presence of glycans may hinder the effective binding of antibodies in those regions or alter the structural position of the protein. Different types of glycosylation have been associated with cancer therapeutic resistance and are an accepted hallmark of cancer (591). N-glycosylation among other glycosylation changes is associated with PCa progression (592). ABCC5 is heavily glycosylated and the eight suggested glycosylation sites are marked in **Figure 6.21** (200). N-glycosylation at Asn684 and Asn897 is up-regulated in the cancer cell line MCF-7 (593) and drug-resistant NCI/ADR-RES cells (594). To further investigate this hypothesis, one could try western blot analysis after deglycosylation of ABCC5 to see if this would improve detection.

The staining results obtained with the Borst antibodies demonstrated the highest sensitivity in detecting the KD of ABCC5 in PCa cells, making them promising candidates for ABCC5 detection. However, it is essential to note that these antibodies have only been tested to a limited extent and require further evaluation, particularly in mouse prostate staining. Indeed, the Borst antibodies also target

the N-terminus, similar to the commercial antibodies, which adds an intriguing dimension to the findings. It highlights the existence of variation in the functionality of N-terminus targeting antibodies, likely dependent on the specific area within the N-terminus they recognise. This variability underscores the complex nature of antibody-antigen interactions and emphasises the need for a comprehensive understanding of the targeted regions within ABCC5. The exact location of epitopes within the N-terminus could have a significant impact on the performance and specificity of the antibodies in ABCC5 detection. In summary, ab90, MON9033, and MON9123 emerge as the most promising candidates for ABCC5 detection in both mouse and human samples and should be further investigated.

6.3.2 Is the ABCC5$^{-/-}$ Mouse a Complete Knockout?

Remarkably, the majority of the antibodies demonstrated stronger staining in the ABCC5 KO samples compared to the WT samples, with ab90, the most promising candidate, displaying particularly notable results in this regard. This result raises intriguing questions regarding the possible explanations for such an observation as off-target staining would result in similar staining between the two groups. The KO mice were created through CRISPR-induced removal of exon 13 following the Walker A catalytic sequence of the initial nucleotide-binding domain, resulting in a frameshift mutation as shown in **Figure 6.22**. Therefore, the potential presence and functional significance of ABCC5 isoforms in the prostate were considered.
In the literature, a short variant of ABCC5 transcript called SMRP was mentioned which was cloned from a human lung cancer cell line (197) and detected in several human tissues (198). However, another group was not able to confirm its presence on the protein level despite detecting small amounts of mRNA (200), and the SMRP transcript was not mentioned in any later studies. Interestingly, a study on human retinas detected three different variants of ABCC5 transcript (226). The

genetic makeup of the three variants of the transcript is shown in **Figure 6.22**. These short transcript variants are located before the CRISPR region responsible for removing exon 13 in the ABCC5 KO mice used in our study. This observation suggests that there is a possibility that unexplored splice variants of ABCC5 could be present in prostate tissue despite the KO which is supported by the western blot staining of WT and KO lysates with ab180274.

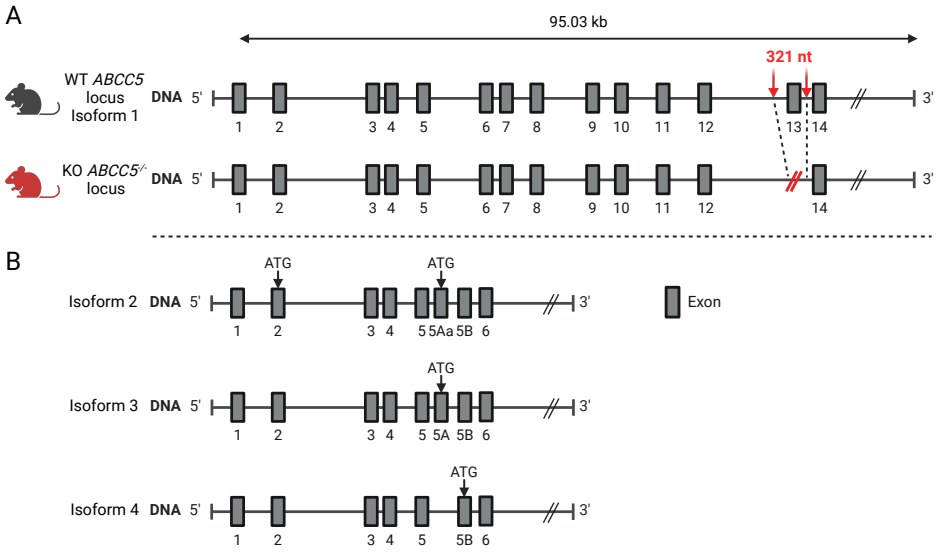

Figure 6.22: Genomic overview of Abcc5$^{-/-}$ CRISPR/Cas9 KO design and mouse ABCC5 isoforms detected in the mouse retina. Created with BioRender.com

Many different ABC transporters within the ABC transporter family have been reported to undergo exon skipping and alternative splicing events (595; 596). ABCB1 exon 2 skipping is associated with lymphoma progression (597). Further, chemotoxic drugs cause significant changes in the expression pattern of specific ABCG2 mRNA isoforms (598). Within the ABCC family, several transporters have reported alternative variants due to alternative splicing. In ovarian tumours,

alternative splicing of the ABCC1 gene occurs more frequently compared to its occurrence in matched normal tissues (599). A homozygous exonic variant in ABCC8 leads to exon skipping, causing severe congenital hyperinsulinism (600). Therefore, there is an association between alternative splicing events and disease. Several transcript variants have been documented for the ABCC5 paralogues ABCC11 and ABCC12. Early research on ABCC12 reported four different splice variants across a variety of tissues including the human liver, pancreas, testis, and fetal thymus. Some of the transcript variants were reported to have higher mRNA levels than the full-length ABCC12 mRNA in the above-mentioned tissues (252). Whereas, a different group identified two transcript variants with the large transcript detected in breast cancer and testis tissue and the smaller transcript in the brain, skeletal muscle, and ovary (271). Another study also detected two short variants of the ABCC12 transcript with 775 and 687 amino acid residues (270). The most recent study on liver tissue was able to detect two of the four previously reported variants in liver tissue (275). So far there has only been one study on variants in ABCC11 which was able to identify a splicing variant which occurred at around 25% in the cDNA clones which was missing exon 28 (252). In conclusion, the presence of different variants seems to be highly tissue-dependent and therefore has to be assessed for various tissues separately. In the next step, it would be imperative to assess whether any transcript variants of ABCC5 are present in prostate tissue and could explain the staining results observed.

Another hypothesis to consider is that despite the KO design, the ABCC5 protein could still be expressed despite the subsequent frameshift, especially as two antibody binding sites are located after the eliminated exon 13 and therefore should not be detected. CRISPR-Cas9 technology that introduces a deletion at the targeted genomic locus, results in premature termination of translation and degradation of mRNA (601). However, it is essential to note that the termination of trans-

lation in the presence of frameshift mutations is not always guaranteed. While frameshift mutations generally lead to the introduction of premature stop codons (PTC), the protein can still be expressed (602). Several studies have shown that PTCs are countered by various cellular mechanisms involving PTC elimination, exon skipping, or alternative translation initiation (603). Ultimately, resulting in N- or C-terminally truncated proteins that exhibit cellular functions (604; 605). Therefore, in the context of a CRISPR-induced frameshift mutation, it is possible that translation of the mRNA may not be fully terminated, and a portion of the ABCC5 protein may still be expressed in the KO mice or it is not a full KO. Taking into account this possibility, the staining observed in ABCC5 KO mouse samples could be attributed to the presence of a dysfunctional or truncated ABCC5 protein. The enhanced staining in comparison to WT could be a result of the higher availability of the antibody epitope due to a changed structural conformation or because of increased expression to compensate for the loss of the fully functional transporter. Given the uncertainties regarding the presence of ABCC5 isoforms, further transcriptomic analysis of the mouse model is warranted to investigate possible aberrant expression in various tissues. Therefore, the model cannot be used to validate antibodies without reservations. Further, the phenotype observed in the mice could be influenced by compensatory overexpression of transcript variants or an abundance of dysfunctional ABCC5.

6.4 Summary and Limitations

Despite the promising results obtained with the Borst antibodies in this study, their efficacy and specificity have not been thoroughly tested. Future investigations should involve testing the Borst antibodies in the KO model to confirm their reliability and validate their potential for further applications, as well as testing the

antibodies in other applications such as IHC and Western Blot. Overall, they show the most promise for studying ABCC5 involvement in PCa. Current research has only indicated ABCC5 isoforms in the retina (226), while their presence and potential variants in PCa tissue remain largely unexplored. Therefore, the ambiguous staining results cannot be traced back to isoforms of ABCC5. Therefore, in the future, there is a need to address ABCC5 isoforms in cancer tissues to ensure a complete analysis of ABCC5 involvement. Furthermore, the lack of an ABCC5 KO cell line imposes limitations on testing antibodies that work on human material as many antibodies only work on species specifically. The unavailability of ABCC5/ABCC11/ABCC12 KO cell lines limits the ability to discern the functional impact of each paralogue and whether there are potential compensatory mechanisms. As a triple KO is not possible in mice, cell lines would present a suitable model to elucidate their respective role.

This chapter has revealed several previously unknown questions about the ABCC5$^{-/-}$ KO model which have to be addressed. Currently, the data is not sufficient to prove that the KO model does not express a dysfunctional or truncated version of ABCC5. Experiments should be conducted to establish whether this KO model is suitable for evaluating the role of ABCC5 in disease. The time constraints imposed by my personal health situation resulted in limitations in the depth of the investigation of functional antibodies. The scope of this chapter was to fully validate functional antibodies to explore the role of ABCC5 in PCa. The ultimate objective was to stain human PCa samples to detect ABCC5 expression in different stages of the disease.

7 | General Discussion and Conclusion

Prostate cancer (PCa) stands out as the most prevalent malignancy in men in the Western world, and caring for patients with PCa represents a substantial global healthcare challenge (606). The increasing frequency of PCa diagnoses underscores the urgent need to develop effective treatment strategies (303). Despite recent improvements, advanced PCa remains a significant contributor to high mortality rates, especially when it metastasises to the bone (607). Current management is predominantly palliative due to the development of resistance to available treatments (608). Overexpression of ABCC5 has been linked to reduced overall survival, shortened progression-free survival, and metastatic progression across various cancer types, including PCa (609; 610). However, the exact mechanisms and pathway involvement of ABCC5 remain unclear, as ABCC5 is often grouped with other ABC transporters in the context of drug export and chemotherapy resistance (279; 238).

The central aim of this thesis was to advance our comprehension of ABCC5's role in PCa. Despite recent advancements, our grasp of ABCC5's precise function, substrates, and pathway involvement is limited by the scarcity of in-depth functional studies and the absence of a 3D-resolution ABCC5 structure. This prevents the establishment of structure-function relationships. Moreover, limited studies have been conducted on ABCC5 due to its status as a niche orphan transporter within the ABCC family. In this thesis, I hypothesised about ABCC5's involvement in PCa and its broader functionalities. Employing a comprehensive approach, I extensively explored ABCC5-associated genes and proteins from large databases to discern potential roles and identify associated pathways. This process unveiled intriguing and unique functions for ABCC5, which are not shared by other ABC transporters, prompting initial functional studies that identified and

validated candidates for further in-depth exploration.

Chapter 3 emphasised the resemblance between the peptidase domain in PCAT1 and the N-terminus of ABCC5, hinting at a potential enzymatic function of ABCC5. Despite the demonstrated structural similarity, the functional context in which the N-terminus operates likely differs between humans and bacteria. Nevertheless, this observation is particularly intriguing given that the short isoforms of ABCC5 in the retina contain this domain. Considering the findings across all of the chapters, ABCC5's involvement can be divided into two main categories: epigenomic regulation and associated processes in the nucleus and apoptosis and heme metabolism in the mitochondria.

7.1 Epigenomic Regulation in Prostate Cancer: Potential ABCC5-Mediated Regulatory Pathways

The dynamics of chromatin and transcriptional regulation are intricately linked, forming a core aspect of cellular function. In the context of PCa, our investigation into ABCC5's role prompts the question of whether ABCC5 could be a contributing factor, playing a role in the orchestration of transcriptional processes and influencing the expression of genes crucial for the progression of PCa? In **Chapter 3**, it was shown that the majority of genes positively correlated with ABCC5 across the entire TCGA dataset were associated with transcription factor activity. Meanwhile, **Chapter 4** revealed the GO Term SUMOylation as a key player in both underexpression and overexpression datasets. SUMOylation influences several cellular processes, spanning gene expression, chromatin remodelling, DNA repair, and cell cycle regulation (365; 366; 367). Notably, this modification prevents FOXM1 dimerisation, a transcription factor pivotal during the G2 and M phases of the cell cycle and a transcription factor of ABCC5 (291; 368).

Furthermore, a comprehensive pan-cancer analysis revealed that genes within the ABCC5 overexpression group were predominantly enriched in pathways related to the cell cycle (611). Interestingly, our data further suggested a specific role in stem cell division, which is likely linked to the previously discussed cell cycle regulation. Significantly, within breast cancer stem cell-like cells, the presence of ABCC5 showed a correlation with increased resistance to chemotherapy. Furthermore, the stem cell transcription factor Bmi1 was shown to modulate ABCC5 expression (298). Moreover, the protein network analysis in **Chapter 5** revealed the presence of ABCB5, which is expressed in various cancer cells containing cancer stem cells (612; 613; 614).

Histone modifications play a crucial role in regulating the cell cycle and add sig-

nificant complexity to transcriptional regulation (615). In **Chapter 4**, significant GO terms associated with ABCC5 in the PCa dataset included chromatin remodelling and histone acetyltransferase complex. Remarkably, SUPT7L expression consistently responded to ABCC5 KD in both cell lines, and it was identified as possessing dual functionality, serving as both an H2BK120 deubiquitinase and an acetyltransferase (616).

This discovery is particularly intriguing in light of the protein network analysis, which highlighted the involvement of ubiquitin C (UBC), and the emphasis on ubiquitination and deubiquitination processes in **Chapter 3**. Further, the protein interaction network also contained two members of the histone linker family, H1.1, namely HIST1H1A and HIST1H1B, with both playing a crucial role in nucleosomes by interacting with DNA and the core histone octamer to enable proper chromatin folding and compaction (617). The dynamic organisation of chromatin is influenced by proteins such as SMC2, another protein identified in the network. SMC2 is an important component of the condensin complex, necessary for chromosome assembly and cell division (618). Remarkably, histone deacetylase (HDAC) inhibitors were found to enhance ABCC5 mRNA and protein expression in lung and colorectal cancer cells (459), a result mirrored in pregnant rats treated with valproic acid, another HDAC inhibitor (460).

Chromatin structure and histone modifications regulate access to damaged DNA sites during the cell cycle. Chromatin remodelling allows repair factors to reach damaged regions, while specific histone modifications act as signals for the recruitment of repair proteins (619; 620). The GO term analysis of genes associated with ABCC5 also identified DNA repair as significant in the TCGA PCa dataset. In the literature, a correlation was observed between ABCC5 and GTF2H2 expression, a component of a complex essential for DNA repair (464). Meanwhile, GSK3beta expression is regulated by the same factor as ABCC5, a pivotal player

in cellular repair and the DNA damage response (466). This connection to DNA repair is further supported by our findings regarding PARP1. PARP1 was identified in the protein network analysis, and qPCR studies revealed consistent expression increase upon ABCC5 KD. Recent evidence underscores the critical role of PARP1 in DNA repair pathways and genomic stability, with its catalytic activity mediating repair and stabilising replication forks (547). The use of PARP inhibitor Olaparib shows promise for treating metastatic castration-resistant PCa (621).
This section highlights the intricate interconnectedness among chromatin dynamics, transcriptional regulation, cell cycle, and DNA repair within the context of ABCC5 and Pca. The presence of ABCC5 isoforms introduces the possibility for short transcript variants to influence the described pathways as modulators, either through an N-terminal enzymatic functionality or as a small effector protein. Although ABCC5 could still function in its fully transcribed version, no nuclear staining has been demonstrated thus far, increasing the likelihood of small transcripts acting as modulators. The cumulative data from all chapters strongly supports the hypothesis that ABCC5 plays a crucial role in epigenomic regulation. The specific findings present promising candidates for more in-depth studies. Nevertheless, to firmly establish the involvement of ABCC5, additional research is essential to validate and expand upon these initial insights.

7.2 Decoding ABCC5's Role in Mitochondria: Unravelling Links to Heme Biosynthesis and Apoptotic Pathways

The intricate interplay among chromatin dynamics, transcriptional regulation, and the cell cycle establishes a connection with mitochondrial processes through the involvement of NRF1. NRF1 plays a pivotal role in influencing essential metabolic genes that are indispensable for growth. Specifically, it regulates genes associated with respiration, heme biosynthesis, and mitochondrial DNA processes, through the EIF2 signalling pathway, among other pathways (622; 623). Notably, the EIF2 signalling pathway also emerged as the most significantly altered GO term pathway in ABCC5 and ABCC12 double knockout mice (224). Furthermore, NRF1 expression exhibited a robust response to ABCC5 KD, with upregulation, as discussed in **Chapter 5**. Additionally, it also has been shown that during mitosis, SENP5 relocates to mitochondria, playing a vital role in deSUMOylation of mitochondrial proteins and contributing to mitochondrial fragmentation (369). Both of these aspects underscore the relationship between nuclear and mitochondrial dynamics, seamlessly leading to our exploration of ABCC5's potential role at the intersection of mitochondrial heme metabolism and apoptosis regulation.

Interestingly, the promoter analysis conducted in **Chapter 5** identified the promoters of MRPS7 and ABCB6 as the most similar, in terms of motifs, to the promoter of the ABCC5 when compared to other members within the cluster. These proteins are interconnected in the context of mitochondrial function and heme metabolism. MRPS7 functions as a small subunit situated in the 28S subunit of the mitochondrial ribosome (624). Remarkably, it stands as the exclusive RNA-binding protein within this structural complex (521). Mitochondrial ribo-

somes play an indispensable role in oxidative phosphorylation by synthesising 13 key proteins essential for the assembly and optimal function of respiratory chain complexes. This synthesis occurs through the translation of mitochondrial DNA (625). On the other hand, ABCB6 is important for facilitating the translocation of porphyrins for heme synthesis into the mitochondria (626). Despite its crucial function, the molecular mechanisms governing the transmembrane transport and substrate recognition of ABCB6 remain unclear (627). Interestingly, ABCG2, also part of the protein network in **Chapter 5**, is involved in porphyrin transport but operates to eliminate excess porphyrins across the plasma membrane (628).

Heme synthesis begins in the mitochondria, where succinyl Co-A and glycine combine to produce 5'-aminolevulinic acid through the catalysis of ALAS, an enzyme dependent on pyridoxal phosphate (629). Heme biosynthesis progresses in the cytoplasm, with the final steps occurring back in the mitochondria (630). SHMT2 converts serine to glycine, generating essential one-carbon units for nucleotide biosynthesis in the mitochondria (567). Overexpression of SHMT2 meets the increased nucleotide demands of rapidly dividing cancer cells, influencing tumour metabolism (572; 573). Moreover, SHMT2's involvement in one-carbon metabolism is associated with heme biosynthesis, as the glycine produced can be utilised in the initial step of heme synthesis. SHMT2 expression levels strongly responded to ABCC5 KD and it was shown in the literature that SHMT2 protein can bind to ABCC5 mRNA (578). ABCC5 downregulation led to an increase in SHMT2, prompting speculation about whether SHMT2 seeks to increase the transport of ABCC5 mRNA to the mitochondria to compensate for the loss of ABCC5 protein. The correlation between ABCC5 and heme metabolism is strengthened by the findings outlined in **Chapter 3**.

Particularly, the DALI alignment revealed a connection to CydDC, a protein responsible for heme transportation in bacteria. Despite our analysis not demon-

strating the conservation of heme transport-related residues, the structural analogy is intriguing, especially considering the emergence of proteins associated with heme biosynthesis in the protein network. As discussed in **Chapter 3**, various studies have proposed ABCC5 as a heme transporter itself (224; 223; 390). Fascinatingly, a study demonstrated that ABCC5 plays an inhibitory role in the induction of ferroptosis within hepatocellular carcinoma (300). Ferroptosis, a form of cell death, is initiated by disturbances in both cellular iron homeostasis and lipid metabolism (631).

Aberrant or mutated TP53 assumes a central role in tumorigenesis by participating in diverse cellular mechanisms, including DNA damage repair, cell cycle regulation, and cell death (611; 632). Beyond its engagements with nuclear target genes, p53 also plays a role in various mitochondrial processes. It contributes to mitochondrial biogenesis, the upkeep of mitochondrial DNA, the regulation of redox homeostasis, and the preservation of oxidative phosphorylation (633; 634). P53 was a central protein in the protein network analysis of **Chapter 5** and interestingly **Chapter 4** showed that ABCC5 overexpression in PC-3 and LNCaP cells led to increased MDM4 expression, a negative regulator of p53 (478). This suggests a potential role for ABCC5 in dysregulating p53 in PCa via MDM4. A study indicated that a metabolic switch to oxidative phosphorylation affects ABCC5 expression through the ERK5/MEF2 pathway in mutated p53 cells (479).

P53 serves as a transcription factor in mediating apoptosis by upregulating the expression of pro-apoptotic proteins such as Bax and PUMA, while suppressing anti-apoptotic proteins like Bcl-2 (635). This regulatory mechanism leads to mitochondrial outer membrane permeabilisation. Consequently, pro-apoptotic proteins, including cytochrome c, are released into the cytoplasm. Upon reaching the cytoplasm, cytochrome c activates caspases, pivotal for executing apoptosis (636). In our investigations, the protein network revealed the presence of

several caspases, and robust qPCR results were observed for various caspases in LNCaP cells. This underscores the correlation between ABCC5 and apoptosis while broadening our understanding of its involvement in mitochondrial pathways. However, additional research is imperative to gain a more in-depth understanding of the underlying mechanisms.

In conclusion, the unchecked proliferation characteristic of cancer cells necessitates a comprehensive understanding of the metabolic rewiring that underlies this process. This thesis has illuminated the complex role of the orphan ABC transporter ABCC5 in the progression of cancer, with a specific focus on prostate cancer. The investigation delved into the interplay of ABCC5 in the realms of epigenomic regulation, mitochondrial metabolism - specifically heme metabolism and the regulation of apoptosis. During our investigation of these pathways, numerous proteins of interest have surfaced as compelling candidates for in-depth exploration. However, a nuanced consideration arises with the identification of ABCC11 and ABCC12, which could potentially serve as compensatory factors for the functions of ABCC5. Subsequent experimental procedures should take into account the suggested compensatory roles of these closely related transporters. This awareness will be important in designing experimental conditions that can distinguish the specific contributions of ABCC5, thereby ensuring a more precise and comprehensive understanding of its distinct functions within the intricate landscape of cancer biology.

Bibliography

[1] H, S. *et al.* Global Cancer Statistics 2020: GLOBOCAN Estimates of Incidence and Mortality Worldwide for 36 Cancers in 185 Countries. *CA: a cancer journal for clinicians* **71** (2021). Publisher: CA Cancer J Clin.

[2] Cancer Research, UK (2019). URL https://www.cancerresearchuk.org/.

[3] Gandaglia, G. *et al.* Epidemiology and Prevention of Prostate Cancer. *European Urology Oncology* **4**, 877–892 (2021).

[4] Bell, K. J. L., Del Mar, C., Wright, G., Dickinson, J. & Glasziou, P. Prevalence of incidental prostate cancer: A systematic review of autopsy studies. *International Journal of Cancer* **137**, 1749–1757 (2015).

[5] Nowroozi, A. *et al.* Global and regional quality of care index for prostate cancer: an analysis from the Global Burden of Disease study 1990-2019. *Archives of Public Health* **81**, 70 (2023).

[6] Tikkinen, K. A. O. *et al.* Rapid Recommendations: Prostate cancer screening with prostate-specific antigen (PSA) test: a clinical practice guideline. *The BMJ* **362** (2018). Publisher: BMJ Publishing Group.

[7] Bostwick, D. G. *et al.* Human prostate cancer risk factors. *Cancer* **101**, 2371–2490 (2004).

[8] Barber, L. *et al.* Family History of Breast or Prostate Cancer and Prostate Cancer Risk. *Clinical Cancer Research* **24**, 5910–5917 (2018).

[9] Johns, L. & Houlston, R. A systematic review and meta-analysis of familial prostate cancer risk. *BJU International* **91**, 789–794 (2003). _eprint: https://onlinelibrary.wiley.com/doi/pdf/10.1046/j.1464-410X.2003.04232.x.

[10] Urabe, F. *et al.* Impact of family history on oncological outcomes in primary therapy for localized prostate cancer patients: a systematic review and meta-analysis. *Prostate Cancer and Prostatic Diseases* **24**, 638–646 (2021). Number: 3 Publisher: Nature Publishing Group.

[11] Kheirandish, P. & Chinegwundoh, F. Ethnic differences in prostate cancer. *British Journal of Cancer* **105**, 481–485 (2011). Number: 4 Publisher: Nature Publishing Group.

[12] Ben-Shlomo, Y. *et al.* The risk of prostate cancer amongst black men in the United Kingdom: the PROCESS cohort study. *European Urology* **53**, 99–105 (2008).

[13] Brookman-May, S. D. *et al.* Latest Evidence on the Impact of Smoking, Sports, and Sexual Activity as Modifiable Lifestyle Risk Factors for Prostate Cancer Incidence, Recurrence, and Progression: A Systematic Review of the Literature by the European Association of Urology Section of Oncological Urology (ESOU). *European Urology Focus* **5**, 756–787 (2019).

[14] Murphy, A. B. *et al.* Smoking and prostate cancer in a multiethnic sample. *The Prostate* **73**, 1518–1528 (2013). _eprint: https://onlinelibrary.wiley.com/doi/pdf/10.1002/pros.22699.

[15] Shahabi, A. *et al.* Tobacco smoking, polymorphisms in carcino-

gen metabolism enzyme genes, and risk of localized and advanced prostate cancer: results from the California Collaborative Prostate Cancer Study. *Cancer Medicine* **3**, 1644–1655 (2014). _eprint: https://onlinelibrary.wiley.com/doi/pdf/10.1002/cam4.334.

[16] Rivera-Izquierdo, M. *et al.* Obesity as a Risk Factor for Prostate Cancer Mortality: A Systematic Review and Dose-Response Meta-Analysis of 280,199 Patients. *Cancers* **13**, 4169 (2021). Number: 16 Publisher: Multidisciplinary Digital Publishing Institute.

[17] Vidal, A. C. *et al.* Obesity Increases the Risk for High-Grade Prostate Cancer: Results from the REDUCE Study. *Cancer Epidemiology, Biomarkers & Prevention* **23**, 2936–2942 (2014).

[18] Rota, M. *et al.* Alcohol consumption and prostate cancer risk: a meta-analysis of the dose-risk relation. *European Journal of Cancer Prevention* **21**, 350 (2012).

[19] Zhao, J., Stockwell, T., Roemer, A. & Chikritzhs, T. Is alcohol consumption a risk factor for prostate cancer? A systematic review and meta-analysis. *BMC Cancer* **16**, 845 (2016).

[20] Tisell, L.-E. & Salander, H. the lobes of the human prostate. *Scandinavian Journal of Urology and Nephrology* **9**, 185–191 (1975). URL https://doi.org/10.3109/00365597509134209. PMID: 1209174, https://doi.org/10.3109/00365597509134209.

[21] McNeal, J. E. The zonal anatomy of the prostate. *The Prostate* **2**, 35–49 (1981). URL https://onlinelibrary.wiley.com/doi/abs/

10.1002/pros.2990020105. https://onlinelibrary.wiley.com/doi/pdf/10.1002/pros.2990020105.

[22] de Kretser, D. M., Temple-Smith, P. D. & Kerr, J. B. *Anatomical and Functional Aspects of the Male Reproductive Organs*, 1–131 (Springer Berlin Heidelberg, Berlin, Heidelberg, 1982). URL https://doi.org/10.1007/978-3-642-65117-5_1.

[23] Dj, G. & Wa, S. Zonal origin of prostatic adenocarcinoma: are there biologic differences between transition zone and peripheral zone adenocarcinomas of the prostate gland? (1994). URL https://api.semanticscholar.org/CorpusID:77012351.

[24] Lopez-Beltran, A., Cheng, L., Montironi, R. & Raspollini, M. R. *Basic Anatomy and Histology of the Prostate*, 1â9 (Cambridge University Press, 2017).

[25] Messner, E. A. *et al.* The androgen receptor in prostate cancer: Effect of structure, ligands and spliced variants on therapy. *Biomedicines* **8** (2020). URL https://www.mdpi.com/2227-9059/8/10/422.

[26] Balk, S. P., Ko, Y.-J. & Bubley, G. J. Biology of prostate-specific antigen. *Journal of Clinical Oncology: Official Journal of the American Society of Clinical Oncology* **21**, 383–391 (2003).

[27] el Shirbiny, A. M. Prostatic specific antigen. *Advances in Clinical Chemistry* **31**, 99–133 (1994).

[28] Rebello, R. J. *et al.* Prostate cancer. *Nature Reviews Disease Primers* **7**, 1–27 (2021). Number: 1 Publisher: Nature Publishing Group.

[29] Ilic, D., Neuberger, M. M., Djulbegovic, M. & Dahm, P. Screening for prostate cancer. *The Cochrane Database of Systematic Reviews* **2013**, CD004720 (2013).

[30] Schröder, F. H. *et al.* Evaluation of the digital rectal examination as a screening test for prostate cancer. Rotterdam section of the European Randomized Study of Screening for Prostate Cancer. *Journal of the National Cancer Institute* **90**, 1817–1823 (1998).

[31] Walsh, A. L., Considine, S. W., Thomas, A. Z., Lynch, T. H. & Manecksha, R. P. Digital rectal examination in primary care is important for early detection of prostate cancer: a retrospective cohort analysis study. *The British Journal of General Practice: The Journal of the Royal College of General Practitioners* **64**, e783–787 (2014).

[32] Dvoracek, J. [Adenocarcinoma of the prostate]. *Casopis Lekaru Ceskych* **137**, 515–521 (1998).

[33] Hoffmann, T. J. *et al.* Genome-wide association study of prostate-specific antigen levels identifies novel loci independent of prostate cancer. *Nature Communications* **8**, 14248 (2017). Number: 1 Publisher: Nature Publishing Group.

[34] Neal, D. E., Clejan, S., Sarma, D. & Moon, T. D. Prostate specific antigen and prostatitis. I. Effect of prostatitis on serum PSA in the human and nonhuman primate. *The Prostate* **20**, 105–111 (1992).

[35] Ilic, D. *et al.* Prostate cancer screening with prostate-specific antigen (PSA) test: a systematic review and meta-analysis. *The BMJ* **362**, k3519 (2018).

[36] Cooner, W. H. *et al.* Prostate cancer detection in a clinical urological practice by ultrasonography, digital rectal examination and prostate specific antigen. *The Journal of Urology* **143**, 1146–1152; discussion 1152–1154 (1990).

[37] Gosselaar, C., Roobol, M. J., Roemeling, S. & Schröder, F. H. The role of the digital rectal examination in subsequent screening visits in the European randomized study of screening for prostate cancer (ERSPC), Rotterdam. *European Urology* **54**, 581–588 (2008).

[38] Nagler, H. M. *et al.* Digital rectal examination is barrier to population-based prostate cancer screening. *Urology* **65**, 1137–1140 (2005).

[39] Teo, C. H., Ng, C. J., Booth, A. & White, A. Barriers and facilitators to health screening in men: A systematic review. *Social Science & Medicine (1982)* **165**, 168–176 (2016).

[40] Ortner, G., Tzanaki, E., Rai, B. P., Nagele, U. & Tokas, T. Transperineal prostate biopsy: The modern gold standard to prostate cancer diagnosis. *Turkish Journal of Urology* **47**, S19–S26 (2021).

[41] Ahmed, H. U. *et al.* Diagnostic accuracy of multi-parametric MRI and TRUS biopsy in prostate cancer (PROMIS): a paired validating confirmatory study. *Lancet (London, England)* **389**, 815–822 (2017).

[42] Harvey, C. J., Pilcher, J., Richenberg, J., Patel, U. & Frauscher, F. Applications of transrectal ultrasound in prostate cancer. *The British Journal of Radiology* **85**, S3–S17 (2012).

[43] Eldred-Evans, D. *et al.* Rethinking prostate cancer screening: could MRI

be an alternative screening test? *Nature Reviews Urology* **17**, 526–539 (2020). Number: 9 Publisher: Nature Publishing Group.

[44] of Health, U. S. N. I. SEER Training Modules, Prostate Cancer, Morphology and Grade, ICD-O-3 Morphology Codes (2024). URL https://training.seer.cancer.gov/.

[45] Epstein, J. I., Allsbrook, W. C., Amin, M. B., Egevad, L. L. & ISUP Grading Committee. The 2005 International Society of Urological Pathology (ISUP) Consensus Conference on Gleason Grading of Prostatic Carcinoma. *The American Journal of Surgical Pathology* **29**, 1228–1242 (2005).

[46] Gleason, D. F. & Mellinger, G. T. Prediction of prognosis for prostatic adenocarcinoma by combined histological grading and clinical staging. *The Journal of Urology* **111**, 58–64 (1974).

[47] Kweldam, C. F., van Leenders, G. J. & van der Kwast, T. Grading of prostate cancer: a work in progress. *Histopathology* **74**, 146–160 (2019). _eprint: https://onlinelibrary.wiley.com/doi/pdf/10.1111/his.13767.

[48] Samaratunga, H., Delahunt, B., Yaxley, J., Srigley, J. R. & Egevad, L. From Gleason to International Society of Urological Pathology (ISUP) grading of prostate cancer. *Scandinavian Journal of Urology* **50**, 325–329 (2016). Publisher: Taylor & Francis _eprint: https://doi.org/10.1080/21681805.2016.1201858.

[49] Short, E., Warren, A. Y. & Varma, M. Gleason grading of prostate cancer: a pragmatic approach. *Diagnostic Histopathology* **25**, 371–378 (2019).

[50] van Leenders, G. J. *et al.* The 2019 International Society of Urological

Pathology (ISUP) Consensus Conference on Grading of Prostatic Carcinoma. *The American Journal of Surgical Pathology* **44**, e87–e99 (2020).

[51] Tolonen, T. T. *et al.* Overall and worst gleason scores are equally good predictors of prostate cancer progression. *BMC Urology* **11**, 21 (2011).

[52] Humphrey, P. A. Gleason grading and prognostic factors in carcinoma of the prostate. *Modern Pathology* **17**, 292–306 (2004).

[53] O'Sullivan, B. *et al.* The TNM classification of malignant tumours-towards common understanding and reasonable expectations. *The Lancet. Oncology* **18**, 849–851 (2017).

[54] UICC. TNM Classification of Malignant Tumours, 8th edition | UICC.

[55] PDQ Adult Treatment Editorial Board. Prostate Cancer Treatment (PDQ): Health Professional Version. In *PDQ Cancer Information Summaries* (National Cancer Institute (US), Bethesda (MD), 2002).

[56] Sekhoacha, M. *et al.* Prostate Cancer Review: Genetics, Diagnosis, Treatment Options, and Alternative Approaches. *Molecules* **27**, 5730 (2022).

[57] Radical prostatectomy versus deferred treatment for localised prostate cancer **2020**, CD006590 (2020).

[58] Carlsson, S. *et al.* Long-term outcomes of active surveillance for prostate cancer - the Memorial Sloan Kettering Cancer Center experience. *The Journal of urology* **203**, 1122–1127 (2020).

[59] Epstein, J. I., Walsh, P. C., Carmichael, M. & Brendler, C. B. Pathologic

and clinical findings to predict tumor extent of nonpalpable (stage T1c) prostate cancer. *JAMA* **271**, 368–374 (1994).

[60] Garisto, J. D. & Klotz, L. Active Surveillance for Prostate Cancer: How to Do It Right. *Oncology (Williston Park, N.Y.)* **31**, 333–340, 345 (2017).

[61] Hamdy, F. C. *et al.* 10-Year Outcomes after Monitoring, Surgery, or Radiotherapy for Localized Prostate Cancer. *The New England Journal of Medicine* **375**, 1415–1424 (2016).

[62] Tosoian, J. J. *et al.* Intermediate and Longer-Term Outcomes From a Prospective Active-Surveillance Program for Favorable-Risk Prostate Cancer. *Journal of Clinical Oncology: Official Journal of the American Society of Clinical Oncology* **33**, 3379–3385 (2015).

[63] Sypre, D. *et al.* Impact of active surveillance for prostate cancer on the risk of depression and anxiety. *Scientific Reports* **12**, 12889 (2022). Number: 1 Publisher: Nature Publishing Group.

[64] Bailey, D. E. & Wallace, M. Critical review: is watchful waiting a viable management option for older men with prostate cancer? *American Journal of Men's Health* **1**, 18–28 (2007).

[65] Van Hemelrijck, M. *et al.* Quantifying the Transition from Active Surveillance to Watchful Waiting Among Men with Very Low-risk Prostate Cancer. *European Urology* **72**, 534–541 (2017).

[66] Bill-Axelson, A. *et al.* Radical prostatectomy or watchful waiting in early prostate cancer. *The New England Journal of Medicine* **370**, 932–942 (2014).

[67] Loeb, S. *et al.* Active Surveillance Versus Watchful Waiting for Localized Prostate Cancer: A Model to Inform Decisions. *European urology* **72**, 899–907 (2017).

[68] Lepor, H. A Review of Surgical Techniques for Radical Prostatectomy. *Reviews in Urology* **7**, S11–S17 (2005).

[69] Rocco, B. *et al.* Robotic vs open prostatectomy in a laparoscopically naive centre: a matched-pair analysis. *BJU International* **104**, 991–995 (2009). _eprint: https://onlinelibrary.wiley.com/doi/pdf/10.1111/j.1464-410X.2009.08532.x.

[70] Carbonara, U. *et al.* Robot-assisted radical prostatectomy versus standard laparoscopic radical prostatectomy: an evidence-based analysis of comparative outcomes. *World Journal of Urology* **39**, 3721–3732 (2021).

[71] Capogrosso, P. *et al.* Are We Improving Erectile Function Recovery After Radical Prostatectomy? Analysis of Patients Treated over the Last Decade. *European Urology* **75**, 221–228 (2019).

[72] Emanu, J. C., Avildsen, I. K. & Nelson, C. J. Erectile dysfunction after radical prostatectomy: prevalence, medical treatments, and psychosocial interventions. *Current Opinion in Supportive and Palliative Care* **10**, 102–107 (2016).

[73] Ficarra, V. *et al.* Systematic review and meta-analysis of studies reporting urinary continence recovery after robot-assisted radical prostatectomy. *European Urology* **62**, 405–417 (2012).

[74] Bejrananda, T. & Pliensiri, P. Prediction of biochemical recurrence after

laparoscopic radical prostatectomy. *BMC Urology* **23**, 183 (2023).

[75] Tourinho-Barbosa, R. *et al.* Biochemical recurrence after radical prostatectomy: what does it mean? *International Brazilian Journal of Urology : official journal of the Brazilian Society of Urology* **44**, 14–21 (2018).

[76] Cookson, M. S. *et al.* Variation in the definition of biochemical recurrence in patients treated for localized prostate cancer: the American Urological Association Prostate Guidelines for Localized Prostate Cancer Update Panel report and recommendations for a standard in the reporting of surgical outcomes. *The Journal of Urology* **177**, 540–545 (2007).

[77] Suarez, J. F. *et al.* Mortality and biochemical recurrence after surgery, brachytherapy, or external radiotherapy for localized prostate cancer: a 10-year follow-up cohort study. *Scientific Reports* **12**, 12589 (2022). Number: 1 Publisher: Nature Publishing Group.

[78] Murgic, J., Fröbe, A. & Kiang Chua, M. L. RECENT ADVANCES IN RADIOTHERAPY MODALITIES FOR PROSTATE CANCER. *Acta Clinica Croatica* **61**, 57–64 (2022).

[79] Wolff, R. F. *et al.* A systematic review of randomised controlled trials of radiotherapy for localised prostate cancer. *European Journal of Cancer* **51**, 2345–2367 (2015).

[80] Parker, C. C. *et al.* Radiotherapy to the prostate for men with metastatic prostate cancer in the UK and Switzerland: Long-term results from the STAMPEDE randomised controlled trial. *PLoS Medicine* **19**, e1003998 (2022).

[81] Pinkawa, M. External beam radiotherapy for prostate cancer. *Panminerva Medica* **52**, 195–207 (2010).

[82] Bauman, G., Rumble, R. B., Chen, J., Loblaw, A. & Warde, P. Intensity-modulated Radiotherapy in the Treatment of Prostate Cancer. *Clinical Oncology* **24**, 461–473 (2012).

[83] Hunte, S. O., Clark, C. H., Zyuzikov, N. & Nisbet, A. Volumetric modulated arc therapy (VMAT): a review of clinical outcomes - what is the clinical evidence for the most effective implementation? *The British Journal of Radiology* **95**, 20201289 (2022).

[84] Lee, J. W. & Chung, M. J. Prostate only radiotherapy using external beam radiotherapy: A clinician's perspective. *World Journal of Clinical Cases* **10**, 10428–10434 (2022).

[85] Booher, J. *et al.* Comparison of Three Groups of Patients Having Low Dose Rate Prostate Brachytherapy: Prostate-Specific Antigen Failure and Overall Survival. *Cureus* **13**, e18185 (2021).

[86] Yang, R., Wang, J. & Zhang, H. Dosimetric study of Cs-131, I-125, and Pd-103 seeds for permanent prostate brachytherapy. *Cancer Biotherapy & Radiopharmaceuticals* **24**, 701–705 (2009).

[87] Yamada, A. *et al.* High expression of ATP-binding cassette transporter ABCC11 in breast tumors is associated with aggressive subtypes and low disease-free survival. *Breast Cancer Research and Treatment* **137**, 773–782 (2013).

[88] Zaorsky, N. G. *et al.* The evolution of brachytherapy for prostate cancer.

Nature Reviews Urology **14**, 415–439 (2017). Number: 7 Publisher: Nature Publishing Group.

[89] Michaelson, M. D. *et al.* Management of Complications of Prostate Cancer Treatment. *CA: a cancer journal for clinicians* **58**, 196–213 (2008).

[90] Sutton, E. *et al.* Men's experiences of radiotherapy treatment for localized prostate cancer and its long-term treatment side effects: a longitudinal qualitative study. *Cancer causes & control: CCC* **32**, 261–269 (2021).

[91] Zietman, A. L. *et al.* Comparison of Conventional-Dose vs High-Dose Conformal Radiation Therapy in Clinically Localized Adenocarcinoma of the ProstateA Randomized Controlled Trial. *JAMA* **294**, 1233–1239 (2005).

[92] Gillessen, S. *et al.* Management of Patients with Advanced Prostate Cancer: Report of the Advanced Prostate Cancer Consensus Conference 2019. *European Urology* **77**, 508–547 (2020).

[93] Huggins, C. & Hodges, C. V. Studies on prostatic cancer. I. The effect of castration, of estrogen and androgen injection on serum phosphatases in metastatic carcinoma of the prostate. *CA: a cancer journal for clinicians* **22**, 232–240 (1972).

[94] Tolis, G. *et al.* Tumor growth inhibition in patients with prostatic carcinoma treated with luteinizing hormone-releasing hormone agonists. *Proceedings of the National Academy of Sciences* **79**, 1658–1662 (1982). Publisher: Proceedings of the National Academy of Sciences.

[95] Loblaw, D. A. *et al.* American Society of Clinical Oncology Recommendations for the Initial Hormonal Management of Androgen-Sensitive

Metastatic, Recurrent, or Progressive Prostate Cancer. *Journal of Clinical Oncology* **22**, 2927–2941 (2004). Publisher: Wolters Kluwer.

[96] Atta, M. A., Elabbady, A., Sameh, W., Sharafeldeen, M. & Elsaqa, M. Is there still a role for bilateral orchidectomy in androgen-deprivation therapy for metastatic prostate cancer? *Arab Journal of Urology* **18**, 9–13 (2019).

[97] Dreicer, R. The evolving role of hormone therapy in advanced prostate cancer. *Cleveland Clinic journal of medicine* **67**, 720–2, 725–6 (2000).

[98] Schally, A. V. Luteinizing hormone-releasing hormone analogs: their impact on the control of tumorigenesis. *Peptides* **20**, 1247–1262 (1999).

[99] Copperman, A. B. & Benadiva, C. Optimal usage of the GnRH antagonists: a review of the literature. *Reproductive Biology and Endocrinology* **11**, 20 (2013).

[100] Nelson, A. J. *et al.* Cardiovascular Effects of GnRH Antagonists Compared With Agonists inÂ Prostate Cancer: A Systematic Review. *JACC. CardioOncology* **5**, 613–624 (2023).

[101] Armstrong, A. J. *et al.* ARCHES: A Randomized, Phase III Study of Androgen Deprivation Therapy With Enzalutamide or Placebo in Men With Metastatic Hormone-Sensitive Prostate Cancer. *Journal of Clinical Oncology: Official Journal of the American Society of Clinical Oncology* **37**, 2974–2986 (2019).

[102] James, N. D. *et al.* Abiraterone for Prostate Cancer Not Previously Treated with Hormone Therapy. *The New England Journal of Medicine* **377**, 338–351 (2017).

[103] Elantably, D., Wang, J., Al Armashi, A. R., Al Zubaidi, A. & Alkrekshi, A. Androgen-deprivation therapy and risk of dementia in patients with prostate cancer: Clinical outcomes from real-world data. *Journal of Clinical Oncology* **41**, 5086–5086 (2023). Publisher: Wolters Kluwer.

[104] Higano, C. Androgen Deprivation Therapy: Monitoring and Managing the Complications. *Hematology/Oncology Clinics of North America* **20**, 909–923 (2006).

[105] Sanda, M. G. *et al.* Quality of life and satisfaction with outcome among prostate-cancer survivors. *The New England Journal of Medicine* **358**, 1250–1261 (2008).

[106] Harris, W. P., Mostaghel, E. A., Nelson, P. S. & Montgomery, B. Androgen deprivation therapy: progress in understanding mechanisms of resistance and optimizing androgen depletion. *Nature Clinical Practice. Urology* **6**, 76–85 (2009).

[107] Amjad, M. T., Chidharla, A. & Kasi, A. Cancer Chemotherapy. In *StatPearls* (StatPearls Publishing, Treasure Island (FL), 2024).

[108] Brunner, R. *et al.* Neoadjuvant chemotherapy for high-risk prostatic adenocarcinoma. *IJU Case Reports* **2**, 61–64 (2019). _eprint: https://onlinelibrary.wiley.com/doi/pdf/10.1002/iju5.12031.

[109] Ge, Q. *et al.* Neoadjuvant Chemohormonal Therapy in Prostate Cancer Before Radical Prostatectomy: A Systematic Review and Meta-Analysis. *Frontiers in Oncology* **12** (2022).

[110] Ma, M. W. *et al.* Effect of Adjuvant Chemotherapy in Highly Ma-

lignant Non-Metastatic Prostate Cancer: An Interim Analysis of Non-Randomized Comparative Trials. *International Journal of Radiation Oncology*Biology*Physics* **117**, e412–e413 (2023).

[111] Zhang, Q., Huang, J., Xie, C. & Wu, T. Adjuvant Chemotherapy in High-Risk Prostate Cancer Patients after Primary Local Therapy: Recurrence, Metastasis, and Survival - A Meta-Analysis. *Urologia Internationalis* **105**, 394–401 (2021).

[112] Kantoff, P. W. *et al.* Sipuleucel-T immunotherapy for castration-resistant prostate cancer. *The New England Journal of Medicine* **363**, 411–422 (2010).

[113] de Bono, J. S. *et al.* Prednisone plus cabazitaxel or mitoxantrone for metastatic castration-resistant prostate cancer progressing after docetaxel treatment: a randomised open-label trial. *Lancet (London, England)* **376**, 1147–1154 (2010).

[114] Cha, H.-R., Lee, J. H. & Ponnazhagan, S. Revisiting Immunotherapy: A Focus on Prostate Cancer. *Cancer research* **80**, 1615–1623 (2020).

[115] Madan, R. A. *et al.* Putting the Pieces Together: Completing the Mechanism of Action Jigsaw for Sipuleucel-T. *Journal of the National Cancer Institute* **112**, 562–573 (2020).

[116] Tucker, M. D. *et al.* Pembrolizumab in men with heavily treated metastatic castrate-resistant prostate cancer. *Cancer Medicine* **8**, 4644–4655 (2019).

[117] Gulley, J. L. *et al.* Phase III Trial of PROSTVAC in Asymptomatic or Minimally Symptomatic Metastatic Castration-Resistant Prostate Cancer.

Journal of Clinical Oncology: Official Journal of the American Society of Clinical Oncology **37**, 1051–1061 (2019).

[118] Noguchi, M. *et al.* A randomized phase III trial of personalized peptide vaccination for castration-resistant prostate cancer progressing after docetaxel. *Oncology Reports* **45**, 159–168 (2021).

[119] Powles, T. *et al.* Atezolizumab with enzalutamide versus enzalutamide alone in metastatic castration-resistant prostate cancer: a randomized phase 3 trial. *Nature Medicine* **28**, 144–153 (2022).

[120] Vogelzang, N. J. *et al.* Efficacy and Safety of Autologous Dendritic Cell-Based Immunotherapy, Docetaxel, and Prednisone vs Placebo in Patients With Metastatic Castration-Resistant Prostate Cancer: The VIABLE Phase 3 Randomized Clinical Trial. *JAMA oncology* **8**, 546–552 (2022).

[121] Stultz, J. & Fong, L. How to turn up the heat on the cold immune microenvironment of metastatic prostate cancer. *Prostate Cancer and Prostatic Diseases* **24**, 697–717 (2021). Number: 3 Publisher: Nature Publishing Group.

[122] Xu, P. *et al.* The Immunotherapy and Immunosuppressive Signaling in Therapy-Resistant Prostate Cancer. *Biomedicines* **10**, 1778 (2022). Number: 8 Publisher: Multidisciplinary Digital Publishing Institute.

[123] Siegel, R. L., Miller, K. D., Fuchs, H. E. & Jemal, A. Cancer statistics, 2022. *CA: A Cancer Journal for Clinicians* **72**, 7–33 (2022). _eprint: https://onlinelibrary.wiley.com/doi/pdf/10.3322/caac.21708.

[124] Draisma, G. *et al.* Lead times and overdetection due to prostate-specific

antigen screening: estimates from the European Randomized Study of Screening for Prostate Cancer. *Journal of the National Cancer Institute* **95**, 868–878 (2003).

[125] Schmidt, C. Metastatic prostate cancer: seeking a fresh chance of recovery. *Nature* **609**, S38–S40 (2022). Bandiera_abtest: a Cg_type: Outlook Number: 7927 Publisher: Nature Publishing Group Subject_term: Cancer, Therapeutics, Imaging.

[126] Siegel, R. L., Miller, K. D. & Jemal, A. Cancer statistics, 2018. *CA: a cancer journal for clinicians* **68**, 7–30 (2018).

[127] Liede, A., Arellano, J., Hechmati, G., Bennett, B. & Wong, S. International prevalence of nonmetastatic (M0) castration-resistant prostate cancer (CRPC). *Journal of Clinical Oncology* **31**, e16052–e16052 (2013). Publisher: Wolters Kluwer.

[128] Hamid, A. A. *et al.* Metastatic Hormone-Sensitive Prostate Cancer: Toward an Era of Adaptive and Personalized Treatment. *American Society of Clinical Oncology Educational Book* e390166 (2023). Publisher: Wolters Kluwer.

[129] Ng, K., Smith, S. & Shamash, J. Metastatic Hormone-Sensitive Prostate Cancer (mHSPC): Advances and Treatment Strategies in the First-Line Setting. *Oncology and Therapy* **8**, 209–230 (2020).

[130] Grino, P. B., Griffin, J. E. & Wilson, J. D. Testosterone at high concentrations interacts with the human androgen receptor similarly to dihydrotestosterone. *Endocrinology* **126**, 1165–1172 (1990).

[131] MacLean, H. E., Chu, S., Warne, G. L. & Zajac, J. D. Related individuals with different androgen receptor gene deletions. *The Journal of Clinical Investigation* **91**, 1123–1128 (1993).

[132] Roy, A. K. *et al.* Regulation of Androgen Action. In Litwack, G. (ed.) *Vitamins & Hormones*, vol. 55, 309–352 (Academic Press, 1998).

[133] Koivisto, P. *et al.* Androgen receptor gene amplification: a possible molecular mechanism for androgen deprivation therapy failure in prostate cancer. *Cancer Research* **57**, 314–319 (1997).

[134] Visakorpi, T. *et al.* In vivo amplification of the androgen receptor gene and progression of human prostate cancer. *Nature Genetics* **9**, 401–406 (1995).

[135] Robinson, D. *et al.* Integrative clinical genomics of advanced prostate cancer. *Cell* **161**, 1215–1228 (2015).

[136] Snaterse, G. *et al.* Androgen receptor mutations modulate activation by 11-oxygenated androgens and glucocorticoids. *Prostate Cancer and Prostatic Diseases* **26**, 293–301 (2023). Number: 2 Publisher: Nature Publishing Group.

[137] Watson, P. A. *et al.* Constitutively active androgen receptor splice variants expressed in castration-resistant prostate cancer require full-length androgen receptor. *Proceedings of the National Academy of Sciences* **107**, 16759–16765 (2010). Publisher: Proceedings of the National Academy of Sciences.

[138] Zhu, Y. & Luo, J. Regulation of androgen receptor variants in prostate cancer. *Asian Journal of Urology* **7**, 251–257 (2020).

[139] Heinlein, C. A. & Chang, C. Androgen receptor (AR) coregulators: an overview. *Endocrine Reviews* **23**, 175–200 (2002).

[140] Senapati, D., Kumari, S. & Heemers, H. V. Androgen receptor co-regulation in prostate cancer. *Asian Journal of Urology* **7**, 219–232 (2020).

[141] Datta, K., Muders, M., Zhang, H. & Tindall, D. J. Mechanism of lymph node metastasis in prostate cancer. *Future Oncology (London, England)* **6**, 823–836 (2010).

[142] Ruppender, N. S., Morrissey, C., Lange, P. H. & Vessella, R. L. Dormancy in solid Tumors: Implications for Prostate Cancer. *Cancer metastasis reviews* **32**, 10.1007/s10555–013–9422–z (2013).

[143] Macedo, F. *et al.* Bone Metastases: An Overview. *Oncology Reviews* **11**, 321 (2017).

[144] Yin, J. J., Pollock, C. B. & Kelly, K. Mechanisms of cancer metastasis to the bone. *Cell Research* **15**, 57–62 (2005). Number: 1 Publisher: Nature Publishing Group.

[145] Higgins, C. F. ABC transporters: from microorganisms to man. *Annual Review of Cell Biology* **8**, 67–113 (1992).

[146] Berger, E. A. & Heppel, L. A. Different mechanisms of energy coupling for the shock-sensitive and shock-resistant amino acid permeases of Escherichia coli. *The Journal of Biological Chemistry* **249**, 7747–7755 (1974).

[147] Higgins, C. F. & Linton, K. J. The ATP switch model for ABC transporters. *Nature Structural & Molecular Biology* **11**, 918–926 (2004).

[148] Young, J. & Holland, I. B. ABC transporters: bacterial exporters-revisited five years on. *Biochimica Et Biophysica Acta* **1461**, 177–200 (1999).

[149] Ames, G. F.-L., Mimura, C. S., Holbrook, S. R. & Shyamala, V. Traffic ATPases: A Superfamily of Transport Proteins Operating from Escherichia coli to Humans. In *Advances in Enzymology and Related Areas of Molecular Biology*, 1–47 (John Wiley & Sons, Ltd, 1992). _eprint: https://onlinelibrary.wiley.com/doi/pdf/10.1002/9780470123119.ch1.

[150] Dean, M., Hamon, Y. & Chimini, G. The human ATP-binding cassette (ABC) transporter superfamily. *Journal of Lipid Research* **42**, 1007–1017 (2001).

[151] Dassa, E. & Bouige, P. The ABC of ABCs: a phylogenetic and functional classification of ABC systems in living organisms. *Research in Microbiology* **152**, 211–229 (2001).

[152] Vasiliou, V., Vasiliou, K. & Nebert, D. W. Human ATP-binding cassette (ABC) transporter family. *Human Genomics* **3**, 281 (2009).

[153] Locher, K. P., Lee, A. T. & Rees, D. C. The E. coli BtuCD Structure: A Framework for ABC Transporter Architecture and Mechanism. *Science* **296**, 1091–1098 (2002). Publisher: American Association for the Advancement of Science.

[154] Hollenstein, K., Dawson, R. J. & Locher, K. P. Structure and mechanism of ABC transporter proteins. *Current Opinion in Structural Biology* **17**, 412–418 (2007).

[155] Oswald, C., Holland, I. B. & Schmitt, L. The motor domains of ABC-

transporters. *Naunyn-Schmiedeberg's Archives of Pharmacology* **372**, 385–399 (2006).

[156] Hyde, S. C. *et al.* Structural model of ATP-binding proteing associated with cystic fibrosis, multidrug resistance and bacterial transport. *Nature* **346**, 362–365 (1990). Number: 6282 Publisher: Nature Publishing Group.

[157] Walker, J. E., Saraste, M., Runswick, M. J. & Gay, N. J. Distantly related sequences in the alpha- and beta-subunits of ATP synthase, myosin, kinases and other ATP-requiring enzymes and a common nucleotide binding fold. *The EMBO journal* **1**, 945–951 (1982).

[158] Hopfner, K.-P. *et al.* Structural Biology of Rad50 ATPase: ATP-Driven Conformational Control in DNA Double-Strand Break Repair and the ABC-ATPase Superfamily. *Cell* **101**, 789–800 (2000). Publisher: Elsevier.

[159] Yoshida, M. & Amano, T. A common topology of proteins catalyzing ATP-triggered reactions. *FEBS Letters* **359**, 1–5 (1995). _eprint: https://onlinelibrary.wiley.com/doi/pdf/10.1016/0014-5793%2894%2901438-7.

[160] Yuan, Y.-R. *et al.* The Crystal Structure of the MJ0796 ATP-binding Cassette: IMPLICATIONS FOR THE STRUCTURAL CONSEQUENCES OF ATP HYDROLYSIS IN THE ACTIVE SITE OF AN ABC TRANSPORTER *. *Journal of Biological Chemistry* **276**, 32313–32321 (2001). Publisher: Elsevier.

[161] Chen, M., Abele, R. & Tampe, R. Functional Non-equivalence of ATP-binding Cassette Signature Motifs in the Transporter Associated with Anti-

gen Processing (TAP). *Journal of Biological Chemistry* **279**, 46073–46081 (2004). Publisher: Elsevier.

[162] Smith, P. C. *et al.* ATP Binding to the Motor Domain from an ABC Transporter Drives Formation of a Nucleotide Sandwich Dimer. *Molecular Cell* **10**, 139–149 (2002). Publisher: Elsevier.

[163] Locher, K. P. Mechanistic diversity in atp-binding cassette (abc) transporters. *Nature structural & molecular biology* **23**, 487–493 (2016).

[164] Hegedus, T. *et al.* Role of individual R domain phosphorylation sites in CFTR regulation by protein kinase A. *Biochimica Et Biophysica Acta* **1788**, 1341–1349 (2009).

[165] Desuzinges-Mandon, E. *et al.* ABCG2 transports and transfers heme to albumin through its large extracellular loop. *The Journal of Biological Chemistry* **285**, 33123–33133 (2010).

[166] Bryan, J. *et al.* ABCC8 and ABCC9: ABC transporters that regulate K+ channels. *Pflgers Archiv - European Journal of Physiology* **453**, 703–718 (2007).

[167] Holland, I. B. & A. Blight, M. ABC-ATPases, adaptable energy generators fuelling transmembrane movement of a variety of molecules in organisms from bacteria to humans. *Journal of Molecular Biology* **293**, 381–399 (1999).

[168] Geisler, M., Aryal, B., di Donato, M. & Hao, P. A Critical View on ABC Transporters and Their Interacting Partners in Auxin Transport. *Plant and Cell Physiology* **58**, 1601–1614 (2017).

[169] Luciani, M. F., Denizot, F., Savary, S., Mattei, M. G. & Chimini, G. Cloning of Two Novel ABC Transporters Mapping on Human Chromosome 9. *Genomics* **21**, 150–159 (1994).

[170] Franco, R. & Zavala-Flores, L. ABCC Transporters. In Schwab, M. (ed.) *Encyclopedia of Cancer*, 1–5 (Springer, Berlin, Heidelberg, 2016).

[171] Contreras, M., Sengupta, T. K., Sheikh, F., Aubourg, P. & Singh, I. Topology of ATP-Binding Domain of Adrenoleukodystrophy Gene Product in Peroxisomes. *Archives of Biochemistry and Biophysics* **334**, 369–379 (1996).

[172] Haimeur, A., Conseil, G., Deeley, R. & Cole, S. (Section A: Molecular, Structural, and Cellular Biology of Drug Transporters) The MRP-Related and BCRP / ABCG2 Multidrug Resistance Proteins: Biology, Substrate Specificity and Regulation. *Current Drug Metabolism* **5**, 21–53 (2004).

[173] Crowe-McAuliffe, C. *et al.* Structural basis of ABCF-mediated resistance to pleuromutilin, lincosamide, and streptogramin A antibiotics in Gram-positive pathogens. *Nature Communications* **12**, 3577 (2021). Number: 1 Publisher: Nature Publishing Group.

[174] Navarro-Quiles, C., Mateo-Bonmati, E. & Micol, J. L. ABCE Proteins: From Molecules to Development. *Frontiers in Plant Science* **9**, 1125 (2018).

[175] Santamarina-Fojo, S. *et al.* Complete genomic sequence of the human ABCA1 gene: analysis of the human and mouse ATP-binding cassette A promoter. *Proceedings of the National Academy of Sciences of the United States of America* **97**, 7987–7992 (2000).

[176] Shulenin, S. *et al.* ABCA3 gene mutations in newborns with fatal surfactant deficiency. *The New England Journal of Medicine* **350**, 1296–1303 (2004).

[177] Webster, A. *et al.* An analysis of allelic variation in the ABCA4 gene. *Investigative Ophthalmology and Visual Science* **42**, 1179–1189 (2001).

[178] Eggensperger, S. & Tampe, R. The transporter associated with antigen processing: a key player in adaptive immunity. *Biological Chemistry* **396**, 1059–1072 (2015). Publisher: De Gruyter.

[179] Paulusma, C. C. *et al.* A mutation in the human canalicular multispecific organic anion transporter gene causes the Dubin-Johnson syndrome. *Hepatology (Baltimore, Md.)* **25**, 1539–1542 (1997).

[180] Cheng, S. H. *et al.* Defective intracellular transport and processing of CFTR is the molecular basis of most cystic fibrosis. *Cell* **63**, 827–834 (1990).

[181] Williams, K., Segard, A. & Graf, G. A. Sitosterolemia: Twenty Years of Discovery of the Function of ABCG5 ABCG8. *International Journal of Molecular Sciences* **22**, 2641 (2021).

[182] Gottesman, M. M., Fojo, T. & Bates, S. E. Multidrug resistance in cancer: role of ATP-dependent transporters. *Nature Reviews. Cancer* **2**, 48–58 (2002).

[183] Doyle, L. A. *et al.* A multidrug resistance transporter from human MCF-7 breast cancer cells. *Proceedings of the National Academy of Sciences of the United States of America* **95**, 15665–15670 (1998).

[184] Marie, J. P., Zittoun, R. & Sikic, B. I. Multidrug resistance (mdr1) gene

expression in adult acute leukemias: correlations with treatment outcome and in vitro drug sensitivity. *Blood* **78**, 586–592 (1991).

[185] Cole, S. P. *et al.* Overexpression of a transporter gene in a multidrug-resistant human lung cancer cell line. *Science (New York, N.Y.)* **258**, 1650–1654 (1992).

[186] Gerk, P. M. & Vore, M. Regulation of expression of the multidrug resistance-associated protein 2 (MRP2) and its role in drug disposition. *The Journal of Pharmacology and Experimental Therapeutics* **302**, 407–415 (2002).

[187] Li, W. *et al.* Overcoming ABC transporter-mediated multidrug resistance: Molecular mechanisms and novel therapeutic drug strategies. *Drug Resistance Updates: Reviews and Commentaries in Antimicrobial and Anticancer Chemotherapy* **27**, 14–29 (2016).

[188] Jedlitschky, G., Leier, I., Buchholz, U., Center, M. & Keppler, D. ATP-dependent transport of glutathione S-conjugates by the multidrug resistance-associated protein. *Cancer Research* **54**, 4833–4836 (1994).

[189] Leier, I. *et al.* The MRP gene encodes an ATP-dependent export pump for leukotriene C4 and structurally related conjugates. *The Journal of Biological Chemistry* **269**, 27807–27810 (1994).

[190] Borst, P., Evers, R., Kool, M. & Wijnholds, J. The multidrug resistance protein family. *Biochimica et Biophysica Acta (BBA) - Biomembranes* **1461**, 347–357 (1999).

[191] Bakos, E. *et al.* Characterization of the amino-terminal regions in the hu-

man multidrug resistance protein (MRP1). *Journal of Cell Science* **113**, 4451–4461 (2000).

[192] Borst, P., Evers, R., Kool, M. & Wijnholds, J. A Family of Drug Transporters: the Multidrug Resistance-Associated Proteins. *JNCI: Journal of the National Cancer Institute* **92**, 1295–1302 (2000).

[193] Ford, R. C., Marshall-Sabey, D. & Schuetz, J. Linker domains: why ABC transporters 'live in fragments no longer'. *Trends in biochemical sciences* **45**, 137–148 (2020).

[194] Bloch, M., Raj, I., Pape, T. & Taylor, N. M. I. Structural and mechanistic basis of substrate transport by the multidrug transporter MRP4. *Structure (London, England: 1993)* **31**, 1407–1418.e6 (2023).

[195] Ravna, A. W., Sylte, I. & Sager, G. Molecular model of the outward facing state of the human P-glycoprotein (ABCB1), and comparison to a model of the human MRP5 (ABCC5). *Theoretical Biology & Medical Modelling* **4**, 33 (2007).

[196] Kool, M. *et al.* Analysis of expression of cMOAT (MRP2), MRP3, MRP4, and MRP5, homologues of the multidrug resistance-associated protein gene (MRP1), in human cancer cell lines. *Cancer Research* **57**, 3537–3547 (1997).

[197] Suzuki, T. *et al.* cDNA Cloning of a Short Type of Multidrug Resistance Protein Homologue,SMRP,from a Human Lung Cancer Cell Line. *Biochemical and Biophysical Research Communications* **238**, 790–794 (1997).

[198] Suzuki, T. *et al.* Detailed structural analysis on both human MRP5 and

mouse mrp5 transcripts. *Gene* **242**, 167–173 (2000).

[199] Sjöstedt, E. *et al.* An atlas of the protein-coding genes in the human, pig, and mouse brain. *Science* **367**, eaay5947 (2020). Publisher: American Association for the Advancement of Science.

[200] Dazert, P. *et al.* Expression and localization of the multidrug resistance protein 5 (MRP5/ABCC5), a cellular export pump for cyclic nucleotides, in human heart. *The American Journal of Pathology* **163**, 1567–1577 (2003).

[201] Berezowski, V., Landry, C., Dehouck, M.-P., Cecchelli, R. & Fenart, L. Contribution of glial cells and pericytes to the mRNA profiles of P-glycoprotein and multidrug resistance-associated proteins in an in vitro model of the blood-brain barrier. *Brain Research* **1018**, 1–9 (2004).

[202] At, N. *et al.* Expression and immunolocalization of the multidrug resistance proteins, MRP1-MRP6 (ABCC1-ABCC6), in human brain. *Neuroscience* **129** (2004). Publisher: Neuroscience.

[203] Klein, D. M., Wright, S. H. & Cherrington, N. J. Localization of Multidrug Resistance-Associated Proteins along the Blood-Testis Barrier in Rat, Macaque, and Human Testis. *Drug Metabolism and Disposition* **42**, 89–93 (2014).

[204] Verscheijden, L. F. M. *et al.* Developmental patterns in human blood-brain barrier and blood-cerebrospinal fluid barrier ABC drug transporter expression. *Histochemistry and Cell Biology* **154**, 265–273 (2020).

[205] de Wolf, C. J. F. *et al.* cGMP transport by vesicles from human and mouse erythrocytes. *The FEBS Journal* **274**, 439–450

(2007). _eprint: https://onlinelibrary.wiley.com/doi/pdf/10.1111/j.1742-4658.2006.05591.x.

[206] Meyer Zu Schwabedissen, H. E. U. *et al.* Expression, localization, and function of MRP5 (ABCC5), a transporter for cyclic nucleotides, in human placenta and cultured human trophoblasts: effects of gestational age and cellular differentiation. *The American Journal of Pathology* **166**, 39–48 (2005).

[207] Matalon, S. T., Drucker, L., Fishman, A., Ornoy, A. & Lishner, M. The Role of heat shock protein 27 in extravillous trophoblast differentiation. *Journal of Cellular Biochemistry* **103**, 719–729 (2008).

[208] Aleksunes, L. M., Cui, Y. & Klaassen, C. D. Prominent expression of xenobiotic efflux transporters in mouse extraembryonic fetal membranes compared with placenta. *Drug Metabolism and Disposition: The Biological Fate of Chemicals* **36**, 1960–1970 (2008).

[209] Shipp, L. E., Hill, R. Z., Moy, G. W. & Hamdoun, A. ABCC5 is required for cAMP-mediated hindgut invagination in sea urchin embryos. *Development (Cambridge, England)* **142**, 3537–3548 (2015).

[210] Long, Y., Li, Q., Li, J. & Cui, Z. Molecular analysis, developmental function and heavy metal-induced expression of ABCC5 in zebrafish. *Comparative Biochemistry and Physiology. Part B, Biochemistry & Molecular Biology* **158**, 46–55 (2011).

[211] Nongpiur, M. E. *et al.* ABCC5, a Gene That Influences the Anterior Chamber Depth, Is Associated with Primary Angle Closure Glaucoma. *PLOS Genetics* **10**, e1004089 (2014). Publisher: Public Library of Science.

[212] Wang, S. *et al.* Association of Single-Nucleotide Polymorphisms in ABCC5 Gene with Primary Angle Closure Glaucoma and the Ocular Biometric Parameters in a Northern Chinese Population. *Ophthalmic Research* **64**, 762–768 (2021).

[213] Karla, P. K. *et al.* Expression of multidrug resistance associated protein 5 (MRP5) on cornea and its role in drug efflux. *Journal of Ocular Pharmacology and Therapeutics: The Official Journal of the Association for Ocular Pharmacology and Therapeutics* **25**, 121–132 (2009).

[214] Vellonen, K.-S. *et al.* Effluxing ABC transporters in human corneal epithelium. *Journal of Pharmaceutical Sciences* **99**, 1087–1098 (2010).

[215] Jansen, R. S. *et al.* N-lactoyl-amino acids are ubiquitous metabolites that originate from CNDP2-mediated reverse proteolysis of lactate and amino acids. *Proceedings of the National Academy of Sciences of the United States of America* **112**, 6601–6606 (2015).

[216] Direk, K., Lau, W., Small, K. S., Maniatis, N. & Andrew, T. ABCC5 transporter is a novel type 2 diabetes susceptibility gene in European and African American populations. *Annals of Human Genetics* **78**, 333–344 (2014).

[217] Cyranka, M. *et al.* Abcc5 Knockout Mice Have Lower Fat Mass and Increased Levels of Circulating GLP-1. *Obesity (Silver Spring, Md.)* **27**, 1292–1304 (2019).

[218] McAleer, M. A., Breen, M. A., White, N. L. & Matthews, N. pABC11 (Also Known as MOAT-C and MRP5), a Member of the ABC Family of Proteins, Has Anion Transporter Activity but Does Not Confer Multidrug

Resistance When Overexpressed in Human Embryonic Kidney 293 Cells. *Journal of Biological Chemistry* **274**, 23541–23548 (1999). Publisher: Elsevier.

[219] Miyauchi, E. *et al.* Quantitative Atlas of Cytochrome P450, UDP-Glucuronosyltransferase, and Transporter Proteins in Jejunum of Morbidly Obese Subjects. *Molecular Pharmaceutics* **13**, 2631–2640 (2016).

[220] Nies, A. T. *et al.* Expression and immunolocalization of the multidrug resistance proteins, MRP1-MRP6 (ABCC1-ABCC6), in human brain. *Neuroscience* **129**, 349–360 (2004).

[221] Wijnholds, J. *et al.* Multidrug-resistance protein 5 is a multispecific organic anion transporter able to transport nucleotide analogs. *Proceedings of the National Academy of Sciences of the United States of America* **97**, 7476–7481 (2000).

[222] García-de Diego, A.-M. C-subfamily ATP binding cassette transporters extrude the calcium fluorescent probe fluo-4 from a cone photoreceptor cell line. *Naunyn-Schmiedeberg's Archives of Pharmacology* **396**, 1727–1740 (2023).

[223] Korolnek, T., Zhang, J., Beardsley, S., Scheffer, G. L. & Hamza, I. Control of Metazoan Heme Homeostasis by a Conserved Multidrug Resistance Protein. *Cell Metabolism* **19**, 1008–1019 (2014). Publisher: Elsevier.

[224] Chambers, I. G. *et al.* MRP5 and MRP9 play a concerted role in male reproduction and mitochondrial function. *Proceedings of the National Academy of Sciences of the United States of America* **119**, e2111617119 (2022).

[225] Gronkowska, K., Michlewska, S. & Robaszkiewicz, A. https://www.cellphysiolbiochem.com/Articles/000663/#discussion. *Cellular Physiology & Biochemistry* **57**, 360–378 (2023).

[226] Stojic, J., Stöhr, H. & Weber, B. H. Three novel ABCC5 splice variants in human retina and their role as regulators of ABCC5 gene expression. *BMC Molecular Biology* **8**, 42 (2007). Publisher: BioMed Central.

[227] Furney, S. J. *et al.* SF3B1 mutations are associated with alternative splicing in uveal melanoma. *Cancer discovery* **3**, 1122–1129 (2013).

[228] Jedlitschky, G., Burchell, B. & Keppler, D. The multidrug resistance protein 5 functions as an ATP-dependent export pump for cyclic nucleotides. *The Journal of Biological Chemistry* **275**, 30069–30074 (2000).

[229] Wielinga, P. R. *et al.* Characterization of the MRP4- and MRP5-mediated transport of cyclic nucleotides from intact cells. *The Journal of Biological Chemistry* **278**, 17664–17671 (2003).

[230] Reid, G. *et al.* Characterization of the Transport of Nucleoside Analog Drugs by the Human Multidrug Resistance Proteins MRP4 and MRP5. *Molecular Pharmacology* **63**, 1094–1103 (2003). Publisher: American Society for Pharmacology and Experimental Therapeutics Section: Article.

[231] Laue, S. *et al.* cCMP is a substrate for MRP5. *Naunyn-Schmiedeberg's Archives of Pharmacology* **387**, 893–895 (2014).

[232] Sager, G. *et al.* Novel cGMP efflux inhibitors identified by virtual ligand screening (VLS) and confirmed by experimental studies. *Journal of Medicinal Chemistry* **55**, 3049–3057 (2012).

[233] Aronsen, L., Orvoll, E., Lysaa, R., Ravna, A. W. & Sager, G. Modulation of high affinity ATP-dependent cyclic nucleotide transporters by specific and non-specific cyclic nucleotide phosphodiesterase inhibitors. *European Journal of Pharmacology* **745**, 249–253 (2014).

[234] Kashgari, F. K. *et al.* Identification and experimental confirmation of novel cGMP efflux inhibitors by virtual ligand screening of vardenafil-analogues. *Biomedicine & Pharmacotherapy = Biomedecine & Pharmacotherapie* **126**, 110109 (2020).

[235] Odland, S. U., Ravna, A. W., Smaglyukova, N., Dietrichs, E. S. & Sager, G. Inhibition of ABCC5-mediated cGMP transport by progesterone, testosterone and their analogues. *The Journal of Steroid Biochemistry and Molecular Biology* **213**, 105951 (2021).

[236] J, W. *et al.* Multidrug-resistance protein 5 is a multispecific organic anion transporter able to transport nucleotide analogs. *Proceedings of the National Academy of Sciences of the United States of America* **97** (2000). Publisher: Proc Natl Acad Sci U S A.

[237] Wielinga, P. R. *et al.* Thiopurine metabolism and identification of the thiopurine metabolites transported by MRP4 and MRP5 overexpressed in human embryonic kidney cells. *Molecular Pharmacology* **62**, 1321–1331 (2002).

[238] Pratt, S. *et al.* The multidrug resistance protein 5 (ABCC5) confers resistance to 5-fluorouracil and transports its monophosphorylated metabolites. *Molecular Cancer Therapeutics* **4**, 855–863 (2005).

[239] Na, H., Ponomarova, O., Giese, G. E. & Walhout, A. J. C. elegans MRP-

5 Exports Vitamin B12 from Mother to Offspring to Support Embryonic Development. *Cell reports* **22**, 3126–3133 (2018).

[240] Wang, Z., Zeng, P. & Zhou, B. Identification and characterization of a heme exporter from the MRP family in Drosophila melanogaster. *BMC Biology* **20**, 126 (2022).

[241] Wielinga, P. *et al.* The human multidrug resistance protein MRP5 transports folates and can mediate cellular resistance against antifolates. *Cancer Research* **65**, 4425–4430 (2005).

[242] S, P., V, C., Wi, P., Jj, S. & Ah, D. Kinetic validation of the use of carboxydichlorofluorescein as a drug surrogate for MRP5-mediated transport. *European journal of pharmaceutical sciences : official journal of the European Federation for Pharmaceutical Sciences* **27** (2006). Publisher: Eur J Pharm Sci.

[243] Minich, T. *et al.* The multidrug resistance protein 1 (Mrp1), but not Mrp5, mediates export of glutathione and glutathione disulfide from brain astrocytes. *Journal of Neurochemistry* **97**, 373–384 (2006).

[244] Jansen, R. S., Mahakena, S., de Haas, M., Borst, P. & van de Wetering, K. ATP-binding Cassette Subfamily C Member 5 (ABCC5) Functions as an Efflux Transporter of Glutamate Conjugates and Analogs. *The Journal of Biological Chemistry* **290**, 30429–30440 (2015).

[245] Aw, R., I, S. & G, S. Binding site of ABC transporter homology models confirmed by ABCB1 crystal structure. *Theoretical biology & medical modelling* **6** (2009). Publisher: Theor Biol Med Model.

[246] Ravna, A. W., Sylte, I. & Sager, G. A molecular model of a putative substrate releasing conformation of multidrug resistance protein 5 (MRP5). *European Journal of Medicinal Chemistry* **43**, 2557–2567 (2008).

[247] Singh, N. Molecular Modelling of Human Multidrug Resistance Protein 5 (ABCC5). *Journal of Biophysical Chemistry* **7**, 61–73 (2016). Number: 3 Publisher: Scientific Research Publishing.

[248] Jumper, J. *et al.* Highly accurate protein structure prediction with AlphaFold. *Nature* **596**, 583–589 (2021). Number: 7873 Publisher: Nature Publishing Group.

[249] Tammur, J. *et al.* Two new genes from the human ATP-binding cassette transporter superfamily, ABCC11 and ABCC12, tandemly duplicated on chromosome 16q12. *Gene* **273**, 89–96 (2001).

[250] Bera, T. K., Lee, S., Salvatore, G., Lee, B. & Pastan, I. MRP8, a new member of ABC transporter superfamily, identified by EST database mining and gene prediction program, is highly expressed in breast cancer. *Molecular Medicine* **7**, 509–516 (2001).

[251] Chen, Z.-S., Guo, Y., Belinsky, M. G., Kotova, E. & Kruh, G. D. Transport of Bile Acids, Sulfated Steroids, Estradiol 17-β-d-Glucuronide, and Leukotriene C4 by Human Multidrug Resistance Protein 8 (ABCC11). *Molecular Pharmacology* **67**, 545–557 (2005). Publisher: American Society for Pharmacology and Experimental Therapeutics Section: ORIGINAL ARTICLE.

[252] Yabuuchi, H., Shimizu, H., Takayanagi, S.-i. & Ishikawa, T. Multiple Splicing Variants of Two New Human ATP-Binding Cassette Transporters,

ABCC11 and ABCC12. *Biochemical and Biophysical Research Communications* **288**, 933–939 (2001).

[253] Maher, J. M., Slitt, A. L., Cherrington, N. J., Cheng, X. & Klaassen, C. D. Tissue Distribution and Hepatic and Renal Ontogeny of the Multidrug Resistance-Associated Protein (mrp) Family in Mice. *Drug Metabolism and Disposition* **33**, 947–955 (2005). Publisher: American Society for Pharmacology and Experimental Therapeutics Section: Article.

[254] Rodriguez, M. R. *et al.* Atrial Natriuretic Factor Stimulates Efflux of cAMP in Rat Exocrine Pancreas via Multidrug Resistance-Associated Proteins. *Gastroenterology* **140**, 1292–1302 (2011). Publisher: Elsevier.

[255] Honorat, M. *et al.* Localization of putative binding sites for cyclic guanosine monophosphate and the anti-cancer drug 5-fluoro-2'-deoxyuridine-5'-monophosphate on ABCC11 in silico models. *BMC Structural Biology* **13**, 7 (2013).

[256] Guo, Y. *et al.* MRP8, ATP-binding Cassette C11 (ABCC11), Is a Cyclic Nucleotide Efflux Pump and a Resistance Factor for Fluoropyrimidines 2',3'-Dideoxycytidine and 9'-(2'-Phosphonylmethoxyethyl)adenine. *Journal of Biological Chemistry* **278**, 29509–29514 (2003).

[257] Bortfeld, M. *et al.* Human multidrug resistance protein 8 (MRP8/ABCC11), an apical efflux pump for steroid sulfates, is an axonal protein of the CNS and peripheral nervous system. *Neuroscience* **137**, 1247–1257 (2006).

[258] Park, S. *et al.* Gene expression profiling of ATP-binding cassette (ABC) transporters as a predictor of the pathologic response to neoadjuvant

chemotherapy in breast cancer patients. *Breast Cancer Research and Treatment* **99**, 9–17 (2006).

[259] Ishiguro, J. *et al.* A functional single nucleotide polymorphism in ABCC11, rs17822931, is associated with the risk of breast cancer in Japanese. *Carcinogenesis* **40**, 537–543 (2019).

[260] Toyoda, Y. & Ishikawa, T. Pharmacogenomics of human ABC transporter ABCC11 (MRP8): potential risk of breast cancer and chemotherapy failure. *Anti-Cancer Agents in Medicinal Chemistry* **10**, 617–624 (2010).

[261] Ota, I. *et al.* Association between breast cancer risk and the wild-type allele of human ABC transporter ABCC11. *Anticancer Research* **30**, 5189–5194 (2010).

[262] Yoshiura, K.-i. *et al.* A SNP in the ABCC11 gene is the determinant of human earwax type. *Nature Genetics* **38**, 324–330 (2006). Number: 3 Publisher: Nature Publishing Group.

[263] Guo, Y. *et al.* Expression of ABCC-type nucleotide exporters in blasts of adult acute myeloid leukemia: relation to long-term survival. *Clinical Cancer Research: An Official Journal of the American Association for Cancer Research* **15**, 1762–1769 (2009).

[264] Trujillo-Paolillo, A. *et al.* Pharmacogenetics of the Primary and Metastatic Osteosarcoma: Gene Expression Profile Associated with Outcome. *International Journal of Molecular Sciences* **24**, 5607 (2023).

[265] Borel, F. *et al.* Adenosine triphosphate-binding cassette transporter genes

up-regulation in untreated hepatocellular carcinoma is mediated by cellular microRNAs. *Hepatology* **55**, 821–832 (2012).

[266] Krizkova, V. *et al.* Protein expression of ATP-binding cassette transporters ABCC10 and ABCC11 associates with survival of colorectal cancer patients. *Cancer Chemotherapy and Pharmacology* **78**, 595–603 (2016).

[267] Uemura, T. *et al.* ABCC11/MRP8 confers pemetrexed resistance in lung cancer. *Cancer Science* **101**, 2404–2410 (2010).

[268] Funazo, T. *et al.* Acquired Resistance to Alectinib in ALK-Rearranged Lung Cancer due to ABCC11/MRP8 Overexpression in a Clinically Paired Resistance Model. *Molecular Cancer Therapeutics* **19**, 1320–1327 (2020).

[269] König, J. *et al.* Expression and localization of human multidrug resistance protein (ABCC) family members in pancreatic carcinoma. *International Journal of Cancer* **115**, 359–367 (2005).

[270] Shimizu, H. *et al.* Characterization of the mouse Abcc12 gene and its transcript encoding an ATP-binding cassette transporter, an orthologue of human ABCC12. *Gene* **310**, 17–28 (2003).

[271] Bera, T. K. *et al.* MRP9, an unusual truncated member of the ABC transporter superfamily, is highly expressed in breast cancer. *Proceedings of the National Academy of Sciences of the United States of America* **99**, 6997–7002 (2002).

[272] Tsyganov, M. M. *et al.* DNA Copy Number Aberrations and Expression of ABC Transporter Genes in Breast Tumour: Correlation with the Effect of

Neoadjuvant Chemotherapy and Prognosis of the Disease. *Pharmaceutics* **14**, 948 (2022).

[273] O'Driscoll, L. *et al.* Investigation of the molecular profile of basal cell carcinoma using whole genome microarrays. *Molecular Cancer* **5**, 74 (2006).

[274] Bierman, W. F. W. *et al.* Protease inhibitors atazanavir, lopinavir and ritonavir are potent blockers, but poor substrates, of ABC transporters in a broad panel of ABC transporter-overexpressing cell lines. *Journal of Antimicrobial Chemotherapy* **65**, 1672–1680 (2010).

[275] Pham, D.-H. *et al.* Deleterious variants in ABCC12 are detected in idiopathic chronic cholestasis and cause intrahepatic bile duct loss in model organisms. *Gastroenterology* **161**, 287–300.e16 (2021).

[276] Mourskaia, A. A. *et al.* ABCC5 supports osteoclast formation and promotes breast cancer metastasis to bone. *Breast cancer research: BCR* **14**, R149 (2012).

[277] Hlavac, V. *et al.* Role of Genetic Variation in ABC Transporters in Breast Cancer Prognosis and Therapy Response. *International Journal of Molecular Sciences* **21**, 9556 (2020).

[278] Lal, S. *et al.* Pharmacogenetics of ABCB5, ABCC5 and RLIP76 and doxorubicin pharmacokinetics in Asian breast cancer patients. *The Pharmacogenomics Journal* **17**, 337–343 (2017). Number: 4 Publisher: Nature Publishing Group.

[279] Chen, J. *et al.* Human drug efflux transporter ABCC5 confers acquired

resistance to pemetrexed in breast cancer. *Cancer Cell International* **21**, 136 (2021).

[280] Bai, F. *et al.* Development of liposomal pemetrexed for enhanced therapy against multidrug resistance mediated by ABCC5 in breast cancer. *International Journal of Nanomedicine* **13**, 1327–1339 (2018).

[281] Oguri, T. *et al.* The determinants of sensitivity and acquired resistance to gemcitabine differ in non-small cell lung cancer: a role of ABCC5 in gemcitabine sensitivity. *Molecular Cancer Therapeutics* **5**, 1800–1806 (2006).

[282] Yu, H., Pang, Z., Li, G. & Gu, T. Bioinformatics analysis of differentially expressed miRNAs in non-small cell lung cancer. *Journal of Clinical Laboratory Analysis* **35**, e23588 (2021). _eprint: https://onlinelibrary.wiley.com/doi/pdf/10.1002/jcla.23588.

[283] Weaver, D. A. *et al.* ABCC5, ERCC2, XPA and XRCC1 transcript abundance levels correlate with cisplatin chemoresistance in non-small cell lung cancer cell lines. *Molecular Cancer* **4**, 18 (2005). Publisher: BMC.

[284] Masetto, F. *et al.* MRP5 nitration by NO-releasing gemcitabine encapsulated in liposomes confers sensitivity in chemoresistant pancreatic adenocarcinoma cells. *Biochimica Et Biophysica Acta. Molecular Cell Research* **1867**, 118824 (2020).

[285] Kohan, H. G. & Boroujerdi, M. Time and concentration dependency of P-gp, MRP1 and MRP5 induction in response to gemcitabine uptake in Capan-2 pancreatic cancer cells. *Xenobiotica; the Fate of Foreign Compounds in Biological Systems* **45**, 642–652 (2015).

[286] Karmakar, S. *et al.* PAF1 Regulates Stem Cell Features of Pancreatic Cancer Cells, Independently of the PAF1 Complex, via Interactions with PHF5A and DDX3. *Gastroenterology* **159**, 1898–1915.e6 (2020).

[287] Duz, M. B. & Karatas, O. F. Expression profile of stem cell markers and ABC transporters in 5-fluorouracil resistant Hep-2 cells. *Molecular Biology Reports* **47**, 5431–5438 (2020).

[288] Mao, X., He, Z., Zhou, F., Huang, Y. & Zhu, G. Prognostic significance and molecular mechanisms of adenosine triphosphate-binding cassette subfamily C members in gastric cancer. *Medicine* **98**, e18347 (2019).

[289] Hagleitner, M. M. *et al.* A First Step toward Personalized Medicine in Osteosarcoma: Pharmacogenetics as Predictive Marker of Outcome after Chemotherapy-Based Treatment. *Clinical Cancer Research* **21**, 3436–3441 (2015).

[290] Xu, L. *et al.* Variants of FasL and ABCC5 are predictive of outcome after chemotherapy-based treatment in osteosarcoma. *Journal of Bone Oncology* **12**, 44–48 (2018).

[291] Hou, Y. *et al.* The FOXM1-ABCC5 axis contributes to paclitaxel resistance in nasopharyngeal carcinoma cells. *Cell Death & Disease* **8**, e2659–e2659 (2017). Number: 3 Publisher: Nature Publishing Group.

[292] Hou, Y. *et al.* FOXM1 Promotes Drug Resistance in Cervical Cancer Cells by Regulating ABCC5 Gene Transcription. *BioMed Research International* **2022**, e3032590 (2022). Publisher: Hindawi.

[293] Ding, Y., Feng, G. & Yang, M. Prognostic role of alternative splicing events

in head and neck squamous cell carcinoma. *Cancer Cell International* **20**, 168 (2020).

[294] Modi, A. *et al.* FOXM1 mediates GDF-15 dependent stemness and intrinsic drug resistance in breast cancer. *Molecular Biology Reports* **49**, 2877–2888 (2022).

[295] Zhang, L., Li, B., Zhang, B., Zhang, H. & Suo, J. miR-361 enhances sensitivity to 5-fluorouracil by targeting the FOXM1-ABCC5/10 signaling pathway in colorectal cancer. *Oncology Letters* **18**, 4064–4073 (2019).

[296] Zhu, Y. *et al.* Reduced miR-128 in breast tumor-initiating cells induces chemotherapeutic resistance via Bmi-1 and ABCC5. *Clinical Cancer Research: An Official Journal of the American Association for Cancer Research* **17**, 7105–7115 (2011).

[297] Li, B., Chen, H., Wu, N., Zhang, W.-J. & Shang, L.-X. Deregulation of miR-128 in ovarian cancer promotes cisplatin resistance. *International Journal of Gynecological Cancer: Official Journal of the International Gynecological Cancer Society* **24**, 1381–1388 (2014).

[298] Ge, G. *et al.* Enhanced SLC34A2 in breast cancer stem cell-like cells induces chemotherapeutic resistance to doxorubicin via SLC34A2-Bmi1-ABCC5 signaling. *Tumor Biology* **37**, 5049–5062 (2016).

[299] Gu, Y.-H. *et al.* Combined BRM270 and endostatin inhibit relapse of NSCLC while suppressing lung cancer stem cell proliferation induced by endostatin. *Molecular Therapy Oncolytics* **22**, 565–573 (2021).

[300] Huang, W. *et al.* ABCC5 facilitates the acquired resistance of sorafenib

through the inhibition of SLC7A11-induced ferroptosis in hepatocellular carcinoma. *Neoplasia (New York, N.Y.)* **23**, 1227–1239 (2021).

[301] Zhang, H., Lian, Z., Sun, G., Liu, R. & Xu, Y. Loss of miR-516a-3p mediates upregulation of ABCC5 in prostate cancer and drives its progression. *OncoTargets and therapy* **11**, 3853–3867 (2018).

[302] Zhang, W. *et al.* Expression of drug pathway proteins is independent of tumour type. *The Journal of Pathology* **209**, 213–219 (2006). _eprint: https://onlinelibrary.wiley.com/doi/pdf/10.1002/path.1955.

[303] Zhang, P. *et al.* Identification and validation of a novel anoikis-related prognostic model for prostate cance. Tech. Rep. (2023). Type: article.

[304] Marzec, J. *et al.* The Transcriptomic Landscape of Prostate Cancer Development and Progression: An Integrative Analysis. *Cancers* **13**, 345 (2021).

[305] Bacolod, M. D. & Barany, F. A Unified Transcriptional, Pharmacogenomic, and Gene Dependency Approach to Decipher the Biology, Diagnostic Markers, and Therapeutic Targets Associated with Prostate Cancer Metastasis. *Cancers* **13**, 5158 (2021).

[306] Sissung, T. M. *et al.* Identification of novel SNPs associated with risk and prognosis in patients with castration-resistant prostate cancer. *Pharmacogenomics* **17**, 1979–1986 (2016).

[307] Bolis, M. *et al.* Dynamic prostate cancer transcriptome analysis delineates the trajectory to disease progression. *Nature Communications* **12**, 7033 (2021). Number: 1 Publisher: Nature Publishing Group.

[308] Ji, G. A new novel gene ABCC5 promotes castration-resistant prostate can-

cer progression through ERK carcinogenic pathway. *Annals of Oncology* **29**, ix71 (2018). Publisher: Elsevier.

[309] Kremer, A., Kremer, T., Kristiansen, G. & Tolkach, Y. Where is the limit of prostate cancer biomarker research? Systematic investigation of potential prognostic and diagnostic biomarkers. *BMC Urology* **19**, 46 (2019).

[310] Chen, H. *et al.* Non-drug efflux function of ABCC5 promotes enzalutamide resistance in castration-resistant prostate cancer via upregulation of P65/AR-V7. *Cell Death Discovery* **8**, 1–13 (2022). Number: 1 Publisher: Nature Publishing Group.

[311] Ji, G. *et al.* Upregulation of ATP Binding Cassette Subfamily C Member 5 facilitates Prostate Cancer progression and Enzalutamide resistance via the CDK1-mediated AR Ser81 Phosphorylation Pathway. *International Journal of Biological Sciences* **17**, 1613–1628 (2021).

[312] Karatas, O. F., Guzel, E., Duz, M. B., Ittmann, M. & Ozen, M. The role of ATP-binding cassette transporter genes in the progression of prostate cancer. *The Prostate* **76**, 434–444 (2016).

[313] Marques, R. B. *et al.* Modulation of Androgen Receptor Signaling in Hormonal Therapy-Resistant Prostate Cancer Cell Lines. *PLOS ONE* **6**, e23144 (2011). Publisher: Public Library of Science.

[314] Ohya, S., Kajikuri, J., Endo, K., Kito, H. & Matsui, M. KCa1.1 K+ Channel Inhibition Overcomes Resistance to Antiandrogens and Doxorubicin in a Human Prostate Cancer LNCaP Spheroid Model. *International Journal of Molecular Sciences* **22**, 13553 (2021).

[315] Mulholland, E. J., Green, W. P., Buckley, N. E. & McCarthy, H. O. Exploring the Potential of MicroRNA Let-7c as a Therapeutic for Prostate Cancer. *Molecular Therapy - Nucleic Acids* **18**, 927–937 (2019). Publisher: Elsevier.

[316] Chandrashekar, D. S. *et al.* UALCAN: A Portal for Facilitating Tumor Subgroup Gene Expression and Survival Analyses. *Neoplasia (New York, N.Y.)* **19**, 649–658 (2017).

[317] Chandrashekar, D. S. *et al.* UALCAN: An update to the integrated cancer data analysis platform. *Neoplasia (New York, N.Y.)* **25**, 18–27 (2022).

[318] Zhou, Y. *et al.* Metascape provides a biologist-oriented resource for the analysis of systems-level datasets. *Nature Communications* **10**, 1523 (2019). Number: 1 Publisher: Nature Publishing Group.

[319] Kolberg, L. *et al.* g:Profiler interoperable web service for functional enrichment analysis and gene identifier mapping (2023 update). *Nucleic Acids Research* **51**, W207–W212 (2023).

[320] Supek, F., BoÅ¡njak, M., Å kunca, N. & Å muc, T. REVIGO Summarizes and Visualizes Long Lists of Gene Ontology Terms. *PLOS ONE* **6**, e21800 (2011). Publisher: Public Library of Science.

[321] Holm, L. Dali server: structural unification of protein families. *Nucleic Acids Research* **50**, W210–W215 (2022).

[322] Santana-Garcia, W. *et al.* RSAT 2022: regulatory sequence analysis tools. *Nucleic Acids Research* **50**, W670–W676 (2022).

[323] Calderone, A., Castagnoli, L. & Cesareni, G. mentha: a resource for brows-

ing integrated protein-interaction networks. *Nature Methods* **10**, 690–691 (2013).

[324] Szklarczyk, D. *et al.* STRING v11: protein-protein association networks with increased coverage, supporting functional discovery in genome-wide experimental datasets. *Nucleic Acids Research* **47**, D607–D613 (2019). Number: D1 Publisher: Oxford University Press.

[325] Samaras, P. *et al.* ProteomicsDB: a multi-omics and multi-organism resource for life science research. *Nucleic Acids Research* **48**, D1153–D1163 (2020).

[326] Schmidt, T. *et al.* ProteomicsDB. *Nucleic Acids Research* **46**, D1271–D1281 (2018).

[327] Wilhelm, M. *et al.* Mass-spectrometry-based draft of the human proteome. *Nature* **509**, 582–587 (2014). Number: 7502 Publisher: Nature Publishing Group.

[328] Aranda, B. *et al.* PSICQUIC and PSISCORE: accessing and scoring molecular interactions. *Nature Methods* **8**, 528–529 (2011). Number: 7 Publisher: Nature Publishing Group.

[329] Oughtred, R. *et al.* The BioGRID interaction database: 2019 update. *Nucleic Acids Research* **47**, D529–D541 (2019).

[330] M, K., C, P., Z, M. & I, J. IID 2018 update: context-specific physical protein-protein interactions in human, model organisms and domesticated species. *Nucleic acids research* **47** (2019). Publisher: Nucleic Acids Res.

[331] Shannon, P. *et al.* Cytoscape: A Software Environment for Integrated Mod-

els of Biomolecular Interaction Networks. *Genome Research* **13**, 2498–2504 (2003). Company: Cold Spring Harbor Laboratory Press Distributor: Cold Spring Harbor Laboratory Press Institution: Cold Spring Harbor Laboratory Press Label: Cold Spring Harbor Laboratory Press Publisher: Cold Spring Harbor Lab.

[332] Doncheva, N. T., Morris, J. H., Gorodkin, J. & Jensen, L. J. Cytoscape StringApp: Network Analysis and Visualization of Proteomics Data. *Journal of Proteome Research* **18**, 623–632 (2019). Publisher: American Chemical Society.

[333] Cunningham, D. & You, Z. In vitro and in vivo model systems used in prostate cancer research. *Journal of Biological Methods* **2**, e17 (2015).

[334] Gorges, T. M. *et al.* Heterogeneous PSMA expression on circulating tumor cells: a potential basis for stratification and monitoring of PSMA-directed therapies in prostate cancer. *Oncotarget* **7**, 34930–34941 (2016).

[335] Sobel, R. E. & Sadar, M. D. Cell lines used in prostate cancer research: a compendium of old and new lines - part 1. *Journal of Urology* **173**, 342–359 (2005). Publisher: WoltersKluwer.

[336] Guzman, C., Bagga, M., Kaur, A., Westermarck, J. & Abankwa, D. ColonyArea: An ImageJ Plugin to Automatically Quantify Colony Formation in Clonogenic Assays. *PLOS ONE* **9**, e92444 (2014). Publisher: Public Library of Science.

[337] Schindelin, J. *et al.* Fiji: an open-source platform for biological-image analysis. *Nat Meth* **9**, 676–682 (2012). URL http://dx.doi.org/10.1038/nmeth.2019.

[338] Jiang, P. *et al.* Big data in basic and translational cancer research. *Nature Reviews. Cancer* **22**, 625–639 (2022).

[339] Wang, Z., Jensen, M. A. & Zenklusen, J. C. A Practical Guide to The Cancer Genome Atlas (TCGA). In Mathe, E. & Davis, S. (eds.) *Statistical Genomics: Methods and Protocols*, Methods in Molecular Biology, 111–141 (Springer, New York, NY, 2016).

[340] Zhu, Y., Qiu, P. & Ji, Y. TCGA-Assembler: open-source software for retrieving and processing TCGA data. *Nature Methods* **11**, 599–600 (2014). Number: 6 Publisher: Nature Publishing Group.

[341] Adhav, V. A. & Saikrishnan, K. The Realm of Unconventional Noncovalent Interactions in Proteins: Their Significance in Structure and Function. *ACS Omega* **8**, 22268–22284 (2023). Publisher: American Chemical Society.

[342] Kuhlman, B. & Bradley, P. Advances in protein structure prediction and design. *Nature Reviews Molecular Cell Biology* **20**, 681–697 (2019). Number: 11 Publisher: Nature Publishing Group.

[343] Kumar, R. & Sharma, A. Chapter 15 - Computational strategies and tools for protein tertiary structure prediction. In Bhatt, A. K., Bhatia, R. K. & Bhalla, T. C. (eds.) *Basic Biotechniques for Bioprocess and Bioentrepreneurship*, 225–242 (Academic Press, 2023).

[344] Altschul, S. F., Gish, W., Miller, W., Myers, E. W. & Lipman, D. J. Basic local alignment search tool. *Journal of Molecular Biology* **215**, 403–410 (1990).

[345] Finn, R. D., Clements, J. & Eddy, S. R. HMMER web server: interactive

sequence similarity searching. *Nucleic Acids Research* **39**, W29–37 (2011).

[346] Hamamsy, T. *et al.* Protein remote homology detection and structural alignment using deep learning. *Nature Biotechnology* 1–11 (2023). Publisher: Nature Publishing Group.

[347] Holm, L., Laiho, A., Törönen, P. & Salgado, M. DALI shines a light on remote homologs: One hundred discoveries. *Protein Science* **32**, e4519 (2023). _eprint: https://onlinelibrary.wiley.com/doi/pdf/10.1002/pro.4519.

[348] Holm, L. Using Dali for Protein Structure Comparison. In Gaspari, Z. (ed.) *Structural Bioinformatics: Methods and Protocols*, Methods in Molecular Biology, 29–42 (Springer US, New York, NY, 2020).

[349] Gebhard, S. ABC transporters of antimicrobial peptides in Firmicutes bacteria - phylogeny, function and regulation. *Molecular Microbiology* **86**, 1295–1317 (2012).

[350] Havarstein, L. S., Diep, D. B. & Nes, I. F. A family of bacteriocin ABC transporters carry out proteolytic processing of their substrates concomitant with export. *Molecular Microbiology* **16**, 229–240 (1995).

[351] van Belkum, M. J., Worobo, R. W. & Stiles, M. E. Double-glycine-type leader peptides direct secretion of bacteriocins by ABC transporters: colicin V secretion in Lactococcus lactis. *Molecular Microbiology* **23**, 1293–1301 (1997).

[352] Kieuvongngam, V. & Chen, J. Structures of the peptidase-containing ABC transporter PCAT1 under equilibrium and nonequilibrium conditions. *Pro-*

ceedings of the National Academy of Sciences **119**, e2120534119 (2022). Publisher: Proceedings of the National Academy of Sciences.

[353] Holyoake, L. V., Poole, R. K. & Shepherd, M. The CydDC Family of Transporters and Their Roles in Oxidase Assembly and Homeostasis. *Advances in Microbial Physiology* **66**, 1–53 (2015).

[354] Lyu, J. *et al.* Structural basis for lipid and copper regulation of the ABC transporter MsbA. *Nature Communications* **13**, 7291 (2022). Number: 1 Publisher: Nature Publishing Group.

[355] Wu, D. *et al.* Dissecting the conformational complexity and mechanism of a bacterial heme transporter. *Nature Chemical Biology* **19**, 992–1003 (2023). Number: 8 Publisher: Nature Publishing Group.

[356] Mahajan, R., Delphin, C., Guan, T., Gerace, L. & Melchior, F. A Small Ubiquitin-Related Polypeptide Involved in Targeting RanGAP1 to Nuclear Pore Complex Protein RanBP2. *Cell* **88**, 97–107 (1997). Publisher: Elsevier.

[357] Miteva, M., Keusekotten, K., Hofmann, K., Praefcke, G. J. K. & Dohmen, R. J. Sumoylation as a Signal for Polyubiquitylation and Proteasomal Degradation. In Groettrup, M. (ed.) *Conjugation and Deconjugation of Ubiquitin Family Modifiers: Subcellular Biochemistry*, Subcellular Biochemistry, 195–214 (Springer, New York, NY, 2010).

[358] Gong, L., Millas, S., Maul, G. G. & Yeh, E. T. Differential regulation of sentrinized proteins by a novel sentrin-specific protease. *The Journal of Biological Chemistry* **275**, 3355–3359 (2000).

[359] Zhang, H., Saitoh, H. & Matunis, M. J. Enzymes of the SUMO Modification Pathway Localize to Filaments of the Nuclear Pore Complex. *Molecular and Cellular Biology* **22**, 6498–6508 (2002).

[360] Di Bacco, A. *et al.* The SUMO-Specific Protease SENP5 Is Required for Cell Division. *Molecular and Cellular Biology* **26**, 4489–4498 (2006). Publisher: Taylor & Francis _eprint: https://doi.org/10.1128/MCB.02301-05.

[361] Gong, L. & Yeh, E. T. H. Characterization of a Family of Nucleolar SUMO-specific Proteases with Preference for SUMO-2 or SUMO-3 *. *Journal of Biological Chemistry* **281**, 15869–15877 (2006). Publisher: Elsevier.

[362] Mendes, A. V., Grou, C. P., Azevedo, J. E. & Pinto, M. P. Evaluation of the activity and substrate specificity of the human SENP family of SUMO proteases. *Biochimica et Biophysica Acta (BBA) - Molecular Cell Research* **1863**, 139–147 (2016).

[363] Shen, L., Geoffroy, M.-C., Jaffray, E. & Hay, R. Characterization of SENP7, a SUMO-2/3-specific isopeptidase. *Biochemical Journal* **421**, 223–230 (2009).

[364] Yeh, E. T. H., Gong, L. & Kamitani, T. Ubiquitin-like proteins: new wines in new bottles. *Gene* **248**, 1–14 (2000).

[365] Eifler, K. & Vertegaal, A. C. SUMOylation-mediated regulation of cell cycle progression and cancer. *Trends in biochemical sciences* **40**, 779–793 (2015).

[366] Psakhye, I. & Jentsch, S. Protein Group Modification and Synergy in the

SUMO Pathway as Exemplified in DNA Repair. *Cell* **151**, 807–820 (2012). Publisher: Elsevier.

[367] Rodriguez, M. S. *et al.* SUMO-1 modification activates the transcriptional response of p53. *The EMBO journal* **18**, 6455–6461 (1999).

[368] Schimmel, J. *et al.* Uncovering SUMOylation Dynamics during Cell-Cycle Progression Reveals FoxM1 as a Key Mitotic SUMO Target Protein. *Molecular Cell* **53**, 1053–1066 (2014). Publisher: Elsevier.

[369] Zunino, R., Braschi, E., Xu, L. & McBride, H. M. Translocation of SenP5 from the Nucleoli to the Mitochondria Modulates DRP1-dependent Fission during Mitosis. *The Journal of Biological Chemistry* **284**, 17783–17795 (2009).

[370] Hall, A. R., Burke, N., Dongworth, R. K. & Hausenloy, D. J. Mitochondrial fusion and fission proteins: novel therapeutic targets for combating cardiovascular disease. *British Journal of Pharmacology* **171**, 1890–1906 (2014).

[371] Kim, C. *et al.* SUMOylation of mitofusins: a potential mechanism for perinuclear mitochondrial congression in cells treated with mitochondrial stressors. *Biochimica et biophysica acta. Molecular basis of disease* **1867**, 166104 (2021).

[372] Bawa-Khalfe, T. & Yeh, E. T. H. SUMO Losing Balance: SUMO Proteases Disrupt SUMO Homeostasis to Facilitate Cancer Development and Progression. *Genes & Cancer* **1**, 748–752 (2010).

[373] Wang, Q. *et al.* SUMO-specific protease 1 promotes prostate cancer pro-

gression and metastasis. *Oncogene* **32**, 2493–2498 (2013). Number: 19 Publisher: Nature Publishing Group.

[374] Wang, Z., Jin, J., Zhang, J., Wang, L. & Cao, J. Depletion of SENP1 suppresses the proliferation and invasion of triple-negative breast cancer cells. *Oncology Reports* **36**, 2071–2078 (2016).

[375] Sun, Z. *et al.* Overexpression of SENP3 in oral squamous cell carcinoma and its association with differentiation. *Oncology Reports* **29**, 1701–1706 (2013).

[376] Ding, X. *et al.* Overexpression of SENP5 in oral squamous cell carcinoma and its association with differentiation. *Oncology Reports* **20**, 1041–1045 (2008).

[377] Jin, Z.-L., Pei, H., Xu, Y.-H., Yu, J. & Deng, T. The SUMO-specific protease SENP5 controls DNA damage response and promotes tumorigenesis in hepatocellular carcinoma. *European Review for Medical and Pharmacological Sciences* **20**, 3566–3573 (2016).

[378] Lin, D. Y.-w., Huang, S. & Chen, J. Crystal structures of a polypeptide processing and secretion transporter. *Nature* **523**, 425–430 (2015). Number: 7561 Publisher: Nature Publishing Group.

[379] Kieuvongngam, V. *et al.* Structural basis of substrate recognition by a polypeptide processing and secretion transporter. *eLife* **9**, e51492 (2020). Publisher: eLife Sciences Publications, Ltd.

[380] Li, J., Vavricka, C. J., Yang, C., Han, Q. & Cooper, A. J. L. Amino Acids | Aromatic Amino Acid Metabolism Across Species. In Jez, J. (ed.) *Encyclo-*

pedia of Biological Chemistry III (Third Edition), 22–42 (Elsevier, Oxford, 2021).

[381] Otto, H. *et al.* Aspartic acid-96 is the internal proton donor in the reprotonation of the Schiff base of bacteriorhodopsin. *Proceedings of the National Academy of Sciences of the United States of America* **86**, 9228–9232 (1989).

[382] Sharma, V., Wang, Y.-S. & Liu, W. R. Probing the Catalytic Charge-Relay System in Alanine Racemase with Genetically Encoded Histidine Mimetics. *ACS chemical biology* **11**, 3305–3309 (2016).

[383] Poole, R., Gibson, F. & Guanghui, W. The cydD gene product, component of a heterodimeric ABC transporter, is required for assembly of periplasmic cytochrome c and of cytochrome bd in Escherichia coli. *FEMS Microbiology Letters* **117**, 217–223 (1994).

[384] Cook, G. M. & Poole, R. K. Oxidase and periplasmic cytochrome assembly in Escherichia coli K-12: CydDC and CcmAB are not required for haem-membrane association. *Microbiology (Reading, England)* **146 (Pt 2)**, 527–536 (2000).

[385] Pittman, M. S., Robinson, H. C. & Poole, R. K. A Bacterial Glutathione Transporter (Escherichia coli CydDC) Exports Reductant to the Periplasm *. *Journal of Biological Chemistry* **280**, 32254–32261 (2005). Publisher: Elsevier.

[386] Yamashita, M. *et al.* Structure and Function of the Bacterial Heterodimeric ABC Transporter CydDC. *The Journal of Biological Chemistry* **289**, 23177–23188 (2014).

[387] Mironov, A. *et al.* CydDC functions as a cytoplasmic cystine reductase to sensitize Escherichia coli to oxidative stress and aminoglycosides. *Proceedings of the National Academy of Sciences* **117**, 23565–23570 (2020). Publisher: Proceedings of the National Academy of Sciences.

[388] Smirnova, G. V. *et al.* Phosphate starvation is accompanied by disturbance of intracellular cysteine homeostasis in Escherichia coli. *Research in Microbiology* 104108 (2023).

[389] Zhu, C. *et al.* Cryo-EM structures of a prokaryotic heme transporter CydDC. *Protein & Cell* pwad022 (2023).

[390] Yuan, X. *et al.* Regulation of intracellular heme trafficking revealed by subcellular reporters. *Proceedings of the National Academy of Sciences of the United States of America* **113**, E5144–E5152 (2016).

[391] Haffner, M. C. *et al.* Genomic and phenotypic heterogeneity in prostate cancer. *Nature Reviews Urology* **18**, 79–92 (2021). Number: 2 Publisher: Nature Publishing Group.

[392] Testa, U., Castelli, G. & Pelosi, E. Cellular and Molecular Mechanisms Underlying Prostate Cancer Development: Therapeutic Implications. *Medicines* **6**, 82 (2019).

[393] Sailer, V. *et al.* Experimental in vitro, ex vivo and in vivo models in prostate cancer research. *Nature Reviews Urology* **20**, 158–178 (2023). Number: 3 Publisher: Nature Publishing Group.

[394] Buskin, A. *et al.* Engineering prostate cancer in vitro: what does it take?

Oncogene **42**, 2417–2427 (2023). Number: 32 Publisher: Nature Publishing Group.

[395] Hepburn, A. C., Sims, C. H. C., Buskin, A. & Heer, R. Engineering Prostate Cancer from Induced Pluripotent Stem Cells-New Opportunities to Develop Preclinical Tools in Prostate and Prostate Cancer Studies. *International Journal of Molecular Sciences* **21**, 905 (2020). Number: 3 Publisher: Multidisciplinary Digital Publishing Institute.

[396] Germain, L. *et al.* Preclinical models of prostate cancer - modelling androgen dependency and castration resistance in vitro, ex vivo and in vivo. *Nature Reviews Urology* **20**, 480–493 (2023). Number: 8 Publisher: Nature Publishing Group.

[397] Martin, P. *et al.* Prostate Epithelial Pten/TP53 Loss Leads to Transformation of Multipotential Progenitors and Epithelial to Mesenchymal Transition. *The American Journal of Pathology* **179**, 422–435 (2011).

[398] Namekawa, T., Ikeda, K., Horie-Inoue, K. & Inoue, S. Application of Prostate Cancer Models for Preclinical Study: Advantages and Limitations of Cell Lines, Patient-Derived Xenografts, and Three-Dimensional Culture of Patient-Derived Cells. *Cells* **8**, 74 (2019).

[399] Russell, P. J. & Kingsley, E. A. Human prostate cancer cell lines. *Methods in Molecular Medicine* **81**, 21–39 (2003).

[400] van Bokhoven, A. *et al.* Molecular characterization of human prostate carcinoma cell lines. *The Prostate* **57**, 205–225 (2003).

[401] Horoszewicz, J. S. *et al.* The LNCaP cell line–a new model for studies on

human prostatic carcinoma. *Progress in Clinical and Biological Research* **37**, 115–132 (1980).

[402] Horoszewicz, J. S. *et al.* LNCaP model of human prostatic carcinoma. *Cancer Research* **43**, 1809–1818 (1983).

[403] Wu, H. C. *et al.* Derivation of androgen-independent human LNCaP prostatic cancer cell sublines: role of bone stromal cells. *International Journal of Cancer* **57**, 406–412 (1994).

[404] Kaighn, M. E., Narayan, K. S., Ohnuki, Y., Lechner, J. F. & Jones, L. W. Establishment and characterization of a human prostatic carcinoma cell line (PC-3). *Investigative Urology* **17**, 16–23 (1979).

[405] Tilley, W. D., Wilson, C. M., Marcelli, M. & McPhaul, M. J. Androgen receptor gene expression in human prostate carcinoma cell lines. *Cancer Research* **50**, 5382–5386 (1990).

[406] Stone, K. R., Mickey, D. D., Wunderli, H., Mickey, G. H. & Paulson, D. F. Isolation of a human prostate carcinoma cell line (DU 145). *International Journal of Cancer* **21**, 274–281 (1978).

[407] Korenchuk, S. *et al.* VCaP, a cell-based model system of human prostate cancer. *In vivo (Athens, Greece)* **15**, 163–168 (2001).

[408] Sramkoski, R. M. *et al.* A new human prostate carcinoma cell line, 22Rv1. *In Vitro Cellular & Developmental Biology - Animal* **35**, 403–409 (1999).

[409] Bello, D., Webber, M. M., Kleinman, H. K., Wartinger, D. D. & Rhim, J. S. Androgen responsive adult human prostatic epithelial cell lines im-

mortalized by human papillomavirus 18. *Carcinogenesis* **18**, 1215–1223 (1997).

[410] Shappell, S. B. *et al.* Prostate Pathology of Genetically Engineered Mice: Definitions and Classification. The Consensus Report from the Bar Harbor Meeting of the Mouse Models of Human Cancer Consortium Prostate Pathology Committee. *Cancer Research* **64**, 2270–2305 (2004).

[411] Gingrich, J. R. *et al.* Androgen-independent prostate cancer progression in the TRAMP model. *Cancer Research* **57**, 4687–4691 (1997).

[412] Abdulkadir, S. A. *et al.* Conditional loss of Nkx3.1 in adult mice induces prostatic intraepithelial neoplasia. *Molecular and Cellular Biology* **22**, 1495–1503 (2002).

[413] Cho, H. *et al.* RapidCaP, a novel GEM model for metastatic prostate cancer analysis and therapy, reveals myc as a driver of Pten-mutant metastasis. *Cancer Discovery* **4**, 318–333 (2014).

[414] Ellwood-Yen, K. *et al.* Myc-driven murine prostate cancer shares molecular features with human prostate tumors. *Cancer Cell* **4**, 223–238 (2003).

[415] Trotman, L. C. *et al.* Pten dose dictates cancer progression in the prostate. *PLoS biology* **1**, E59 (2003).

[416] Logothetis, C. J. & Lin, S.-H. Osteoblasts in prostate cancer metastasis to bone. *Nature Reviews Cancer* **5**, 21–28 (2005). Number: 1 Publisher: Nature Publishing Group.

[417] Navone, N. M. *et al.* Movember GAP1 PDX project: An international col-

lection of serially transplantable prostate cancer patient-derived xenograft (PDX) models. *The Prostate* **78**, 1262–1282 (2018).

[418] Park, S. I., Kim, S. J., McCauley, L. K. & Gallick, G. E. Pre-Clinical Mouse Models of Human Prostate Cancer and their Utility in Drug Discovery. *Current protocols in pharmacology / editorial board, S.J. Enna (editor-in-chief) ... [et al.]* **51**, 14.15–14.15.27 (2010).

[419] Nguyen, H. M. *et al.* LuCaP Prostate Cancer Patient-Derived Xenografts Reflect the Molecular Heterogeneity of Advanced Disease anÂÂd Serve as Models for Evaluating Cancer Therapeutics. *The Prostate* **77**, 654–671 (2017). _eprint: https://onlinelibrary.wiley.com/doi/pdf/10.1002/pros.23313.

[420] Shi, C., Chen, X. & Tan, D. Development of patient-derived xenograft models of prostate cancer for maintaining tumor heterogeneity. *Translational Andrology and Urology* **8**, 519–528 (2019).

[421] Jin, J., Yoshimura, K., Sewastjanow-Silva, M., Song, S. & Ajani, J. A. Challenges and Prospects of Patient-Derived Xenografts for Cancer Research. *Cancers* **15**, 4352 (2023).

[422] D'haeseleer, P. What are DNA sequence motifs? *Nature Biotechnology* **24**, 423–425 (2006).

[423] Slattery, M. *et al.* Absence of a simple code: how transcription factors read the genome. *Trends in Biochemical Sciences* **39**, 381–399 (2014). Publisher: Elsevier.

[424] Peter, I. S. & Davidson, E. H. Evolution of Gene Regulatory Networks

Controlling Body Plan Development. *Cell* **144**, 970–985 (2011). Publisher: Elsevier.

[425] Spitz, F. & Furlong, E. E. M. Transcription factors: from enhancer binding to developmental control. *Nature Reviews. Genetics* **13**, 613–626 (2012).

[426] Levine, M. Transcriptional enhancers in animal development and evolution. *Current biology: CB* **20**, R754–763 (2010).

[427] Petrykowska, H. M., Vockley, C. M. & Elnitski, L. Detection and characterization of silencers and enhancer-blockers in the greater CFTR locus. *Genome Research* **18**, 1238–1246 (2008).

[428] Gaszner, M. & Felsenfeld, G. Insulators: exploiting transcriptional and epigenetic mechanisms. *Nature Reviews. Genetics* **7**, 703–713 (2006).

[429] Batut, P. J. *et al.* Genome organization controls transcriptional dynamics during development. *Science (New York, N.Y.)* **375**, 566–570 (2022).

[430] Isbel, L., Grand, R. S. & Schübeler, D. Generating specificity in genome regulation through transcription factor sensitivity to chromatin. *Nature Reviews Genetics* **23**, 728–740 (2022). Number: 12 Publisher: Nature Publishing Group.

[431] Vicent, G. P. *et al.* Two chromatin remodeling activities cooperate during activation of hormone responsive promoters. *PLoS genetics* **5**, e1000567 (2009).

[432] Wingender, E., Schoeps, T. & Dönitz, J. TFClass: an expandable hierarchical classification of human transcription factors. *Nucleic Acids Research* **41**, D165–D170 (2013).

[433] Xie, T. *et al.* FOXM1 evokes 5-fluorouracil resistance in colorectal cancer depending on ABCC10. *Oncotarget* **8**, 8574–8589 (2016).

[434] Zhu, X. *et al.* The FoxM1-ABCC4 axis mediates carboplatin resistance in human retinoblastoma Y-79 cells. *Acta Biochimica et Biophysica Sinica* **50**, 914–920 (2018).

[435] Liu, C., Barger, C. J. & Karpf, A. R. FOXM1: A Multifunctional Oncoprotein and Emerging Therapeutic Target in Ovarian Cancer. *Cancers* **13**, 3065 (2021). Number: 12 Publisher: Multidisciplinary Digital Publishing Institute.

[436] Wierstra, I. The transcription factor FOXM1 (Forkhead box M1): proliferation-specific expression, transcription factor function, target genes, mouse models, and normal biological roles. *Advances in Cancer Research* **118**, 97–398 (2013).

[437] Wu, Z. *et al.* Role of Nuclear Receptor Coactivator 3 (Ncoa3) in Pluripotency Maintenance*. *Journal of Biological Chemistry* **287**, 38295–38304 (2012).

[438] Timmerman, D. M., Remmers, T. L., Hillenius, S. & Looijenga, L. H. J. Mechanisms of TP53 Pathway Inactivation in Embryonic and Somatic Cells-Relevance for Understanding (Germ Cell) Tumorigenesis. *International Journal of Molecular Sciences* **22**, 5377 (2021).

[439] Hoffmann, I. Centrosomes in mitotic spindle assembly and orientation. *Current Opinion in Structural Biology* **66**, 193–198 (2021).

[440] Kodani, A. *et al.* Centriolar satellites assemble centrosomal microcephaly

proteins to recruit CDK2 and promote centriole duplication. *eLife* **4**, e07519.

[441] Gujral, P., Mahajan, V., Lissaman, A. C. & Ponnampalam, A. P. Histone acetylation and the role of histone deacetylases in normal cyclic endometrium. *Reproductive Biology and Endocrinology* **18**, 84 (2020).

[442] Cassandri, M. *et al.* Zinc-finger proteins in health and disease. *Cell Death Discovery* **3**, 17071 (2017).

[443] Pace, N. J. & Weerapana, E. Zinc-Binding Cysteines: Diverse Functions and Structural Motifs. *Biomolecules* **4**, 419–434 (2014). Number: 2 Publisher: Multidisciplinary Digital Publishing Institute.

[444] Maeda, T. Regulation of hematopoietic development by ZBTB transcription factors. *International journal of hematology* **104**, 310–323 (2016).

[445] Ramsey, J. E. & Fontes, J. D. The zinc finger transcription factor ZXDC activates CCL2 gene expression by opposing BCL6-mediated repression. *Molecular immunology* **56**, 768–780 (2013).

[446] Hirai, H. & Sherr, C. J. Interaction of D-type cyclins with a novel myb-like transcription factor, DMP1. *Molecular and Cellular Biology* **16**, 6457–6467 (1996).

[447] Woodfield, S. E. *et al.* MDM4 inhibition: a novel therapeutic strategy to reactivate p53 in hepatoblastoma. *Scientific Reports* **11**, 2967 (2021). Number: 1 Publisher: Nature Publishing Group.

[448] Mzoughi, S. *et al.* PRDM15 is a key regulator of metabolism critical to

sustain B-cell lymphomagenesis. *Nature Communications* **11**, 3520 (2020). Number: 1 Publisher: Nature Publishing Group.

[449] Martinez, E. *et al.* Human STAGA Complex Is a Chromatin-Acetylating Transcription Coactivator That Interacts with Pre-mRNA Splicing and DNA Damage-Binding Factors In Vivo. *Molecular and Cellular Biology* **21**, 6782–6795 (2001). Publisher: Taylor & Francis _eprint: https://doi.org/10.1128/MCB.21.20.6782-6795.2001.

[450] Robinson, M. M. *et al.* Mapping and Functional Characterization of the TAF11 Interaction with TFIIA. *Molecular and Cellular Biology* **25**, 945–957 (2005).

[451] Fan, W. *et al.* TRIM52: A nuclear TRIM protein that positively regulates the nuclear factor-kappa B signaling pathway. *Molecular Immunology* **82**, 114–122 (2017).

[452] Dozmorov, M. G. *et al.* Unique Patterns of Molecular Profiling between Human Prostate Cancer LNCaP and PC-3 Cells. *The Prostate* **69**, 1077 (2009). Publisher: NIH Public Access.

[453] Probert, C. *et al.* Communication of prostate cancer cells with bone cells via extracellular vesicle RNA; a potential mechanism of metastasis. *Oncogene* **38**, 1751–1763 (2019). Number: 10 Publisher: Nature Publishing Group.

[454] Whitburn, J. *The role of metabolism in prostate cancer progression and bone metastases*. http://purl.org/dc/dcmitype/Text, University of Oxford (2019).

[455] Ching, K. Z. *et al.* Expression of mRNA for epidermal growth factor, transforming growth factor-alpha and their receptor in human prostate tissue and cell lines. *Molecular and Cellular Biochemistry* **126**, 151–158 (1993).

[456] Pan, Y. *et al.* Characterization of chromosomal abnormalities in prostate cancer cell lines by spectral karyotyping. *Cytogenetic and Genome Research* **87**, 225–232 (1999).

[457] Karanika, S., Karantanos, T., Li, L., Corn, P. G. & Thompson, T. C. DNA damage response and prostate cancer: defects, regulation and therapeutic implications. *Oncogene* **34**, 2815 (2015). Publisher: NIH Public Access.

[458] Trtkova, K., Paskova, L., Matijescukova, N., Strnad, M. & Kolar, Z. Binding of AR to SMRT/N-CoR complex and its co-operation with PSA promoter in prostate cancer cells treated with natural histone deacetylase inhibitor NaB. *Neoplasma* **57**, 406–414 (2010).

[459] Wang, H. *et al.* Effects of histone deacetylase inhibitors on ATP-binding cassette transporters in lung cancer A549 and colorectal cancer HCT116 cells. *Oncology Letters* **18**, 63–71 (2019).

[460] Jinno, N. *et al.* Effects of single and repetitive valproic acid administration on the gene expression of placental transporters in pregnant rats: An analysis by gestational period. *Reproductive Toxicology* **96**, 47–56 (2020).

[461] Strachowska, M. *et al.* I-CBP112 declines overexpression of ATP-binding cassette transporters and sensitized drug-resistant MDA-MB-231 and A549 cell lines to chemotherapy drugs. *Biomedicine & Pharmacotherapy* **168**, 115798 (2023).

[462] Josling, G. A., Selvarajah, S. A., Petter, M. & Duffy, M. F. The Role of Bromodomain Proteins in Regulating Gene Expression. *Genes* **3**, 320–343 (2012).

[463] Zhou, J., Zhou, X. A., Zhang, N. & Wang, J. Evolving insights: how DNA repair pathways impact cancer evolution. *Cancer Biology & Medicine* **17**, 805–827 (2020).

[464] Rimel, J. K. & Taatjes, D. J. The essential and multifunctional TFIIH complex. *Protein Science : A Publication of the Protein Society* **27**, 1018–1037 (2018).

[465] Mattick, J. S. *et al.* Long non-coding RNAs: definitions, functions, challenges and recommendations. *Nature Reviews Molecular Cell Biology* **24**, 430–447 (2023). Number: 6 Publisher: Nature Publishing Group.

[466] Lin, J., Song, T., Li, C. & Mao, W. GSK-3β in DNA repair, apoptosis, and resistance of chemotherapy, radiotherapy of cancer. *Biochimica et Biophysica Acta (BBA) - Molecular Cell Research* **1867**, 118659 (2020).

[467] Moltzahn, F. & Thalmann, G. N. Cancer stem cells in prostate cancer. *Translational Andrology and Urology* **2**, 242–253 (2013).

[468] Peng, Y. *et al.* MicroRNA-155 promotes bladder cancer growth by repressing the tumor suppressor DMTF1. *Oncotarget* **6**, 16043–16058 (2015).

[469] Schrankel, C. S. & Hamdoun, A. Early patterning of ABCB, ABCC, and ABCG transporters establishes unique territories of small molecule transport in embryonic mesoderm and endoderm. *Developmental Biology* **472**, 115–124 (2021).

[470] Alliance of Genome Resources (2023).

[471] Cho, J. G. *et al.* ZNF224, Krüppel like zinc finger protein, induces cell growth and apoptosis-resistance by down-regulation of p21 and p53 via miR-663a. *Oncotarget* **7**, 31177–31190 (2016).

[472] Bauer, M. How does an organism extract relevant information from transcription factor concentrations? *Biochemical Society Transactions* **50**, 1365–1376 (2022).

[473] Brown, J. C. Involvement of promoter/enhancers in a feedback loop to regulate human gene expression. *Heliyon* **6**, e04934 (2020).

[474] Göös, H. *et al.* Human transcription factor protein interaction networks. *Nature Communications* **13**, 766 (2022). Number: 1 Publisher: Nature Publishing Group.

[475] Swift, J. & Coruzzi, G. A Matter of Time - How Transient Transcription Factor Interactions Create Dynamic Gene Regulatory Networks. *Biochimica et biophysica acta* **1860**, 75–83 (2017).

[476] Yagil, Z. *et al.* The enigma of the role of Protein inhibitor of Activated STAT3 (PIAS3) in the immune response. *Trends in Immunology* **31**, 199–204 (2010).

[477] Aubrey, B. J., Strasser, A. & Kelly, G. L. Tumor-Suppressor Functions of the TP53 Pathway. *Cold Spring Harbor Perspectives in Medicine* **6**, a026062 (2016).

[478] Toledo, F. & Wahl, G. M. MDM2 and MDM4: p53 regulators as targets

in anticancer therapy. *The International Journal of Biochemistry & Cell Biology* **39**, 1476–1482 (2007).

[479] Belkahla, S. *et al.* Changes in metabolism affect expression of ABC transporters through ERK5 and depending on p53 status. *Oncotarget* **9**, 1114–1129 (2018).

[480] Valkenburg, K. C., de Groot, A. E. & Pienta, K. C. Targeting the tumour stroma to improve cancer therapy. *Nature reviews. Clinical oncology* **15**, 366–381 (2018).

[481] Braun, P. & Gingras, A.-C. History of protein-protein interactions: from egg-white to complex networks. *Proteomics* **12**, 1478–1498 (2012).

[482] Ofran, Y. & Rost, B. Analysing six types of protein-protein interfaces. *Journal of Molecular Biology* **325**, 377–387 (2003).

[483] Perkins, J. R., Diboun, I., Dessailly, B. H., Lees, J. G. & Orengo, C. Transient Protein-Protein Interactions: Structural, Functional, and Network Properties. *Structure* **18**, 1233–1243 (2010).

[484] Sharan, R. *et al.* Conserved patterns of protein interaction in multiple species. *Proceedings of the National Academy of Sciences* **102**, 1974–1979 (2005). Publisher: Proceedings of the National Academy of Sciences.

[485] Berggard, T., Linse, S. & James, P. Methods for the detection and analysis of protein-protein interactions. *PROTEOMICS* **7**, 2833–2842 (2007). _eprint: https://onlinelibrary.wiley.com/doi/pdf/10.1002/pmic.200700131.

[486] Kovacs, I. A. *et al.* Network-based prediction of protein interactions. *Na-*

ture Communications **10**, 1240 (2019). Number: 1 Publisher: Nature Publishing Group.

[487] Lv, Q. *et al.* Genome-wide protein-protein interactions and protein function exploration in cyanobacteria. *Scientific Reports* **5**, 15519 (2015). Number: 1 Publisher: Nature Publishing Group.

[488] Aydinli, M., Liang, C. & Dandekar, T. Motif and conserved module analysis in DNA (promoters, enhancers) and RNA (lncRNA, mRNA) using AlModules. *Scientific Reports* **12**, 17588 (2022). Number: 1 Publisher: Nature Publishing Group.

[489] Coppe, A. *et al.* Motif discovery in promoters of genes co-localized and co-expressed during myeloid cells differentiation. *Nucleic Acids Research* **37**, 533–549 (2009).

[490] van Dam, S., Vosa, U., van der Graaf, A., Franke, L. & de Magalhaes, J. P. Gene co-expression analysis for functional classification and gene-disease predictions. *Briefings in Bioinformatics* **19**, 575–592 (2017).

[491] M. Ribeiro, D., Ziyani, C. & Delaneau, O. Shared regulation and functional relevance of local gene co-expression revealed by single cell analysis. *Communications Biology* **5**, 876 (2022).

[492] Gaudet, P. *et al.* Gene Ontology representation for transcription factor functions. *Biochimica et Biophysica Acta (BBA) - Gene Regulatory Mechanisms* **1864**, 194752 (2021).

[493] Lovering, R. C. *et al.* A GO catalogue of human DNA-binding transcription

factors. *Biochimica et Biophysica Acta (BBA) - Gene Regulatory Mechanisms* **1864**, 194765 (2021).

[494] Hanahan, D. & Weinberg, R. A. The Hallmarks of Cancer. *Cell* **100**, 57–70 (2000). Publisher: Elsevier.

[495] Hanahan, D. Hallmarks of Cancer: New Dimensions. *Cancer Discovery* **12**, 31–46 (2022).

[496] Feitelson, M. A. *et al.* Sustained proliferation in cancer: mechanisms and novel therapeutic targets. *Seminars in cancer biology* **35**, S25–S54 (2015).

[497] Raftopulos, N. L. *et al.* Prostate cancer cell proliferation is influenced by LDL-cholesterol availability and cholesteryl ester turnover. *Cancer & Metabolism* **10**, 1 (2022).

[498] Reed, J. C. Dysregulation of apoptosis in cancer. *Journal of Clinical Oncology: Official Journal of the American Society of Clinical Oncology* **17**, 2941–2953 (1999).

[499] Brand, M., Orr, A., Perevoshchikova, I. & Quinlan, C. The role of mitochondrial function and cellular bioenergetics in ageing and disease. *The British journal of dermatology* **169**, 1–8 (2013).

[500] Wang, C. & Youle, R. J. The Role of Mitochondria in Apoptosis. *Annual review of genetics* **43**, 95–118 (2009).

[501] Wang, R., Liu, G. & Wang, C. Identifying protein complexes based on an edge weight algorithm and core-attachment structure. *BMC Bioinformatics* **20**, 471 (2019).

[502] Wang, J., Li, M., Deng, Y. & Pan, Y. Recent advances in clustering methods for protein interaction networks. *BMC Genomics* **11**, S10 (2010).

[503] Bailey, T. L. & Grant, C. E. SEA: Simple Enrichment Analysis of motifs (2021). Pages: 2021.08.23.457422 Section: New Results.

[504] Shi, Y. Mechanisms of Caspase Activation and Inhibition during Apoptosis. *Molecular Cell* **9**, 459–470 (2002). Publisher: Elsevier.

[505] Rees, D. C., Johnson, E. & Lewinson, O. ABC transporters: the power to change. *Nature Reviews Molecular Cell Biology* **10**, 218–227 (2009). Number: 3 Publisher: Nature Publishing Group.

[506] Lin, L., Yee, S. W., Kim, R. B. & Giacomini, K. M. SLC transporters as therapeutic targets: emerging opportunities. *Nature Reviews Drug Discovery* **14**, 543–560 (2015). Number: 8 Publisher: Nature Publishing Group.

[507] Guggino, W. B. & Stanton, B. A. New insights into cystic fibrosis: molecular switches that regulate CFTR. *Nature Reviews Molecular Cell Biology* **7**, 426–436 (2006). Number: 6 Publisher: Nature Publishing Group.

[508] Hegedüs, T. *et al.* C-terminal phosphorylation of MRP2 modulates its interaction with PDZ proteins. *Biochemical and Biophysical Research Communications* **302**, 454–461 (2003).

[509] Fitzgerald, M. L. *et al.* Naturally Occurring Mutations in the Largest Extracellular Loops of ABCA1 Can Disrupt Its Direct Interaction with Apolipoprotein A-I. *Journal of Biological Chemistry* **277**, 33178–33187 (2002). Publisher: Elsevier.

[510] Krishna, S. S., Majumdar, I. & Grishin, N. V. Structural classification of

zinc fingers: survey and summary. *Nucleic Acids Research* **31**, 532–550 (2003).

[511] Johnson, P. F. & McKnight, S. L. Eukaryotic Transcriptional Regulatory Proteins. *Annual Review of Biochemistry* **58**, 799–839 (1989). _eprint: https://doi.org/10.1146/annurev.bi.58.070189.004055.

[512] Laity, J. H., Lee, B. M. & Wright, P. E. Zinc finger proteins: new insights into structural and functional diversity. *Current Opinion in Structural Biology* **11**, 39–46 (2001).

[513] McConnell, B. B. & Yang, V. W. Mammalian Krüppel-like factors in health and diseases. *Physiological Reviews* **90**, 1337–1381 (2010).

[514] Meng, J. *et al.* Characterization of the prognostic values and response to immunotherapy/chemotherapy of Krüppel-like factors in prostate cancer. *Journal of Cellular and Molecular Medicine* **24**, 5797–5810 (2020). _eprint: https://onlinelibrary.wiley.com/doi/pdf/10.1111/jcmm.15242.

[515] Suske, G., Bruford, E. & Philipsen, S. Mammalian SP/KLF transcription factors: Bring in the family. *Genomics* **85**, 551–556 (2005).

[516] Safe, S., Abbruzzese, J., Abdelrahim, M. & Hedrick, E. Specificity Protein Transcription Factors and Cancer: Opportunities for Drug Development. *Cancer Prevention Research* **11**, 371–382 (2018).

[517] Lai, W. *et al.* GTSE1 promotes prostate cancer cell proliferation via the SP1/FOXM1 signaling pathway. *Laboratory Investigation* **101**, 554–563 (2021). Number: 5 Publisher: Nature Publishing Group.

[518] Shin, S.-H., Kim, I., Lee, J. E., Lee, M. & Park, J.-W. Loss of EGR3

is an independent risk factor for metastatic progression in prostate cancer. *Oncogene* **39**, 5839–5854 (2020).

[519] Donohue, L. K. H. *et al.* A cis-regulatory lexicon of DNA motif combinations mediating cell-type-specific gene regulation. *Cell Genomics* **2**, 100191 (2022).

[520] Tyzack, J. K., Wang, X., Belsham, G. J. & Proud, C. G. ABC50 Interacts with Eukaryotic Initiation Factor 2 and Associates with the Ribosome in an ATP-dependent Manner*. *Journal of Biological Chemistry* **275**, 34131–34139 (2000).

[521] Koc, E. C., Burkhart, W., Blackburn, K., Moseley, A. & Spremulli, L. L. The Small Subunit of the Mammalian Mitochondrial Ribosome: IDENTIFICATION OF THE FULL COMPLEMENT OF RIBOSOMAL PROTEINS PRESENT *. *Journal of Biological Chemistry* **276**, 19363–19374 (2001). Publisher: Elsevier.

[522] Sztal, T. E., McKaige, E. A., Williams, C., Ruparelia, A. A. & Bryson-Richardson, R. J. Genetic compensation triggered by actin mutation prevents the muscle damage caused by loss of actin protein. *PLoS genetics* **14**, e1007212 (2018).

[523] Traunmüller, L., Bornmann, C. & Scheiffele, P. Alternative Splicing Coupled Nonsense-Mediated Decay Generates Neuronal Cell Type-Specific Expression of SLM Proteins. *Journal of Neuroscience* **34**, 16755–16761 (2014). Publisher: Society for Neuroscience Section: Articles.

[524] Ohno, S. *Evolution by Gene Duplication* (Springer Science & Business Media, 2013). Google-Books-ID: 5SjqCAAAQBAJ.

[525] Fraimovitch, E. & Hagai, T. Promoter evolution of mammalian gene duplicates. *BMC Biology* **21**, 80 (2023).

[526] Kuzmin, E. *et al.* Exploring whole-genome duplicate gene retention with complex genetic interaction analysis. *Science* **368**, eaaz5667 (2020). Publisher: American Association for the Advancement of Science.

[527] Lan, X. & Pritchard, J. K. Coregulation of tandem duplicate genes slows evolution of subfunctionalization in mammals. *Science* **352**, 1009–1013 (2016). Publisher: American Association for the Advancement of Science.

[528] Loker, R. & Mann, R. S. Divergent expression of paralogous genes by modification of shared enhancer activity through a promoter-proximal silencer. *Current biology: CB* **32**, 3545–3555.e4 (2022).

[529] Liu, A. Y. Differential Expression of Cell Surface Molecules in Prostate Cancer Cells1. *Cancer Research* **60**, 3429–3434 (2000).

[530] Ölken, E. A. *et al.* SFRP2 Overexpression Induces an Osteoblast-like Phenotype in Prostate Cancer Cells. *Cells* **11** (2022). Publisher: Multidisciplinary Digital Publishing Institute (MDPI).

[531] Hanahan, D. & Weinberg, R. A. Hallmarks of Cancer: The Next Generation. *Cell* **144**, 646–674 (2011). Publisher: Elsevier.

[532] Chen, L. *et al.* Downregulation of SHMT2 promotes the prostate cancer proliferation and metastasis by inducing epithelial-mesenchymal transition. *Experimental Cell Research* **415**, 113138 (2022).

[533] Weiss, W. A., Taylor, S. S. & Shokat, K. M. Recognizing and exploiting

differences between RNAi and small-molecule inhibitors. *Nature chemical biology* **3**, 739–744 (2007).

[534] Schaller, M. D. *et al.* pp125FAK a structurally distinctive protein-tyrosine kinase associated with focal adhesions. *Proceedings of the National Academy of Sciences of the United States of America* **89**, 5192–5196 (1992).

[535] Provenzano, P. P. & Keely, P. J. The role of focal adhesion kinase in tumor initiation and progression. *Cell Adhesion & Migration* **3**, 347–350 (2009). Publisher: Taylor & Francis _eprint: https://doi.org/10.4161/cam.3.4.9458.

[536] Tan, X. *et al.* Focal adhesion kinase: from biological functions to therapeutic strategies. *Experimental Hematology & Oncology* **12**, 83 (2023).

[537] Figel, S. & H. Gelman, I. Focal Adhesion Kinase Controls Prostate Cancer Progression Via Intrinsic Kinase and Scaffolding Functions. *Anti-Cancer Agents in Medicinal Chemistry- Anti-Cancer Agents)* **11**, 607–616 (2011).

[538] Wu, Y. *et al.* Focal adhesion kinase inhibitors, a heavy punch to cancer. *Discover. Oncology* **12**, 52 (2021).

[539] Chauhan, A. & Khan, T. Focal adhesion kinase-An emerging viable target in cancer and development of focal adhesion kinase inhibitors. *Chemical Biology & Drug Design* **97**, 774–794 (2021). _eprint: https://onlinelibrary.wiley.com/doi/pdf/10.1111/cbdd.13808.

[540] Murphy, J. M., Rodriguez, Y. A. R., Jeong, K., Ahn, E.-Y. E. & Lim, S.-T. S. Targeting focal adhesion kinase in cancer cells and the tumor mi-

croenvironment. *Experimental & Molecular Medicine* **52**, 877–886 (2020). Number: 6 Publisher: Nature Publishing Group.

[541] Zhou, J., Yi, Q. & Tang, L. The roles of nuclear focal adhesion kinase (FAK) on Cancer: a focused review. *Journal of Experimental & Clinical Cancer Research : CR* **38**, 250 (2019).

[542] Omoto, Y. & Iwase, H. Clinical significance of estrogen receptor β in breast and prostate cancer from biological aspects. *Cancer Science* **106**, 337–343 (2015).

[543] Lafront, C., Germain, L., Weidmann, C. & Audet-Walsh, E. A Systematic Study of the Impact of Estrogens and Selective Estrogen Receptor Modulators on Prostate Cancer Cell Proliferation. *Scientific Reports* **10**, 4024 (2020). Number: 1 Publisher: Nature Publishing Group.

[544] Nelson, A. W. *et al.* Comprehensive assessment of estrogen receptor beta antibodies in cancer cell line models and tissue reveals critical limitations in reagent specificity. *Molecular and Cellular Endocrinology* **440**, 138–150 (2017).

[545] Ame, J.-C., Spenlehauer, C. & de Murcia, G. The PARP superfamily. *BioEssays: News and Reviews in Molecular, Cellular and Developmental Biology* **26**, 882–893 (2004).

[546] Smulson, M. E. *et al.* Roles of poly(ADP-ribosyl)ation and PARP in apoptosis, DNA repair, genomic stability and functions of p53 and E2F-1. *Advances in Enzyme Regulation* **40**, 183–215 (2000).

[547] Ray Chaudhuri, A. & Nussenzweig, A. The multifaceted roles of PARP1

in DNA repair and chromatin remodelling. *Nature Reviews Molecular Cell Biology* **18**, 610–621 (2017). Number: 10 Publisher: Nature Publishing Group.

[548] Schiewer, M. J. *et al.* Dual roles of PARP-1 promote cancer growth and progression. *Cancer discovery* **2**, 1134–1149 (2012).

[549] Schiewer, M. J. & Knudsen, K. E. Transcriptional Roles of PARP1 in Cancer. *Molecular Cancer Research* **12**, 1069–1080 (2014).

[550] Lai, Y. *et al.* PARP1-siRNA suppresses human prostate cancer cell growth and progression. *Oncology Reports* **39**, 1901–1909 (2018). Publisher: Spandidos Publications.

[551] Bryce, A. H., Sartor, O. & de Bono, J. DNA Repair and Prostate Cancer: A Field Ripe for Harvest. *European Urology* **78**, 486–488 (2020).

[552] Kelly, D. P. & Scarpulla, R. C. Transcriptional regulatory circuits controlling mitochondrial biogenesis and function. *Genes & Development* **18**, 357–368 (2004). Company: Cold Spring Harbor Laboratory Press Distributor: Cold Spring Harbor Laboratory Press Institution: Cold Spring Harbor Laboratory Press Label: Cold Spring Harbor Laboratory Press Publisher: Cold Spring Harbor Lab.

[553] Bugno, M., Daniel, M., Chepelev, N. L. & Willmore, W. G. Changing gears in Nrf1 research, from mechanisms of regulation to its role in disease and prevention. *Biochimica et Biophysica Acta (BBA) - Gene Regulatory Mechanisms* **1849**, 1260–1276 (2015).

[554] Northrop, A., Byers, H. A. & Radhakrishnan, S. K. Regulation of NRF1,

a master transcription factor of proteasome genes: implications for cancer and neurodegeneration. *Molecular Biology of the Cell* **31**, 2158–2163 (2020).

[555] WU, C.-H. *et al.* Nuclear Respiratory Factor 1 Overexpression Inhibits Proliferation and Migration of PC3 Prostate Cancer Cells. *Cancer Genomics & Proteomics* **19**, 614–623 (2022).

[556] Schultz, M. A. *et al.* Nrf1 and Nrf2 Transcription Factors Regulate Androgen Receptor Transactivation in Prostate Cancer Cells. *PLOS ONE* **9**, e87204 (2014). Publisher: Public Library of Science.

[557] Kiyama, T. *et al.* Essential roles of mitochondrial biogenesis regulator Nrf1 in retinal development and homeostasis. *Molecular Neurodegeneration* **13**, 56 (2018).

[558] Zhang, J. *et al.* EglN2 associates with the NRF1-PGC1α complex and controls mitochondrial function in breast cancer. *The EMBO Journal* **34**, 2953–2970 (2015).

[559] Kim, K., Pang, K. M., Evans, M. & Hay, E. D. Overexpression of β-Catenin Induces Apoptosis Independent of Its Transactivation Function with LEF-1 or the Involvement of Major G1 Cell Cycle Regulators. *Molecular Biology of the Cell* **11**, 3509–3523 (2000).

[560] Iurlaro, R. & Munoz-Pinedo, C. Cell death induced by endoplasmic reticulum stress. *The FEBS Journal* **283**, 2640–2652 (2016). _eprint: https://onlinelibrary.wiley.com/doi/pdf/10.1111/febs.13598.

[561] McGilvray, P. T. *et al.* An ER translocon for multi-pass membrane protein

biogenesis. *eLife* **9**, e56889 (2020).

[562] Li, P. *et al.* Caspase-9: structure, mechanisms and clinical application. *Oncotarget* **8**, 23996–24008 (2017).

[563] McStay, G. P. & Green, D. R. Measuring Apoptosis: Caspase Inhibitors and Activity Assays. *Cold Spring Harbor Protocols* **2014**, pdb.top070359 (2014). Publisher: Cold Spring Harbor Laboratory Press.

[564] Nabih, H. K., Hamed, A. R. & Yahya, S. M. M. Anti-proliferative effect of melatonin in human hepatoma HepG2 cells occurs mainly through cell cycle arrest and inflammation inhibition. *Scientific Reports* **13**, 4396 (2023).

[565] Wang, G., Zhao, D., Spring, D. J. & DePinho, R. A. Genetics and biology of prostate cancer. *Genes & Development* **32**, 1105–1140 (2018).

[566] de Koning, T. J. *et al.* L-serine in disease and development. *Biochemical Journal* **371**, 653–661 (2003).

[567] Ducker, G. S. & Rabinowitz, J. D. One-Carbon Metabolism in Health and Disease. *Cell Metabolism* **25**, 27–42 (2017). Publisher: Elsevier.

[568] Minton, D. R. *et al.* Serine Catabolism by SHMT2 Is Required for Proper Mitochondrial Translation Initiation and Maintenance of Formylmethionyl-tRNAs. *Molecular Cell* **69**, 610–621.e5 (2018). Publisher: Elsevier.

[569] Lucas, S., Chen, G., Aras, S. & Wang, J. Serine catabolism is essential to maintain mitochondrial respiration in mammalian cells. *Life Science Alliance* **1**, e201800036 (2018).

[570] Morscher, R. J. *et al.* Mitochondrial translation requires folate-dependent

tRNA methylation. *Nature* **554**, 128–132 (2018). Number: 7690 Publisher: Nature Publishing Group.

[571] Farber, S. & Diamond, L. K. Temporary remissions in acute leukemia in children produced by folic acid antagonist, 4-aminopteroyl-glutamic acid. *The New England Journal of Medicine* **238**, 787–793 (1948).

[572] Jain, M. *et al.* Metabolite profiling identifies a key role for glycine in rapid cancer cell proliferation. *Science (New York, N.Y.)* **336**, 1040–1044 (2012).

[573] Ye, J. *et al.* Serine catabolism regulates mitochondrial redox control during hypoxia. *Cancer Discovery* **4**, 1406–1417 (2014).

[574] Puyo, S., Robert, J., Richaud, P., Pourquier, P. & Houede, N. Abstract 2692: Overexpression of serine hydroxy methyl transferase 2 (SHMT2) in high grade prostate cancers as a marker of tumor response to oxaliplatin. *Cancer Research* **70**, 2692 (2010).

[575] Puyo, S. *et al.* Abstract 4478: SHMT2 modulates DNA methylation and differentially affects prostate cancer cell response to platinum derivatives. *Cancer Research* **73**, 4478 (2013).

[576] Marrocco, I. *et al.* Shmt2: A Stat3 Signaling New Player in Prostate Cancer Energy Metabolism. *Cells* **8**, 1048 (2019).

[577] Sant'Anna-Silva, A. C. B. *et al.* Succinate Anaplerosis Has an Onco-Driving Potential in Prostate Cancer Cells. *Cancers* **13**, 1727 (2021).

[578] Castello, A. *et al.* Insights into RNA Biology from an Atlas of Mammalian mRNA-Binding Proteins. *Cell* **149**, 1393–1406 (2012).

[579] Hentze, M. W., Castello, A., Schwarzl, T. & Preiss, T. A brave new world of RNA-binding proteins. *Nature Reviews Molecular Cell Biology* **19**, 327–341 (2018). Number: 5 Publisher: Nature Publishing Group.

[580] Bordeaux, J. *et al.* Antibody validation. *BioTechniques* **48**, 197–209 (2010).

[581] Uhlen, M. *et al.* A proposal for validation of antibodies. *Nature Methods* **13**, 823–827 (2016). Number: 10 Publisher: Nature Publishing Group.

[582] Frank, S. A. Specificity and Cross-Reactivity. In *Immunology and Evolution of Infectious Disease* (Princeton University Press, 2002).

[583] Kuhre, R. E. *et al.* Peptide production and secretion in glutag, nci-h716 and stc-1 cells: a comparison to native l-cells. *Journal of molecular endocrinology* **56**, 201 (2016).

[584] Aleksunes, L. M., Augustine, L. M., Scheffer, G. L., Cherrington, N. J. & Manautou, J. E. Renal xenobiotic transporters are differentially expressed in mice following cisplatin treatment. *Toxicology* **250**, 82–88 (2008).

[585] Dallas, S., Schlichter, L. & Bendayan, R. Multidrug resistance protein (MRP) 4- and MRP 5-mediated efflux of 9-(2-phosphonylmethoxyethyl)adenine by microglia. *The Journal of Pharmacology and Experimental Therapeutics* **309**, 1221–1229 (2004).

[586] Prime-Chapman, H. M., Fearn, R. A., Cooper, A. E., Moore, V. & Hirst, B. H. Differential multidrug resistance-associated protein 1 through 6 isoform expression and function in human intestinal epithelial Caco-2 cells.

The Journal of Pharmacology and Experimental Therapeutics **311**, 476–484 (2004).

[587] Scheffer, G. L. *et al.* Specific detection of multidrug resistance proteins MRP1, MRP2, MRP3, MRP5, and MDR3 P-glycoprotein with a panel of monoclonal antibodies. *Cancer Research* **60**, 5269–5277 (2000).

[588] Soontornmalai, A., Vlaming, M. L. H. & Fritschy, J.-M. Differential, strain-specific cellular and subcellular distribution of multidrug transporters in murine choroid plexus and blood-brain barrier. *Neuroscience* **138**, 159–169 (2006).

[589] Ambudkar, S. V., Kim, I.-W., Xia, D. & Sauna, Z. E. The A-loop, a novel conserved aromatic acid subdomain upstream of the Walker A motif in ABC transporters, is critical for ATP binding. *FEBS Letters* **580**, 1049–1055 (2006).

[590] Lipman, N. S., Jackson, L. R., Trudel, L. J. & Weis-Garcia, F. Monoclonal versus polyclonal antibodies: distinguishing characteristics, applications, and information resources. *ILAR journal* **46**, 258–268 (2005).

[591] Reily, C., Stewart, T. J., Renfrow, M. B. & Novak, J. Glycosylation in health and disease. *Nature Reviews Nephrology* **15**, 346–366 (2019). Number: 6 Publisher: Nature Publishing Group.

[592] Butler, W. & Huang, J. Glycosylation Changes in Prostate Cancer Progression. *Frontiers in Oncology* **11**, 809170 (2021).

[593] Xu, F. *et al.* Quantitative site- and structure-specific N-glycoproteomics

characterization of differential N-glycosylation in MCF-7/ADR cancer stem cells. *Clinical Proteomics* **17**, 3 (2020).

[594] Ji, Y. *et al.* Integrated proteomic and N-glycoproteomic analyses of doxorubicin sensitive and resistant ovarian cancer cells reveal glycoprotein alteration in protein abundance and glycosylation. *Oncotarget* **8**, 13413–13427 (2017).

[595] Dean, M., Moitra, K. & Allikmets, R. The human ATP-binding cassette (ABC) transporter superfamily. *Human Mutation* **43**, 1162–1182 (2022). _eprint: https://onlinelibrary.wiley.com/doi/pdf/10.1002/humu.24418.

[596] Park, J. E., Ryoo, G. & Lee, W. Alternative Splicing: Expanding Diversity in Major ABC and SLC Drug Transporters. *The AAPS Journal* **19**, 1643–1655 (2017).

[597] Leivonen, S.-K. *et al.* Alternative splicing discriminates molecular subtypes and has prognostic impact in diffuse large B-cell lymphoma. *Blood Cancer Journal* **7**, e596–e596 (2017). Number: 8 Publisher: Nature Publishing Group.

[598] Sandor, S. *et al.* Functional characterization of the ABCG2 5' non-coding exon variants: Stem cell specificity, translation efficiency and the influence of drug selection. *Biochimica et Biophysica Acta (BBA) - Gene Regulatory Mechanisms* **1859**, 943–951 (2016).

[599] He, X., Ee, P. L. R., Coon, J. S. & Beck, W. T. Alternative Splicing of the Multidrug Resistance Protein 1/ATP Binding Cassette Transporter Subfamily Gene in Ovarian Cancer Creates Functional Splice Variants and Is Asso-

ciated with Increased Expression of the Splicing Factors PTB and SRp20. *Clinical Cancer Research* **10**, 4652–4660 (2004).

[600] Reyes Diaz, J. V. *et al.* A homozygous exonic variant leading to exon skipping in ABCC8 as the cause of severe congenital hyperinsulinism. *American Journal of Medical Genetics. Part A* **188**, 2429–2433 (2022).

[601] Cong, L. *et al.* Multiplex Genome Engineering Using CRISPR/Cas Systems. *Science* **339**, 819–823 (2013). Publisher: American Association for the Advancement of Science.

[602] Ketteler, R. On programmed ribosomal frameshifting: the alternative proteomes. *Frontiers in Genetics* **3**, 242 (2012).

[603] Tuladhar, R. *et al.* CRISPR-Cas9-based mutagenesis frequently provokes on-target mRNA misregulation. *Nature Communications* **10**, 4056 (2019).

[604] Reber, S. *et al.* CRISPR-Trap: a clean approach for the generation of gene knockouts and gene replacements in human cells. *Molecular Biology of the Cell* **29**, 75–83 (2018).

[605] Smits, A. H. *et al.* Biological plasticity rescues target activity in CRISPR knock outs. *Nature Methods* **16**, 1087–1093 (2019). Number: 11 Publisher: Nature Publishing Group.

[606] Bergengren, O. *et al.* 2022 Update on Prostate Cancer Epidemiology and Risk Factors-A Systematic Review. *European Urology* **84**, 191–206 (2023).

[607] Elmehrath, A. O. *et al.* Causes of Death Among Patients With Metastatic Prostate Cancer in the US From 2000 to 2016. *JAMA Network Open* **4**, e2119568 (2021).

[608] Wu, X., Swedek, M., Malouff, T. D. & Silberstein, P. T. Palliative care utilization in metastatic prostate cancer: An analysis of the National Cancer Database. *Journal of Clinical Oncology* **40**, 202–202 (2022). Publisher: Wolters Kluwer.

[609] Gazzaniga, P. *et al.* Molecular markers in circulating tumour cells from metastatic colorectal cancer patients. *Journal of Cellular and Molecular Medicine* **14**, 2073–2077 (2010).

[610] Liu, L., Guo, K., Liang, Z., Li, F. & Wang, H. Identification of candidate genes that may contribute to the metastasis of prostate cancer by bioinformatics analysis. *Oncology Letters* **15**, 1220–1228 (2018).

[611] Chen, J. The Cell-Cycle Arrest and Apoptotic Functions of p53 in Tumor Initiation and Progression. *Cold Spring Harbor Perspectives in Medicine* **6**, a026104 (2016).

[612] Cheung, S. T., Cheung, P. F. Y., Cheng, C. K. C., Wong, N. C. L. & Fan, S. T. Granulin-Epithelin Precursor and ATP-Dependent Binding Cassette (ABC)B5 Regulate Liver Cancer Cell Chemoresistance. *Gastroenterology* **140**, 344–355.e2 (2011).

[613] Schatton, T. *et al.* Identification of cells initiating human melanomas. *Nature* **451**, 345–349 (2008). Number: 7176 Publisher: Nature Publishing Group.

[614] Wilson, B. J. *et al.* ABCB5 Identifies a Therapy-Refractory Tumor Cell Population in Colorectal Cancer Patients. *Cancer Research* **71**, 5307–5316 (2011).

[615] Ma, Y., Kanakousaki, K. & Buttitta, L. How the cell cycle impacts chromatin architecture and influences cell fate. *Frontiers in Genetics* **6** (2015).

[616] Clouaire, T. *et al.* Comprehensive Mapping of Histone Modifications at DNA Double-Strand Breaks Deciphers Repair Pathway Chromatin Signatures. *Molecular Cell* **72**, 250–262.e6 (2018).

[617] Happel, N. & Doenecke, D. Histone H1 and its isoforms: contribution to chromatin structure and function. *Gene* **431**, 1–12 (2009).

[618] Wang, H., Liu, Y., Yuan, J., Zhang, J. & Han, F. The condensin subunits SMC2 and SMC4 interact for correct condensation and segregation of mitotic maize chromosomes. *The Plant Journal* **102**, 467–479 (2020). _eprint: https://onlinelibrary.wiley.com/doi/pdf/10.1111/tpj.14639.

[619] Arnould, C. *et al.* Chromatin compartmentalization regulates the response to DNA damage. *Nature* **623**, 183–192 (2023). Number: 7985 Publisher: Nature Publishing Group.

[620] Stadler, J. & Richly, H. Regulation of DNA Repair Mechanisms: How the Chromatin Environment Regulates the DNA Damage Response. *International Journal of Molecular Sciences* **18**, 1715 (2017).

[621] de Bono, J. *et al.* Olaparib for Metastatic Castration-Resistant Prostate Cancer. *New England Journal of Medicine* **382**, 2091–2102 (2020). Publisher: Massachusetts Medical Society _eprint: https://doi.org/10.1056/NEJMoa1911440.

[622] Satoh, J.-i., Kawana, N. & Yamamoto, Y. Pathway Analysis of ChIP-Seq-Based NRF1 Target Genes Suggests a Logical Hypothesis of their Involve-

ment in the Pathogenesis of Neurodegenerative Diseases. *Gene Regulation and Systems Biology* **7**, 139–152 (2013).

[623] Scarpulla, R. C. Transcriptional Paradigms in Mammalian Mitochondrial Biogenesis and Function. *Physiological Reviews* **88**, 611–638 (2008). Publisher: American Physiological Society.

[624] Brown, A. *et al.* Structure of the large ribosomal subunit from human mitochondria. *Science (New York, N.Y.)* **346**, 718–722 (2014).

[625] Miller, J. L., Cimen, H., Koc, H. & Koc, E. C. Phosphorylated proteins of the mammalian mitochondrial ribosome: implications in protein synthesis. *Journal of proteome research* **8**, 4789–4798 (2009).

[626] Krishnamurthy, P. C. *et al.* Identification of a mammalian mitochondrial porphyrin transporter. *Nature* **443**, 586–589 (2006).

[627] Song, G. *et al.* Molecular insights into the human ABCB6 transporter. *Cell Discovery* **7**, 1–11 (2021). Number: 1 Publisher: Nature Publishing Group.

[628] Krishnamurthy, P. & Schuetz, J. D. The role of ABCG2 and ABCB6 in porphyrin metabolism and cell survival. *Current Pharmaceutical Biotechnology* **12**, 647–655 (2011).

[629] Shemin, D. & Rittenberg, D. The biological utilization of glycine for the synthesis of the protoporphyrin of hemoglobin. *The Journal of Biological Chemistry* **166**, 621–625 (1946).

[630] Ajioka, R. S., Phillips, J. D. & Kushner, J. P. Biosynthesis of heme in mammals. *Biochimica et Biophysica Acta (BBA) - Molecular Cell Research* **1763**, 723–736 (2006).

[631] Li, J. *et al.* Ferroptosis: past, present and future. *Cell Death & Disease* **11**, 1–13 (2020). Number: 2 Publisher: Nature Publishing Group.

[632] Sengupta, S. & Harris, C. C. p53: traffic cop at the crossroads of DNA repair and recombination. *Nature Reviews Molecular Cell Biology* **6**, 44–55 (2005). Number: 1 Publisher: Nature Publishing Group.

[633] Phan, T. T. T., Lin, Y.-C., Chou, Y.-T., Wu, C.-W. & Lin, L.-Y. Tumor suppressor p53 restrains cancer cell dissemination by modulating mitochondrial dynamics. *Oncogenesis* **11**, 1–14 (2022). Number: 1 Publisher: Nature Publishing Group.

[634] Park, J.-H., Zhuang, J., Li, J. & Hwang, P. M. p53 as guardian of the mitochondrial genome. *FEBS Letters* **590**, 924–934 (2016). _eprint: https://onlinelibrary.wiley.com/doi/pdf/10.1002/1873-3468.12061.

[635] Wei, H. *et al.* Structural insight into the molecular mechanism of p53-mediated mitochondrial apoptosis. *Nature Communications* **12**, 2280 (2021). Number: 1 Publisher: Nature Publishing Group.

[636] Garrido, C. *et al.* Mechanisms of cytochrome c release from mitochondria. *Cell Death & Differentiation* **13**, 1423–1433 (2006). Number: 9 Publisher: Nature Publishing Group.

A | Appendices

A.1 Appendix

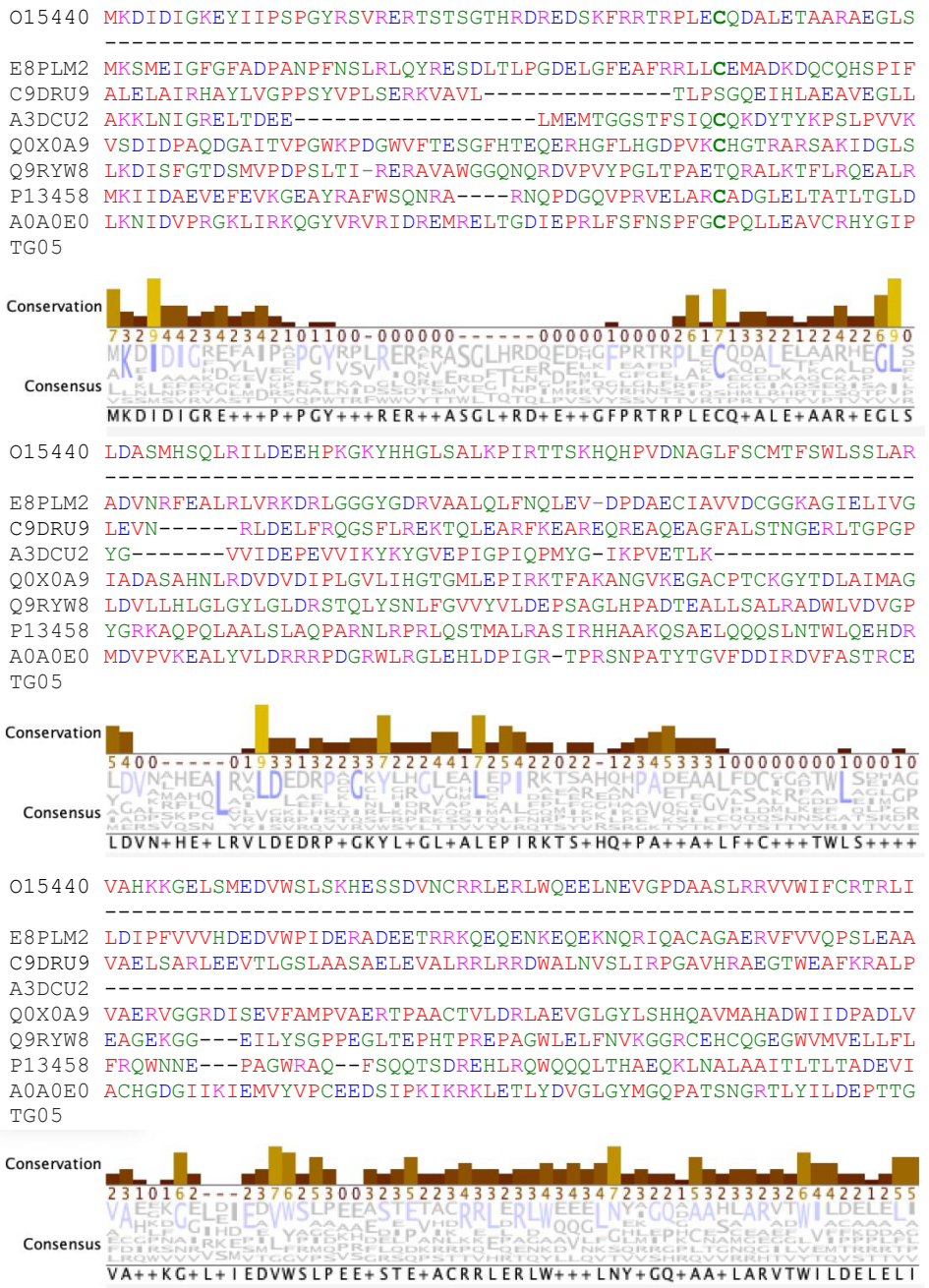

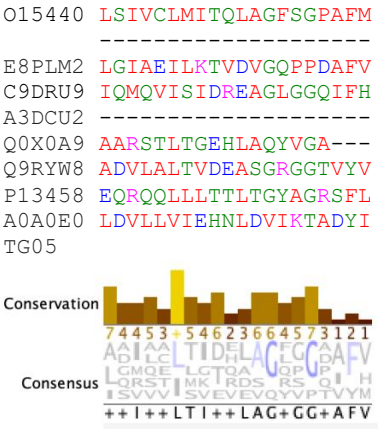

Figure A.1: Multiple Sequence Alignment of Proteins identified in DALI analysis with ABCC5 (015440).

Table A.1: Homology modelling of ABCC11 and ABCC12 against human and *E. coli* AlphaFold structural database.

Human ABCC12 against human AlphaFold database						
Chain	**Z-score**	**rmsd**	**lali**	**nres**	**$id**	**PDB Description**
e7l9-A	17.3	2.8	275	1437	32	HUMAN:AF-O15440-F1 MULTIDRUG RESISTANCE ASSOCIATED PROTEIN 5
fa2p-A	16.0	1.8	283	1359	93	HUMAN:AF-Q96J65-F1 ATP-BINDING CASSETTE SUB-FAMILY C MEMBER 12
e8h6-A	15.1	1.8	269	1382	40	HUMAN:AF-Q96J66-F1 ATP-BINDING CASSETTE SUB-FAMILY C MEMBER 11
Human ABCC12 against *E. coli* AlphaFold database						
Chain	**Z-score**	**rmsd**	**lali**	**nres**	**$id**	**PDB Description**
etv6-A	9.7	2.7	175	588	11	ECOLI:AF-P29018-F1 ATP-BINDING/PERMEASE PROTEIN CYDD
esk7-A	9.4	2.6	175	590	8	ECOLI:AF-P77265-F1 MULTIDRUG RESISTANCE-LIKE ATP-BINDING PROTEIN MDL
ermm-A	9.3	3.2	78	79	17	ECOLI:AF-P68699-F1 ATP SYNTHASE SUBUNIT C
Human ABCC11 against human AlphaFold database						
Chain	**Z-score**	**rmsd**	**lali**	**nres**	**$id**	**PDB Description**
fa2p-A	5.8	12.7	112	1359	46	HUMAN:AF-Q96J65-F1 ATP-BINDING CASSETTE SUB-FAMILY C MEMBER 12
e7l9-A	4.8	4.0	114	1437	36	HUMAN:AF-O15440-F1 MULTIDRUG RESISTANCE-ASSOCIATED PROTEIN 5
Human ABCC11 against *E. coli* AlphaFold database						
Chain	**Z-score**	**rmsd**	**lali**	**nres**	**$id**	**PDB Description**
no hits						

```
                10         :         :         :        50         :         :
ABCC5  LLLLLLLLLLLLLLLLLLLLLLLLLLLLLLLLLLLLLLLLLLLLLLLLLHHHHHHLLLLLLLLLLLLHHH
CydC   ----------------------------------------------------------------------

                 :         :       100         :         :         :         :
ABCC5  HHHHLLLLLLLHHHHHHHLLLLLLLLLLLHHHHLLHHHHHHLHHHHHHHHHHHHHLLLLHHHLLLLLLLL
CydC   ----------------------------------------------------------------------

               150         :         :         :         :       200         :
ABCC5  LHHHHHHHHHHHHHHHHHHHLLLLLLHHHHHHHHHHHHHHHHHHHHHHHHHHHHHHHHHHHHHHHHHHHL
CydC   ----------------------------------------------------------------------

                 :         :         :       250         :         :         :
ABCC5  LLLLHHHHHHHHHHHHHHHHHHHHHHHHHHHHHHHHHHHHHHHHHHHHHHHHLLLLLLLLLLHHHHHHHL
CydC.  ----------------------------------------------------------------------

                 :       300         :         :         :         :       350
ABCC5  LHHHHHHHHHHHHHHHHHHHHHHHHHHHHHHHHHHHHHHHHHHHHHHHHHHHHHHHHHHHHHHHHHHHHH
CydC.  ----------------------------------------------------------------------

                 :         :         :         :       400         :         :
ABCC5  HHHHHHHHHHHHHLHHHHHHLLLHHHHHHHHHHHHHHHHHHHHHHHHHHHHHHHHHHHHHHHHHHHHHHH
CydC.  ----------------------------------------------------------------------

                 :         :       450         :         :         :         :
ABCC5  HHHLLLLLLHHHHHHHHHHHHHHHHHHHHHHHHHHHHHHHHHHHHHHHHHHLLLLLLLLLLLLLLLLEEE
CydC   ----------------------------------------------------------------------

               500         :         :         :         :       550         :
ABCC5  EEEEEEEEEELLLLLLLLLLLLLLLLLLLLLLLLLLLLLLHHHHHHHHHHHLLLLLLLLLLLLLLLLLLLL
CydC   ----------------------------------------------------------------------

                 :         :         :       600         :         :         :
ABCC5  LLLLLLLLLLLLLEEEEEEEEEEEEELLLEEEEELLLLLLHHHHHHHHLLLLEEEEEEEEELLLEEEELL
CydC   ----------------------------------------------------------------------

                 :       650         :         :         :         :       700
ABCC5  LLLLLLLLHHHHHHLLLLLLHHHHHHHHHHLLLHHHHLLLLLHHHLLLLHHHLLLLHHHHHHHHHHHHHH
CydC   ----------------------------------------------------------------------

                 :         :         :         :       750         :         :
ABCC5  HLLLEEEEELLLLLLLHHHHHHHHHHHHHHHLLLLEEEEELLLHHHHHHLLEEEEEELLEEEEEELHHHH
CydC   ----------------------------------------------------------------------

                 :         :       800         :         :         :         :
ABCC5  HHHLLHHHHHHHHHHHLLLLLLLLLLLLLLLLLLLLLLLLLLLLLLLLLLLLLLLLLLLLLLLLLLLLLL
CydC   ----------------------------------------------------------------------

               850         :         :         :         :       900         :
ABCC5  LLHHHHHHHHHHHLLHHHHHHHHHHHHHHHHHHHHHHHHHHHHHHLLLLLLEEEELLEEEELLLHHHLLL
CydC   --LHHHHHHHHHHHHHHHHHHHHHHHHHHHHHHHHHHHHHHHHHHHHHLHH-------------HHLLLL

                 :         :         :       950         :         :         :
ABCC5  HHHHHHHHHHHHHHHHHHHHHHHHHHHHHHHHHHHHHHHHHHHHHHLLLHHHHLLLLHHHHHHHHLHHHH
CydC   LHHHHHHHHHHHHHHHHHHHHHHHHHHHHHHHHHHHHHHHHHHHHHHHLLHHHHLLLHHHHHHHHLHHHH
```

Figure A.2: Structural alignment of ABCC5 and CydC (PDB: essr) from the DALI server alignment. The letters describe different structural elements: H: helix, E: strand, L: coil

A.2 Appendix

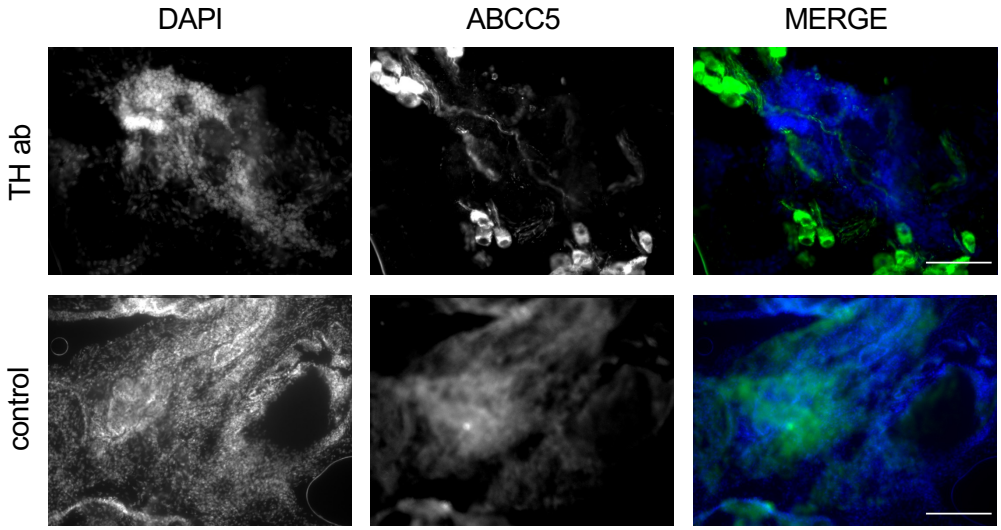

Figure A.3: Staining of wild-type mouse prostate tissue with commercial anti-TH antibody compared to the primary control.

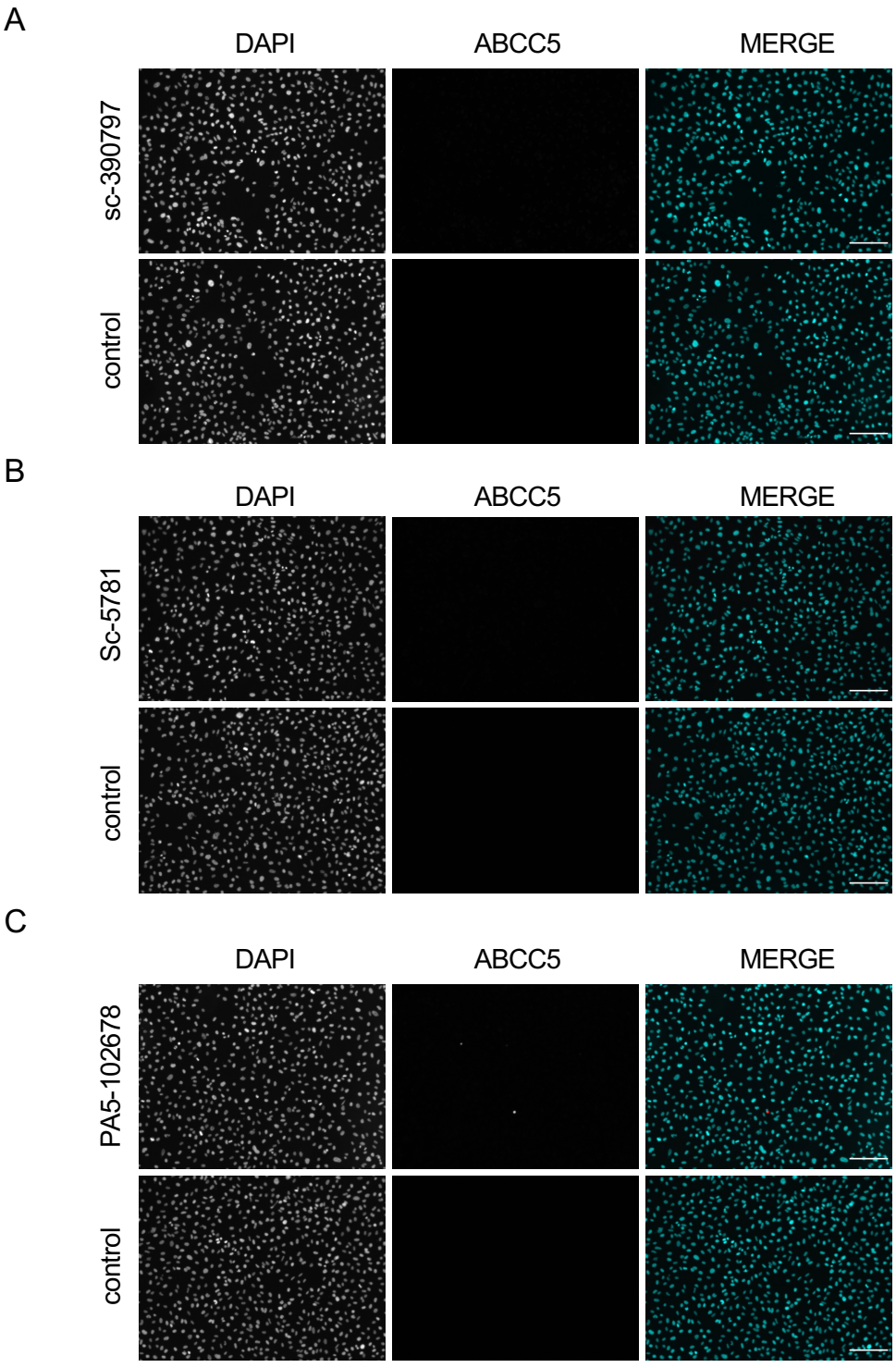
A
DAPI
ABCC5
MERGE
sc-390797
control
B
DAPI
ABCC5
MERGE
Sc-5781
control
C
DAPI
ABCC5
MERGE
PA5-102678
control

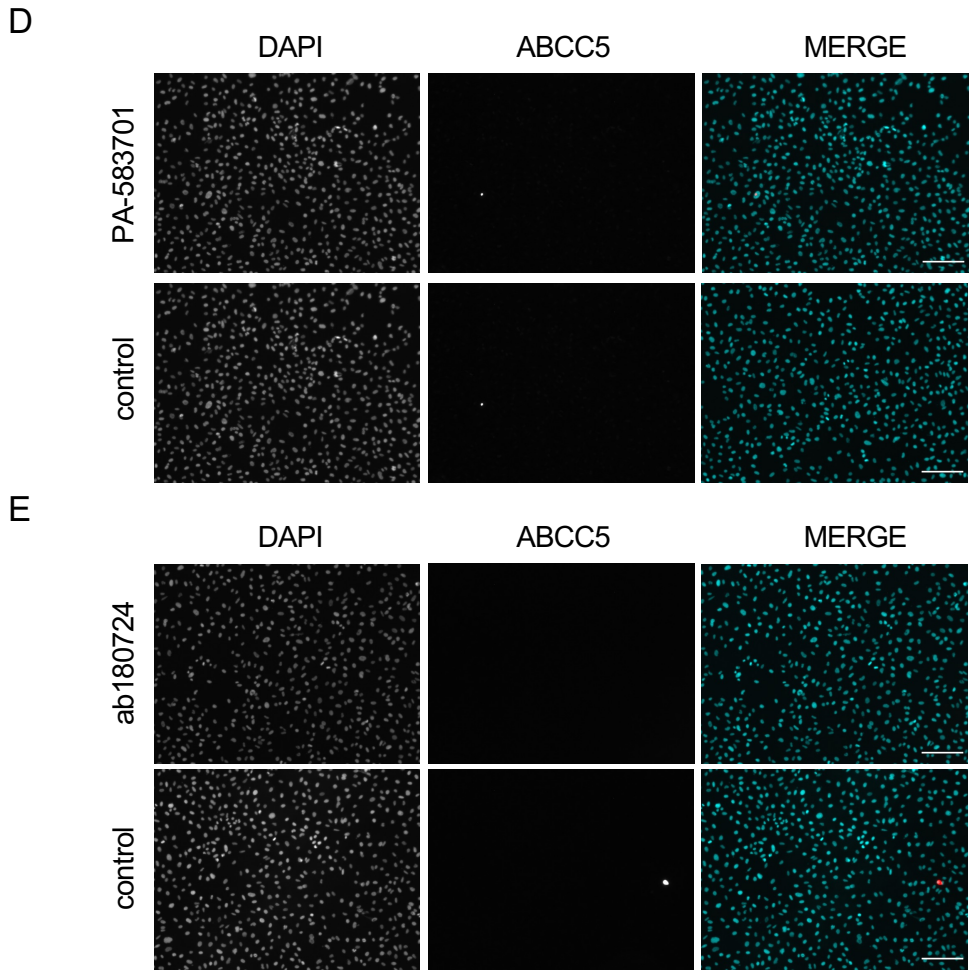

Figure A.4: Staining of PC-3 cells with commercial anti-ABCC5 antibodies. Images of ABCC5 staining with **A)** sc-390797 **B)** sc-5781 **C)** ab180724 **D)** PA583701 **E)** PA5102678 of PC-3 cells compared to no primary control (n=1). Antibody concentration at 1/200. The scale bar is 200 μm.

A

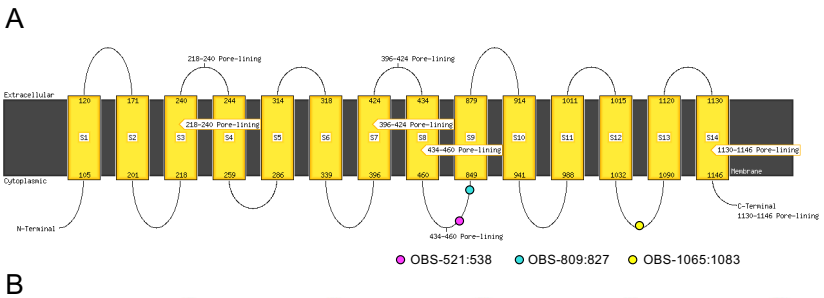
218-240 Pore-lining
396-424 Pore-lining
Extracellular
Cytoplasmic
N-Terminal
C-Terminal
Membrane
434-460 Pore-lining
1130-1146 Pore-lining
OBS-521:538
OBS-809:827
OBS-1065:1083

B


Strand
Helix
Coil
Disordered
Disordered, protein binding
Putative Domain Boundary
Membrane Interaction
Transmembrane Helix
Extracellular
Re-entrant Helix
Cytoplasmic
Signal Peptide

C

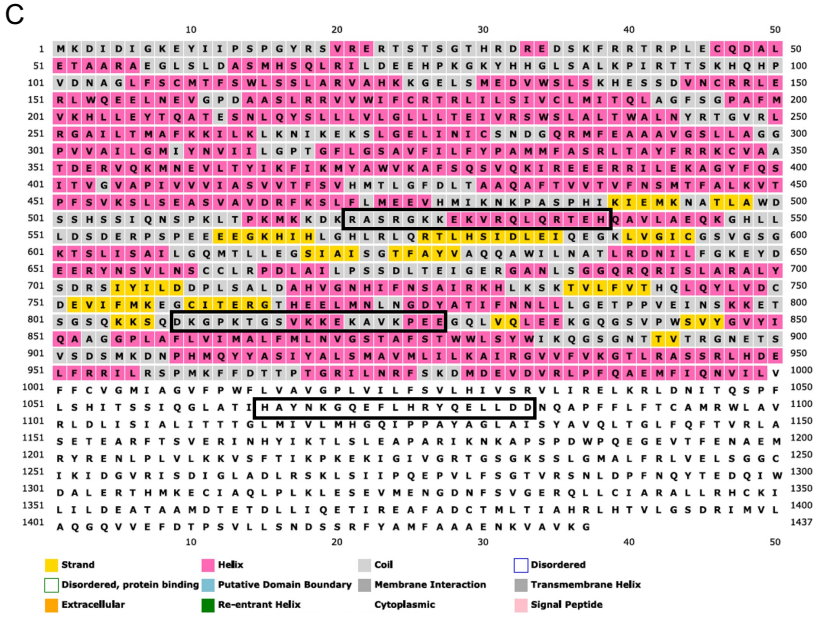
Strand
Helix
Coil
Disordered
Disordered, protein binding
Putative Domain Boundary
Membrane Interaction
Transmembrane Helix
Extracellular
Re-entrant Helix
Cytoplasmic
Signal Peptide

Figure A.5: Prediction of ABCC5 all-helical membrane protein by MEMSAT-SVM and MEMSAT3 servers. **A)** Cartoon diagram that displays the predicted topology of ABCC5. The locations of the antibody binding sites are added; OBS-521:538 (magenta), OBS-809:827 (cyan) and OBS-1065:1083 (yellow). **B)** The plot highlights areas that are extracellular (orange) and have membrane interaction (grey). The sequences of the antibody-binding sites are highlighted in black. **C)** Prediction of the secondary structure of ABCC5 using the Predict Secondary Structure (PSIPRED) algorithm. The plot highlights the areas that are coils (light grey), beta-strands (yellow) and alpha-helices (pink). The sequences of the antibody-binding sites are highlighted in black.